DASA-1892-3

Weapons Radiation Shielding Handbook

Chapter 3 / Methods for Calculating Neutron and Gamma-Ray Attenuation

by Paul N. Stevens and David K. Trubey

Bower

Sh

Handbook Editors

Lorraine S. Abbott, H. Clyde Claiborne, and Charles E. Clifford

DEFENSE ATOMIC SUPPORT AGENCY

Washington, D. C. 20301

Printed in the United States of America. Available from Clearinghouse for Federal
Scientific and Technical Information, National Bureau of Standards,
U.S. Department of Commerce, Springfield, Virginia 22151
Price: Printed Copy $3.00; Microfiche $0.65

DASA-1892-3

WEAPONS RADIATION SHIELDING HANDBOOK

Chapter 3. Methods for Calculating Neutron and Gamma-Ray Attenuation

by

Paul N. Stevens and David K. Trubey

Handbook Editors

Lorraine S. Abbott, H. Clyde Claiborne, and Charles E. Clifford

DEFENSE ATOMIC SUPPORT AGENCY

Washington, D.C. 20301

MARCH 1968

Preparing Agency

OAK RIDGE NATIONAL LABORATORY

Oak Ridge, Tennessee

Operated by UNION CARBIDE CORPORATION

for the U.S. ATOMIC ENERGY COMMISSION

DASA Order No. EO-806-65,

Task A2-11.033

Preface

At the request of the Defense Atomic Support Agency, Oak Ridge National Laboratory has undertaken the preparation of a handbook to aid engineers charged with the responsibility of designing shields to protect military equipment and personnel in the vicinity of a nuclear weapons burst. This document constitutes the third chapter of the Handbook issued thus far, the first one being Chapter 5, entitled "Methods for Calculating Effects of Ducts, Access Ways, and Holes in Shields," and the second one being Chapter 4, entitled "Neutron and Gamma-Ray Albedos." These three chapters, together with an introductory first chapter, will eventually be combined with Chapter 2, which will define the radiation sources insofar as is possible and practicable, to form Volume I of the Handbook. Volume II will consist of two or more additional chapters presenting engineering design methods that are based on the more sophisticated techniques described in Volume I. The intent is that the shield designer will use Volume I as a textbook and ready reference and Volume II as a guide for handling most of the problems with which he will be confronted.

In order to prepare this Handbook, it has been necessary for Oak Ridge National Laboratory to obtain the assistance of several consultants and subcontractors. For this chapter on attenuation, for example, Paul N. Stevens, a consultant from the University of Tennessee, together with David K. Trubey of the Laboratory prepared the first draft with which the editors worked. Other chapters will similarly represent a cooperative effort of ORNL staff members and those of other organizations.

As is always the case for handbooks, the authors and editors rely heavily on the reviews of others as an aid in the development of the various chapters. The list of individuals who have contributed in this manner has already grown very large, and it would be almost impossible to acknowledge each person here. However, there are always reviewers who we feel have made such significant contributions as to warrant individual acknowledgment. With respect to this chapter, we particularly wish to acknowledge the help given by F. R. Mynatt of the Oak Ridge Computing Technology Center, who is largely responsible for the final version of Section 3.3. In addition, several persons at the Laboratory familiar with the various methods for calculating radiation transport through shields were able to serve as on-the-spot authorities to help resolve problem areas as they arose. For this type of help we are especially grateful to F. H. Clark and P. H. Pitkanen, who reviewed the section on the moments method (Section 3.4), to Clark and V. R. Cain, who contributed to the section on the Monte Carlo method (Section 3.5), and to R. R. Coveyou, who reviewed the section on the invariant imbedding technique (Section 3.7). We also wish to thank Mrs. Betty F. Maskewitz for providing the information on the computer code abstracts used in Appendix A.

Appreciation is also expressed to Lt. Cols. Charles D. Daniel and William A. Alfonte, who as past DASA Shielding Project Officers handled the early administration of the contract and assisted in establishing the scope of the Handbook. The work they began is currently being ably performed by Captain R. W. Enz.

Finally, we wish to thank Mrs. Virginia M. Hamrick, who by carefully reading each draft of this chapter, including galley and page proofs, has both improved the rhetoric and helped eliminate some of the usual errors that are inevitably found in formal publications.

December 1967

Contents

3.0 Introduction

The design of shields for protection against the neutrons and gamma rays given off by a weapons burst or an operating reactor usually requires the appropriate interpretation and use of computer programs that implement mathematical models representing the transport of radiation through attenuating media. Numerical, and in some cases analytical, solutions of these models can be obtained by one of several calculational techniques. Selection of the proper technique for a specific shield design problem is usually governed by the type of problem to be solved and the degree of accuracy required, the best technique being, of course, the most economical one that will show beyond a reasonable doubt that the design criteria have been met. The purpose of this chapter of the Handbook is to help the shield designer choose the best method by providing him with reasonably simplified and generalized descriptions of the more commonly used techniques. As a further aid, summaries of digital computer programs which solve the models by the various techniques are presented in an appendix, and other appendixes include basic data and functions of general utility.

The calculational methods covered here are those of spherical harmonics, discrete ordinates, moments, Monte Carlo, diffusion theory, invariant imbedding, and kernels, plus a method which combines a removal kernel with diffusion theory. Except for the invariant imbedding method, all these techniques are either approximate solutions to the well-known Boltzmann equation or are based on kernels obtained from solutions to the equation.* The Boltzmann equation, which is discussed in Section 3.1, is a precise mathematical description of neutron or gamma-ray behavior in terms of position, energy, direction and time.

Both neutrons and gamma rays are considered to be particles which move unchanged in straight lines until they collide with an atom. These collisions result in the fission of the atomic nucleus (primarily by neutron collisions), the scattering of the incident particle, or the absorption of the incident particle. Fission reactions are not normally of interest in shield design except when the sources of radiation need to be considered. Thus the interactions treated in calculating neutron or gamma-ray attenuation in shields are either scattering, in which case the particle emerges from the interaction deflected in direction and degraded in energy, or absorption, in which case the particle effectively disappears. When the absorbed particle is a neutron, either a charged particle or a gamma ray is emitted by the absorbing nucleus. The charged particle is of interest in shielding calculations only in certain special cases, but the gamma rays resulting from neutron absorption (called "radiative capture") are important secondary sources and must be taken into account. Inelastic scattering by neutrons results in the emission of gamma rays, which can be important secondary sources in some cases. Secondary particles emitted as a result of gamma-ray interactions (electrons, positrons, and low-energy gamma rays) do not normally create a shielding problem.

The relative importance of the different interactions is described by basic nuclear parameters called "cross sections." The cross section of greatest importance in shielding is the macroscopic total cross section (called the linear absorption coefficient for gamma rays). The total cross section is the probability per unit length of particle travel that an interaction will occur. It is usually given in units of cm^{-1}, and its reciprocal is the mean free path between interactions for the neutron or gamma ray of a particular energy in a particular material. The total cross section can be divided into partial cross sections representing each nuclide in the shield and each interaction contributing to the total attenuation. These include cross sections that describe the energy and angular distributions of the resulting particles, which are required for a detailed treatment of the transport process.

Most of the calculational methods that have been proposed would in principle apply equally well to both gamma rays and neutrons. However, the differences in their interaction mechanisms as exemplified by their cross sections lead to many real differences in the implemented solutions. For example, gamma-ray cross sections are smooth functions of both energy and atomic number. In contrast, neutron cross sections usually exhibit complex resonance structure, with the total and differential scattering cross sections varying

*Kernels may also be obtained from experiments.

irregularly with respect to energy and having little similarity for nuclides of nearly the same atomic number or atomic mass. Also, gamma-ray cross sections are relatively well known, whereas the neutron cross-section data are not complete in many regions of special interest to shield design. Most neutron cross-section work to date has been performed in support of reactor design, and because of this the work in the resonance energy regions has concentrated on the peaks rather than the valleys in the cross-section curve as a function of energy. In shield design the valleys are of more interest since neutrons with energies corresponding to these valleys tend to dominate the penetration process.

Finally, it is becoming increasingly clear that the limiting factor in calculating the attenuation of neutrons and gamma rays in bulk media is the availability and accuracy of the basic data – the cross sections and the source distributions. In other words, the more sophisticated methods described in this chapter have been developed to the point that, with proper care and accurate basic data, radiation transport can be calculated for deep penetration with considerable reliability.

3.1 The General Boltzmann Transport Equation

The Boltzmann transport equation describes the general behavior of uncharged radiation particles (e.g., neutrons) or quanta of electromagnetic radiation (e.g., gamma rays) in terms of the seven-dimensional phase space $(\bar{r}, E, \bar{\Omega}, t)$. This phase space consists of three spatial coordinates, two direction-defining angles, the particle energy, and time. Knowledge of the radiation particle density over all phase space for some prescribed physical situation is in fact the complete solution to the transport problem. However, experience has shown that the particle flux, which is simply related to the particle density (particle flux = particle density × particle speed), is a more convenient variable for analysis. Accordingly, *particle flux*, rather than current, is used as the dependent variable in the Boltzmann equation.

The flux quantity used is the angular flux, denoted by $\Phi(\bar{r}, E, \bar{\Omega}, t)$ and defined as the number of particles that cross a unit area normal to the $\bar{\Omega}$ direction per unit time with energies in dE about E and in a direction that lies in $d\bar{\Omega}$ about $\bar{\Omega}$. This function is more properly called the *differential energy and angle spectrum of the number flux density*, but the simple expression *angular flux* has become standard terminology. Integrating the angular flux over all directions yields the *scalar flux*, given by

$$\Phi(\bar{r}, E, t) = \int_{\Omega} \Phi(\bar{r}, E, \bar{\Omega}, t)\, d\bar{\Omega} \qquad (3.1)$$

and having the units neutrons cm^{-2} sec^{-1} MeV^{-1}. This scalar flux is sometimes referred to as a total flux, although it is differential with respect to energy. A second integration over some specified energy range will produce $\Phi(\bar{r})$, which is truly a total flux (neutrons cm^{-2} sec^{-1}).

Derivation of the Boltzmann transport equation can be regarded as a bookkeeping process that sets particle losses equal to particle gains within a differential element of phase space $(d\bar{r}\, dE\, d\bar{\Omega})$. One of its more familiar and useful forms is for the time-independent problem, given by

$$\nabla\cdot\bar{\Omega}\, \Phi(\bar{r}, E, \bar{\Omega}) + \Sigma_t(\bar{r}, E)\, \Phi(\bar{r}, E, \bar{\Omega}) = S(\bar{r}, E, \bar{\Omega})$$

$$+\iint \Sigma_s(\bar{r}, E' \rightarrow E, \bar{\Omega}' \rightarrow \bar{\Omega})\, \Phi(\bar{r}, E', \bar{\Omega}')\, dE'\, d\bar{\Omega}', \qquad (3.2)$$

where

$\nabla\cdot\bar{\Omega}\, \Phi(\bar{r}, E, \bar{\Omega})\, dE\, d\bar{\Omega}$ = net *convective loss* at $\bar{r}$ of particles with energies in dE about E and with directions which lie in $d\bar{\Omega}$ about $\bar{\Omega}$ per unit volume per unit time,

$\Sigma_t(\bar{r}, E)\, \Phi(\bar{r}, E, \bar{\Omega})\, dE\, d\bar{\Omega}$ = *collision loss* at $\bar{r}$ of particles with energies in dE about E and directions which lie in $d\bar{\Omega}$ about $\bar{\Omega}$ per unit volume per unit time,

$S(\bar{r},E,\bar{\Omega})\ dE\ d\bar{\Omega}$ = *source particles emitted* at $\bar{r}$ with energies in dE about E and directions which lie in $d\bar{\Omega}$ about $\bar{\Omega}$ per unit volume per unit time,

$$\left[\iint \Sigma_s(\bar{r},E' \rightarrow E,\bar{\Omega}' \rightarrow \bar{\Omega})\ \Phi(\bar{r},E',\bar{\Omega}')\ dE'\ d\bar{\Omega}'\right]$$

$\times\ dE\ d\bar{\Omega}$ = *inscattering gain* at $\bar{r}$ of particles with energies in dE about E and directions which lie in $d\bar{\Omega}$ about $\bar{\Omega}$ per unit volume per unit time,

$\Sigma_t(\bar{r},E)$ = total macroscopic cross section at $\bar{r}$ evaluated at the energy of the incident particle,

$\Sigma_s(\bar{r},E' \rightarrow E,\bar{\Omega}' \rightarrow \bar{\Omega})\ dE\ d\bar{\Omega}$ = differential scattering cross section which describes the probability that a particle with an initial energy E' and an initial direction $\bar{\Omega}'$ undergoes a scattering collision at $\bar{r}$ which places it into a direction that lies in $d\bar{\Omega}$ about $\bar{\Omega}$ with a new energy in dE about E.

The solution of the transport equation represents the average value of the particle flux or particle density. In real systems, there will be fluctuations from the average; in some cases these fluctuations will be important, but, in general, they will not have a bearing on the validity of the equation predicting the expected value.

Solutions of the transport equation are inherently complex due to its integrodifferential form, and exact solutions are limited to a few highly specialized problems. The most practical techniques are approximate and essentially numerical in nature, the more familiar ones being the spherical harmonics method, the discrete ordinates (S_n) technique, and the moments method. It is interesting to note that diffusion theory actually corresponds to a low-order approximation of the transport equation. Also, integral forms of the transport equation are generally regarded as the formal basis for the Monte Carlo method, the results of which can in principle be made to approach the exact solution. More complete descriptions of these and other approximate methods are presented in the following sections of this chapter.

3.2 Spherical Harmonics Method

The method of "spherical harmonics" as applied to the solution of the Boltzmann transport equation (Eq. 3.2) consists of representing the various angle-dependent terms as expansions in the spherical harmonics polynomials. These polynomials, commonly called associated spherical harmonics, are described by Weinberg and Wigner[1] and are given by the following expressions:

where $\bar{\Omega}$ is the unit vector specifying the direction of the particle motion, and θ and ϕ are the polar and azimuthal angles respectively.

Applying the spherical harmonics technique to the transport problem is inherently complex and involves mathematical procedures and concepts beyond the scope of this handbook. However, a simplified and lucid illustration of the method can

$$P_{jm}(\bar{\Omega}) = \sum_k (-1)^{k-m} \frac{j[(j+m)!\,(j-m)!]^{1/2}}{(j-m-k)!\,(m+k)!\,k!\,(j-k)!}\, e^{im\phi}\left(\cos\frac{1}{2}\theta\right)^{2j-m-2k}\left(\sin\frac{1}{2}\theta\right)^{2k+m}$$

$$= e^{im\phi}\,\frac{(-\sin\theta)^m}{j!\,2^j}\left[\frac{(j-m)!}{(j+m)!}\right]^{1/2}\frac{d^{j+m}(\cos^2\theta-1)^j}{(d\cos\theta)^{j+m}}, \quad (3.3)$$

be shown for the case of a steady-state (no time dependence), one-speed (no energy dependence), one-dimensional (slab geometry with azimuthal symmetry), homogeneous (constant system parameters) neutron transport problem. Consistent with these simplifications, the general Boltzmann transport equation as given by Eq. 3.2 can be written as

$$\mu \frac{\partial \Phi(x,\mu)}{\partial x} + \Sigma_t \Phi(x,\mu) = S(x,\mu) + \int_0^{2\pi} \int_0^{2\pi} \int_{-1}^{+1} \Sigma_s(\bar{\Omega},\bar{\Omega}') \, \Phi(x,\bar{\Omega}') \, d\mu' \, d\phi' \, d\phi , \tag{3.4}$$

where

$\Phi(x,\mu)$ = angular flux (neutron flux per unit μ),

ϕ = azimuthal angle with respect to x axis,

x = spatial variable in slab geometry, the direction of which is specified by the unit vector $\bar{i}$,

μ = direction cosine with respect to the x axis
$= \bar{\Omega} \cdot \bar{i} = \cos \theta$,

Σ_t = total macroscopic cross section,

$\Sigma_s(\bar{\Omega},\bar{\Omega}') \, d\Omega$ = differential scattering cross section, the macroscopic cross section for scattering through an angle $\cos^{-1} \bar{\Omega} \cdot \bar{\Omega}'$ into the differential solid angle $d\bar{\Omega}$ about $\bar{\Omega}$,

$S(x,\mu)$ = source neutrons per unit μ, volume, and time.

The angle-dependent terms in Eq. 3.4 can each be represented as a series of spherical harmonics of the first kind, the Legendre polynomials $P_j(\mu)$. These polynomials are the degenerate form of the associated spherical harmonics and are given by Eq. 3.3 when the index m is set equal to zero; that is,

$$P_j(\mu) \equiv P_{j,0}(\bar{\Omega}) .$$

The first few Legendre polynomials are

$$P_0(\mu) = 1 ,$$

$$P_1(\mu) = \mu ,$$

$$P_2(\mu) = \frac{1}{2}(3\mu^2 - 1) ,$$

$$\ldots . \tag{3.5}$$

Expanding the angular neutron flux and source term in terms of these polynomials yields

$$\Phi(x,\mu) = \sum_{j=0}^{\infty} \frac{2j+1}{2} \Phi_j(x) P_j(\mu) , \tag{3.6}$$

$$S(x,\mu) = \sum_{j=0}^{\infty} \frac{2j+1}{2} S_j(x) P_j(\mu) , \tag{3.7}$$

where

$\Phi_j(x)$ = position-dependent Legendre coefficients corresponding to the neutron flux

$$= \int_{-1}^{+1} \Phi(x,\mu) P_j(\mu) \, d\mu , \tag{3.8}$$

$S_j(x)$ = position-dependent Legendre coefficients corresponding to the source term

$$= \int_{-1}^{+1} S(x,\mu) P_j(\mu) \, d\mu , \tag{3.9}$$

$j = 0, 1, 2, \ldots$.

Since for most practical situations the differential scattering cross section depends only on the change in direction as denoted by $\mu_0 = \bar{\Omega} \cdot \bar{\Omega}'$, the series expansion for $\Sigma_s(\bar{\Omega},\bar{\Omega}')$ is made in terms of the Legendre polynomials $P_j(\mu_0)$:

$$\Sigma_s(\bar{\Omega},\bar{\Omega}') = \sum_{j=0}^{\infty} \frac{2j+1}{2} \eta_j P_j(\mu_0) , \tag{3.10}$$

where

η_j = Legendre coefficients ($j = 0, 1, 2, \ldots \infty$) corresponding to the differential scattering cross section

$$= \int_{-1}^{+1} \Sigma_s(\bar{\Omega},\bar{\Omega}') P_j(\mu_0) \, d\mu_0 . \tag{3.11}$$

The spherical harmonics form of the Boltzmann equation is obtained by introducing the above series representations for $\Phi(x,\mu)$, $S(x,\mu)$, and $\Sigma_s(\bar{\Omega},\bar{\Omega}')$ into Eq. 3.4, multiplying each term by the Legendre polynomial $P_n(\mu)$, and integrating over all μ (−1 to +1). When Eqs. 3.6, 3.7, and

3.10 are substituted into Eq. 3.4 and the orthogonality property of Legendre polynomials,

$$\int_{-1}^{+1} P_j(\mu) P_n(\mu)\, d\mu = 0 \quad \text{if } j \neq n$$

$$= \frac{2}{2j+1} \quad \text{if } j = n\,, \qquad (3.12)$$

is used along with the addition theorem for Legendre polynomials,*

$$P_j(\mu_0) = P_j(\mu) P_j(\mu') + 2 \sum_{m=1}^{j} \frac{j-m}{j+m} P_j^m(\mu) P_j^m(\mu') \cos m(\phi - \phi')\,, \qquad (3.13)$$

the following set of coupled differential equations is obtained:

$$\frac{n+1}{2n+1} \frac{d}{dx} \Phi_{n+1}(x) + \frac{n}{2n+1} \frac{d}{dx} \Phi_{n-1}(x) + \Sigma \Phi_n(x) + \eta_n \Phi_n(x) + S_n(x) = 0$$

$$\text{for } n = 0, 1, 2, \ldots \infty\,. \qquad (3.14)$$

This set of equations, which no longer involves the directional variables and therefore is more amenable to solution than Eq. 3.4, is called the second (or spherical harmonics component) form of the Boltzmann equation by Weinberg and Wigner[1] and others. Solution of this set of equations can be accomplished by rather straightforward although sometimes complex techniques.

Practical methods of solution require that the series of representations of $\Phi(x,\mu)$ be limited to a finite number of terms, for example, to $(n + 1)$ terms; n is commonly called the truncation number, and the corresponding calculation is referred to as the P_n approximation. The P_1 approximation is equivalent to diffusion theory (see Section 3.6) and involves only a linear representation, which restricts its application to situations wherein the neutron flux is nearly isotropic, a condition not characteristic of the penetrating components of neutrons that traverse a shield.

In a similar fashion the accuracy of the spherical harmonics calculation is also influenced by the number of terms used to represent the differential scattering cross section. Only a few terms are necessary for nearly isotropic scattering, but a large number of terms are required for adequate treatment of anisotropic scattering, and in the past this has limited the use of the spherical harmonics treatment. However, recent advances in cross-section technology and increased computer capacity have for all practical considerations removed this limitation.

It has been shown[1] that the accuracy of the spherical harmonics method is improved when the truncation number n is equal to or greater than 3. This is demonstrated in Table 3.1, in which the results obtained with P_1, P_3, P_5, and P_{15} approximations are compared with those obtained from a rigorous calculation by the Wiener-Hopf method for the well-known Milne problem with spherically symmetric scattering and no absorption. These results indicate that the P_3 approximation is a vast improvement over diffusion theory (P_1 approximation) and that computer implementation of the P_3 approximation is reasonable.

Shure[2] found that a multigroup P_3 approach in one dimension for calculating spatial and spectral neutron distributions in metal hydrogenous reactor shields yielded satisfactory estimates of neutron attenuation for reasonable amounts of computer time. Further, it was recognized by Lanning[3] that for some design problems the low-order approximations were sufficiently accurate. He successfully calculated the spatial distribution of the gamma-ray energy flux in one-dimensional slab geometry.

*The use of the addition theorem makes possible the evaluation of the inscattering-integral term containing $\Sigma_s(\bar{\Omega},\bar{\Omega}')$, which is necessarily expanded in terms of $P_j(\mu_0)$ rather than $P_j(\mu)$.

Table 3.1. Comparison of Normalized Total Fluxes Obtained with Various P_n Approximations with a Rigorous Solution by the Wiener-Hopf Method[a]

Scattering (mfp)	Total Flux				
	P_1	P_3	P_5	P_{15}	Wiener-Hopf Method
0.0	1	1	1	1	1
0.1	1.1732	1.2094	1.2263	1.2528	1.2608
0.2	1.3464	1.4123	1.4389	1.4680	1.4714
0.3	1.5196	1.6099	1.6414	1.6664	1.6685
0.4	1.6928	1.8031	1.8365	1.8564	1.8587
0.5	1.8660	1.9927	2.0261	2.0417	2.0443
0.6	2.0392	2.1794	2.2117	2.2241	2.2271
0.7	2.2124	2.3637	2.3944	2.4045	2.4077
0.8	2.3856	2.5460	2.5749	2.5834	2.5868
0.9	2.5589	2.7267	2.7537	2.7613	2.7652
1.0	2.7321	2.9060	2.9312	2.9382	2.9419
2.0	4.4641	4.6623	4.6792	4.6853	4.6902

[a]Table taken from: A. M. Weinberg and E. P. Wigner, *The Physical Theory of Neutron Chain Reactors*, University of Chicago Press, Chicago, 1958.

3.3 Discrete Ordinates S_n Method*

The discrete ordinates S_n method is a means of effecting a numerical solution of the energy-dependent linear Boltzmann transport equation. The most recent versions of the method permit anisotropic scattering to be included, thus making it suitable for both neutron and gamma-ray deep-penetration calculations in a wide variety of shielding problems. Since the method is fundamentally formulated as a finite difference equation (rather than as finite differencing of an analytic approximation), a minimum number of limiting assumptions is required, and the solutions apparently approach the exact solution of the Boltzmann equation as the space, angle, and energy mesh approaches differential size. The method can be applied without significant restrictions to the general core criticality problem, and it can be used for both homogeneous and laminated shields with a variety of source configurations, including surface- and volume-distributed sources.

The original method of discrete ordinates is attributed to Wick[4] and to Chandrasekhar.[5] Early applications were primarily limited to simple problems such as the transport of monoenergetic neutrons isotropically scattered in one-dimensional slabs. The fundamental assumption in the method was that the integral in the Boltzmann equation could be approximated by a Gaussian quadrature formula; consequently, functions involved in the integral had to be evaluated only at the angles corresponding to the Gaussian zeros. Although this original discrete ordinates method could

*This section is primarily the work of F. R. Mynatt of the Computing Technology Center, Oak Ridge, Tennessee.

be extended to anisotropic scattering, it was limited to slab geometry.

A discrete ordinates technique which could be extended to curved geometries such as spheres or cylinders was introduced by Carlson,[6] and it is this method that is commonly referred to as the discrete ordinates S_n method. The S_n technique serves as the basis for several widely used codes, such as the one-dimensional codes DTF II,[7] DTF IV,[8] ANISN,[9] and DSN[10] and the two-dimensional codes TDC[10] and DOT.[11]

Other approaches that can be classified as discrete ordinates methods are the direct numerical integration techniques employed by the NIOBE* and BIGGI-3P** computer programs, but these techniques have not been utilized to a large extent for shielding problems in the United States.

As applied to one-dimensional spherical geometry, early versions of the S_n method assumed that the angular flux varies with angle as connected line segments in an even number of equally spaced angular increments. This representation, although very accurate for homogeneous one-dimensional systems, was found to be unsuitable for the general problem because it fails to preserve optical reciprocity (i.e., the method consists of a nonsymmetric angular quadrature). Also, recursions involving many terms are required, and an extension of the method to multidimensional geometries is most difficult. These shortcomings are largely alleviated by the use of the "diamond difference" technique,[10] which relates in a more general fashion the angular flux within each particular angular increment to the endpoint values of the increment. With the diamond difference method the Boltzmann equation can be integrated over an angular increment, yielding, for the derivative terms, a two-point difference equation involving the angular flux evaluated at the increment endpoints.

The linear Boltzmann equation of transport theory is not derived from first principles of physics but is a flow balance for a differential phase space cell, treating in a phenomenological manner the events causing an increase or a decrease in the number of particles contained in the cell. The discrete ordinates difference equations can be formulated in an equivalent manner but considering a finite-difference cell – the way it is presented in most references. For some time it was not clear that the difference equations would in general approach the analytic form of the Boltzmann equation as the finite-difference phase space cell approached differential size. Lathrop[8] showed that they would for the one-dimensional geometries, and this is established implicitly in the following paragraphs in which the difference equations for spherical geometry are derived directly from the analytic Boltzmann equation. This geometry, although simple, illustrates all the characteristics of the discrete ordinates equations except for discrete ray streaming, which occurs only in two- or three-dimensional geometry.

Transport Equation and Phase Space Geometry. – The differential phase space cell is defined by three variables: the radius of the sphere (r), the cosine of the angle of the particle direction relative to the radius (μ), and the energy of the particle (E); that is,

$$\text{differential phase space cell} = dV\, d\mu\, dE$$

$$= 4\pi r^2\, dr\, d\mu\, dE\,. \qquad (3.15)$$

The finite-difference cell is obtained by integrating Eq. 3.15 over any particular finite intervals of radius, angle, and energy; it is given by

$$\text{finite-difference cell} = V_I\, \Delta\mu_D\, \Delta E_G$$

$$= \frac{4\pi}{3} (r_{i+1}^3 - r_i^3)\, (\mu_{d+1} - \mu_d)$$

$$\times (E_{g+1} - E_g)^*\,. \qquad (3.16)$$

*See, for example, S. Preiser, G. Rabonowitz, and E. deDufour, *A Program for the Numerical Integration of Boltzmann Transport Equation – NIOBE*, Nuclear Development Corp. of America, Aeronautical Research Laboratories, Report ARL-TR-60-314 (1960).

**See Appendix 3A.

*The following subscript notation is used throughout this section: subscripts I, D, and G denote functions whose values are associated with the Ith space interval, Dth angular interval, and Gth energy group respectively; i and $i+1$ refer to a function evaluated at the lower and upper limits of the Ith space interval; d and $d+1$ refer to a function evaluated at the lower and upper limits of the Dth angular interval; and g and $g+1$ refer to a function evaluated at the lower and upper limits of the Gth energy group.

For this problem (one-dimensional spherical geometry), the following two analytic forms of the Boltzmann transport equation can be considered:

$$\mu \frac{\partial}{\partial r} \Phi(r, \mu, E) + \frac{(1-\mu^2)}{r} \frac{\partial}{\partial \mu} \Phi(r, \mu, E) + \Sigma^T \Phi(r, \mu, E) = S(r, \mu, E) + \int_{-1}^{+1} \int_{0}^{\infty} \Sigma_S(r, E' \rightarrow E, \mu_0) \times \Phi(r, E', \mu') \, dE' \, d\mu' , \quad (3.17)$$

and

$$\frac{\mu}{r^2} \frac{\partial}{\partial r} [r^2 \Phi(r, \mu, E)] + \frac{1}{r} \frac{\partial}{\partial \mu} [(1-\mu^2) \Phi(r, \mu, E)] + \Sigma^T(r, E) \Phi(r, \mu, E) = S(r, \mu, E) + \int_{-1}^{+1} \int_{0}^{\infty} \Sigma^S(r, E' \rightarrow E, \mu_0) \Phi(r, E', \mu') \, dE' \, d\mu' , \quad (3.18)$$

where

$\Phi(r, \mu, E)$ = particle track length per unit volume (flux) about r per unit time per unit energy about E per unit direction cosine about μ,

$\Sigma^T(r, E)$ = position- and energy-dependent macroscopic total cross section,

$\Sigma^S(r, E' \rightarrow E, \mu_0) \, dE \, d\mu$ = differential scattering cross section describing the probability that a particle with an initial energy E' and direction cosine μ' undergoes a collision at r, resulting in a change of flight direction described by the cosine of the scattering angle μ_0, which places it into a new direction which lies in $d\mu$ about μ with a new energy in dE about E,

μ_0 = the scattering angle = $\bar{\Omega} \cdot \bar{\Omega}'$,

$\bar{\Omega}, \bar{\Omega}'$ = final and initial flight direction unit vectors respectively,

$S(r, \mu, E)$ = source particles per unit volume about r per unit time per unit energy about E per unit direction cosine about μ.

Integration of both Eqs. 3.17 and 3.18 would yield particle balance equations; however, the same would not be true for the numerical approximation of Eq. 3.17. Equation 3.18 is called the "conservative" form of the transport equation, and its integration over any phase space volume results in interface terms, which may be identified as leakage terms, that satisfy the divergence theorem exactly. As a consequence, the "conservative" equation (Eq. 3.18) is the preferred formal basis for numerical analyses.

Derivation of Finite-Difference Equation. – The discrete ordinates difference equation is obtained by applying the following simple integral operator to the transport equation (Eq. 3.18) in a manner consistent with the classical technique for obtaining difference equations:

$$\text{integral operator} = \int_{r \epsilon V_I} \int_{\mu \epsilon \Delta \mu_D} \int_{E \epsilon \Delta E_G} \times 4\pi r^2 \, dr \, d\mu \, dE . \quad (3.19)$$

This operator integrates* each term of the transport equation over the difference cell. Application of the operator to the first term of Eq. 3.18 gives

$$T_1 = \int_{r \epsilon V_I} \int_{\mu \epsilon \Delta \mu_D} \int_{E \epsilon \Delta E_G} \frac{\mu}{r^2} \times \frac{\partial}{\partial r} [r^2 \Phi(r, \mu, E)] \, 4\pi r^2 \, dr \, d\mu \, dE , \quad (3.20)$$

which on rearranging becomes

$$T_1 = 4\pi \int_{r \epsilon V_I} \int_{\mu \epsilon \Delta \mu_D} \mu \frac{\partial}{\partial r} \left[r^2 \int_{E \epsilon \Delta E_G} \Phi(r, \mu, E) \, dE \right] d\mu \, dr . \quad (3.21)$$

The integral of the flux over the energy group G may be identified as the multigroup flux

$$\Phi_G(r, \mu) \equiv \int_{E \epsilon \Delta E_G} \Phi(r, \mu, E) \, dE , \quad (3.22)$$

*The integration limits are expressed symbolically by $x \epsilon X$, which implies a definite integral with respect to the variable x over the interval X.

in which case Eq. 3.21 becomes

$$T_1 = 4\pi \int_{\mu\epsilon\Delta\mu_D} \mu d\mu \times \int_{r\epsilon V_I} \frac{\partial}{\partial r}[\, r^2\, \Phi_G(r,\mu)\,]\, dr\,. \quad (3.23)$$

Since Eq. 3.23 is integrated independently with respect to each variable,

$$\int_{r\epsilon V_I} \frac{\partial}{\partial r}[r^2\, \Phi_G(r,\mu)]\, dr = \int_{r\epsilon V_I} d[r^2\, \Phi_G(r,\mu)]\,. \quad (3.24)$$

Therefore the volume integral in Eq. 3.23 can now be evaluated directly:

$$T_1 = 4\pi \int_{\mu\epsilon\Delta\mu_D} \mu r_{i+1}^2\, \Phi_{G,i+1}(\mu)\, d\mu - 4\pi \int_{\mu\epsilon\Delta\mu_D} \mu r_i^2\, \Phi_{G,i}(\mu)\, d\mu\,, \quad (3.25)$$

where $\Phi_{G,i+1}(\mu) = \Phi_G(r_{i+1}, \mu)$ and $\Phi_{G,i}(\mu) = \Phi_G(r_i, \mu)$. It follows from the mean value theorem that any integral can be approximated by

$$\int_{x_1}^{x_2} x\, f(x)\, dx \cong \bar{x}\, f(\bar{x})\, \Delta x\,, \quad \text{for } x_1 < \bar{x} < x_2\,, \quad (3.26)$$

where $\bar{x}$ may be adjusted to give the equality; for well-behaved functions the closer $\bar{x}$ is to the true mean, the better the approximation.

Applying the mean value theorem to Eq. 3.25 to evaluate the solid angle intervals results in

$$T_1 = 4\pi\, (\bar{\mu}_D\, r_{i+1}^2\, \Phi_{G,i+1,D}\, \Delta\mu_D - \bar{\mu}_D\, r_i^2\, \Phi_{G,i,D}\, \Delta\mu_D)\,, \quad (3.27)$$

where $\Phi_{G,i,D} \equiv \Phi_{G,i}(\bar{\mu}_D)$ and $\bar{\mu}_D$ is a mean value approximation for the direction cosine over the direction increment $\Delta\mu_D$. Identifying the surface areas of the volume increment by

$$A_i = 4\pi r_i^2\,, \quad A_{i+1} = 4\pi r_{i+1}^2 \quad (3.28)$$

yields the final form for the first term:

$$T_1 = \bar{\mu}_D\, \Delta\mu_D\, [A_{i+1}\, \Phi_{G,i+1,D} - A_i\, \Phi_{G,i,D}]\,. \quad (3.29)$$

The integral operator (Eq. 3.19) is next applied to the second term in Eq. 3.18 and the result rearranged:

$$T_2 = 4\pi \int_{r\epsilon V_I} \int_{\mu\epsilon\Delta\mu_D} r\, \frac{\partial}{\partial\mu}\Big[\,(1-\mu^2) \times \int_{E\,\epsilon\Delta\mu_D} \Phi(r,\mu,E)\, dE\,\Big]\, d\mu\, dr\,. \quad (3.30)$$

Defining the multigroup flux as before, Eq. 3.30 becomes

$$T_2 = 4\pi \int_{r\epsilon V_I} r\, dr \int_{\mu\epsilon\Delta\mu_D} \frac{\partial}{\partial\mu}\,[(1-\mu^2) \times \Phi_G(r,\mu)]\, d\mu\,. \quad (3.31)$$

The integration over μ is accomplished by the procedure suggested by Eq. 3.24 with the following result:

$$T_2 = 4\pi\Big[\int_{r\epsilon V_I} (1-\mu_{d+1}^2)\, \Phi_{G,d+1}(r)\, r\, dr - \int_{r\epsilon V_I} (1-\mu_d^2)\, \Phi_{G,d}(r)\, r\, dr\Big]\,. \quad (3.32)$$

The remaining integration over the radius variable is performed by using the mean value approximation (Eq. 3.26):

$$T_2 = 4\pi\,[(1-\mu_{d+1}^2)\, \Phi_{G,d+1,I}\, \bar{r}_I\, \Delta r_I - (1-\mu_d^2)\, \Phi_{G,d,I}\, \bar{r}_I\, \Delta r_I]\,. \quad (3.33)$$

Equation 3.33 reduces to a two-point difference in the angle index

$$T_2 = 2[B_{d+1}\, \Phi_{G,d+1,I} - B_d\, \Phi_{G,d,I}] \quad (3.34)$$

if the curvature coefficient B_{d+1} is defined by the expression

$$B_d \equiv 4\pi \bar{r}_I\, \Delta\bar{r}_I (1-\mu_d^2)\,. \quad (3.35)$$

Consistent with the conservation property of the technique, Eq. 3.34 gives an overall neutron balance. This is apparent since incoming and outgoing flows cancel and the curvature coefficients become zero for the end values ($\mu = \pm 1$). Equation 3.35, which defines the curvature coefficients, can be recast in the form of a recursion relation which involves the coefficients B_{d+1} and B_d. First, B_d is subtracted from B_{d+1} (where B_d and B_{d+1} are given by Eq. 3.35), yielding

$$B_{d+1} - B_d = -4\pi \bar{r}_I \, \Delta r_I (\mu_{d+1}^2 - \mu_d^2) \, . \qquad (3.36)$$

It is assumed that $\bar{r}_I$ in Eq. 3.36 is the arithmetic mean, that is, that

$$\bar{r}_I = \frac{r_{I+1} + r_I}{2} \, . \qquad (3.37)$$

Then it follows that

$$\bar{r}_I \, \Delta r_I = \frac{(r_{I+1}^2 - r_I^2)}{2} \, . \qquad (3.38)$$

Following similar arguments, the factor $(\mu_{d+1}^2 - \mu_d^2)$ can be expressed as

$$(\mu_{d+1}^2 - \mu_d^2) = 2\bar{\mu}_D \, \Delta\mu_d \, . \qquad (3.39)$$

Introducing Eqs. 3.38 and 3.39 into Eq. 3.36 yields the following recursion relation:

$$B_{d+1} - B_d = -4\pi (r_{I+1}^2 - r_I^2) \, \bar{\mu}_D \, \Delta\mu_D \, . \qquad (3.40)$$

The final form for the recursion relation is obtained by introducing the cell areas A_{I+1} and A_I (see Eq. 3.28) and rearranging, with the result that

$$B_{d+1} = B_d - \bar{\mu}_D \, \Delta\mu_D (A_{I+1} - A_I) \, , \qquad (3.41)$$

where $B_1 = 0$. Equation 3.41 is the form of the curvature coefficient found in the literature. The only approximation made in the preceding derivation is in the definition of mean values.

When the integral operator, Eq. 3.19, is applied to the fifth term of Eq. 3.18 (which is called the inscattering integral), the result is

$$T_5 = \int_{r \epsilon V_I} \int_{\mu \epsilon \Delta\mu_D} \int_{E \epsilon \Delta E_G} \int_{-1}^{+1} \int_0^{\infty} \Sigma^S(r, E' \rightarrow E, \mu_0) \, \Phi(r, E', \mu') \, dE' \, d\mu' \times 4\pi r^2 \, dr \, d\mu \, dE \, . \qquad (3.42)$$

The differential scattering cross section can be approximated by a truncated Legendre polynomial expansion in the cosine of the scattering angle:

$$\Sigma^S(r, E' \rightarrow E, \mu_0) = \frac{1}{2} \sum_{n=0}^{N} \Sigma^n(r, E' \rightarrow E) \, P_n(\mu_0) \, , \qquad (3.43)$$

where the Σ^n's are Legendre coefficients of the expansion.

The scattering angle is related to the initial and final angles in the problem coordinate system by the addition theorem for Legendre polynomials, which for spherically symmetric geometry is simply

$$P_n(\mu_0) = P_n(\mu) \, P_n(\mu') \, . \qquad (3.44)$$

In adapting Eq. 3.42 to a multigroup calculation, the integrals over all incident energies and all incident angles are replaced by sums of integrals over the primed phase space cell. Symbolically this is denoted by

$$\int_0^{\infty} f(E') \, dE' = \sum_{G'=1}^{NOG} \int_{E' \epsilon \Delta E_{G'}} f(E') \, dE' \, , \qquad (3.45)$$

$$\int_{-1}^{+1} f(\mu') \, d\mu' = \sum_{D'=1}^{NOA} \int_{\mu' \epsilon \Delta\mu'_D} f(\mu') \, d\mu' \, ,$$

where *NOG* and *NOA* signify the number of energy groups and number of angular increments respectively.

Combining Eqs. 3.43 and 3.44 with Eq. 3.42, approximating the incident energy and angle integrals by Eq. 3.45, and evaluating all remaining integrals by the mean value approximation yields

(after considerable rearrangement of terms) the following forms for the inscattering integral:

$$T_5 = V_I \Delta\mu_D \sum_{G'=1}^{NOG} \sum_{n=0}^{N} P_n(\bar{\mu}_D) \Sigma_{G' \to G}^{n,I} \sum_{D'=1}^{NOA} \Phi_{I,G',D'} P_n(\bar{\mu}_{D'}) \Delta\mu_{D'}$$

$$= \frac{V_I \Delta\mu_D}{2} \sum_{G'=1}^{NOG} \sum_{n=0}^{N} P_n(\mu_D) \Sigma_{G' \to G}^{n,I} j_{I,G'}^{n} , \quad (3.46)$$

where $\Sigma_{G' \to G}^{n,I}$ is the nth Legendre moment of the multigroup scattering cross section (multigroup macroscopic transfer coefficient), defined by

$$\Sigma_{G' \to G}^{n,I} \equiv \frac{4\pi \int_{r \in V_I} \int_{E \in \Delta E_G} \int_{E' \in \Delta E_{G'}} \Sigma^n(r, E' \to E) \int_{-1}^{+1} \Phi(r, E', \mu') P_n(\mu') \, d\mu' \, dE' \, dE \, r^2 \, dr}{V_I \int_{E' \in \Delta E_{G'}} \int_{-1}^{+1} \Phi(r, E', \mu') P_n(\mu') \, d\mu' \, dE} , \quad (3.47)$$

and $j_{I,G'}^{n}$ is the nth Legendre coefficient of the angular dependence of the flux, calculated from

$$j_{I,G'}^{n} = \sum_{D'=1}^{NOA} \Phi_{I,G',D'} P_n(\bar{\mu}_{D'}) \Delta\mu_{D'} . \quad (3.48)$$

Application of the integral operator (Eq. 3.19) to the removal term (third term) of Eq. 3.18 gives

$$T_3 = \int_{r \in V_I} \int_{\mu \in \Delta\mu_D} \int_{E \in \Delta E_G} \Sigma^T(r, E) \times \Phi(r, \mu, E) \, 4\pi r^2 \, dr \, d\mu \, dE . \quad (3.49)$$

The evaluation of Eq. 3.49 requires some effort in order to avoid the assumption of angle-energy separability in the weighting of the multigroup cross sections. As the first step in evaluating Eq. 3.49 in terms of a cross section that is independent of angle, the energy integral of Eq. 3.49 is written as

$$T_3^E = \int_{E \in \Delta E_G} \Sigma^T(r, E) \Phi(r, \mu, E) \, dE = \Sigma_G^T(r) \Phi_G(r, \mu) - R , \quad (3.50)$$

where

R = correction factor that is to be determined,

$\Sigma_G^T(r)$ = flux-weighted group-G total cross section defined by

$$\Sigma_G^T(r) \equiv \frac{\int_{E \in \Delta E_G} \Sigma^T(r, E) \, j^0(r, E) \, dE}{\int j^0(r, E) \, dE} , \quad (3.51)$$

in which $j^0(r, E)$ is the zeroth Legendre coefficient of the angular dependence of the flux, which is identical to the differential flux $\Phi(r, E)$.

Rearrangement of Eq. 3.50 provides an explicit expression for R:

$$R = \Sigma_G^T(r) \Phi_G(r, \mu) - \int_{E \in \Delta E_G} \Sigma^T(r, E) \Phi(r, \mu, E) \, dE , \quad (3.52)$$

which has only a small effect when the energy group structure is reasonably fine.

The correction factor R is determined by expressing the angular fluxes as truncated Legendre series and then combining the two terms which comprise Eq. 3.52. The truncated Legendre series representation of the flux is

$$\Phi(r, \mu, E) \cong \sum_{n=0}^{N} \frac{2n+1}{2} j^n(r, E) P_n(\mu) . \quad (3.53)$$

When Eq. 3.53 is substituted into Eq. 3.52, the result is

$$R = \Sigma_G^T(r) \sum_{n=0}^{N} \frac{2n+1}{2} j_G^n(r)\, P_n(\mu) - \int_{E \in \Delta E_G} \Sigma^T(r,E) \times \sum_{n=0}^{N} \frac{2n+1}{2} j^n(r,E)\, P_n(\mu)\, dE \ , \quad (3.54)$$

which can be written as

$$R = \sum_{n=0}^{N} \frac{2n+1}{2} \left[\Sigma_G^T(r) - \Sigma_G^{Tn}(r) \right] j_G^n(r)\, P_n(\mu) \ , \quad (3.55)$$

where

$$j_G^n(r) = \int_{E \in \Delta E_G} j^n(r,E)\, dE \ ,$$

and the moments of the cross section are defined by

$$\Sigma_G^{Tn}(r) \equiv \frac{\int_{E \in \Delta E_G} \Sigma^T(r,E)\, j^n(r,E)\, dE}{j_G^n(r)} \ . \quad (3.56)$$

Substitution of Eq. 3.55 into Eq. 3.51 yields the final form for the energy integral:

$$T_3^E = \Sigma_G^T(r) \sum_{n=0}^{N} \frac{2n+1}{2} j_G^n(r)\, P_n(\mu) - \sum_{n=0}^{N} \frac{2n+1}{2} \left[\Sigma_G^T(r) - \Sigma_G^{Tn}(r) \right] j_G^n(r)\, P_n(\mu) \ . \quad (3.57)$$

Using this form for the energy integral in Eq. 3.49, the remaining integrals are evaluated by the mean value approximation, yielding

$$T_3 = V_I\, \Delta\mu_D \left[\Sigma_{G,I}^T \Phi_{G,I,D} - \sum_{n=0}^{N} \frac{2n+1}{2} (\Sigma_{G,I}^T - \Sigma_{G,I}^{Tn})\, j_{G,I}^n P_n(\bar{\mu}_D) \right] . \quad (3.58)$$

The series in Eq. 3.58 is very similar in form to the inscattering integral term (T_5) and may be included there by replacing $\Sigma^{n,I}_{G' \to G}$ in Eq. 3.46 with

$$\Sigma^{n,I\,(\mathrm{mod})}_{G' \to G} = \Sigma^{n,I}_{G' \to G} + (2n+1) \left(\Sigma_{G,I}^T - \Sigma_{G,I}^{Tn} \right) \delta_{G,G'} \ , \quad (3.59)$$

where $\delta_{G,G'} = 1$ if $G' = G$ and $= 0$ if $G' \neq G$. The modified removal term then has the desired form

$$T_3 = V_I\, \Delta\mu_D\, \Sigma_{G,I}^T \Phi_{G,I,D} \ . \quad (3.60)$$

Application of the integral operator to the source term of Eq. 3.18 is straightforward since, with the exception of defining multigroup constants, the mean value approximation is used for all variables. The final result for a general fixed source is

$$T_4 = V_I\, \Delta\mu_D\, S_{I,G,D} \ . \quad (3.61)$$

If multiplication is present (eigenvalue problem),

$$S(r,\mu,E) = \frac{1}{k_{\mathrm{eff}}} \chi(E) \times \int_0^{\infty} \nu\Sigma_f(r,E')\, \Phi(r,E')\, dE' \ , \quad (3.62)$$

which gives

$$T_4 = V_I\, \Delta\mu_D \frac{\chi_G}{k_{\mathrm{eff}}} \sum_{G'=1}^{NOG} \nu\Sigma_{fG'}^I \Phi_{I,G'} \ , \quad (3.63)$$

where

k_{eff} = effective multiplication constant of the medium,

$\Sigma_{fG'}$ = macroscopic fission cross section at energy G',

ν = number of neutrons per fission by neutrons of energy G',

χ_G = fission spectrum defined by

$$\chi_G \equiv \int_{E \in \Delta E_G} \chi(E)\, dE \ ,$$

$$\nu\Sigma_{fG'}^I = \frac{\int_{E' \in \Delta E_{G'}} \nu\Sigma_f^I(E')\, \Phi_{I,G'}\, dE'}{\int_{E' \in \Delta E_{G'}} \Phi_{I,G'}\, dE'} \ .$$

The discrete ordinates difference equation is obtained by substituting the derived expressions for each of the five terms into Eq. 3.18 and then dividing through by $\Delta\mu_D$. The result is

$$\bar{\mu}_D (A_{i+1}\,\Phi_{G,i+1,D} - A_i\,\Phi_{G,i,D}) + \frac{1}{\Delta\mu_D}(B_{d+1}\,\Phi_{G,I,D+1} - B_d\,\Phi_{G,I,d}) + V_I\,\Sigma^T_{G,I}\,\Phi_{G,I,D} = V_I\,S_{G,I,D} + \frac{V_I}{2} \times \sum_{n=0}^{N} P_n(\bar{\mu}_D) \sum_{G'=1}^{NOG} \Sigma^{n,I\,(\mathrm{mod})}_{G' \to G} \times \sum_{D'=1}^{NOA} \Phi_{I,G',D'}\,P_n(\bar{\mu}_{D'})\,\Delta\mu_{D'}. \quad (3.64)$$

Although derived for spherical geometry, that is, for

$$A_i = 4\pi r_i^2 \text{ and } V_I = \frac{4\pi}{3}(r_{i+1}^3 - r_i^3) \quad ,$$

Eq. 3.64 is the general discrete ordinates difference equation for the one-dimensional geometries. The equations for the other geometries are obtained from Eq. 3.64, with $A_i = 1.0$ and $V_I = \Delta r_I$ for a slab and with $A_i = 2\pi r_i$ and $V_I = \pi(r_{i+1}^2 - r_i^2)$ for a cylinder.

Numerical Solution of the Discrete Ordinates Equation. – Equation 3.64 contains discrete-flux variables having both centered and endpoint subscripts. This in effect increases the number of unknowns such that an insufficient number of determining relations are available for their solution. This difficulty can be resolved by relating the "centered" and "endpoint" fluxes in some consistent fashion. The diamond difference technique is the most widely used method for this purpose and includes two relationships for the spatial variable,

$$\Phi_{G,I,D} = A_{G,i+1,D} + (1 - A)\,\Phi_{G,i,D} \quad , \qquad \mu > 0 \quad , \quad (3.65)$$

and

$$\Phi_{G,I,D} = (1 - A)\,\Phi_{G,i+1,D} + A\Phi_{G,i,D} \quad , \qquad \mu < 0 \quad , \quad (3.66)$$

and a single expression for the angular variable,

$$\Phi_{G,I,D} = B\Phi_{G,I,d+1} + (1 - B)\,\Phi_{G,I,d} \quad , \quad (3.67)$$

where A and B are constants which can be assigned values of the interval $(\frac{1}{2}, 1)$. When $A = B = \frac{1}{2}$, Eqs. 3.65 and 3.66 are the same for all values of μ and together with Eq. 3.67 are known as the "ordinary" diamond difference equations which form the basis for most current computer solutions. If $A = B = 1$, the step function relationship is obtained which equates the centered fluxes to the appropriate endpoint fluxes. The step-function relationship is less accurate than the ordinary diamond difference scheme for the same mesh; however, it has the advantage of always giving positive fluxes for positive sources and is used for the correction of negative fluxes, which occasionally occur with other diamond difference schemes.

The choice of the discrete directions plays an important role in the discrete ordinates or S_n method. It does not appear that a most accurate (or best) quadrature scheme for a specific problem can be selected *a priori*. The efficiency of a given set of discrete directions (quadrature set) depends on problem parameters such as geometry, optical thickness, energy group structure, spatial mesh size, etc., and a generalization of these dependencies is not altogether impossible.

The discrete directions and associated weights (which represent solid angle) define the quadrature used in the inscattering integral; the directions define the mean values for the angles, such as $\bar{\mu}_D$, and thus affect the approximations in the convection term. In Wick's original method the discrete directions corresponded to Gaussian zeroes, and the quadrature affected only the source integral. In the early S_n method the connected line segment technique was found to imply discrete directions; however, they are not symmetric about $\mu = 0$ and thus introduce difficulties with boundary conditions and symmetry requirements.

Although the later S_n codes all use essentially the same form of the difference equation, they differ markedly in the type of discrete directions used. In all cases the discrete directions are represented as points on the surface of a unit sphere located at the point in space for which the flux is to be defined and oriented in a fixed manner with respect to the coordinate system. The points or directions are located on the sphere in a

reflective manner with respect to the three planes defining an octant such that the point description of one octant defines the whole sphere. This is not an absolute necessity but is usually required because of reflecting boundaries.

In the DSN and TDC codes the discrete direction weights are defined by dividing the surface area of the unit sphere octant into equal segments. In one-dimensional spheres and slabs the octant is divided by latitudes about the radial axis which are often referred to as levels. In two-dimensional geometry the octant is divided by latitudes about the polar axis and longitudinal sections such that the first latitude division contains one segment, the second latitude division contains two segments, etc. In either case the equal-area method completely defines the solid-angle weights once the number of direction weights is specified. This leaves the directions adjustable, with the restriction that they lie interior to their area segment.

The more recent S_n codes allow specification of direction weights as well as the directions themselves. Lee[10] developed a rather elegant method of areas which computes directions and direction weights that are symmetric with respect to rotational interchange of the axes of the unit sphere. Although the directions and weights in the area method are somewhat adjustable, the best results occur with Lee's recommended values, which satisfy various approximate moment conditions and asymptotic theories. The area method has the advantage of rotation symmetry, which is extolled in the reference, and the important advantage of all positive weights for any order of S_n.

Although rotation reflection symmetry has desirable qualities, only three-dimensional calculations would benefit from full symmetry; two-dimensional problems thus require twofold symmetry, and one-dimensional problems require no symmetry conditions within the octant. Thus for one- and two-dimensional geometries and especially for problems where other conditions outweigh the symmetry considerations, some liberty in choosing directions may be exercised.

For one-dimensional plane and spherical geometry, experience has shown that Gauss-Legendre quadrature is well suited for deep-penetration problems. For thin shields involving isotropic plane or spherical shell sources, a double Gauss-Legendre quadrature is preferable. For specific problems, increased accuracy is usually obtained by using a higher-order Gaussian quadrature rather than by developing a special biased quadrature to exploit special characteristics of the problem.

In two-dimensional geometries or one-dimensional cylindrical geometry less experience is available on which to base the selection of the quadrature scheme. Good results have been obtained using quadratures that are designed to integrate specified orders of a spherical harmonic. In this method the direction set is left to be specified, and is often based on Gaussian zeroes or complete symmetry requirements. For specific problems increased accuracy is gained by using a proven quadrature to a higher order rather than by developing special biased sets. It is usually more expensive to develop and test a biased quadrature than to use the standard quadrature with a higher order.

A typical computer solution of the discrete ordinates problem is basically one of iterating the solution to some prescribed degree of convergence. The sweep of the mesh points is carefully ordered to "follow" the neutrons (or gamma rays). Beginning at a boundary along which the inwardly directed flux values are specified, the sweep is made across the geometric cell at one angle, then back. After progressing through all angles at one energy, the next lower energy group is treated in a similar fashion and so on. Details are omitted here but can be found in the descriptions of codes DTF IV,[8] ANISN,[9] and DOT.[11]

Advantages and Disadvantages. – From the results of calculations made with S_n codes, it appears that for shielding applications the discrete ordinates methods have the following advantages:

1. Depending somewhat on the sophistication desired, the S_n calculations are easy to prepare.
2. The method is not stochastic, and flux errors at deep penetration are systematic rather than statistical.
3. Production problems having similar characteristics benefit from knowledge of fluxes calculated in a similar case.
4. Secondary gamma rays may be calculated by the same method, either as a second calculation or simultaneously with the neutrons. The gamma-ray yield distribution may also be made a function of the energy of the captured neutron.
5. The range of neutron energies from highest fission energies to thermal, including upscattering, may be calculated by the same method.

6. The one-dimensional calculations are much faster (in computer time) than similar Monte Carlo calculations (see Section 3.5). In two dimensions the type of problem and the desired answers determine whether S_n or Monte Carlo is better.

The following disadvantages are evident, but additional development can alleviate or eliminate them:

1. Convergence of the iterative method is not always uniform and well defined. The best method currently used is to determine from each iterate the maximum error in the scalar flux at any point in space relative to the previous iterate value. Iterations proceed until the error falls below a specified limit.

2. Flux aberrations are frequently observed in two dimensions due to localized sources and the propagation of neutrons in discrete directions.

3. No basic ground rules exist which define for a particular problem the best direction set, space mesh, multigroup structure, and polynomial expansion limit.

3.4 Moments Method

Another technique that can be used to solve the Boltzmann transport equation is the moments method.* This method has some important advantages not shared by other methods, one being that foreknowledge about the behavior of the solution can be incorporated analytically in a very natural way, thereby often greatly reducing the effort required to achieve a specific result and/or a desired accuracy. Another is that the type of recursion relation developed precludes a truncation at a crucial part of the calculation; that is, a finite number of moments may be calculated exactly (ignoring errors due to the numerical solution) without considering the influence of higher moments.

In the moments method one considers first the formal definition for the moments and the manner in which they relate to the system parameter of interest, $f(x)$. If $f(x)$ is defined for all x within the interval $A \leqq x \leqq B$, then the nth moment of $f(x)$ is

$$M_n = \int_A^B x^n f(x)\, dx \,, \qquad (3.68)$$

provided that the integral exists. Only nonnegative integral values of n are considered in practical applications.

Definite interpretations may be associated with the various moments. For example, the zeroth moment is a normalizing number, and the first, second, third, and fourth moments are closely related to the mean value, variance, skewness, and kurtosis respectively. In the physics of statics and dynamics the first moment of the mass is the center of gravity and the second is the moment of inertia.

No such particular meanings are given to the moments as they are used in the solution of radiation transport problems. Rather, they may be regarded as a transform, much the same as Laplace, Fourier, or finite trigonometric transforms. The major portion of the calculation is performed in terms of the transform (moments) space; then, by an appropriate inversion, the desired answer of interest is reconstructed.

The application of the moments method to the solution of the Boltzmann transport equation is limited with respect to the source-shield configuration. It is usually applied only to infinite homogeneous media with plane, line, or point sources. The method as applied to gamma rays has been described by Goldstein and Wilkins,[12] and as applied to neutrons by Goldstein,[13] Certaine,[14] and Aronson *et al.*[15,16] The technique is basically the same for both neutrons and gamma rays, and a description for one should suffice for the other. The most significant differences lie in the treatment of the scattering integral

*Brief descriptions of a few computer codes based on the moments method are given in Appendix 3A.

and in the more complex nature of the neutron cross sections. The description presented below is for slab geometry in terms of the simpler gamma-ray problem, in which the dependent variable is the angular energy flux $I(x, \lambda, \omega)$, and the Compton wavelength is taken as the energy variable.

Consider the following specialized form of the Boltzmann equation:

$$\omega \frac{\partial I}{\partial x} + \mu(\lambda)\, I(x,\lambda,\omega) = \int_0^{\lambda} \int_{4\pi} I(x,\lambda',\omega')\, k(\lambda',\lambda)\, \frac{\delta(1+\lambda'-\lambda-\overline{\Omega}\cdot\overline{\Omega}')}{2\pi}\, d\Omega'\, d\lambda' + S(\lambda,\omega)\, \delta(x) \quad , \quad (3.69)$$

where

$I(x,\lambda,\omega)\, dE\, d\omega$ = energy flux (MeV per unit area and time) due to gamma rays with energies in dE about E and direction cosines which lie in $d\omega$ about ω,

x = spatial coordinate in slab geometry,

λ = gamma-ray energy after scattering expressed in terms of its Compton wavelength,

λ' = gamma-ray wavelength prior to scattering,

ω = x direction cosine with respect to x axis,

$\mu(\lambda)$ = total macroscopic cross section evaluated at the energy corresponding to the gamma-ray wavelength λ,

$\overline{\Omega}\cdot\overline{\Omega}'$ = cos θ, cosine of the scattering angle between initial and final gamma-ray directions, where $\overline{\Omega}'$ and $\overline{\Omega}$ are the initial and final unit direction vectors respectively,

$$k(\lambda',\lambda) = 2\pi \frac{\lambda}{\lambda'}\, \sigma(\lambda',\theta) \quad ,$$

$\sigma(\lambda',\theta)$ = cross section for Compton scattering given by the well-known Klein-Nishina formula,

$\delta(x)$ = Dirac delta function, which has the property

$$\int_a^b f(x)\, \delta(x-X)\, dx = f(X) \quad ,$$

$$a < X < b \quad ,$$

$\delta(1+\lambda'-\lambda-\overline{\Omega}\cdot\overline{\Omega}')$ = Dirac delta function which prescribes that the angular change $(\overline{\Omega}\cdot\overline{\Omega}')$ be consistent with the change in wavelength $(\lambda - \lambda')$ as given by the Compton scattering equation, $\lambda - \lambda' = 1 - \overline{\Omega}\cdot\overline{\Omega}'$,

$S(\lambda,\omega)\, dE\, d\omega$ = plane source of gamma rays (energy emission per unit area and time of gamma rays with energies in dE about E and direction cosines which lie in $d\omega$ about ω).

Solving Eq. 3.69 by the moments method is similar to the spherical harmonics treatment (see Section 3.2) in that the angular energy flux is first expanded as a Legendre polynomial series:

$$I(x,\lambda,\omega) = \sum_{j=0}^{\infty} \frac{2j+1}{2}\, I_j(x,\lambda)\, P_j(\omega) \quad , \quad (3.70)$$

where the Legendre coefficients are given by

$$I_j(x,\lambda) = \int_{-1}^{+1} I(x,\lambda,\omega)\ P_j(\omega)\ d\omega\ . \tag{3.71}$$

It can be shown that $I_0(x,\lambda)$ is the energy flux and that $I_1(x,\lambda)$ is the energy current density.

With this series representation for the angular energy flux the integrodifferential equation (Eq. 3.68) with the dependent variable $I(x,\lambda,\omega)$ and three continuous independent variables can be transformed into a sequence of integrodifferential equations for the variables $I_j(x,\lambda)$, which are dependent on only two independent variables. This desired result is obtained by multiplying Eq. 3.68 by the Legendre polynomial $P_j(\omega)$ and integrating over all solid angle, yielding (after some manipulation) the following sequence of equations:

$$\frac{j+1}{2j+1}\frac{\partial I_{j+1}}{\partial x} + \frac{j}{2j+1}\frac{\partial I_{j-1}}{\partial x} + \mu(\lambda)\ I_j = S_j(\lambda)\ \delta(x) + \int_0^{\lambda} P_j(1+\lambda'-\lambda)\ k(\lambda',\lambda)\ I_j(x,\lambda')\ d\lambda'\ ,\quad j = 0,1,2,\ldots\infty\ . \tag{3.72}$$

Elimination of the spatial variable in this sequence of equations is accomplished by the generation of the moments of the Legendre coefficients of the angular energy flux, which are defined as

$$b_{nj}(\lambda) \equiv \frac{\mu_0^{n+1}}{n!}\int_{-\infty}^{+\infty} I_j(x,\lambda)\ x^n\ dx\ , \tag{3.73}$$

where μ_0 is the total macroscopic cross section evaluated at the source energy. The equations satisfied by $b_{nj}(\lambda)$ are obtained by multiplying Eq. 3.72 by $\mu_0^{n+1}x^n/n!$ and integrating with respect to x from $-\infty$ to $+\infty$. It is because of this integration over all space that the application of the moments method to the transport problem becomes inextricably restricted to the infinite-medium geometry. Using Eq. 3.73 permits the original Boltzmann equation to be reduced to the following doubly indexed sequence of linear integral equations of the Volterra type:

$$\mu(\lambda)\ b_{nj}(\lambda) = \int_0^{\lambda} k(\lambda',\lambda)\ P_j(1+\lambda'-\lambda)\ b_{nj}(\lambda')\ d\lambda' + \frac{\mu_0}{2j+1}\left[(j+1)\ b_{n-1,j+1} + j b_{n-1,j-1}\right] + \mu_0\ S_j(\lambda)\ \delta_{n0}\ , \tag{3.74}$$

where $j = 0, 1, 2, \ldots \infty$, and $n = 0, 1, 2, \ldots \infty$. The Kronecker delta function $\delta_{n0} = 1$ if $n = 0$ and $= 0$ if $n \neq 0$.

The evaluation of the moments for a given problem can be accomplished by a rather straightforward numerical solution of Eq. 3.74. The ease of numerical calculation depends on the form of the source function $S_j(\lambda)$. Many problems involve monoenergetic sources. Since the presence of the delta function is undesirable for machine calculation, the following transformation is made:

$$b_{nj}(\lambda) = B_{nj}(\lambda) + \lambda_0\delta(\lambda-\lambda_0)C_{nj}\ , \tag{3.75}$$

where

$$C_{nj} = S_j\ ,\ \text{for } n = 0\ ,$$

$$= \frac{j+1}{2j+1}C_{n-1,j+1} + \frac{1}{2j+1}C_{n-1,j-1}\ ,\quad \text{for } n = 1, 2, 3, \ldots\ .$$

Introducing the transformation defined by Eq. 3.75 into Eq. 3.74 yields the defining equations for B_{nj} and C_{nj}:

$$\mu\, B_{nj} = \int_{\lambda_0}^{\lambda} k(\lambda',\lambda)\ P_j(1+\lambda'-\lambda)\ B_{nj}(\lambda')\ d\lambda' + \frac{\mu_0}{2j+1}\left[(j+1)\,B_{n-1,j+1} + jB_{n-1,j-1}\right] + \lambda_0 k(\lambda_0,\lambda)\ P_j(1+\lambda_0-\lambda)\ C_{nj}\ , \tag{3.76}$$

$$\mu C_{nj} = \mu_0\left(\frac{j+1}{2j+1}C_{n-1,j+1} + \frac{j}{2j+1}C_{n-1,j-1}\right) + \mu_0 S_j\,\delta_{n0}\ . \tag{3.77}$$

The equations that define C_{nj} are similar in form to the equations that define b_{nj} and B_{nj} except that the inscattering integral does not appear, which suggests that all collisions are considered to be removals. It follows that $\lambda_0 \delta(\lambda - \lambda_0) C_{nj}$ must be the moments for the unscattered energy flux. Therefore the transformation given by Eq. 3.75 separates the unscattered energy flux (energy flux corresponding to C_{nj}) from the total energy flux (energy flux corresponding to b_{nj}). The solution to Eq. 3.76 requires values of C_{nj} as input, and the calculated moments B_{nj} are associated only with the scattered energy flux. This is most convenient since the uncollided angular energy flux $I^0(x,\lambda,\omega)$ is easily calculated and values of C_{nj} are then uniquely determined.

For a typical calculation, the quantity of greatest interest is the total, or scalar, energy flux $I_0(x,\lambda)$. Therefore only the moments B_{n0} $(n = 0, 1, 2, \ldots N)$ are required. However, the calculation of a given B_{nj} requires the prior calculation of $B_{n-1,j+1}$ and $B_{n-1,j-1}$; therefore moments other than the B_{n0} moments must be calculated. In general the moments B_{0j} $(j = 0, 1, 2, \ldots J)$ can be calculated directly, while a B_{nj} moment cannot be calculated until calculations have been made of all the $B_{n'j'}$'s for which $(n + j) - (n' + j')$ is a non-negative even integer (including zero) and $n' < n$. Table 3.2 illustrates a typical calculation sequence (for $N = 5$). It is noted that all the moments shown in the table must be calculated in order to determine B_{n0} for $n \leq 5$.

Since Eq. 3.76 is a Volterra type of equation, it can be written as

$$\mu(\lambda_n)\, v(\lambda_n) = \int_{\lambda_0}^{\lambda_n} H(\lambda_n,\lambda')\, v(\lambda')\, d\lambda' + T(\lambda_n) \quad , \quad (3.78)$$

where

$$\lambda_n = \lambda_0 + n\Delta\lambda \ ,$$

$\Delta\lambda$ = arbitrary increment of wavelength,

$$v(\lambda_n) = B_{nj}(\lambda) \ ,$$

$$H(\lambda_n,\lambda') = k(\lambda',\lambda)\, P_j(1 + \lambda' - \lambda) \ ,$$

$$T(\lambda_n) = \frac{\mu_0}{2j+1} \left[(j+1)\, B_{n-1,j+1} + jB_{n-1,j+1} \right] + \lambda_0 k(\lambda_0,\lambda)\, P_j(1 + \lambda_0 - \lambda)\, C_{nj} \ .$$

Equation 3.78 is characterized by (1) the limit of integration being the independent variable λ_n, (2) the value of the dependent variable $v(\lambda_n)$ depending on the values of $v(\lambda')$ if $\lambda' < \lambda_n$ but not if $\lambda' > \lambda_n$, and (3) $T(\lambda_n)$ involving only known or previously calculated quantities. A numerical evaluation of the integral is required, for which several schemes are available. Regardless of

Table 3.2. Sequence of Moments Calculation for $N = 5$

n	B_{nj}					
	$j = 0$	$j = 1$	$j = 2$	$j = 3$	$j = 4$	$j = 5$
0	B_{00}	B_{01}	B_{02}	B_{03}	B_{04}	B_{05}
1	B_{10}	B_{11}	B_{12}	B_{13}	B_{14}	
2	B_{20}	B_{21}	B_{22}	B_{23}		
3	B_{30}	B_{31}	B_{32}			
4	B_{40}	B_{41}				
5	B_{50}					

which scheme is employed, there are coefficients M_{nk} such that Eq. 3.78 can be rewritten as

$$\mu(\lambda_n)\ v(\lambda_n) = \sum_{k=0}^{n-1} H(\lambda_n,\lambda_k)\ v(\lambda_k)\ M_{nk} + H(\lambda_n,\lambda_n)\ v(\lambda_n)\ M_{nn} + T(\lambda_n)\ . \quad (3.79)$$

Note that

$$H(\lambda_n,\lambda_n) = k(\lambda_n,\lambda_n)\ P_j(1+\lambda_n-\lambda_n) = \tfrac{3}{4} \quad (3.80)$$

and that, by the trapezoidal rule, $M_{nn} = \Delta\lambda/2$ for $n = 1$, and $M_{nn} = \Delta\lambda/3$ for $n > 1$. Then for $n = 1$

$$v(\lambda_1) = \frac{T(\lambda_1) + H(\lambda_1,\lambda_0)\ v(\lambda_0)\ (\Delta\lambda/2)}{\mu(\lambda_1) - (3\Delta\lambda/8)}\ , \quad (3.81)$$

and for $n > 1$

$$v(\lambda_n) = \frac{T(\lambda_n) + \sum_{k=0}^{n-1} H(\lambda_n,\lambda_k)\ v(\lambda_k)\ M_{nk}}{\mu(\lambda_n) - (\Delta\lambda/4)}\ . \quad (3.82)$$

The gamma-ray scattering process is such that

$$H(\lambda_n,\lambda_k) = 0 \text{ when } \lambda_n > \lambda_k + 2\ . \quad (3.83)$$

It follows that

$$H(\lambda_n,\lambda_0) = 0 \text{ when } \lambda_n > \lambda_0 + 2\ . \quad (3.84)$$

Therefore the sums on the index k involve only a fixed number of terms, and the second term in $T(\lambda_n > \lambda_0 + 2)$ also vanishes; $H(\lambda_n,\lambda_k)$ can be calculated directly, since only the Klein-Nishina formula and the Legendre polynomials are involved.

At this point it is presumed that the required moments for a given problem can be calculated, and the problem of reconstructing the fluxes is considered. It should be emphasized that the calculation to this point can be performed with very few approximations, excluding the approximations involved in the numerical procedures. The major source of error will lie in the subsequent reconstruction process since only a finite number of moments are available. In fact, for a finite number of moments there is an infinite number of allowable functions. The problem is basically one of choice: the selection of a functional form that will come as close as possible to describing the spatial dependence of $I_j(x,\lambda)$.

Two methods can be used to reconstruct the fluxes: the polynomial expansion method and the method of undetermined parameters. The polynomial expansion method assumes that $I_j(\rho,\lambda)$ behaves roughly as some trial function $f(\rho)$, where ρ is measured in mean free paths at the initial energy; i.e., $\rho \equiv \mu_0 x$. Then

$$I_j(\rho,\lambda) = f(\rho)\ g_j(\rho,\lambda)\ , \quad (3.85)$$

where $g_j(\rho,\lambda)$ contains the λ dependence and provides a correction for the ρ dependence. If a reasonable choice of $f(\rho)$ can be made, then $g_j(\rho,\lambda)$ need be only a gently varying smooth function of ρ, for example, a polynomial of degree N in ρ when $(N+1)$ moments are available; $g_j(\rho,\lambda)$ could be represented as an infinite series with respect to a set of orthogonal polynomials of degree n:

$$g_j(\rho,\lambda) = \sum_{n=0}^{\infty} A_{nj}(\lambda)\ P_n(\rho)\ . \quad (3.86)$$

The orthogonality relationship is given by

$$\int_{-\infty}^{+\infty} P_n(x)\ P_m(x)\ f(x)\ dx = \delta_{nm}\ , \quad (3.87)$$

where $f(x)$ is a weighting function as well as the trial function $f(\rho)$. This representation of $g_j(\rho,\lambda)$ is limited to a truncated series since only $(N+1)$ values of A_{nj} can be obtained, given $(N+1)$ moments.

The approximation for $I_j^s(\rho,\lambda)$ can then be written as

$$I_j^s(\rho,\lambda) = f(\rho) \sum_{n=0}^{N} A_{nj}(\lambda)\ P_n(\rho)\ , \quad (3.88)$$

where $I_j^s(\rho,\lambda)$ is the jth Legendre coefficient of the scattered component of the angular flux. This assumes that values of $(N+1)$ moments B_{nj} are available for the reconstruction of $I_j^s(\rho,\lambda)$.

The reconstruction is accomplished by evaluating the $(N+1)$ coefficient A_{nj} in terms of the known $(N+1)$ moments B_{nj} for a given value of j. To this end, $I_j^s(\rho,\lambda)$ is multiplied by $P_m(\rho)\ d\rho$ and the product is integrated from $-\infty$ to $+\infty$:

$$A_{nj}(\lambda') = \int_{-\infty}^{+\infty} I_j^s(\rho,\lambda)\ P_n(\rho)\ d\rho\ . \quad (3.89)$$

The polynomial $P_n(\rho)$ can be written as

$$P_n(\rho) = \sum_{i=0}^{n} a_i \rho^i \ , \qquad (3.90)$$

where the a_i's are known parameters for a given type of polynomial. The expression for $A_{nj}(\lambda)$ then becomes

$$A_{nj}(\lambda) = \sum_{j=0}^{n} a_i \int_{-\infty}^{+\infty} I_j^s(\rho,\lambda)\ \rho^i\, d\rho \ . \qquad (3.91)$$

The moments B_{ij} are defined as

$$B_{ij}(\lambda) \equiv \frac{1}{i!} \int_{-\infty}^{+\infty} I_j^s(\rho,\lambda)\ \rho^i\, d\rho \ . \qquad (3.92)$$

Elimination of the integrals between the above expressions for $A_{nj}(\lambda)$ and $B_{ij}(\lambda)$ provides the desired relationship

$$A_{nj}(\lambda) = \sum_{i=0}^{n} (i!)\ a_i B_{ij} \ . \qquad (3.93)$$

Practical considerations will usually restrict accurate calculation to $I_0^s(\rho,\lambda)$ and then only the $A_{n0}(\lambda)$'s are required; that is

$$I_0^s(\rho,\lambda) = f(\rho) \sum_{n=0}^{N} A_{n0}(\lambda)\ P_n(\rho) \ , \qquad (3.94)$$

where

$$A_{n0}(\lambda) = \sum_{i=0}^{n} (i!)\ A_i B_{i0} \ .$$

In principle, $A_{nj}(\lambda)$ for $j > 0$ can be calculated. However, since the angular flux $I(x,\lambda,\omega)$ is usually highly peaked in the forward direction, the series

$$I^s(x,\lambda,\omega) = \sum_{j=0}^{L} \frac{2j+1}{2}\ I_j^s(x,\lambda)\ P_j(\omega) \qquad (3.95)$$

converges slowly, thereby requiring a large number of values of $I_j^s(x,\lambda)$, which in turn would require an unreasonably large number of moments. Finally, the scattered and unscattered energy fluxes are easily combined for most simple geometries:

$$I_0(x,\lambda) = I_0^0(x,\lambda) + I_0^s(x,\lambda) \ . \qquad (3.96)$$

The polynomial expansion method described above is most often used for reconstructing the energy flux of the gamma-ray problem. This is partly for historical reasons and partly due to the ability of the method to make full use of large numbers of moments within the same systematic framework of analysis. For the neutron problem the selection of a suitable weighting (or test) function is not obvious and the method loses much of its flexibility.

In using the method of undetermined parameters to reconstruct the fluxes, $I_j(\rho,\lambda)$ is represented as

$$I_j(\rho,\lambda) = \sum_i a_i(\lambda)\ h_i(\rho) \ , \qquad (3.97)$$

where $h_i(\rho)$ is a function having the general expected behavior of $I_j(\rho,\lambda)$ but containing one or more undetermined parameters, and a_i is an undetermined parameter which includes the λ dependence. In particular, let $j = 0$ and assume that $(N+1)$ values of the $B_{n0}(\lambda)$ moments are known; then

$$I_0^s(\rho,\lambda) = \sum_i a_i(\lambda)\ h_i(\rho) \ . \qquad (3.98)$$

The moments corresponding to $j = 0$ can be written as

$$B_{n0}(\lambda) = \frac{1}{n!} \int_{-\infty}^{+\infty} I_0^s(\rho,\lambda)\ \rho^n\, d\rho \ ,$$

$$n = 0, 1, 2, \ldots N \ . \qquad (3.99)$$

Substituting Eq. 3.98 into 3.99 yields the following set of $(N+1)$ equations:

$$B_{n0}(\lambda) = \frac{1}{n!} \sum_i a_i(\lambda) \int_{-\infty}^{+\infty} h_i(\rho)\ \rho^n\, d\rho \ ,$$

$$n = 0, 1, 2, \ldots N \ . \qquad (3.100)$$

Values of $h_i(\rho)$ should be selected so that the above integration can be evaluated either analytically or numerically, and if $(N+1)$ moments are available, then a total of $(N+1)$ undetermined parameters are allowed.

Problems not amenable to other methods can sometimes be solved by the method of undetermined parameters because of the much greater choice that can be made in the $h_i(\rho)$ values. As a result, this method has been more widely applied to the neutron penetration problem. A characteristic of

the method is that when it fails it fails catastrophically, leaving no doubt about its applicability. Usually not all of the moments available are needed to obtain a satisfactory solution. The surplus moments can be used to check the accuracy by constructing moments corresponding to the unused moments, a feature not so easily accomplished by the other methods.

3.5 Monte Carlo Method

A fourth technique which can be applied to the solution of the Boltzmann transport equation is the Monte Carlo method. The Monte Carlo method is a mathematical technique used to approximate a desired quantity by random sampling from the probabilities describing the true stochastic processes that affect the magnitude of the quantity. With sufficient sampling it is assumed that the average value obtained is an accurate estimate of the quantity. For example, a game of chance may be played in which the probability of success P is a number whose value is desired. If the game is played N times with r wins, then r/N is an estimate of P.

Many types of problems in physics and mathematics can be solved successfully by random sampling or stochastic techniques.[17,18] For simple problems, such as the evaluation of single or double integrals, the usual numerical integration schemes will give accurate results with less effort, but for four- or fivefold integrals, Monte Carlo becomes a practical tool.[19]

The method can be demonstrated by considering the Monte Carlo evaluation of a single integral, for example, the integral

$$J = \int_a^b g(x)\, f(x)\, dx\,, \qquad (3.101)$$

which generates the average of the function $g(x)$ weighted by the function $f(x)$. Let the values of the random variable x be sampled from $f(x)$, a normalized probability density function (pdf); the normalization condition is

$$\int_a^b f(x)\, dx = 1\,. \qquad (3.102)$$

With this sampling procedure the integral can be rewritten as

$$J = \int_a^b g(x)\, dF(x)\,, \qquad (3.103)$$

with

$$F(x) = \int_a^x f(x')\, dx'\,. \qquad (3.104)$$

The function $F(x)$ is the cumulative distribution function (cdf) corresponding to $f(x)$. With this transformation a selection of values of $F(x)$ with uniform probability over the interval (0,1) is equivalent to the selection of values of x according to $f(x)$ over the interval (a,b). Then for the ith selection there is a value $g(x_i)$, and an estimation for the value of J is given by

$$\bar{J} = \frac{1}{N} \sum_{i=1}^{N} g(x_i)\,, \qquad (3.105)$$

where $\bar{J}$ is the Monte Carlo estimate of J and N is the arbitrary number of samples.

When generalized to multidimensional integrals Q, the above procedure gives

$$Q = \int g(P)\, f(P)\, dP\,, \qquad (3.106)$$

where P denotes the multidimensional phase space. Then the Monte Carlo estimate of Q is given by

$$\bar{Q} = \frac{1}{N} \sum_{i=1}^{N} g(P_i)\,, \qquad (3.107)$$

where the P_i's are selected according to a complicated set of probabilities giving rise to the probability density function $f(P)$.

The application of this technique to radiation transport becomes clear if the transport equation is written in terms of successive collisions. Following Goertzel and Kalos,[20] a particle is described by the six-dimensional phase space whose coordinates are the components of the position variable $\bar{x}$ and the energy vector $\bar{\omega}E$, where E is its kinetic energy and $\bar{\omega}$ is a unit direction vector.

The motion of the particle may be completely described in terms of the flux density $\Phi(P)$, the collision density $\psi(P)$, or the density of particles leaving collisions $X(P)$. The collision density is so defined that the expected number of collisions of the particle within the medium in the volume of phase space V is given by the integral

$$\int_V \psi(P)\, dP .$$

The flux density may be defined as the collision density divided by the total cross section $\Sigma_t(x,E)$; then

$$\Sigma_t(x,E)\, \Phi(P) = \psi(P) . \tag{3.108}$$

The density of particles leaving collisions is defined so that the expected number of particles appearing in the volume V of phase space either as a result of a collision or directly from a particle source is given by

$$\int_V X(P)\, dP .$$

An important point is that the behavior of a particle is independent of its past history and is determined only by its position in phase space. Nevertheless, it is convenient to indicate the number of collisions n that a particle has undergone. Thus with the collision density of particles that have undergone exactly $n-1$ collisions (and are thus entering their nth collision) denoted by ψ_n, the relation between ψ and ψ_n is given by

$$\psi(P) = \sum_{n=1}^{\infty} \psi_n(P) . \tag{3.109}$$

Similarly,

$$\Phi(P) = \sum_{1}^{\infty} \Phi_n(P) \tag{3.110}$$

and

$$X(P) = \sum_{0}^{\infty} X_n(P) . \tag{3.111}$$

The transport equation can now be expressed in terms of equations for the average values of the source distributions and the collision density:

$$X_0(P) = S(P) , \tag{3.112}$$

$$X_n(x,E) = \int \psi_n(x,E')\, C(E',E,x)\, dE' ,$$

$$n = 1, 2, \ldots , \tag{3.113}$$

$$\psi_{n+1}(x,E) = \int X_n(x',E)\, T(x',x,E)\, dx' ,$$

$$n = 0, 1, 2, \ldots . \tag{3.114}$$

In these equations $S(P)$ is the source distribution and $T(x', x, E)$ denotes the transport kernel and is so defined that for particles leaving a collision (or the source) at (x', E) the expected number of next collisions in the spatial volume V is given by

$$\int_V T(x', x, E)\, dx .$$

Similarly, the collision kernel $C(E', E, x)$ is so defined that for a particle entering a collision at (x, E') the expected number of particles leaving the collision within the volume V of energy space is given by

$$\int_V C(E', E, x)\, dE .$$

For simplicity, the direction variable $\bar{\omega}$ has been dropped but should be interpreted as being carried with E.

In solving for the basic quantities mentioned above or for others determined by these quantities, the sampling in phase space is accomplished by following particle case histories from birth [sampling from $S(P)$] to death by absorption or leakage. This analogy to real particles has led some to call Monte Carlo a theoretical experiment. For adequate numbers of case histories to be traced, a computing machine is necessary; so it is no coincidence that the development of Monte Carlo methods has closely paralleled the development of high-speed computers.

When generating the sequence of events in the life of a case history, certain quantities of interest are selected or computed at each step of the random walk. Each step may be regarded as a collision or as a flight. The quantities associated with the collision, called "collision parameters," are the phase-space coordinates such as x, y, and z (spatial coordinates), α, β, and γ (directional coordinates before or after the collision at x,y,z), the energy E (before or after the collision), and

other quantities deemed useful, such as $\Sigma_t(x,y,z,E)$. The steps proceed as follows:

1. selection of the initial position, energy, and direction from the source function $S(P)$,
2. selection of the next collision site from e^{-y}, which is the distribution of flight lengths in units of the mean free path $[1/\Sigma(E)]$,
3. selection of the energy and direction after collision from the appropriate collision kernel $C(E',E,x)$.

Termination of a history generally takes place when the particle is absorbed, reaches a portion of phase space not allowed, or is killed according to some prescription such as Russian roulette (see discussion below). The most common areas of phase space not allowed are spatial regions exterior to the system considered or energy regions below an arbitrary cutoff.

Sampling Procedures. – Selecting a sample from a distribution usually requires first the selection of one or more random numbers, which customarily are numbers uniformly distributed between 0 and 1. The rigorous definition of this uniform random number is that the probability of it being selected from an interval of length ℓ, contained in the interval between 0 and 1, is simply ℓ. In actual practice there are computational algorithms adapted to digital computers that serve the purpose. One can find descriptions of such methods in the literature, together with discussions of tests of randomness that have been applied.

Once a random number has been selected, there are a number of possible ways to select from a distribution. Consider the following examples:

1. Select a nuclide from N nuclides in a mixture. [The scattering function $C(E',E,x)$ will, in general, depend on the particular nuclide, and hence it is simpler to select a scattering angle and energy for a particular nuclide than for a mixture.]

Each nuclide has a total macroscopic cross section Σ_n, and the total macroscopic cross section for the medium, Σ, is given by

$$\Sigma = \sum_{n=1}^{N} \Sigma_n . \tag{3.115}$$

Nuclide 1 is selected if a random number R is less than Σ_1/Σ, and the ith nuclide is selected if

$$\sum_{n=1}^{i-1} \frac{\Sigma_n}{\Sigma} \leqq R < \sum_{n=1}^{i} \frac{\Sigma_n}{\Sigma} . \tag{3.116}$$

Once the nuclide has been selected, a choice is made between an absorption or a scattering reaction. If another random number R is less than Σ_s/Σ, where Σ_s is the scattering cross section, a scattering reaction will occur; otherwise, it will be an absorption.

2. Select the azimuthal scattering angle ϕ from its uniform pdf, $f(\theta) = 1/2\pi$, and from its corresponding cdf, $F(\phi) = \int_0^{\phi} f(\phi')\, d\phi' = \phi/2\pi$. A value for ϕ is obtained by setting $F(\phi) = R$ and solving for ϕ:

$$\phi = 2\pi R , \tag{3.117}$$

where R is a new random number.

3. Select a value of x from the pdf $f(x)$, where

$$\int_{-\infty}^{\infty} f(x)\, dx = 1 , \tag{3.118}$$

and define the cdf $F(x)$:

$$F(x) = \int_{-\infty}^{x} f(x')\, dx' . \tag{3.119}$$

A value of x is selected by setting $R = F(x)$ and solving for x:

$$x = F^{-1}(R) . \tag{3.120}$$

As an example, pick the distance from one collision site to the next. The pdf is given by

$$f(x) = \Sigma e^{-\Sigma x} , \tag{3.121}$$

and the cdf by

$$F(x) = \Sigma \int_0^x e^{-\Sigma x'}\, dx' = 1 - e^{-\Sigma x} . \tag{3.122}$$

Let

$$R = 1 - e^{-\Sigma x} ; \tag{3.123}$$

then

$$x = -\frac{1}{\Sigma} \ln (1 - R) . \tag{3.124}$$

The quantity $(1 - R)$ is a random number and consequently can be replaced by the random number R', giving

$$x = -\frac{1}{\Sigma} \ln R' . \qquad (3.125)$$

Often it is difficult or impossible to solve for x explicitly, as was done in this example. A table can be constructed with $F(x)$ inverted; that is, x can be regarded as the dependent variable, and $F(x)$ (or R) as the independent variable. Thus a value of x can be obtained from the table for any given value of R.

Many prescriptions for picking from various distributions have been given by Kahn.[21] Cashwell and Everett[22] also give many procedures useful in radiation transport applications.

Importance Sampling. – In any numerical integration scheme it is essential for accuracy to process a sufficient number of points in the phase-space regions where large contributions are made by the integrand. In many Monte Carlo problems adequate sampling becomes a crucial problem. For example, in deep-penetration shielding problems analog sampling may not within a reasonable period of time yield any histories for particles traveling through the regions of interest. Even when a few histories that make important contributions are obtained, the probable error may be too large, and increasing the number of histories decreases the error only slowly (inversely to the square root of the number of histories). A possible solution to the problem is to alter the sampling scheme to one which samples primarily from the important regions.

In importance-sampling techniques, the basic stochastic process is so modified that the event density of the basic process is multiplied by a chosen function (importance function) which measures the importance of an event at x on the quite reasonable basis that important regions of the phase space should be sampled most frequently. Important regions are those in which events contribute, directly or potentially, most heavily to the desired answer, the consideration of which provides some insight to the selection of the importance function.

When the sampling schemes are altered, the concept of statistical weight is introduced to correct for the altered or biased probability, so that the expected value of the mean will not be affected. For example, the information obtained from a case history is increased (and thus the probable error is decreased), generally, by not permitting absorption. Absorption is accounted for by reducing the weight of each particle by the factor Σ_s/Σ_t or, to be more general, by the ratio of the average number of particles emerging from a collision to the number entering a collision. The weighted particle whose history is being traced may be thought of as a bundle consisting of a number of particles, the number being proportional to the weight. At each collision some of the particles in the bundle are absorbed, resulting in a decrease in the weight.

If absorption is not allowed, the particle must eventually be killed by another means. The normal way is by Russian roulette. Thus when the weight becomes lower than some arbitrary value, a game is played in which a particle is killed if $R > C$, where C is the survival probability ($0 \leqq C \leqq 1$). If $R \leqq C$, the particle survives and the weight is increased by the factor $1/C$. The surviving particle then represents all those particles killed in the game.

Russian roulette can also be used to decrease the sampling in any region of phase space by arbitrary tests, in which case it is often coupled with the inverse process splitting. That is, with certain criteria satisfied, a particle can split into two or more particles with the appropriate weight reduction. This is done when a particle crosses into an important region of phase space or at the first collision site in such a region.

Importance sampling can be considered in a general way by referring back to Eq. 3.101, which can be rewritten as

$$J = \int_a^b g^*(x)\, f^*(x)\, dx , \qquad (3.126)$$

where

$$g^*(x)\, f^*(x) = g(x)\, f(x) , \qquad (3.127)$$

with the restrictions that $f^*(x) = 0$ only for $f(x) = 0$ and that

$$\int_a^b f^*(x)\, dx = 1 . \qquad (3.128)$$

The expected value of J remains the same in a Monte Carlo solution involving sampling from $f^*(x)$ and evaluating $g^*(x_i)$. However, it can be shown that the variance is not the same, making

it possible to improve the variance if $f^*(x)$ is selected properly. It is obvious that

$$g^*(x) = g(x)\frac{f(x)}{f^*(x)}, \qquad (3.129)$$

which shows that the statistical weight correction factor $f(x)/f^*(x)$ is to be used when sampling from $f^*(x)$ and evaluating $g(x)$.

For example, it is well known that in shielding problems the high-energy neutrons from a fission source dominate the penetration. In sampling from the Watt fission spectrum,[23] however, less than 1% of the samples have energies greater than 7.5 MeV. Obviously, importance sampling is needed. One way is to pick from a uniform distribution over only the range of importance bounded, for example, by the energies E_1 and E_2. If it is assumed that the fission spectrum is given by the pdf $f(E)$, the pdf can be modified (without change) by the pdf $f^*(E) = (E_2 - E_1)^{-1}$ in the following manner:

$$f(E) = f(E)\frac{f^*(E)}{f^*(E)} = f^*(E)\frac{f(E)}{f^*(E)} \cdot \qquad (3.130)$$

The selection of energy is made from $f^*(E)$, and the particle weight is corrected by the factor $f(E)/f^*(E)$. The cdf corresponding to $f^*(E)$ is given by

$$F^*(E) = \int_{E_1}^{E} f^*(E)\,dE = \frac{E - E_1}{E_2 - E_1}. \qquad (3.131)$$

The selection of an energy E is accomplished by setting $F^*(E)$ equal to a random number R and solving the resulting equation for E, which yields

$$E = E_1 + R(E_2 - E_1). \qquad (3.132)$$

Further discussions of importance sampling can be found in refs. 17–22. In many cases the importance function is selected arbitrarily and intuitively. A more systematic (and generally successful) approach is to use value functions.[24] The value function, a solution of a transport equation adjoint to the Boltzmann transport equation, has been shown to be a very good, and sometimes an optimum, importance function for biasing the original Monte Carlo procedure. In most cases, a reasonable approximation to the actual value function will produce quite good results. A useful specialization of these techniques is the exponential transformation, which can be quite helpful if parameters for its use are obtained from a value function approximation.[25,26]

Scoring. – Thus far, only the generation of histories has been considered. At some point with each history a score must be evaluated, a score being the contribution to the quantity of interest. (Typical quantities of interest are flux density, current, absorption, heating, leakage, transmission, reflection, and dose.) For example, suppose that it is desired to estimate a reaction rate integrated over a volume V of phase space, where $\Sigma(x,E)$ is the macroscopic cross section for the reaction of interest. This reaction rate is given by

$$\int_V \Sigma(P)\,\Phi(P)\,dP\,.$$

One way of estimating it is to record $\Sigma(P)/\Sigma_a(P)$ for every particle absorbed in the volume V, where $\Sigma_a(P)$ is the macroscopic absorption cross section. Another commonly used estimator records $\Sigma(P)\cdot d$ for every flight of length d in the volume of interest, where it is assumed that $\Sigma(P)$ does not vary over the track d. It is possible to reduce the variance of the estimate by using computed means in connection with the basic collision data. An example of this is the next-event estimator, which records at each collision site the probability of scoring in one additional flight. There are many other possible means of combining analytical computation with random sampling, but they will not be discussed here.

Statistical Accuracy. – The mean is usually the quantity of most interest in a Monte Carlo problem, but in a study of the statistical properties of the problem higher moments are often calculated, particularly the second moment, or the estimate of the variance. The sample variance (an estimate of the second moment) is given by

$$s^2 = \frac{1}{n-1}\sum_{i=1}^{n}(x_i - \bar{x})^2$$

$$= \frac{1}{n-1}\left[\Sigma x_i^2 - \frac{(\Sigma x_i)^2}{n}\right], \qquad (3.133)$$

where

n = number of samples,

x_i = value of a sample,

$\bar{x} = \frac{1}{n}\Sigma x_i$ = mean value of n samples.

The estimate of the variance of the mean is

$$\mathrm{var}(\bar{x}) = \sigma^2 = \frac{s^2}{n}. \qquad (3.134)$$

The sample x_i may be regarded as the result from one case history, or it might be the mean of many histories taken as a batch. Only in the limit of many histories will the estimate of the variance be the same for a particular set of case histories divided into arbitrary batches.

For a normal distribution, σ is called the standard deviation and has the following properties: When samples are taken, the probability that the estimate of the mean will be within one standard deviation of the true mean (limiting value with an infinite number of samples) is about 67%, within two standard deviations about 95%, and within three standard deviations about 99%. Thus one generally computes the sum x_i^2 as well as x_i during a Monte Carlo calculation so that σ can be calculated as well as $\bar{x}$.

There are some principles that should be kept in mind at this point. With adequate sampling of the important regions of phase space in shielding problems the distribution of the mean might be expected to be close to the normal distribution, but there is a good possibility that it will be skewed, and the above interpretation of the sample variance will be far from correct. From a practical standpoint the above interpretations of the variance are overly optimistic. In many cases (especially in deep-penetration problems) it is typical to undersample important regions of phase space and to obtain an underestimate of the mean. Then the estimate of the variance is likely to be even worse (frequently much worse[27]) and hence completely unreliable. If the standard deviation approaches 30 to 50% of the mean, the mean itself should be regarded as very unreliable.

Use of Monte Carlo Methods Today. – Monte Carlo techniques may be designed to reproduce a physical model in as much detail as is necessary, and so provide a powerful tool to solve problems with very few compromises with the physics. The Monte Carlo method is capable of incorporating any geometry. To use Monte Carlo successfully, however, generally requires a considerable investment in analysis, programming, and computer machine time. The importance of machine time is often overemphasized, with analysis and programming being underemphasized. It is important for the user to keep in mind that a well-developed theory exists which specifies, in principle, a near-optimum procedure for solving a given problem. This procedure consists of obtaining the best possible approximation to the value function for the problem and then using this function to obtain parameters for importance-sampling techniques or to guide development of new biasing techniques.

To aid the programmer, the concept of a Monte Carlo programming system, as opposed to a particular general-purpose code, is now utilized. For example, a system known as the O5R system[28] can, in principle, be utilized to solve any neutron transport problem. The framework is there (cross-section handling, geometry-solving routines, random-walk procedures, etc.), but the programmer must incorporate the special features he desires by adding subroutines to the framework.

In general, Monte Carlo methods will not be applied to one-dimensional problems, since discrete ordinates codes are likely to be much faster than Monte Carlo codes. For two-dimensional problems, Monte Carlo and discrete ordinates methods are somewhat comparable, but for three-dimensional or time-dependent problems there is no competitor to Monte Carlo for a rigorous solution of transport problems.

3.6 Application of Diffusion Theory

An approach to the particle transport problem that neglects the detailed directional aspects of the particle motion is that of diffusion theory. A neutron balance in the four-dimensional phase space $(\bar{r}, t)$ leads to the following equation of continuity for the one-speed neutron transport problem:

$$\frac{\partial n(\bar{r}, t)}{\partial t} = S(\bar{r}, t) - \Sigma_a \Phi(\bar{r}, t) - \nabla \cdot J(\bar{r}, t), \quad (3.135)$$

where

$n(\bar{r}, t)$ = neutron density (neutrons cm^{-3}),

Σ_a = macroscopic absorption cross section (cm^{-1}),

$S(\bar{r}, t)$ = general source term (neutrons cm^{-3} sec^{-1}),

$\Phi(\bar{r}, t)$ = total neutron flux (neutrons cm^{-2} sec^{-1}),

$J(\bar{r}, t)$ = net neutron current (neutrons cm^{-2} sec^{-1}),

$\frac{\partial n}{\partial t}$ = time rate of change of the neutron density (neutrons cm^{-3} sec^{-1}),

$\Sigma_a \Phi(\bar{r}, t)$ = loss of neutrons due to absorption (neutrons cm^{-3} sec^{-1}),

$\nabla \cdot J(\bar{r}, t)$ = loss of neutrons due to convection (neutrons cm^{-3} sec^{-1}).

Equation 3.135 can be regarded as a precise relationship that can be applied without restriction to the general problem of particle transport. However, a basic limitation in its use is that except for certain very restricted situations a tractable form for the net neutron current $J(\bar{r}, t)$ does not exist. Diffusion theory in its usual form is based on the following time-independent expression for the net current:

$$J(\bar{r}) = -D \nabla \Phi(\bar{r}) , \quad (3.136)$$

where D is the position-independent diffusion coefficient (cm), and $\nabla\Phi(\bar{r})$ is the gradient of the total neutron flux. It is noted that with the steady-state assumption, phase space has been reduced to three position variables as denoted in general vector notation by $(\bar{r})$. Equation 3.136 is identical in form with Fick's law, which simply states that the net diffusion of particles (or molecules) in liquids and gases will be from regions of high particle density to regions of low particle density, with the gradient of the particle flux as the driving potential. The derivation of Eq. 3.136 can be found in any nuclear reactor theory textbook, for example, in the text by Weinberg and Wigner.[1]

Substitution of Eq. 3.136 into the steady-state form of Eq. 3.135 leads to the "diffusion equation"

$$D\nabla^2 \Phi(\bar{r}) - \Sigma_a \Phi(\bar{r}) + S(\bar{r}) = 0 . \quad (3.137)$$

Equation 3.137 has the same form as the steady-state form of the P_1 approximation to the spherical harmonics treatment of the Boltzmann equation (see Section 3.2).

Certain limitations are inherent to diffusion theory: (1) the scattering process is assumed to be isotropic in the laboratory frame of reference, (2) the directional distribution of the particle flux is nearly isotropic, (3) the diffusing medium must be a poor absorber, i.e., $\Sigma_a \ll \Sigma_s$, and (4) the results are invalid for regions within 2 to 3 mean free paths of boundaries, strong sources, and strong sinks. The existence of these limitations is a clear indication of the approximate nature of diffusion theory insofar as the physical situation is concerned. In reality the above conditions of applicability for diffusion theory are seldom satisfied. However, with the judicious selection of system parameters the diffusion theory solutions of certain problems* compare favorably with solutions obtained with more exact theories or with the physical situation itself.

A neutron shielding problem that can be solved by diffusion theory would involve neutrons having a continuous energy spectra over a wide energy range (typically from a low keV region to 10 MeV) so that a "group" approach is required to adequately describe the diffusion process. The energy range is divided into G energy groups with the gth group corresponding to the energy width $E_{i+1} - E_i$. The group-diffusion equation for the gth group is given by

$$D_g \nabla^2 \Phi_g(\bar{r}) - \Sigma_a^g \Phi(\bar{r}) + S_g(\bar{r}) = 0 , \quad (3.138)$$

*For example, diffusion theory is used in fast reactor shielding design since the leakage spectrum peaks below 0.5 MeV and the materials involved are non-hydrogenous (sodium and graphite). Also, the small source (reactor core) requires two-dimensional calculations, which are much simpler with diffusion theory.

where

D_g = group-averaged diffusion coefficient

$$= \frac{\int_{E_i}^{E_{i+1}} D(E)\, \Phi(\bar{r}, E)\, dE}{\Phi_g(\bar{r})} ,$$

$\Phi_g(\bar{r})$ = total flux corresponding to the gth energy group ($g = 1, 2, \ldots G$)

$$= \int_{E_i}^{E_{i+1}} \Phi(\bar{r}, E)\, dE ,$$

Σ_a^g = group-averaged macroscopic absorption cross section

$$= \frac{\int_{E_i}^{E_{i+1}} \Sigma_a(E)\, \Phi(\bar{r}, E)\, dE}{\Phi_g(\bar{r})} ,$$

$S_g(\bar{r})$ = general source term for the gth group

$$= \int_{E_i}^{E_{i+1}} S(\bar{r}, E)\, dE .$$

However, the typical neutron shielding problem is not amenable to solution by the straightforward application of diffusion theory, because the neutrons are on the average very energetic and possess a strong forward directional bias. The limitations of diffusion theory under these conditions are clearly violated and results thus obtained would be meaningless. But when applied to certain special problems in combination with other methods, diffusion theory has proved useful. Applications of diffusion theory to the neutron shielding problem are discussed further in Section 3.9.

The use of diffusion theory to predict gamma-ray energy fluxes seems to be unjustified on superficial examination of the gamma-ray transport phenomenon. Certainly deep penetration by gamma radiation cannot be described by diffusion theory, because the resultant gamma-ray flux is due to photons that have maintained a strong directional correlation. But diffusion theory seems to be adequate for small-to-moderate penetrations relatively near the source under conditions where the low-energy end of the spectrum predominates and the scattering is more nearly isotropic. These restricted conditions exist, for example, for gamma-ray heating calculations.[29]

3.7 Invariant Imbedding Method

The method of "invariant imbedding" is not another method for solving the Boltzmann transport equation. Rather it is a different fundamental approach to the mathematical description of particle transport. The method has for its historical basis the early works of a Russian astrophysicist, V. A. Ambarzumian, who confined his interest to the transport problems of astrophysics.[30] Recent investigations[31,32] have shown that the invariant imbedding approach can be applied to a much broader class of problems, including the neutron and gamma-ray transport problems encountered in radiation shielding.

The dependent variables of the invariant imbedding formulation are the reflection and transmission functions, with the region dimensions (shield thickness) and the energy and direction of the particle comprising the six-dimensional phase space. In this context a particular shielding problem is viewed as being "imbedded" in a more general class of shields having different dimensions. Characteristically, and in contrast with solutions of the Boltzmann transport equation, the invariant imbedding method provides transmission and reflection information for a large variety of shields, as well as for the specific problem of interest. However, the detailed behavior of the radiation during transport through the shield is not explicit during the analysis and for that reason is unavailable, a not too serious shortcoming – if not a real advantage – for the typical shielding problem.

The reflection and transmission functions of invariant imbedding are each defined by an integro-differential equation. These equations can be derived by applying the usual conservation principles of radiation transport to a shield system, the dimensions of which are allowed to vary by differential amounts. For simplicity and greater clarity, the derivations are performed in slab geometry with azimuthal symmetry. Phase space becomes three-dimensional: the shield thickness X, the energy variable E, and the direction variable μ ($=\cos\theta$). A schematic representation of this configuration is shown in Fig. 3.1.

The reflection function $R(X;\mu,E;\mu_0,E_0)\,d\mu\,dE$ is defined as the number of particles incident with energy E_0 and direction μ_0 that are reflected from a slab of thickness X with energies in dE about E and directions that lie in $d\mu$ about μ per unit area on the emergent surface; the function can be regarded as an angular flux within the differential slab thickness dX. The reflection equation describes the change in the reflection function due to changes in the shield thickness and is formulated without involving the transmission function. The derivation is accomplished by equating the difference in the reflection functions for slabs of thicknesses $X + dX$ and X with the net change in the reflection function which results from collisions suffered by the particles within the differential slab dX:

where $\Sigma_t(\bar{x},E_0)$ is the position-dependent total macroscopic cross section evaluated at the particle energy E_0, and $\Sigma_s(\bar{x};\mu',E';\mu_0,E_0)\,d\mu'dE'$ represents the position-dependent differential scattering cross section which describes the probability that a particle with an initial energy E_0 and an initial direction μ_0 undergoes a scattering collision that places it into a direction which lies in $d\mu'$ about μ' with a new energy in dE' about E'.

The first and second terms on the right-hand side of Eq. 3.139 represent the particle losses due to collisions within dX (any collision is presumed to alter the particle's energy and direction).

ORNL-DWG 67-12748

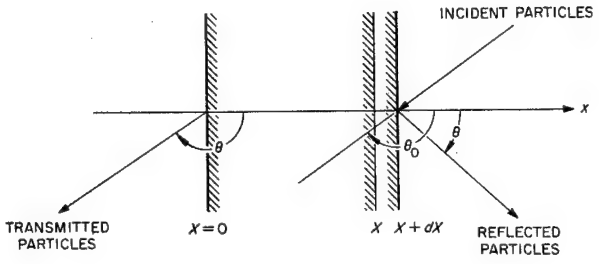

Fig. 3.1. Geometry for Invariant Imbedding Technique.

$$R(X+dX;\mu,E;\mu_0,E_0) - R(X;\mu,E;\mu_0,E_0) = -\Sigma_t(X,E_0)\,R(X;\mu,E;\mu_0,E_0)\frac{dX}{\mu_0}\,d\mu\,dE$$

$$-\Sigma_t(X,E)\,R(X;\mu,E;\mu_0,E_0)\frac{dX}{\mu}\,d\mu\,dE$$

$$+\int_{-1}^{0} d\mu' \int_{0}^{\infty} dE'\,\Sigma_s(X;\mu',E';\mu_0,E_0)\,R(X;\mu,E;\mu',E')\frac{dX}{\mu_0}\,d\mu\,dE$$

$$+\int_{0}^{1}\frac{d\mu'}{\mu'}\int_{0}^{\infty} dE'\,R(X;\mu',E';\mu_0,E_0)\,\Sigma_s(X;\mu,E;\mu',E')\,dX\,d\mu\,dE$$

$$+\int_{0}^{1}\frac{d\mu'}{\mu'}\int_{-1}^{0} d\mu''\int_{0}^{\infty} dE'\int_{0}^{\infty} dE''\,R(X;\mu',E';\mu_0,E_0)\,\Sigma_s(X;\mu'',E'';\mu',E')$$

$$\times R(X;\mu,E;\mu'',E'')\,dX\,d\mu\,dE\,, \quad (3.139)$$

The first term is the loss of incident particles scattered within dX such that they do not enter the slab of thickness X, and the second term is the loss of particles that are scattered within dX such that they are prevented from emerging from the slab of thickness $X + dX$. The third, fourth, and fifth terms represent the inscattering gains due to scattering collisions within dX. The third term is the gain from particles that scatter from dX into the slab of thickness X with energies in dE' about E' and directions $d\mu'$ about μ', and then are reflected from the slab of thickness X with the proper emergent angle and direction. The fourth term is the gain from particles that scatter from the slab of thickness X into dX with energies in dE' about E' and directions $d\mu'$ about μ' and then are scattered within dX with the proper emergent energy and direction. The fifth term is the gain from particles that scatter from the slab of thickness X into dX with energies in dE' about E' and direction $d\mu'$ about μ', are scattered back into the slab of thickness X with energies in dE'' about E'' and directions $d\mu''$ about μ'', and are finally reflected from the slab of thickness X with the proper emergent energy and direction. A rearrangement of terms leads to the usual form of the reflection equation:

$$\frac{d}{dX} R(X;\mu,E;\mu_0,E_0) = -\left[\frac{\Sigma_t(X,E_0)}{\mu_0} + \frac{\Sigma_t(X,E)}{\mu}\right] R(X;\mu,E;\mu_0,E_0)$$

$$+ \int_{-1}^{0} d\mu' \int_{0}^{\infty} dE' \, \Sigma_s(X;\mu',E';\mu_0,E_0)\, R(X;\mu,E;\mu',E') \frac{1}{\mu_0}$$

$$+ \int_{0}^{1} \frac{d\mu'}{\mu'} \int_{0}^{\infty} dE' \, R(X;\mu',E';\mu_0,E_0)\, \Sigma_s(X;\mu,E;\mu',E')$$

$$+ \int_{0}^{1} \frac{d\mu'}{\mu'} \int_{-1}^{0} d\mu'' \int_{0}^{\infty} dE' \int_{0}^{\infty} dE'' \, R(X;\mu',E';\mu_0,E_0)\, \Sigma_s(X;\mu'',E'';\mu',E')$$

$$\times R(X;\mu,E;\mu'',E'') , \qquad (3.140)$$

with the initial condition that

$$R(0;\mu,E;\mu_0,E_0) = 0 . \qquad (3.141)$$

The transmission function $T(X;\mu,E;\mu_0,E_0)\,d\mu\,dE$ is defined as the number of particles incident with energy E_0 and direction μ_0 that are transmitted through a slab of thickness X, emerging with energies in dE about E and directions in $d\mu$ about μ per unit area on the exit surface. The derivation of the transmission equation is accomplished in a manner similar to that used to derive the reflection equation and follows the argument that the difference in the transmission functions for slabs of thickness $X + dX$ and X is due to collisions suffered by the particles within the differential slab dX. A familiar form of the transmission equation is

$$\frac{d}{dX} T(X;\mu,E;\mu_0,E_0) = -\frac{\Sigma_t(X,E_0)}{\mu_0} T(X;\mu,E;\mu_0,E_0)$$

$$+ \int_{-1}^{0} d\mu' \int_{0}^{\infty} dE' \, \Sigma_s(X;\mu',E';\mu_0,E_0)\, T(X;\mu,E;\mu',E')$$

$$+ \int_{0}^{1} \frac{d\mu'}{\mu'} \int_{-1}^{0} d\mu'' \int_{0}^{\infty} dE' \int_{0}^{\infty} dE'' \, R(X;\mu',E';\mu_0,E_0)\, \Sigma_s(X;\mu'',E'';\mu',E')$$

$$\times T(X;\mu,E;\mu'',E'') , \qquad (3.142)$$

with the initial condition that

$$T(0;\mu,E;\mu_0,E_0) = \delta(\mu-\mu_0)\,\delta(E-E_0)\,. \qquad (3.143)$$

The first term in the right-hand side of Eq. 3.142 represents the loss of incident particles scattered within dX such that they do not enter the slab of thickness X. The second and third terms represent the inscattering gains due to scattering collisions within dX. The second term is the gain from particles that scatter from dX into the slab of thickness X with energies in dE' about E' and directions in $d\mu'$ about μ', finally emerging with energies in dE about E and directions in $d\mu$ about μ. The third term is the gain from particles that are reflected from the slab of thickness X into dX and are then scattered back into the slab of thickness X, finally emerging with energies in dE about E and directions in $d\mu$ about μ.

The reflection equation (Eq. 3.140) and the transmission equation (Eq. 3.142) are both nonlinear integrodifferential equations which for the radiation transport problems of nuclear engineering form problems of the "initial-value" type. The reflection equation involves only the reflection function as the dependent variable, thereby allowing its solution without consideration of the transmission equation. The transmission equation appears simpler in form (fewer terms) but contains the reflection function, which must be known before a solution can be effected. Therefore a typical shielding transmission problem (initial-value) would involve the solution of a coupled pair of nonlinear integrodifferential equations. This is in contrast to the Boltzmann equation (Eq. 3.2), which is a linear integrodifferential equation and for the same application forms a "boundary-value" type problem.

Analytical solutions of the reflection and transmission equations for practical problems are not possible because of their integrodifferential form; the nonlinearities are a further complication. As a consequence, all useful solutions are numerical in nature and are accomplished through the use of digital computers. The numerical techniques are similar to those used to solve the Boltzmann equation by the discrete ordinates technique, in which a specific combination of the independent variables defines discrete values of the neutron flux $\Phi_{G,I,D}$ (see Section 3.3 for a more complete description).

In invariant imbedding, specific combinations of the energy and direction of the particle define the particle's state "*i*." In this context, the discrete reflection variable $R_{ij}(X)$ is the number of particles in state i per unit area normal to the x direction reflected by a slab of thickness X due to a unit source of particles in state j that are incident on the slab. The discrete transmission variable $T_{ij}(X)$ is the number of particles in state i per unit area normal to the x direction that penetrate a slab of thickness X due to a unit source of particles in state j that are incident on the slab. The reflection and transmission equations in discrete variable notation, along with a general description of numerical techniques used in their solution, are given by Mathews, Hansen, and Mason.[33]

The paper of Mathews *et al.* also describes the application of invariant imbedding to practical energy-dependent neutron shielding problems, such as for a thick water shield and a thinner heterogeneous iron-polyethylene-iron shield. A very detailed set of reflection and transmission equations in particle-state notation for the monoenergetic neutron transport problem in slab geometry is given by Mingle,[34] who includes applications of the method of escape probabilities, blackness coefficients, and critical size determinations. Solutions for the gamma-ray transport problem in slab geometry, including results for slabs of iron, water, lead, and concrete, are given by Shimizu and Mizuta.[35]

The advantages and disadvantages of the invariant imbedding method relative to other techniques should strongly influence the extent and directions of future applications. The advantages of the method are that it yields very detailed solutions (gives energy and angular distributions), it is efficient for deep penetrations with reasonably short computer times, it is well suited for heterogeneous shield configurations, the effects of boundaries are implicitly and exactly included in the solution, and it has the computational advantages of being an initial-value problem. The disadvantages of the method are that it is inefficient for thin shields (the method is very slow during initial phases of solution), it is difficult to apply to other than slab geometries, it does not generate detailed particle-state information within the shield (actually an advantage from a computational point of view), the basic equations are nonlinear (not too serious if solution is obtained numerically), and the calculational techniques and "user" computer programs are not as advanced as those for the solutions of the Boltzmann equation.

3.8 Kernel Techniques

The kernel technique, which in the language of mathematical physics is known as the method of Green's functions, is one of the more widely used methods for the solution of both gamma-ray and neutron shielding problems.* The point kernel $K(|\bar{r} - \bar{r}'|)$ is formally the solution to the unit point source problem and is defined as the desired response of a detector (particle flux, energy flux, dose, or energy absorption) at the space point $\bar{r}$ due to a unit point source of radiation at the space point $\bar{r}'$. This kernel provides the means for solving a variety of problems which involve distributed sources. As an illustration of the procedure, consider the surface-source problem.** In terms of the point kernel, the detector response at a distance $|\bar{r} - \bar{r}'| = R$ away from a differential source area $dA(R)$ of intensity $S_A(R)$ (particles cm^{-2} sec^{-1}) is

$$d\Phi = [S_A(R)\, dA(R)]\, K(R) . \qquad (3.144)$$

The differential area $dA(R)$ is selected so that the term $[S_A(R)\, dA(R)]$ can be considered as a point source located at a distance R from the detector. The total detector response (the desired answer to the surface-source problem) is obtained by integrating over the entire surface:

$$\Phi = \int d\Phi = \int_A S_A(R)\, K(R)\, dA(R) . \qquad (3.145)$$

The utility of the method is considerably enhanced if the integral can be evaluated analytically.

Kernels that are used in practical shielding calculations almost invariably result from solutions (either analytical or numerical) for infinite homogeneous media. Consequently, applications of these kernels to finite-geometry configurations lead to systematic errors, the sign and severity of the errors depending on the particular conditions.

3.8.1. GAMMA-RAY CALCULATIONS

Point Kernels

In the analysis of gamma-ray transport problems, the uncollided flux (i.e., the flux due to source gamma rays that arrive at the point of interest without suffering an interaction) is usually easily calculated. For example, for the case of a monoenergetic point isotropic source in an infinite medium, the uncollided flux is given by

$$\Phi^0(R) = S\, \frac{e^{-\mu(E)R}}{4\pi R^2} \text{ (gamma rays cm}^{-2}\text{ sec}^{-1}) , \qquad (3.146)$$

where

S = source strength (gamma rays/sec),
$\mu(E)$ = macroscopic total cross section evaluated at the initial gamma-ray energy E (cm^{-1}),
$e^{-\mu(E)R}$ = material attenuation factor, which is the probability that a gamma ray of energy E travels a distance R (cm) without suffering a collision,
$\frac{1}{4\pi R^2}$ = geometric attenuation for a point source (cm^{-2}).

Calculation of the scattered flux is in general much more complex. The scattered component is handled by introducing a buildup factor, which accounts for the increase (i.e., buildup) in the flux at some point $\bar{r}$ that is due to the scattered gamma rays. It is this buildup factor, defined as

$$B \equiv \frac{\text{some desired property (particle flux, energy flux, dose, etc.) of the total gamma-ray flux at } R}{\text{same property due to the uncollided flux at } R} , \qquad (3.147)$$

that serves as the basis for formulating the point kernels required for gamma-ray shield analysis. For the calculation of dose, the kernel is given by

$$K_r(R) = \frac{\mu_{at}(E)\, E\, \Phi^0(R)}{S} B_r = \frac{\mu_{at}(E)\, E\, e^{-\mu(E)R}}{4\pi R^2} B_r , \qquad (3.148)$$

where $\mu_{at}(E)$ is the macroscopic energy absorption cross section for tissue evaluated at the initial

*Brief descriptions of several computer codes based on the kernel technique are given in Appendix 3A.

**The volumetric source problem is handled in a similar fashion.

gamma-ray energy E, and B_r is the dose buildup factor, which is the ratio of the actual dose at R to the uncollided dose at R. Similarly, if the desired property is the energy absorbed, the kernel is given by

$$K_a(R) = \frac{\mu_a(E)\, E\, \Phi^0(R)}{S} B_a = \frac{\mu_a(E)\, E\, e^{-\mu(E)R}}{4\pi R^2} B_a , \quad (3.149)$$

where $\mu_a(E)$ is the macroscopic energy absorption cross section evaluated at the initial gamma-ray energy E for the material in which the energy is absorbed, and B_a is the energy absorption buildup factor, which is the ratio of the actual energy absorbed at R to the uncollided energy absorbed at R.

Buildup Factors

The results of many accurate gamma-ray attenuation calculations are reported in terms of buildup factors, which in combination with the kernel technique provide a relatively simple and, in many cases, quite accurate calculational method. Most of the buildup factors in current use are those published in 1954 by Goldstein and Wilkins,[13] who give the results of infinite-medium calculations for seven materials and up to nine source energies, which cover the range of interest for reactor and weapons shielding. Results for other materials and energies may be obtained by interpolation since the buildup factors are smooth functions of energy and atomic number.

Various approximate equations have been used for the buildup factors, the coefficients usually being determined by a best fit of the available data. Some of these are discussed below.

Early Linear Form. – Probably the oldest formula used for a buildup factor was a simple linear form given by

$$B(E,\mu R) = 1 + \mu R , \quad (3.150)$$

where

E = source energy,
μ = linear attenuation coefficient, evaluated at the source energy,
R = distance to source.

This particular linear form of the buildup factor has the advantage of being simple, but it is not very good over a significant range.

Taylor Form. – A frequently used form of the buildup factor is that of Taylor,[36] written as

$$B(E,\mu R) = A\, e^{-\alpha_1(E)\mu R} + (1 - A)\, e^{-\alpha_2(E)\mu R} . \quad (3.151)$$

It is apparent that substitution of Eq. 3.151 into 3.149 does not change the form of the kernel but merely generates two terms. Consequently, all available analytical solutions for the uncollided flux can be corrected for the scattered flux by simply using modified attenuation coefficients represented by $(1 + \alpha_1)\mu$ and $(1 + \alpha_2)\mu$ and multiplying the respective terms by A and $(1 - A)$. Addition of these two terms then gives the total dose (uncollided plus scattered).

Values of A, α_1, and α_2 were given in Taylor's original report for a number of materials, and subsequently coefficients for the energy absorption buildup factor for aluminum, tungsten, and lead and coefficients for the dose buildup factor for uranium were published by Strobel.[37]

Only recently Buscaglione and Manzini[38] published a rather complete set of coefficients for dose buildup factors, including those for ordinary, barytes, ferrophosphorous, and magnetite concretes. The values for concrete are based on data published by Walker and Grotenhuis.[39] Since the data are so complete, covering all the point sources used by Goldstein and Wilkins,[13] the dose coefficients are reprinted in Table 3B.1 in Appendix B. The values for concrete should be better than those published previously[40,41] because a more realistic effective atomic number was assumed.

Polynomial Form. – The use of a buildup factor given by a four-term polynomial capable of good accuracy became feasible when in 1958 Capo[42] published a rather complete set of coefficients for many materials. The form of the buildup factor is

$$B(E,\mu R) = \sum_{n=0}^{3} \beta_n(E)\, (\mu R)^n , \quad (3.152)$$

and Capo gives the coefficients β for several sets of energies, as well as coefficients for a bivariant fit which allows a set of β values to be generated for any energy. Unlike all other formulations considered here, Capo's coefficients result in an expression that does not reduce to exactly unity for

$\mu R = 0$; however, the values of β_0 are extremely close to 1.

A more recent set of coefficients for this form of the dose buildup factor has been published by Buscaglione and Manzini[43] for various concretes. Their values, based on the data of Walker and Grotenhuis,[39] are reproduced in Table 3B.2 in Appendix B.

Empirical Linear and Quadratic Forms. – By least-squares fits to the data of Goldstein and Wilkins[13] for various materials and to the data of Walker and Grotenhuis[39] for four types of concrete, Trubey[44] determined values of the dose coefficient A_1 in the linear form of the buildup factor given by

$$B(E,\mu R) = 1 + A_1(E)\,\mu R\,, \qquad (3.153)$$

and the dose coefficients A_2 and b in the quadratic form given by

$$B(E,\mu R) = 1 + A_2(E)\,\mu R + b(E)(\mu R)^2. \qquad (3.154)$$

Two sets of data were used, one based on data for $\mu R \leqq 7$ mean free paths, and another based on data for $\mu R \leqq 20$ mean free paths. In the fitting procedure used, the results obtained for large values of the argument were better than those obtained for small values. With heavy elements, when the fit is from 0 to 20 or more mean free paths, a large error occurs in the fitting function at small distances such that the value of B as determined by Eq. 3.154 goes to zero or is negative. This causes the absurd result of a maximum error ratio of infinity, which limits the use of the quadratic form with these parameters to deep-penetration calculations for such cases.

Values of the coefficients A_1, A_2, and b are presented in columns 2, 4, and 5 in Tables 3B.3 and 3B.4 in Appendix B. The maximum errors shown in columns 3 and 6 are those encountered over the fitted range. The error is reported either in percentage or as a factor indicated by the letter F.

Berger Form. – A two-parameter dose buildup formula proposed by Berger[45] and reintroduced by Chilton *et al.*[46] has the simplicity of the linear form but fits the buildup factor data well over a long range. This formula is

$$B(E,\mu R) = 1 + C(E)\,\mu R\,e^{D(E)\mu R}\,. \qquad (3.155)$$

In an effort to investigate the adequacy of the formula and to make it generally useful, Trubey[44] used a least-squares procedure to obtain values of C and D for all the materials included by Goldstein and Wilkins[13] and the four types of concrete covered by Walker and Grotenhuis,[39] again using two sets of data corresponding to $\mu R \leqq 7$ and 20 mean free paths. These values are given in columns 7 and 8 of Tables 3B.3 and 3B.4 of Appendix B, with the maximum error encountered over the fitted range given in column 9. It was found that this formula could reproduce the calculated buildup factor functions extremely well and had the advantages of being easily integrable over the various source regions and (unlike the Taylor form) resulting in two terms (unscattered and scattered) which have significance. Consequently, this form was highly recommended.[44] Other values for C and D were published by Rudloff[47] and by Chilton[48] for $\mu R \leqq 15$ and 10 mean free paths respectively. Chilton's values are reproduced in Figs. 3.2 and 3.3 as functions of energy for various materials. It can be seen in Fig. 3.3 that for several materials and certain energies the value of D is zero, which means that the Berger formula reduces to the linear form.

Other Forms. – There are many other possible forms of buildup factors, such as those cited by Hubbell,[49] but they are generally more complicated than the forms given here. Hubbell's power series form, for example, converges adequately at short distances only and thus usually requires many

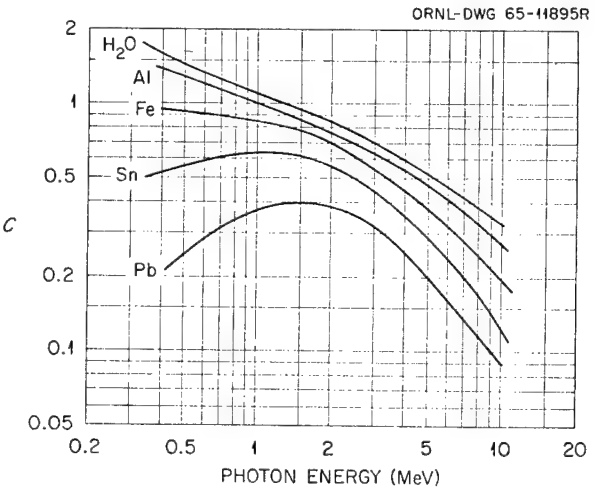

Fig. 3.2. The Coefficient C for the Berger Form of the Gamma-Ray Dose Buildup Factor. (From Chilton, ref. 48.)

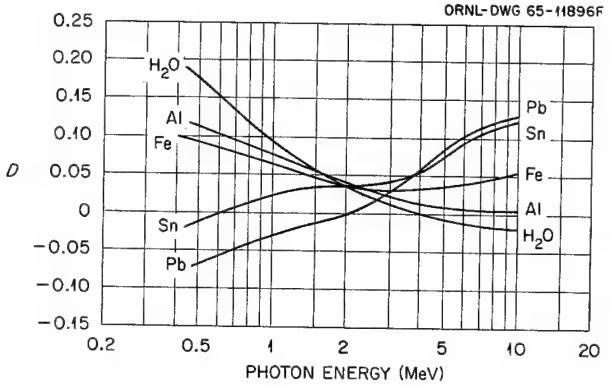

Fig. 3.3. The Coefficient D for the Berger Form of the Gamma-Ray Dose Buildup Factor. (From Chilton, ref. 48.)

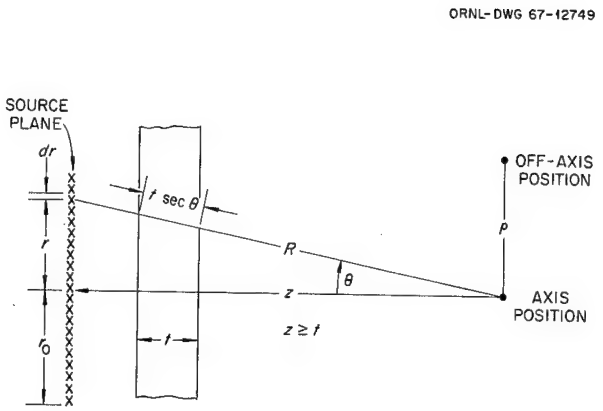

Fig. 3.4. Schematic of Disk Source.

terms, but it has the advantage of allowing separation of the variables dependent on the medium properties, geometry, and thickness.

Application of Point Kernels to Disk and Rectangular Sources

Sometimes solutions to shielding problems can be reasonably approximated from attenuation data for a disk or rectangular source and a slab shield. These simple plane source problems are amenable to analytic or numerical solution by integrating a point kernel of the form of Eq. 3.146 over the source area. The results when tabulated or plotted are directly usable in practical applications.

Disk Source. – Consider, for example, a detector shielded from a plane disk source that is uniformly emitting S photons cm^{-2} sec^{-1} isotropically in 4π steradians (see Fig. 3.4). Applying the point kernel as given by Eq. 3.146, the unscattered dose rate along the disk axis is

$$\Gamma(\mu t, r_0, z) = S\, G(E) \int_0^{r_0} \frac{e^{-\mu t \sec\theta}\,(2\pi r)\,dr}{4\pi R^2} . \qquad (3.156)$$

Since $R^2 = r^2 + z^2$, Eq. 3.156 can be transformed to

$$\Gamma(\mu t,\, z/r_0) = \frac{S\, G(E)}{2} \int_{\mu t}^{\mu t\sqrt{1+(r_0/z)^2}} \frac{e^{-y}}{y}\, dy , \qquad (3.157)$$

where $y \equiv \mu t \sec\theta$. When integrated, Eq. 3.157 becomes

$$\Gamma(\mu t, z/r_0) = \frac{S\, G(E)}{2} \times \left\{ E_1(\mu t) - E_1\left(\mu t \sqrt{1 + [r_0/z]^2}\right)\right\}, \qquad (3.158)$$

where E_1 is the exponential integral function* of the first order and is defined by

$$E_1(x) \equiv \int_x^{\infty} \frac{e^{-y}}{y}\, dy . \qquad (3.159)$$

[Equation 3.158, as well as the equations given below for computing uncollided doses, can be used to determine the total dose (uncollided + scattered) by using the Taylor form of the buildup factor (see Section 3.8.1).]

For the case of an isotropic flux $\Phi(0)$ at the source plane, which is equivalent to a current with a $\cos\theta$ angular distribution,** the unscattered dose is

$$\Gamma(\mu t, r_0, z) = \Phi(0)\, G(E) \int_0^{r_0} + \frac{e^{-\mu t \sec\theta} \cos\theta (2\pi r)\, dr}{4\pi R^2} , \qquad (3.160)$$

*Plots of this function are given in Appendix C.

**See Section 5.1.1 in Chapter 5 for a discussion of fluxes, currents, and sources.

which integrates to

$$\Gamma(\mu t, z/r_0) = \frac{\Phi(0)\, G(E)}{2} \left\{ E_2(\mu t) - \frac{1}{\sqrt{1 + (r_0/z)^2}}\, E_2(\mu t \sqrt{1 + [r_0/z]^2}) \right\}, \quad (3.161)$$

where E_2 is the exponential function of the second order.

The equivalent angular current $I(\theta)$ in the forward hemisphere is $[\Phi(0)/4\pi] \cos\theta$, defined as the number of photons per unit solid angle crossing a unit area on the source plane in the directions within the interval $-1 \leq \cos\theta \leq 1$ as measured normal to the source plane. Therefore

$$I(0) = \int_{\Omega/2} \frac{\Phi(0)}{4\pi} \cos\theta\, d\Omega = \int_0^1 \frac{\Phi(0)\cos\theta}{4\pi} 2\pi \times d(\cos\theta) = \frac{\Phi(0)}{4}. \quad (3.162)$$

If the current in the forward direction is used, $4I(0)$ must be substituted for $\Phi(0)$ in Eq. 3.161.

In general, for the $\cos^n\theta$ angular distribution in the forward direction,

$$\Phi(\theta) = \frac{(n+1)\,\Phi'(0)\cos^n\theta}{2\pi}, \quad (3.163)$$

where $\Phi'(0)$ is the total or scalar flux in the forward direction only, and

$$\Gamma(\mu t, z/r_0) = \frac{(n+1)\,\Phi(0)\,G(E)}{2} \left\{ E_{n+2}(\mu t) - \frac{E_{n+2}(\mu t \sqrt{1 + [r_0/z]^2})}{(\sqrt{1 + [r_0/z]^2})^{n+1}} \right\}. \quad (3.164)$$

For the off-axis position at a distance ρ measured perpendicularly to the disk axis (see Fig. 3.4), integrations must be done numerically. Hubbell *et al.*[50] integrated an expression similar to Eq. 3.156, the isotropic source case, for off-axis positions and tabulated the results in terms of the parameters μt, z/r_0, and ρ/r_0. These results are shown in Table 3D.1 of Appendix D. The quantity tabulated is $4\pi\Gamma(\mu t, z/r_0, \rho/r_0)/S\ G(E)$, which is the same as $4\pi\Phi^0(\rho/r_0)/S$, where $\Phi^0(\rho/r_0)$ is the uncollided flux at ρ/r_0.

In a similar manner Trubey[51] determined the data for an isotropic flux. The results are given in Table 3D.2 of Appendix D as $2\Gamma(\mu t, z/r_0, \rho/r_0)/\Phi(0)\ G(E)$, which is the same as $2\Phi^0/\Phi(0)$.

Certain circular aperture and disk source configurations to which these results might be applied are shown in Fig. 3.5.

Rectangular Sources. – A solution was developed by Hubbell *et al.*[52] for the uncollided flux a distance z from a plane isotropic rectangular source.* Expressed as the product of separable source and geometry functions, the uncollided flux is given by

$$\Phi^0(a,b) = \sum_{n=0}^{\infty} \frac{2n+1}{2}\, g_n\, p_n(a,b), \quad (3.165)$$

where g_n and $p_n(a,b)$ are Legendre coefficients of the source and geometry functions respectively.

If $a = H/z$ and $b = W/z$, where H and W are the height and width of the source plane (see Fig. 3.6), then Eq. 3.165 gives the flux at the corner position, that is, the flux at a distance z along the normal to the corner of the rectangular source. It follows that using the half-height and half-width gives one-fourth of the flux at z along a normal to the center of the source plane. The source function is

$$g_n = \int_{-1}^{1} g(\cos\theta)\, P_n(\cos\theta)\, d(\cos\theta), \quad (3.166)$$

where $g(\cos\theta)$ represents the angular flux at the source plane for the case of a slab shield of thickness t ($z \geq t$) located between the source and the detector at a distance z from the source; that is,

$$g(\mu t, \cos\theta) = \frac{S\, e^{-\mu t/\cos\theta}}{4\pi\cos\theta}. \quad (3.167)$$

Substituting Eq. 3.167 into Eq. 3.166, Hubbell *et al.* evaluated g_n and p_n numerically and solved Eq. 3.165. The results for a corner position ($a = H/z$, $b = W/z$) are given in Table 3D.3 of Appendix D as $4\Gamma/S\ G(E)$, or $4\Phi^0/S$, in terms of the parameters μt, a, and b.

---

*The application of the work of Hubbell *et al.* to rectangular ducts, which is the special case of a zero shield thickness, is described in Section 5.1.1 in Chapter 5.

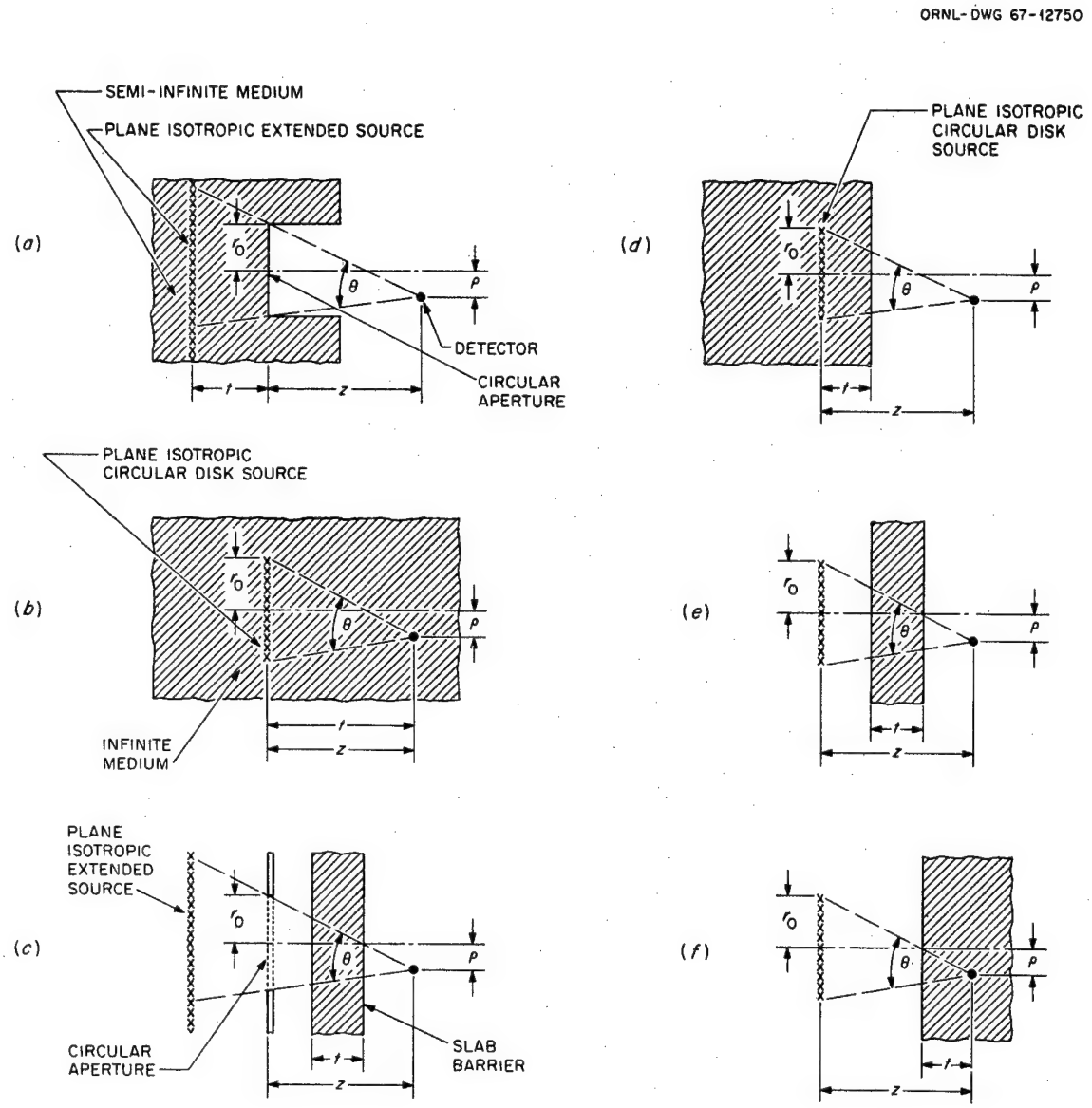

Fig. 3.5. Some Circular Aperture or Disk Source–Shield Configurations to Which Point Kernels Are Applicable. (From Hubbell *et al.*, ref. 50.)

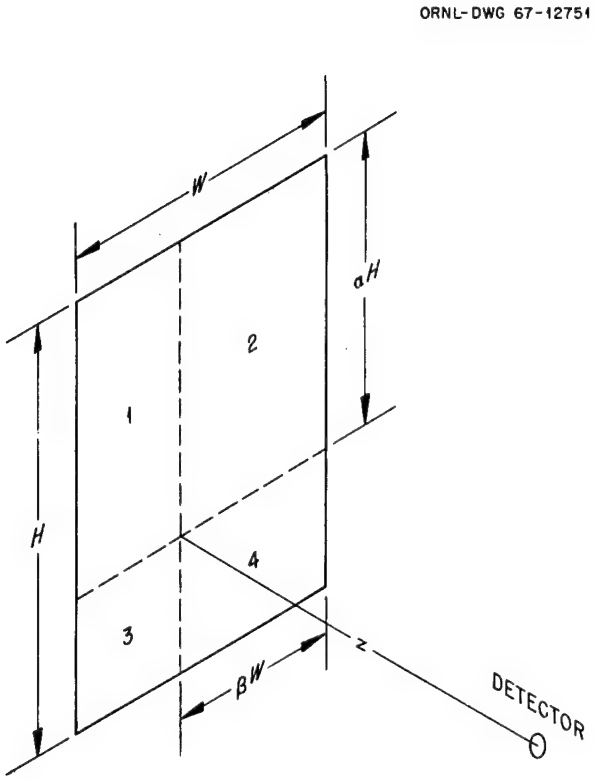

Fig. 3.6. Schematic Demonstrating Use of Corner Position of a Rectangular Source to Calculate Dose at an Arbitrary Position by Point Kernel Techniques.

In a similar manner Trubey[51] numerically evaluated the equivalent of Eq. 3.165 for an isotropic flux (cosine distribution of the angular current), that is, for

$$g(\mu t,\cos\theta) = \frac{\Phi(0)\, e^{-\mu t/\cos\theta}}{4\pi} \qquad (3.168)$$

These results for a corner position are given in Table 3D.4 of Appendix D as $2\Gamma/\Phi(0)$ $G(E)$, or $2\Phi^0/\Phi(0)$, which is the same quantity tabulated for the disk source in Table 3D.2. For the case of a square the dose will be slightly greater than that from a disk of radius W.

Although these results relate directly to the response of a detector in a corner position, they are also applicable to any arbitrary position lying within the projection of the source plane. It is obvious from Fig. 3.6 that the dose at the detector is

$$\Gamma(H/z,W/z) = \Gamma_1\left(\frac{\alpha H}{z}, \frac{[1-\beta]\,W}{z}\right) + \Gamma_2\left(\frac{\alpha H}{z}, \frac{\beta W}{z}\right) + \Gamma_3\left(\frac{[1-\alpha]\,H}{z}, \frac{[1-\beta]\,W}{z}\right) + \Gamma_4\left(\frac{[1-\alpha]\,H}{z}, \frac{\beta W}{z}\right). \qquad (3.169)$$

3.8.2. NEUTRON CALCULATIONS

The use of buildup factors in the attenuation function, or kernel, for neutrons has not developed to a large extent, primarily because neutron interactions are much more complex than gamma-ray interactions, and consequently the uncollided neutron flux is not as easily determined as the uncollided gamma-ray flux. However, a simple kernel developed by Albert and Welton[53] which uses an energy-dependent hydrogen cross section has been widely applied to hydrogenous shields. This section is devoted primarily to a description of the Albert-Welton kernel, together with a discussion of removal cross sections that are required in the kernel when other shield materials are used in conjunction with the hydrogenous medium.

Other kernels that can be used to calculate differential energy spectra of neutrons in hydrogenous media can be developed from moments method or Monte Carlo calculations. For example, the moments method code RENUPAK was used[51] to calculate the differential energy flux as a function of distance from a point fission source in an infinite medium of lithium hydride, and an empirical attenuation function based on the results was then incorporated in the point kernel code QAD (ref. 54) for use in space reactor shield designs. Because these kernels require large efforts to develop and have limited applicability, the method is not widely used. However, simple neutron dose attenuation functions determined from such calculations can be used for preliminary shield design applications, and some of these functions for concrete and several other materials are included in this section.

Removal Cross Sections

Measurements in the Oak Ridge National Laboratory Lid Tank Shielding Facility[55] showed that the insertion of relatively thin slabs of material

between a fission source and a thick water shield gives an effect which can be correlated by a simple exponential attenuation factor that is characteristic of absorption processes alone. This behavior might not be expected since nonabsorption effects predominate in fast-neutron attenuation. However, the large thickness of water filters out the neutrons deflected by the sample, thereby effecting their complete removal. Therefore the effect of slabs of shield materials when followed by large thicknesses of hydrogenous material can be described by an equivalent absorption cross section, called the "removal cross section."

An ideal way to experimentally determine the validity of the concept would be to use a plane monodirectional source of fission neutrons incident on a tank of water. For such a configuration the removal cross-section concept would be valid if the doses measured at the source distance z in water could be correlated by

$$D_2(z) = D_1(z)\, e^{-\Sigma_R t}, \qquad (3.170)$$

where

$D_1(z)$ = observed neutron dose attenuated through a distance z of water,

$D_2(z)$ = observed neutron dose attenuated through a slab of material of thickness t (inserted between source and water) plus water of thickness z,

Σ_R = macroscopic removal cross section.

In the actual experimental shielding facility where this concept was originally tested, the source was a finite isotropic disk rather than a plane monodirectional source. However, by making a few simple assumptions about the behavior of neutron penetration, an analog to Eq. 3.170 was derived and used in obtaining removal cross sections from experimental data.[56]

Values of microscopic removal cross sections (σ_R) determined from measurements at the ORNL Lid Tank Shielding Facility for several elements and compounds are shown in Table 3.3. Empirical functions useful for interpolation in the experimental data have been derived by Zoller:[57]

$$\Sigma_R/\rho = 0.19Z^{-0.743}\ \text{cm}^2/\text{g}, \text{ for } Z \leqq 8,$$
$$= 0.125Z^{-0.565}\ \text{cm}^2/\text{g}, \text{ for } Z > 8; \qquad (3.171)$$

$$\Sigma_R/\rho = 0.206A^{-1/3}\, Z^{-0.294} \approx 0.206\,(AZ)^{-1/3}, \qquad (3.172)$$

Table 3.3. Microscopic Removal Cross Sections of Various Elements and Compounds Measured at the ORNL Lid Tank Shielding Facility[a,b]

Material	σ_R (barns/atom)
Aluminum	1.31 ± 0.05
Beryllium	1.07 ± 0.06
Bismuth	3.49 ± 0.35
Boron[c]	0.97 ± 0.10
Carbon	0.81 ± 0.05
Chlorine[c]	1.2 ± 0.8
Copper	2.04 ± 0.11
Fluorine[c]	1.29 ± 0.06
Iron	1.98 ± 0.08
Lead	3.53 ± 0.30
Lithium	1.01 ± 0.05
Nickel	1.89 ± 0.10
Oxygen[c]	0.99 ± 0.10
Tungsten	3.36[d]
Zirconium	2.36 ± 0.12[e]
Uranium	3.6 ± 0.4
Boric oxide, B_2O_3	4.30 ± 0.41
Boron carbide, B_4C	4.7 ± 0.3[f]
Fluorothene, C_2F_3Cl	6.66 ± 0.8
Heavy water, D_2O	2.76 ± 0.11
Hevimet (90 wt % W, 6 wt % Ni, 4 wt % Cu)	3.22 ± 0.18
Lithium fluoride, LiF	2.43 ± 0.34
Oil, CH_2	2.84 ± 0.11
Paraffin, $C_{30}H_{62}$	80.5 ± 5.2
Perfluoroheptane, C_7F_{16}	26.3 ± 0.8

[a] Except where noted these values were taken from G. T. Chapman and C. L. Storrs, *Effective Neutron Removal Cross Sections for Shielding*, Oak Ridge National Laboratory Report ORNL-1843 (Sept. 19, 1955), AECD-3978 (Dec. 2, 1955).

[b] A measurement not included here yielded a removal cross-section value of 0.036 ± 0.002 cm^2/g for concrete. [From E. P. Blizard and J. M. Miller, *Radiation Attenuation Characteristics of Structural Concrete*, Oak Ridge National Laboratory Report ORNL-2913 (Aug. 13, 1958).]

[c] Cross-section value determined from measurements behind compounds of the elements.

[d] Weighted average of two values, 3.5 ± 0.2 and 3.13 ± 0.25 barns/atom. [From P. B. Hemmig in *Second Semi-annual ANP Shielding Information Meeting, November 14–15, 1956*, Convair Report NARF-56-41T (Vol. 4) (classified); and J. M. Miller in *Applied Nuclear Phys. Div. Ann. Prog. Rept. Sept. 1, 1957*, Oak Ridge National Laboratory Report ORNL-2389, p. 187.]

[e] From J. M. Miller in *Neutron Phys. Div. Ann. Prog. Rept. Sept. 1, 1959*, Oak Ridge National Laboratory Report ORNL-2842, p. 168.

[f] Average of two reported values, 4.3 ± 0.4 and 5.1 ± 0.4 barns/atom.

where Z is the atomic number. Most of the macroscopic removal cross sections given in Table 3.4 were obtained with Eq. 3.171.

It is emphasized that most of the removal cross sections determined by experiment were obtained for a slab-type configuration with water following the shield material and may not be applicable to other configurations. It has been demonstrated, for example, that in a homogeneous medium the removal cross section for oxygen[58] is (0.75 ± 0.05) barn rather than (0.99 ± 0.10) barn as shown in Table 3.3. It is also pointed out that the removal cross section may vary with sample thickness (the value for oxygen[59] obtained from the homogeneous-medium measurements increased from 0.72 barn at a distance 90 cm from the source to 0.79 barn at a distance 140 cm from the source). There is really no reason to expect the removal cross section to remain constant with sample thickness since the removal concept is the result of a crude application of theoretical principles; however, the variation should not be very great up to about 5 relaxation lengths. Another point that should be emphasized is that the removal cross section for a material can be applied only when that material is used in conjunction with a hydrogenous shield since hydrogen is required to moderate and absorb the scattered neutrons, as occurred in the experiments from which the removal cross sections were determined.

It follows from the removal cross-section concept that the removal cross sections of elements in a series of slabs or mixed together should be additive; that is, the number of relaxation lengths becomes

$$\sum_i \Sigma_{R_i} t_i ,$$

where the index i refers to the various elements. This additive property has been generally accepted, even though some discrepancies have been noted, particularly in regard to compounds.

Removal cross sections can be predicted by theory. Phenomenologically, the removal process can be considered equivalent to the total reaction rate minus the forward component of the scattering process. This suggests that an estimate of the removal cross section could be obtained from the transport cross section. As it turns out, $\Sigma_R \cong \Sigma_{tr}$ for neutrons between 6 and 8 MeV; therefore

$$\Sigma_R = \Sigma_{tr} = \Sigma_t - \Sigma_s \overline{\cos}\,\theta . \qquad (3.173)$$

Removal cross sections may also be estimated from

$$\Sigma_R \cong \frac{2}{3}\Sigma_t , \qquad (3.174)$$

where Σ_t is the average total macroscopic cross section between 6 and 8 MeV, and from

$$\Sigma_R/\rho = 0.21\, A^{-0.58} \qquad (3.175)$$

where ρ is the density and A is the atomic weight. Figure 3.7 compares plots of measured values of Σ_R/ρ and Σ_t/ρ at 8 MeV as a function of atomic weight. It can be seen that a reasonably good fit to the curve for $A > 10$ is obtained by Eq. 3.175.

Albert-Welton Kernel

The experimentally determined removal cross section provides a simple method for determining the attenuation through nonhydrogenous portions of shield material, but cannot be applied to the hydrogenous portion of the shield. Albert and Welton[53] developed a semi-empirical theory of neutron attenuation which provides a simple method for calculating neutron attenuation through the complete shield, providing the shield contains hydrogen. Basic to the Albert-Welton model is the assumption that any collision with hydrogen has the effect of an absorption. This, in effect, neglects the buildup of scattered neutrons which have undergone only small-angle scatterings by hydrogen. Inelastic scatterings with heavier nuclei are also regarded as absorptions because of the characteristically large energy loss. Other collisions are mainly small-angle elastic scatterings within the forward peak of the angular distribution, which amount to virtually no collisions. Attenuation through the materials in the shield are described in terms of removal cross sections. For hydrogen the removal cross section is taken to be its energy-dependent total cross section, and for the heavier nuclides it is taken to be an empirical energy-independent removal cross section such as the removal cross sections described in the preceding paragraphs. Thus the Albert-Welton model provides a theoretical basis for the removal cross-section concept.

The Albert-Welton formulation for fission neutrons from a plane monodirectional source that

penetrate through a mixture of water and heavy materials is given by

$$\Phi(r) \propto \exp\left(-\sum_i f_i \Sigma_{R_i} r\right) \times \int_0^\infty S(E)\, e^{-\Sigma_H(E) r}\, dE\,, \quad (3.176)$$

where

$\Phi(r)$ = number flux at a distance r from the source,

Σ_{R_i} = macroscopic removal cross section of ith element (other than hydrogen),

f_i = volume fraction of ith nonhydrogenous material,

$S(E)\,dE$ = fraction of fission neutrons at E in interval dE for a total source of 1 fission cm^{-2} sec^{-1},

Σ_H = total macroscopic cross section for hydrogen.

Table 3.4. Fast-Neutron Removal Cross Sections and Mass Attenuation Coefficients[a]

Element	Atomic Number	ρ (g/cm^3)	Σ_R/ρ (Calc.) (cm^2/g)	Σ_R (cm^{-1})	Σ_R/ρ (Exp.) (cm^2/g)
Aluminum	13	2.699	0.0293	0.0792	0.0292 ± 0.0012
Antimony	51	6.691	0.0136	0.0907	
Argon	18		0.0244		
Arsenic	33	5.730	0.0173	0.0993	
Barium	56	3.500	0.0129	0.0450	
Beryllium	4	9.013	0.0678	0.1248	0.0717 ± 0.0043
Bismuth	83	9.747	0.0103	0.1003	0.010 ± 0.0010
Boron	5	3.330	0.0575	0.1914	0.0540 ± 0.0054
Bromine	35	3.120	0.0168	0.0523	
Cadmium	48	8.648	0.0140	0.1213	
Calcium	20	1.540	0.0230	0.0354	
Carbon	6	1.670	0.0502	0.0838	0.0407 ± 0.0024
Cerium	58	6.900	0.0126	0.0870	
Cesium	55	1.873	0.0130	0.0243	
Chlorine	17		0.0252		0.020 ± 0.014
Chromium	24	6.920	0.0208	0.1436	
Cobalt	27	8.900	0.0194	0.1728	
Copper	29	8.940	0.0186	0.1667	0.0194 ± 0.0011
Dysprosium	66	8.562	0.0117	0.1003	
Erbium	68	4.770	0.0115	0.0550	
Europium	63	5.166	0.0120	0.0621	
Fluorine	9		0.0361		0.0409 ± 0.0020
Gadolinium	64	7.868	0.0119	0.0938	
Gallium	31	5.903	0.0180	0.1060	
Germanium	32	5.460	0.0176	0.0963	
Gold	79	19.320	0.0106	0.2045	
Hafnium	72	13.300	0.0112	0.1484	
Helium	2		0.1135		
Holmium	67		0.0116		
Indium	49	7.280	0.0139	0.1009	
Iodine	53	4.930	0.0133	0.0654	
Iridium	77	22.420	0.0107	0.2408	
Iron	26	7.865	0.0198	0.1560	0.0214 ± 0.0009
Krypton	36		0.0165		
Lanthanum	57	6.150	0.0127	0.0783	
Lead	82	11.347	0.0104	0.1176	0.0103 ± 0.0009
Lithium	3	0.534	0.0840	0.0449	0.094 ± 0.007
Lutetium	71		0.0112		
Magnesium	12	1.741	0.0307	0.0535	
Manganese	25	7.420	0.0203	0.1505	
Mercury	80	13.546	0.0105	0.1424	
Molybdenum	42	10.200	0.0151	0.1543	
Neodymium	60	6.960	0.0124	0.0861	
Neon	10		0.0340		
Nickel	28	8.900	0.0190	0.1693	0.0190 ± 0.0010
Niobium	41	8.400	0.0153	0.1288	
Nitrogen	7		0.0448		
Osmium	76	22.480	0.0108	0.2432	
Oxygen	8		0.0405		0.031 ± 0.002
Palladium	46	12.160	0.0144	0.1747	
Phosphorus	15	1.820	0.0271	0.0493	
Platinum	78	21.370	0.0107	0.2279	
Potassium	19	6.475	0.0237	0.1533	
Praseodymium	59	6.500	0.0125	0.0812	
Radium	88	5.000	0.0100	0.0498	
Rhenium	75	20.530	0.0109	0.2238	
Rhodium	45	12.440	0.0145	0.1810	
Rubidium	37	1.532	0.0163	0.0249	
Ruthenium	44	12.060	0.0147	0.1777	
Samarium	62	7.750	0.0121	0.0941	
Scandium	21	3.020	0.0224	0.0676	
Selenium	34	4.800	0.0170	0.0818	
Silicon	14	2.420	0.0281	0.0681	
Silver	47	10.503	0.0142	0.1491	
Sodium	11	0.971	0.0322	0.0313	
Stronium	38	2.540	0.0160	0.0407	
Sulfur	16	2.070	0.0261	0.0540	
Tantalum	73	16.600	0.0111	0.1838	
Tellurium	52	6.240	0.0134	0.0837	
Terbium	65		0.0118		
Thallium	81	11.860	0.0104	0.1238	
Thorium	90	11.300	0.0098	0.1111	
Thulium	69		0.0114		
Tin	50	6.550	0.0137	0.0898	
Titanium	22	4.500	0.0218	0.0981	
Tungsten	74	19.300	0.0110	0.2120	0.0082 ± 0.0018
Uranium	92	18.700	0.0097	0.1816	0.0091 ± 0.0010
Vanadium	23	5.960	0.0213	0.1267	
Xenon	54		0.0131		
Ytterbium	70		0.0113		
Yttrium	39	3.800	0.0158	0.0599	
Zinc	30	7.140	0.0183	0.1306	
Zirconium	40	6.440	0.0156	0.1001	

[a]Table taken from L. K. Zoller, "Fast-Neutron-Removal Cross Sections," *Nucleonics* 22(8), 128–129 (1964).

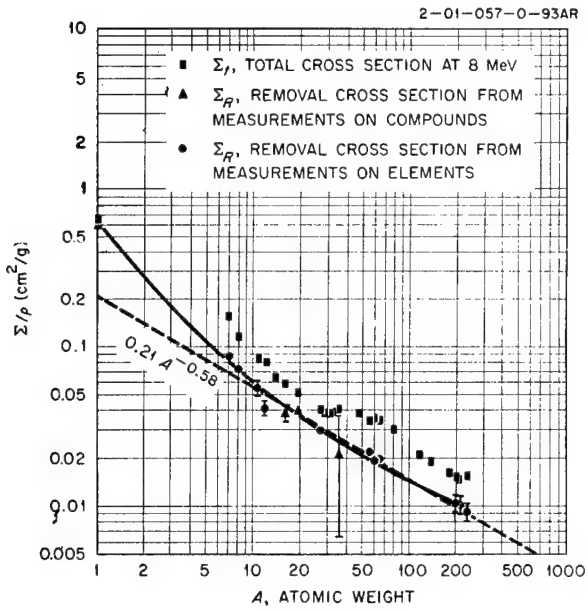

Fig. 3.7. Removal Cross Sections per Unit Mass for Fission Neutrons as a Function of Atomic Weight. (From Chapman and Storrs, ref. 55.)

The proportionality constant included in the original Albert-Welton derivation has been removed from the inequality 3.176 to avoid the implication that the actual number flux can be computed from this.

Integration of the inequality 3.176 yields the original Albert-Welton kernel for the hydrogenous portion of the shield, which is included in the brackets of the following equation:

$$\Phi(r) \propto \left[(f_w r)^{0.29}\, e^{-0.928(f_w r)^{0.58}}\right] \times \exp\left[-f_w r\Sigma_{RO} - (1-f_w) r \sum_i f_i \Sigma_{Ri}\right], \quad (3.177)$$

where

f_w = volume fraction of water,
Σ_{RO} = removal cross section of oxygen,
Σ_{R_i} = removal cross section of nonhydrogenous materials other than the oxygen in the water.

Although the derivation was for a plane source, Eq. 3.177 holds for a point source when multiplied by the geometric factor $1/4\pi r^2$ and the integral of $S(E)$ is normalized to 1 fission/sec. The equation is also valid when slabs of heavy material are laminated with the water. A minimum of about 50 or 60 cm of water is required between the dose point and the last of the heavy materials (whether as slabs or in a mixture) in order to comply with the limitations of the removal cross-section concept.

Based on more recent experimental results, Casper[60] evaluated new constants for the Albert-Welton kernel. The result for a point fission spectrum source is

$$4\pi r^2\, D(r) = 2.78 \times 10^{-5} \left[(f_w r)^{0.349} \times e^{-0.422(f_w r)^{0.58}}\right] e^{-0.0308 f_w r}, \quad (3.178)$$

where $D(r)$ is the neutron dose r cm from the source in (rads/hr)/(neutron/sec). When shield materials are inserted between the water and the fission source, Eq. 3.178 is multiplied by

$$\cdot \exp\left[-(1-f_w) \sum_i \Sigma_{R_i} f_i\right]$$

to obtain the dose at the shield surface.

The Albert-Welton kernel is especially useful in the following two applications:

1. It can be used to correct measured or calculated data when small changes are made in the heavy elements of a shield. For example, suppose that a lead layer and a water layer surround a point source. If the lead layer is increased and the water thickness remains the same, the new dose rate will be given by

$$4\pi r_2^2\, D(r_2) = 4\pi r_1^2\, D_1(r_1)\, e^{-\Sigma_R t}, \quad (3.179)$$

where

Σ_R = removal cross section for lead,
t = change in lead thickness = $r_1 + t$,
r_2 = new distance from source,
$D(r_2)$ = new dose rate,
r_1 = original distance,
$D(r_1)$ = original dose rate.

It will be noticed that the assumption is made that the water thickness (and its effect) remains unchanged. Consequently, the dose rates are evaluated at different positions.

2. It can be used to correct results obtained for one hydrogenous medium so that they apply for

another hydrogenous medium. The basic assumption is that the hydrogen effect remains constant for a given "hydrogen length," with the effects of other elements accounted for on the basis of removal cross sections. Thus the hydrogen attenuation kernel in one medium is set equal to the hydrogen attenuation in the other, giving

$$4\pi r_2^2 D(r_2) e^{\Sigma_{R_2} r_2} = 4\pi r_1^2 D_1(r_1) e^{\Sigma_{R_1} r_1} , \quad (3.180)$$

with the constraint, to ensure the equivalence of the hydrogen effect, of

$$\rho_2 r_2 = \rho_1 r_1 , \quad (3.181)$$

where

ρ_2 = hydrogen density in medium for which $D(r_2)$ is unknown,
ρ_1 = hydrogen density in reference medium for which $D(r_1)$ is known,
Σ_{R_2} = removal cross section for all elements except hydrogen in the medium being analyzed,
Σ_{R_1} = removal cross section for all elements except hydrogen in the reference medium.

Combining the above equations yields

$$D(r_2) = D_1(\rho_2 r_2 / \rho_1) [\rho_2/\rho_1]^2 \times \exp\left(\Sigma_{R_1} \frac{\rho_2 r_2}{\rho_1} - \Sigma_R r_2\right) . \quad (3.182)$$

A word of caution is appropriate here. The above equations represent a simple model of rather complex phenomena, and rather large errors are possible.

Attenuation Kernels from Monte Carlo Calculations

Results from Monte Carlo calculations (or from other sophisticated methods) for dose transmission through slab shields with an incident beam of neutrons can be quite useful when expressed in terms of attenuation kernels, that is, as plots of transmission factors or dose attenuation as a function of slab thickness. With such graphs it is a simple matter to estimate the fraction of the dose that is transmitted for each incident energy group of neutrons, the total dose being the sum of the doses from all energy groups.

Clark *et al.*[61] performed Monte Carlo calculations for monoenergetic beams of neutrons normally incident on slabs of ordinary concrete and also on a semi-infinite medium (half-space) of concrete. The neutron energies were 0.7, 1.2, 2, 3, 4, 6, 8, 10, 12, and 14 MeV. The density of the concrete was assumed to be 2.43 g/cm^3, and its composition, other than its water content, was representative of that given for ordinary concrete 01 in ANL-5800 (ref. 62). The resulting dose attenuation curves are shown in Figs. 3E.1 through 3E.10 in Appendix E.

In addition to being useful directly, these results can be helpful in adjusting the large body

Table 3.5. Compositions of Materials Used for Neutron Transmission Calculations[a]

Material	Density (g/cm^3)	Composition	
		Element	Atoms/cm^3
			$\times 10^{21}$
Borated polyethylene (8 wt % B_4C)[b]	0.97	H	76.80
		C	39.20
		^{10}B	0.658
		^{11}B	2.67
Water	1.00	H	66.90
		O	33.45
Concrete	2.26	H	13.75
		O	45.87
		Al	1.743
		Si	20.15
Nevada Test Site soil (dry)	1.15	H	8.553
		O	22.68
		Al	2.014
		Si	9.533
Nevada Test Site soil (100% saturated)	1.25	H	16.87
		O	27.00
		Al	1.976
		Si	8.963

[a]Table taken from F. J. Allen and A. T. Futterer, "Neutron Transmission Data," *Nucleonics* 21(8), 120 (1963).

[b]Several calculations made for pure polyethylene slabs (ρ = 0.925 g/cm^3) up to 6 in. thick yielded approximately the same neutron transmission results as those for the borated polyethylene.

of neutron attenuation data[63] that have been obtained for an infinite concrete medium so that the infinite-medium data can be applied to finite systems. This results from the fact that after 1 or 2 relaxation lengths the penetrating characteristics of neutrons in an infinite medium of concrete should differ very little from those of neutrons in a semi-infinite medium. Therefore such data, which in all other respects appear to be appropriate for application to a particular situation, might be fairly well adapted to a finite system by correcting the data in proportion to the ratio of the curve for the semi-infinite medium (dashed curve) to the curve for the slab configuration (solid curve) at the proper penetration distance and energy.

Other useful results were calculated by Allen and Futterer,[64] who determined the attenuation of the multicollision dose in the materials listed in Table 3.5 due to monoenergetic neutron beams incident at various angles. The neutron energies used were 5, 3, 2, 1, and 0.5 MeV, and the results are plotted in Figs. 3E.11 through 3E.15 in Appendix E. In order to use these curves, the multicollision dose (rate) must be known at the inner surface of a slab of one of these materials due to neutrons incident in a broad beam at an angle (or angle band) and energy (or energy band) close to the angle and energy for which the attenuation data are given. The attenuation factor appropriate to the material, thickness, energy, and angle is read from the curve, and the incident dose multiplied by that factor should approximate the dose that has penetrated the slab.

3.9 Combination Removal-Diffusion Methods

The removal cross-section concept described in Section 3.8.2 provides a method for calculating the dose due to high-energy neutrons that penetrate a hydrogenous shield; however, the technique cannot be used to predict the dose due to neutrons that have been moderated to epithermal and thermal energies or to predict the thermal-neutron flux, which is used to obtain the capture gamma-ray source distribution within the shield.*

The energy and spatial distributions of the moderated neutrons throughout a shield have sometimes been calculated by using the elementary theories of neutron diffusion and moderation (see Section 3.6). But these methods of reactor physics are normally used to predict the average behavior of neutrons involved in reactor criticality problems, and in the typical shielding problem the neutron of significance is the unusual fission neutron, born with an energy much greater than the average and contributing very little to reactor criticality. It is this unusual neutron that penetrates into regions deep within the shield.

The inadequacy of both the removal concept and the elementary methods of reactor core physics to calculate the whole shielding problem has resulted in neutron transport being regarded as a two-step process: a step in which a high-energy neutron penetrates to a position deep within the shield, where it suffers a collision that degrades its energy significantly; and another step in which the resulting low-energy neutron enters a diffusion process. Characteristically, the distance traveled by the neutron during the diffusion process is very much less than that which it traveled as a fast neutron, and once it has entered this second phase, the methods of reactor physics conceivably could apply. It was such reasoning that prompted the first-flight correction to the age in Fermi age theory.[1] This correction was necessary because a neutron cannot enter a process described as continuous slowing down (as required by Fermi age theory) until it has had at least one collision.

The development of high-speed computers and the resulting extensive use of multigroup diffusion theory for reactor criticality problems made the development of a technique that utilized diffusion theory even more attractive. In one of the first

*Calculations of capture gamma-ray doses are discussed in Section 3.10.

attempts to develop such a technique, Haffner[65] in 1958 used diffusion theory to calculate thermal-neutron fluxes within a reactor shield and then normalized the results at each space point according to the fast-neutron dose rate obtained with the Albert-Welton kernel (see Section 3.8.2). Anderson and Shure[66] used a similar technique when they applied a known pure water kernel to normalize diffusion (actually P_1 multigroup) results for a metal-water mixture. In general, they obtained good results for laminated iron-water shields. (Shure[2,67] later showed that a straightforward P_3 calculation without the use of a kernel also gave good results.) The main assumption in the Anderson-Shure technique is that the multigroup procedure correctly calculates the ratio between the fluxes in water and those in a metal-water mixture.

After several attempts had been made to develop a technique by correcting diffusion theory results, a different approach to the problem evolved: a first-flight correction was made *before* the diffusion theory calculation was performed. In the early calculations this was done by computing the singly scattered neutron flux from the uncollided flux and then using it as a source for the diffusion theory calculation. A difficulty inherent in this procedure, especially for hydrogenous media, is that the penetrating component does not consist of uncollided neutrons alone, but rather is composed largely of neutrons that have had one or more collisions but have suffered only small angular deflections. When these neutrons were accounted for, the first successful two-step model for neutron-penetration calculations became available. Combining the fast-neutron removal concept and age-diffusion theory, the method is commonly referred to as the "Spinney method," after its chief developer. The remainder of this section is devoted to a description of the original version of this removal-age-diffusion method and subsequent variations of it.

3.9.1. THE SPINNEY METHOD

The Spinney method as first described by Avery *et al.*[68] is characterized by the following basic physical assumptions:

1. The penetrating component of the source neutrons consists of the high-energy neutrons that suffer only small energy loss through small-angle elastic collisions plus the uncollided neutrons.

2. Neutrons that suffer large energy loss through either wide-angle elastic or inelastic scattering are regarded as being removed from the fast beam.

3. The removed neutrons are degraded in energy in accordance with age theory and do not travel significantly from the point of removal.

4. The removed neutrons have a spectral and spatial distribution closely described by the conventional age-diffusion theory near the source.

5. Neutrons removed after they have penetrated deep into a homogeneous medium develop an equilibrium spectrum and are attenuated at the same rate that the penetrating component is attenuated.

6. The equilibrium spectrum of the degraded neutrons is disturbed near the boundaries between dissimilar media.

The neutron flux that corresponds to the penetrating component of the source neutrons is given by the kernel

$$\Phi^0(r) = \frac{S_0 e^{-\Sigma_R r}}{4\pi r^2} \qquad (3.183)$$

where

S_0 = source strength of high-energy neutrons of energy E,

Σ_R = removal cross section evaluated at the source energy E (determined experimentally or approximated by the transport cross section),*

r = distance traveled by the neutron to its first collision.

The removed neutrons are regarded as a local source of degraded neutrons, the behavior of which can be adequately described by diffusion theory. The intensity of this source is given by

$$S(r) = \Phi^0(r)\,\Sigma_R = \frac{S_0 \Sigma_R e^{-\Sigma_R r}}{4\pi r^2}. \qquad (3.184)$$

These neutrons (that is, the removed neutrons) are then introduced into the highest energy group of an appropriate set of multigroup diffusion equations in order to calculate the distribution of the

*See Section 3.8.

low-energy neutron flux. The equations comprising the multigroup set are given by

$$\nabla^2 \Phi_1(r) - k_1^2 \Phi_1(r) - \frac{\Sigma_{a1}}{D_1} \Phi_1(r) + \frac{S(r)}{D_1} = 0, \qquad i = 1 ,$$

$$\nabla^2 \Phi_i(r) = k_i^2 \Phi_i(r) - \frac{\Sigma_{ai}}{D_i} \Phi_i(r) + \frac{D_{i-1}\, k_{i-1}^2\, \Phi_{i-1}(r)}{D_i} = 0, \qquad i > 1 , \quad (3.185)$$

where

Φ_i = group flux for the ith group,

Σ_{ai} = group-averaged macroscopic absorption cross section,

D_i = group-averaged diffusion coefficient,

k_i^{-1} = slowing-down length for the ith group.

The slowing-down length is calculated according to age theory and for the ith group is given by

$$\left(\frac{1}{k_i}\right)^2 = \int_{E_{i-1}}^{E_i} \frac{dE}{3\, \xi(E)\, \Sigma_s(E)\, \Sigma_{tr}(E)\, E} , \quad (3.186)$$

where

$\xi(E)$ = average change in lethargy per collision for neutrons of energy E,

$\Sigma_s(E)$ = macroscopic scattering cross section for neutrons of energy E,

$\Sigma_{tr}(E)$ = macroscopic transport cross section for neutrons of energy E.

In the original formulation of the Spinney method, five energy groups were taken for the multigroup diffusion calculation. The bottom group, which was a thermal group, had an upper energy of 2.81 kT ($k = 8.61 \times 10^{-5}$ eV/°K), and the highest group ($i = 1$) had an upper energy of 2 MeV. It was assumed that all removed source neutrons were placed directly into the highest group. Solution of the group diffusion equations, of course, required that boundary conditions be specified at the inner and outer surfaces of the shield. A zero reentrant condition was imposed at the outer boundary; this was stated in terms of the extrapolated boundary condition, which requires the fluxes to vanish at a distance $3.13D_i$ beyond the physical boundary. The boundary conditions at the inner surface of the shield were established by requiring that the fluxes and currents be equal to those determined from reactor core calculations.

This original formulation was used with some success to predict the distribution of low-energy neutrons in concrete shields for existing graphite-moderated reactors, but it was not suited for general application. Some of its inadequacies were that (1) all the removed neutrons were placed in one group, which neglected any additional diffusion-type transport that could have been accomplished at energies greater than 2 MeV, (2) not enough groups were used to adequately represent the continuous slowing-down process, and (3) the transfer of neutrons from one energy group to the next lower group did not describe the large energy losses experienced by neutrons that had suffered an inelastic scattering or a collision with hydrogen.

3.9.2. MODERN VARIATIONS OF THE SPINNEY METHOD

Many modifications to and variations of the Spinney method have been developed, the most recent of which are exemplified by the RASH E, MAC, and NRN codes. In the RASH E* formulation[69,70] the modifications include an increase in the number of groups to 16 and a broader energy range (0–10 MeV). Also, the multigroup equations have been modified to include a direct source of removed neutrons into the nine highest energy groups. The equations so modified are as follows:

$$\nabla^2 \Phi_1(r) - k_1^2 \Phi_1(r) - \frac{\Sigma_{a1}}{D_1} \Phi_1(r) + \frac{\psi_1(r)}{D_1} = 0, \qquad i = 1 ,$$

$$\nabla^2 \Phi_i(r) - k_i^2 \Phi_i(r) - \frac{\Sigma_{ai}}{D_i} \Phi_i(r) + \frac{D_{i-1}\, k_{i-1}^2}{D_i} \Phi_{i-1}(r) + \frac{\psi_i(r)}{D_i} = 0, \qquad i = 2, 3, \ldots 9 ,$$

*RASH E is the latest member of the RASH family of codes utilizing the Spinney method. RASH E is included in a FORTRAN code package known as COMPRASH and can be obtained from the Radiation Shielding Information Center (RSIC) (see Appendix 3A).

$$\nabla^2 \Phi_i(r) - k_i^2 \Phi_i(r) - \frac{\Sigma_{ai}}{D_i}\Phi_i(r) + \frac{D_{i-1} k_{i-1}^2}{D_i} \Phi_{i-1}(r) = 0, \quad i = 10, 11, \ldots 15 ,$$

$$\nabla^2 \Phi_T(r) - \frac{\Sigma_a^T}{D_T} \Phi_T(r) + \frac{D_{15} k_{15}^2}{D_T} \Phi_{15}(r) = 0, \quad i = 16 , \quad (3.187)$$

where T corresponds to $i = 16$ and designates the thermal group flux.

The source term for the ith group resulting from removed neutrons is designated as $\psi_i(r)$ and is determined in the following manner. The fission spectrum is divided into 18 energy bands of 1-MeV width. Neutrons removed from the jth energy band are given by

$$S_j(r) = S_0 \int_{E_j}^{E_{j+1}} \frac{F(E)\, \Sigma_R(E)\, e^{-\Sigma_R(E) r}}{4\pi r^2} dE, \quad j = 1, 2, \ldots 18 , \quad (3.188)$$

where S_0 is a magnitude factor determined by the power level of the reactor, and $F(E)$ is the normalized fission spectrum.

The neutrons from each of the removal bands in the energy range 0 to 8 MeV (j = 18, 17, 16, ... 11) are introduced into the energy group whose upper energy limit corresponds to the mid-energy of the band. Neutrons from all the bands above 8 MeV (j = 10, 4, 8, ... 1) have a mean energy of about 10 MeV and are all introduced into the highest energy group (group 1), which has an upper energy of 10.5 MeV. This transfer scheme, along with the removal-band and energy-group structures for RASH E, is presented in Table 3.6.

In the MAC* formulation[71,72] the number of energy groups for the group-diffusion calculation is increased to 31 over an energy range from 0 to 10 MeV. Again the fission spectrum is divided into 18 removal bands of 1-MeV width. The flux from the removed neutrons (usually called "removal flux") corresponding to the gth removal band, which is introduced into the ith energy group, is given by

$$\Phi_{gi}^0 = S_0 \int_{E_g}^{E_{g+1}} \frac{F(E)\, e^{-\Sigma_R(E) r}}{4\pi r^2} dE . \quad (3.189)$$

The removed neutrons are introduced into the five highest energy groups only. The transfer scheme, along with the removal-band and energy-group structures, is presented in Table 3.7.

The MAC formulation differs from the original Spinney method in two major respects: (1) the removal flux is added directly to the group-diffusion flux after the diffusion calculation has been performed, and the combined flux is then used to calculate source neutrons for the lower-energy groups, and (2) the general treatment of the downscatter transfer of neutrons allows for a more accurate representation of inelastic scattering and collisions with hydrogen.

The highest energy group (i = 1) in the diffusion part of the calculation is not actually treated as a diffusion group. The collision density,

$$\Sigma_{1k} \left[\sum_{g=1}^{12} \Phi_{g1}^0(\bar{r}) \right],$$

which is based on the removal fluxes (corresponding to the energy bands 1 through 12), provides neutrons by downscattering from the first group into the kth group, k = 2, 3, ... K. The kinds of possible interactions, as described by their respective group-to-group removal cross section Σ_{1k}, will determine the extent of the downscatter. A diffusion calculation is then performed on the second group, with the neutrons removed from group 1 used as the source. Solution of the group-2 diffusion equation,

$$D_2 \nabla^2 \Phi_2(\bar{r}) - \sum_{k=3}^{K} \Sigma_{2k} \Phi_2(\bar{r}) - \Sigma_{a2} \Phi_2(\bar{r}) + \Sigma_{12} \left(\sum_{g=1}^{12} \Phi_{g1}^0 \right) = 0 , \quad (3.190)$$

yields the group-diffusion flux $\Phi_2(\bar{r})$. The group-2 removal fluxes are then added to the diffusion flux

*Available from RSIC in several versions (see Appendix 3A).

Table 3.6. Removal-Band and Energy-Group Structures Used in RASH E[a]

Removal Bands			Diffusion Groups			Band-to-Group Transfer Scheme
Band No.	Energy Limits (MeV)		Group No.	Energy Limits (MeV)		
	Upper	Lower		Upper	Lower	
1	18	17	1	1.05×10^{1}	7.5×10^{0}	1 → 1
2	17	16	2	7.5×10^{0}	6.5×10^{0}	2 → 1
3	16	15	3	6.5×10^{0}	5.5×10^{0}	3 → 1
4	15	14	4	5.5×10^{0}	4.5×10^{0}	4 → 1
5	14	13	5	4.5×10^{0}	3.5×10^{0}	5 → 1
6	13	12	6	3.5×10^{0}	2.5×10^{0}	6 → 1
7	12	11	7	2.5×10^{0}	1.5×10^{0}	7 → 1
8	11	10	8	1.5×10^{0}	5.0×10^{-1}	8 → 1
9	10	9	9	5.0×10^{-1}	5.0×10^{-2}	9 → 1
10	9	8	10	5.0×10^{-2}	5.0×10^{-3}	10 → 1
11	8	7	11	5.0×10^{-3}	5.0×10^{-4}	11 → 2
12	7	6	12	5.0×10^{-4}	5.0×10^{-5}	12 → 3
13	6	5	13	5.0×10^{-5}	5.0×10^{-6}	13 → 4
14	5	4	14	5.0×10^{-6}	5.5×10^{-7}	14 → 5
15	4	3	15	5.5×10^{-7}	7.0×10^{-8}	15 → 6
16	3	2	16	Thermal		16 → 7
17	2	1				17 → 8
18	1	0				18 → 9

[a]From D. E. Bendall, *RASH D – A Mercury Programme for Neutron Shielding Calculations*, Great Britain Atomic Energy Establishment Report AEEW-M-261 (August 1962).

in order to calculate the downscatter source of neutrons from group 2 into the lower-energy groups. The downscatter source into group k (k = 3, 4, ... K) is given by

$$\Sigma_{2k}\left[\Phi_2(\bar{r}) + \sum_{g=13}^{15} \Phi^0_{g2}(\bar{r})\right].$$

The calculation proceeds in a similar fashion from one group to the next lower group and so on. In general, for $i > 2$, the group-diffusion equations are given by

$$D_i \nabla^2 \Phi_i(\bar{r}) - \sum_{k=i+1}^{K} \Sigma_{ik} \Phi_i(\bar{r}) - \Sigma_{ai} \Phi_i(\bar{r}) + \sum_{j=i-1}^{1} \Sigma_{ji}\left[\Phi_j(\bar{r}) + \sum_g \Phi^0_{gj}\right] = 0, \quad i = 3, 4, \ldots, \quad (3.191)$$

and the downscatter source term from the ith group into the kth group is

$$\Sigma_{ik}\left[\Phi_i(\bar{r}) + \Phi^0_{gi}\right].$$

Table 3.7. Removal-Band and Energy-Group Structures Used in MAC[a]

Removal Bands			Diffusion Groups			Band-to-Group Transfer Scheme
Band No.	Energy Limits (MeV)		Group No.	Energy Limits (MeV)		
	Upper	Lower		Upper	Lower	
1	18	17	1	6.065×10^{0}	1.000×10^{-1}	1 → 1
2	17	16	2	3.679×10^{0}	6.065×10^{0}	2 → 1
3	16	15	3	2.231×10^{0}	3.679×10^{0}	3 → 1
4	15	14	4	1.353×10^{0}	2.231×10^{0}	4 → 1
5	14	13	5	8.208×10^{-1}	1.353×10^{0}	5 → 1
6	13	12	6	3.876×10^{-1}	8.208×10^{-1}	6 → 1
7	12	11	7	1.830×10^{-1}	3.876×10^{-1}	7 → 1
8	11	10	8	6.733×10^{-2}	1.830×10^{-1}	8 → 1
9	10	9	9	2.600×10^{-2}	6.733×10^{-2}	9 → 1
10	9	8	10	2.000×10^{-2}	2.600×10^{-2}	10 → 1
11	8	7	11	9.118×10^{-3}	2.000×10^{-2}	11 → 1
12	7	6	12	3.355×10^{-3}	9.118×10^{-3}	12 → 1
13	6	5	13	1.234×10^{-3}	3.355×10^{-3}	13 → 2
14	5	4	14	4.540×10^{-4}	1.234×10^{-3}	14 → 2
15	4	3	15	3.199×10^{-4}	4.540×10^{-4}	15 → 2
16	3	2	16	2.255×10^{-4}	3.199×10^{-4}	16 → 3
17	2	1	17	1.120×10^{-4}	2.255×10^{-4}	17 → 4
18	1	0	18	6.147×10^{-5}	1.120×10^{-4}	18 → 5
			19	3.374×10^{-5}	6.147×10^{-5}	
			20	1.515×10^{-5}	3.374×10^{-5}	
			21	1.016×10^{-5}	1.515×10^{-5}	
			22	4.565×10^{-6}	1.016×10^{-5}	
			23	1.375×10^{-6}	4.565×10^{-6}	
			24	9.214×10^{-7}	1.375×10^{-6}	
			25	6.716×10^{-7}	9.214×10^{-7}	
			26	4.140×10^{-7}	6.716×10^{-7}	
			27	2.775×10^{-7}	4.140×10^{-7}	
			28	1.860×10^{-7}	2.775×10^{-7}	
			29	1.247×10^{-7}	1.860×10^{-7}	
			30	7.595×10^{-8}	1.247×10^{-7}	
			31	0	7.595×10^{-8}	

[a]From E. G. Peterson, *MAC — A Bulk Shielding Code*, Hanford Atomic Products Operation Report HW-73381 (April 1962).

In the NRN* formulation[73,74] the energy structure for the removal bands and energy groups differs significantly from that used in the RASH and MAC formulations. The group structure for the group-diffusion calculation consists of 24 groups over an energy range 0 to 18 MeV, and the fission spectrum is divided into 30 bands of varying widths. The removal-band and energy-group structures are presented in Table 3.8.

The NRN method allows for the transfer of removed neutrons from each removal band to many diffusion groups. The source for the ith diffusion group arising from all removal collisions is

$$\sum_{g} \Sigma^{0}_{gi} \Phi^{0}_{g} ,$$

where Φ^{0}_{g} = removal flux in the gth energy band, and Σ^{0}_{gi} = energy-averaged removal cross section for the transfer of neutrons from the gth removal band into the ith energy group.

The calculation also allows transfer from each diffusion group to all lower-energy diffusion groups. The group-diffusion equation for the ith group is given by

$$D_i \nabla^2 \Phi_i(\bar{r}) - \sum_{k=i+1}^{K} \Sigma_{ik} \Phi_i(\bar{r}) - \Sigma_{ai} \Phi_i(\bar{r}) + \sum_{j=i-1}^{1} \Sigma_{ji} \Phi_j(\bar{r}) + \Sigma^{0}_{gi} \Phi^{0}_{g} = 0, \quad (3.192)$$

where the various diffusion theory parameters have conventional definitions.

3.9.3. DIFFERENCES IN MODERN METHODS

A comparison of the three preceding formulations shows that, with respect to the removal-band and energy-group schemes, RASH E and MAC are similar in concept and identical in many respects. The NRN approach is more general and should provide the most accurate model if the required removal and transfer cross sections are known.

With regard to removal cross sections, RASH E and MAC use the cross sections suggested by the original Spinney formulation, which have the general form

$$\Sigma_R = \Sigma_t - f \Sigma_{el} , \quad (3.193)$$

where

Σ_R = removal cross section,

Σ_t = total macroscopic cross section,

Σ_{el} = elastic scattering cross section,

f = fraction of elastic collisions that can be regarded as glancing.

If f is taken to be the average cosine of scattering in the laboratory system, $\bar{\mu}_0$, the removal cross section becomes the transport cross section originally used by Spinney. In general, the parameter f cannot be determined intrinsically, and so a value must be assumed or determined empirically. This has been accomplished for a large variety of typical shield configurations, and the removal cross sections thus determined are used with a high degree of confidence.

NRN removal cross sections are obtained by experimentally determining the angles of scatter above which elastic collisions can be considered as removals. The removal cross section is given by

$$\Sigma_R = \Sigma_t - 2\pi \int_{\cos\theta_{rem}}^{1} \sigma(\theta)\, d(\cos\theta) , \quad (3.194)$$

where $\sigma(\theta)$ = differential elastic scattering cross section per unit solid angle about the scattering angle θ in the center-of-mass system, and θ_{rem} = scattering angle above which the collision is considered to be a removal. The value of θ_{rem} is determined by comparison of predicted neutron reaction rates with experimental values. A "best" value of $\cos\theta_{rem} = 0.45$ was obtained for hydrogen, and $\cos\theta_{rem} = 0.60$ was obtained for other nuclides. With these values of θ_{rem} a full set of removal cross sections can be derived.

The NRN removal cross sections do not appear to have any advantage over the Spinney cross sections since each scheme involves only a single adjustable parameter, θ_{rem} and f respectively.

The MAC scheme for transferring removed neutrons into energy groups differs significantly from that used by either RASH E or NRN. The practice in MAC of adding the removal flux to the newly calculated group-diffusion flux in order to establish the group-to-group downscatter source violates

*Available from RSIC (see Appendix 3A).

Table 3.8. Removal-Band and Energy-Group Structures Used in NRN[a]

Removal Bands			Diffusion Group		
Band No.	Energy Limits (MeV)		Group No.	Energy Limits (MeV)	
	Upper	Lower		Upper	Lower
1	1.8×10^{1}	1.43×10^{1}	1	1.8×10^{1}	1.35×10^{1}
2	1.43×10^{1}	1.136×10^{1}	2	1.35×10^{1}	1.0×10^{1}
3	1.136×10^{1}	9.021×10^{0}	3	1.0×10^{1}	7.8×10^{0}
4	9.021×10^{0}	7.166×10^{0}	4	7.8×10^{0}	5.9×10^{0}
5	7.166×10^{0}	5.692×10^{0}	5	5.9×10^{0}	4.4×10^{0}
6	5.692×10^{0}	4.521×10^{0}	6	4.4×10^{0}	3.4×10^{0}
7	4.521×10^{0}	3.591×10^{0}	7	3.4×10^{0}	2.6×10^{0}
8	3.591×10^{0}	2.853×10^{0}	8	2.6×10^{0}	2.0×10^{0}
9	2.853×10^{0}	2.267×10^{0}	9	2.0×10^{0}	1.5×10^{0}
10	2.267×10^{0}	1.800×10^{0}	10	1.5×10^{0}	1.2×10^{0}
11	1.800×10^{0}	1.430×10^{0}	11	1.2×10^{0}	9.0×10^{-1}
12	1.430×10^{0}	1.136×10^{0}	12	9.0×10^{-1}	7.0×10^{-1}
13	1.136×10^{0}	9.021×10^{-1}	13	7.0×10^{-1}	5.1×10^{-1}
14	9.021×10^{-1}	7.166×10^{-1}	14	5.1×10^{-1}	3.8×10^{-1}
15	7.166×10^{-1}	5.692×10^{-1}	15	3.8×10^{-1}	3.0×10^{-1}
16	5.692×10^{-1}	4.521×10^{-1}	16	3.0×10^{-1}	1.0×10^{-1}
17	4.521×10^{-1}	3.591×10^{-1}	17	1.0×10^{-1}	3.10×10^{-2}
18	3.591×10^{-1}	2.853×10^{-1}	18	3.10×10^{-2}	1.10×10^{-2}
19	2.853×10^{-1}	2.267×10^{-1}	19	1.10×10^{-2}	1.10×10^{-3}
20	2.267×10^{-1}	1.800×10^{-1}	20	1.10×10^{-3}	1.10×10^{-4}
21	1.800×10^{-1}	1.430×10^{-1}	21	1.10×10^{-4}	1.10×10^{-5}
22	1.430×10^{-1}	1.136×10^{-1}	22	1.10×10^{-5}	1.10×10^{-6}
23	1.136×10^{-1}	9.021×10^{-2}	23	1.10×10^{-6}	1.05×10^{-7}
24	9.021×10^{-2}	7.166×10^{-2}	24	Thermal	
25	7.166×10^{-2}	5.692×10^{-2}			
26	5.692×10^{-2}	4.521×10^{-2}			
27	4.521×10^{-2}	3.591×10^{-2}			
28	3.591×10^{-2}	2.853×10^{-2}			
29	2.853×10^{-2}	2.267×10^{-2}			
30	2.267×10^{-2}	1.80×10^{-2}			

[a]From L. Hjarne and M. Leimdorfer, "A Method for Predicting the Penetration and Slowing Down of Neutrons in Reactor Shields," *Nucl. Sci. Eng.* **24**, 165 (1966).

the "conservation of neutrons" precept usually intrinsic to the group-diffusion concept. This could result in serious calculational errors that are difficult to diagnose.

In contrast, RASH E and NRN introduce the removed neutrons into given groups as source neutrons to that group, a more natural procedure for the group-diffusion calculation. RASH E has a very restricted transfer scheme wherein the removed neutrons from a given removal band are introduced into a prescribed energy group and into no other. NRN provides for a much more general scheme, employing a removal matrix to describe the transfer of removed neutrons from a given removal band into any of the lower-energy groups.

Of the three methods, the slowing-down model embodied in NRN gives the most accurate description of the slowing-down process. It involves a general-group to any lower-energy-group transfer matrix using detailed elastic and inelastic scattering cross sections for all nuclides. A similar scheme is employed by MAC; however, some inaccuracy is allowed in the description of the nonhydrogen elastic scattering.

RASH E uses a group-to-group transfer cross section based on the continuous slowing-down (age) model, which allows transfer to the next lower energy group only. This could lead to serious inaccuracies, particularly with respect to inelastic scatterings and collisions with hydrogen.

3.10 Application of Kernel Technique to Secondary Gamma-Ray Dose Calculations

Often a large fraction of the radiation dose behind reactor and shelter shields is the gamma-ray dose due to neutron capture, and possibly to inelastic scattering, within the shield. If the spatial distribution of the neutron flux is known, the gamma-ray dose rate may be calculated for a large number of configurations by integrating the dose kernel over the source volume. Using the kernel technique as exemplified by Eq. 3.148 and slab geometry as shown in Fig. 3.8, the dose rate $\Gamma(t,a,b)$ on the shield surface due to a distributed monoenergetic isotropic gamma-ray source $S(x)$ bounded by planes at a and b is given by

$$\Gamma(t,a,b) = G(E) \int_a^b S(x)\,dx \int_0^\infty B_r(\mu R) \frac{e^{-\mu R}}{4\pi R^2} 2\pi\rho\,d\rho \quad , \tag{3.195}$$

where

x = one-dimensional spatial coordinate measured from the reference plane,

t = shield thickness,

ρ = radial distance to source point measured from the detector axis,

R = distance from the source point to the detector,

μ = total macroscopic cross section for gamma rays of source energy E,

$G(E)$ = flux-to-dose conversion factor, which for conversion to rads/hr is $5.767 \times 10^{-5} \dfrac{\mu_a(E)}{\rho} E$, where $\dfrac{\mu_a}{\rho}$ is the mass energy absorption coefficient for tissue,

$B_r(\mu R)$ = dose buildup factor for gamma rays of energy E.

Since $R^2 = \rho^2 + z^2$,

$$\Gamma(t,a,b) = \frac{G(E)}{2} \int_a^b S(x)\,dx \int_{t-x}^\infty B_r(\mu R) \frac{e^{-\mu R}}{R}\,dR \ . \tag{3.196}$$

The gamma-ray source term usually can be represented quite well either by fitting with several terms or by piecewise fitting of the thermal-neutron flux distribution* (or of the fast flux distribution

*The production of secondary gamma rays by the capture of nonthermal neutrons is usually insignificant in shelter design.

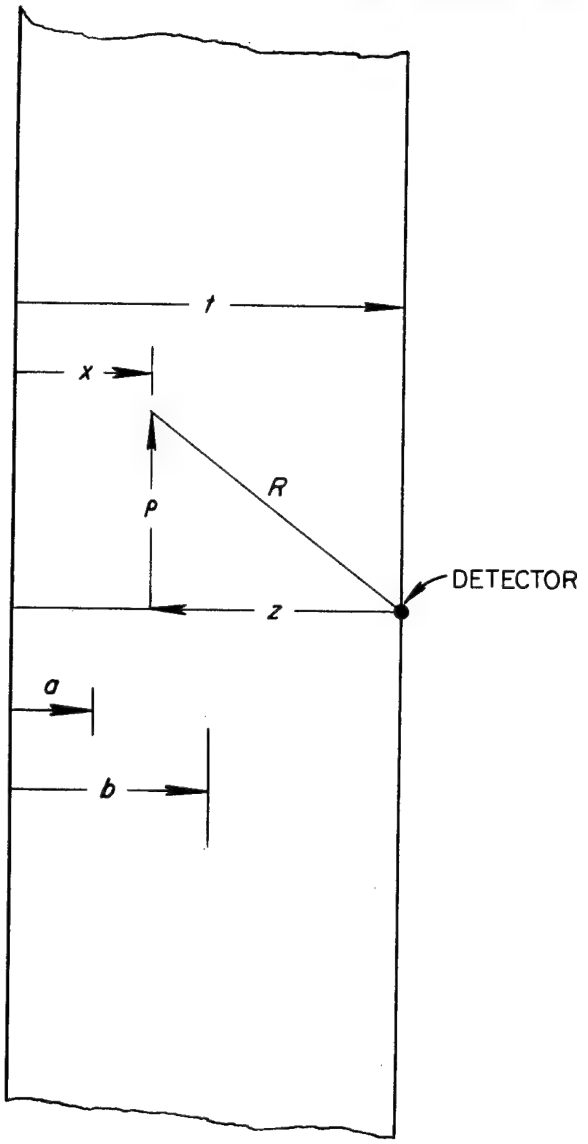

Fig. 3.8. Geometry for Integration over Exponential Source Distribution.

if inelastic scattering is being considered) with a function of the form

$$S(x) = S_a\, e^{-kx} , \qquad (3.197)$$

where S_a is the gamma-ray source at a in the interval (a,b) and k is the reciprocal of the effective neutron relaxation length. Usually S_a can be calculated by

$$S_a = y\,\Phi(a)\,\Sigma , \qquad (3.198)$$

where

y = number of photons of energy E released per neutron capture (or per inelastic scattering),

$\Phi(a)$ = neutron flux (usually thermal flux for capture and fast flux for inelastic scattering),

Σ = macroscopic neutron cross section for thermal-neutron capture (or for inelastic scattering).

When exponential or polynomial forms of the buildup factor are used (see Section 3.8.1), together with the source description given by Eq. 3.197, then Eq. 3.196 can be integrated analytically and very useful results obtained. In the paragraphs given below, examples of such integrations are given for two cases of interest: a slab shield of finite thickness t and a semi-infinite shield ($t = \infty$), the latter corresponding to a real problem in which the shield is very thick.

3.10.1. CALCULATION FOR SLAB SHIELD

Trubey[40] calculated the secondary gamma-ray dose rate for a slab shield by using the Berger form of the buildup factor,

$$B_r(E,\mu R) = 1 + C(E)\,\mu R\, e^{D\,\mu R} , \qquad (3.199)$$

in Eq. 3.196. The equation then becomes

$$\Gamma(t,a,b) = \frac{G(E)}{2} S_a \int_a^b e^{-kx}\, dx \left[\int_{\mu(t-x)}^{\infty} \frac{e^{-\mu R}}{R}\, dR + \int_{\mu(t-x)}^{\infty} C(E)\, e^{\mu(D-1)R}\, d(\mu R) \right] , \qquad (3.200)$$

where the uncollided dose rate $\Gamma_0(t,a,b)$ is represented by the first term, and the scattered dose rate $\Gamma_s(t,a,b)$ is given by the second term.

Letting $\mu(t - x) = y$ and integrating the first term of Eq. 3.200 by parts, the dose rate from the uncollided gamma-ray dose rate is given by

$$\Gamma_0(t,a,b) = \frac{G(E)\,S_a\,e^{-\alpha\mu t}}{2\alpha\mu}\left[e^{\alpha y}\,E_1(y)\Big|_{\mu(t-b)}^{\mu(t-a)} + \int_{\mu(t-b)}^{\mu(t-a)} e^{\alpha y}\,\frac{e^{-y}}{y}\,dy\right]$$

$$= \frac{G(E)\,S_a\,e^{-\alpha\mu t}}{2\alpha\mu}\{e^{\alpha\mu(t-a)}\,E_1(\mu[t-a]) - E_1([1-\alpha]\,\mu[t-a])$$

$$+ E_1([1-\alpha]\,\mu[t-b]) - e^{\alpha\mu(t-b)}\,E_1(\mu[t-b])\}\ , \qquad (3.201)$$

where $\alpha = k/\mu$ and E_1 is an exponential function of the first order and is defined by

$$E_1(x) = \int_x^\infty \frac{e^{-y}}{y}\,dy\ . \qquad (3.202)$$

Graphs of the exponential functions and other details of their properties are shown in Appendix 3C.

If $\alpha = 1$ or 0 (case of uniform source distribution) or if $b = t$, indeterminate forms result which may be resolved by L'Hôpital's rule, by series expansions, or by integrating Eq. 3.200 for $k = \mu$, $k = 0$, and $b = t$, respectively. These cases are as follows:

For $b < t$ and $\alpha = 0$

$$\Gamma_0(t,a,b) = \frac{G(E)\,S_a}{2\mu}\{\mu[b-a]\,E_1(\mu[t-b])$$

$$+ \mu t\,E_1(\mu[t-a]) - \mu t\,E_1(\mu[t-b])\}\ . \qquad (3.203)$$

For $b < t$ and $\alpha = 1$

$$\Gamma_0(t,a,b) = \frac{G(E)\,S_a}{2\mu}\left\{e^{-\mu a}\,E_1(\mu[t-a])\right.$$

$$\left. - e^{-\mu b}\,E_1(\mu[t-b]) + e^{-\mu t}\ln\frac{t-a}{t-b}\right\}\ . \qquad (3.204)$$

For $b = t$ and $\alpha \neq 0$ or 1

$$\Gamma_0(t,a,t) = \frac{G(E)\,S_a}{2\mu\alpha}\left(e^{-\alpha\mu a}\,E_1(\mu[t-a])\right.$$

$$\left. - e^{-\alpha\mu t}\{E_1(\mu|1-\alpha|[t-a]) + \ln|1-\alpha|\}\right) \qquad (3.205)$$

For $b = t$ and $\alpha = 0$

$$\Gamma_0(t,a,t) = \frac{G(E)\,S_a}{2\mu}\{1 + \mu[t-a]\,E_1(\mu[t-a])$$

$$- e^{-\mu[t-a]}\}\ . \qquad (3.206)$$

For $b = t$ and $\alpha = 1$

$$\Gamma_0(t,a,t) = \frac{G(E)\,S_a}{2\mu}\{e^{-\mu a}\,E_1(\mu[t-a])$$

$$- e^{-\mu t}\ln\gamma\mu[t-a]\}\ , \qquad (3.207)$$

where $\ln\gamma = 0.577215665\ldots$, Euler's constant.

For the special case of $b = t$ and $a = 0$, Eq. 3.205 can be represented by

$$\Gamma_0(t,0,t) = \frac{G(E)\,S_a}{\mu}\,\psi_0(\mu t,\alpha)\ , \qquad (3.208)$$

where

$$\psi_0(\mu t,\alpha) = \frac{1}{2\alpha}\left(E_1(\mu t) - e^{-\alpha\mu t}\{E_1([1-\alpha]\,\mu t)\right.$$

$$\left. + \ln|1-\alpha|\}\right)\ . \qquad (3.209)$$

Equation 3.209 is shown plotted in Fig. 3F.1 of Appendix F as a function of the number of mean free paths μt with α as a parameter.

[Note: Equations 3.203 through 3.209 can be used to calculate the *total* gamma-ray dose (uncollided + scattered) when the Taylor form of the buildup factor is used (see Section 3.8.1).]

Since $z = t - x$, the scattered dose rate behind a slab shield can be determined by expressing the second term of Eq. 3.200 (i.e., the Berger term) as

$$\Gamma_s(t,a,b) = \frac{G(E)\,C(E)\,S_a\,e^{-\alpha\mu t}}{2} \int_{t-b}^{t-a} dz \int_z^{\infty} e^{\alpha\mu z}\, e^{-(1-D)\mu R}\, d(\mu R)\ . \tag{3.210}$$

Integrating Eq. 3.210 gives

$$\Gamma_s(t,a,b) = \frac{G(E)\,C(E)\,S_a\,e^{-\alpha\mu t}}{2(1-D)(1-D-\alpha)\,\mu} \left[e^{-(1-D-\alpha)\mu(t-b)} - e^{-(1-D-\alpha)\mu(t-a)}\right]\ . \tag{3.211}$$

Examination of Eq. 3.210 and Eq. 3.211 reveals that unless $D < 1$, negative doses are obtained. However, D is always significantly <1, as is shown in Fig. 3.3 in Section 3.8.

When $\alpha + D = 1$, Eq. 3.211 gives an indeterminate form which, when resolved, becomes

$$\Gamma_s(t,a,b) = \frac{G(E)\,C(E)\,S_a\,e^{-\alpha\mu t}(b-a)}{2(1-D)}\ . \tag{3.212}$$

For the special case when $b = t$ and $a = 0$, Eq. 3.212 can be expressed as

$$\Gamma_s(t,0,t) = \frac{G(E)\,C(E)\,S_a\,e^{D\mu t}}{\mu(1-D)}\,\psi_1(\mu t,\alpha')\ , \tag{3.213}$$

where

$$\psi_1(\mu t,\alpha') = \frac{e^{-\alpha'\mu t}\left[1 - e^{-\mu t(1-\alpha')}\right]}{2} \tag{3.214}$$

and $\alpha' = \alpha + D$. The function given by Eq. 3.214 is shown in Fig. 3F.2 in Appendix F.

3.10.2. CALCULATION FOR SEMI-INFINITE SHIELD

Solutions of Eq. 3.196 for a semi-infinite shield, that is, for $b = \infty$, give useful results that are generally applicable for the special case in which $a = 0$, particularly if one is interested in a gamma-ray heating rate within a shield. Using the polynomial form of the buildup factor,

$$B_r(\mu R) = \sum_{n=0}^{3} A_n(\mu R)^n\ , \tag{3.215}$$

Claiborne[75] determined solutions to Eq. 3.196 for this case, which were all in the form

$$\Gamma(\mu x) = \frac{G(E)\,S_a}{\mu} \sum_{n=0}^{3} n!\, A_n\,\psi_n\ . \tag{3.216}$$

The dose rate from the uncollided flux is represented by the first term and is given by

$$\psi_0(\mu t) = \frac{1}{2\alpha}\left(E_1(\mu t) - e^{-\alpha\mu t}\left\{E_1([1-\alpha]\,\mu t) - \ln\left|\frac{1+\alpha}{1-\alpha}\right|\right\}\right)\ , \tag{3.217}$$

and the sum of the next three terms represents the scattered contribution. The terms are

$$\psi_1(\mu t) = \frac{e^{-\alpha\mu t}}{2}\left[\frac{1 - e^{-(1-\alpha)\mu t}}{1-\alpha} + \frac{1}{1+\alpha}\right]\ , \tag{3.218}$$

$$\psi_2(\mu t) = \frac{4e^{-\alpha\mu t} - (1+\alpha)^2(2-\alpha)e^{-\mu t} - (1+\alpha)^2(1-\alpha)\mu t\,e^{-\mu t}}{4(1-\alpha)^2(1+\alpha)^2}\ , \tag{3.219}$$

$$\psi_3(\mu t) = \frac{2}{3}\psi_2 + \left[\frac{1}{(1-\alpha)^3} + \frac{1}{(1+\alpha)^3}\right]\frac{e^{-\alpha\mu t}}{6}$$

$$- \left[\frac{(\mu t)^2}{2(1-\alpha)} + \frac{\mu t}{(1-\alpha)^2} + \frac{1}{(1-\alpha)^3}\right]\frac{e^{-\mu t}}{6} . \quad (3.220)$$

When $\alpha = 0$, an indeterminate form occurs in Eq. 3.162, and when $\alpha = 1$, indeterminate forms occur in Eqs. 3.218 through 3.220. The following equations result when the indeterminate forms are evaluated:

For $\alpha = 0$

$$\psi_0(\mu t) = 1 + \frac{\mu t}{2} E_1(\mu t) - \frac{e^{-\mu t}}{2} = 1 - \frac{1}{2} E_2(\mu t) . \quad (3.221)$$

For $\alpha = 1$

$$\psi_0(\mu t) = \frac{E_1(\mu t)}{2} + \frac{e^{-\mu t}}{2} \ln(2\gamma\mu t) , \quad (3.222)$$

$$\psi_1(\mu t) = \left(\mu t + \frac{1}{2}\right)\frac{e^{-\mu t}}{2} , \quad (3.223)$$

$$\psi_2(\mu t) = \frac{\psi_1}{2} + \left[2(\mu t)^2 + 1\right]\frac{e^{-\mu t}}{16} , \quad (3.224)$$

$$\psi_3(\mu t) = \frac{2\psi_2}{3} + \left[\frac{(\mu t)^3}{3} + \frac{1}{4}\right]\frac{e^{-\mu t}}{12} . \quad (3.225)$$

The functions given by Eqs. 3.222 through 3.225 for the semi-infinite medium are plotted in Figs. 3F.3 through 3F.4 in Appendix F for various values of α. Figures 3F.3 and 3F.4 may be compared with Figs. 3F.1 and 3F.2, which are the corresponding functions evaluated for a slab shield.

These solutions contain the contribution from the gamma-ray sources between the detector position at t and infinity, since integration of Eq. 3.196 from $x = 0$ to $x = \infty$ produces two integrals: one giving the contribution from the interval $0 \leqq x \leqq t$ and the other giving the contribution from the interval $t \leqq x \leqq \infty$. In the usual shield, however, the contribution from the second interval at deep penetrations is small, and the gamma-ray dose rate outside a shield of thickness μt will be only slightly less than that calculated for a distance μt within a semi-infinite shield.

If Eq. 3.216 is used for gamma-ray heating calculations within a shield, the coefficients A_n must correspond to the polynomial fit of the energy absorption buildup factor, and the conversion factor for expressing the heating rate in W/g becomes

$$G(E) = 1.6 \times 10^{-13} \frac{\mu_a}{\rho} E , \quad (3.226)$$

where μ_a/ρ is the mass energy absorption coefficient of the material in which heat is generated.

Appendix 3A. Computer Code Abstracts

Computer codes which utilize the methods described in this chapter are abstracted below. These abstracts also appear in ORNL-RSIC-13,[76] a publication of the Radiation Shielding Information Center which is continually updated to include new codes as they become available. It is emphasized that the abstracts given here do not represent all the codes available from RSIC, nor the many shielding codes not in the RSIC collection for reasons such as obsolescence, nonavailability due to proprietary interests, or insufficient testing or documentation.

All codes and auxiliary routines received by RSIC are checked out for operability; that is, sample problems are run by the RSIC staff. If the code is operable, it is packaged and assigned a CCC number, and a code abstract is written and distributed.

Inquiries or requests for a code package should be mailed to

CODES COORDINATOR
Radiation Shielding Information Center
Oak Ridge National Laboratory
P.O. Box X
Oak Ridge, Tennessee 37830

or telephoned to

Area Code 615; 483-8611, Ext. 3-6944, or to
FTS 615-483-6944.

A reel of magnetic tape should accompany each request for a code.

Members of the RSIC staff are always available for consultation in connection with the shielding code packages, either in regard to operation of the code or to its applicability for a particular shielding problem. Also, RSIC maintains a file indicating whether a code package has been made available in additional machine languages, made operable on other machines, etc.

3A.1. DISCRETE ORDINATES PROGRAMS

DTF-IV (CCC-42*). – The Los Alamos Scientific Laboratory program DTF-IV[8,77,78] solves the multigroup, one-dimensional Boltzmann transport equation for plane, cylindrical, or spherical geometries. Anisotropic scattering is represented by Legendre polynomial expansion of the differential scattering cross section. Energy dependence is treated by the multigroup approximation and angular dependence by a general discrete ordinates approximation. Iteration processes for within-group scattering and upscattering are accelerated by system-wide renormalization procedures.

General anisotropic scattering capability is provided in each of the three geometries, upscattering convergence acceleration is used, an optional group- and pointwise convergence test is available, and a neutron-conserving negative flux correction routine is used.

An auxiliary routine, GAMLEG, provides cross sections for photon transport problems in a form suitable for input to DTF-IV.

DTF-IV is written in FORTRAN IV language and is operable on IBM-7090 and -7030 computers.

ANISN (CCC-82). – ANISN,[79] a code developed jointly by the Oak Ridge Computing Technology Center and Oak Ridge National Laboratory, solves the one-dimensional Boltzmann transport equation in slab, spherical, or cylindrical geometry. The source may be a fixed source, a fission source, or a subcritical combination of the two. A criticality search may be performed on any one of several parameters. Cross sections may be weighted using the space- and energy-dependent flux generated in solving the transport equation.

The solution technique is an advanced discrete ordinates method which represents a generalization of the method originated by G. C. Wick and greatly developed and extended to curvilinear geometry by B. G. Carlson at Los Alamos Scientific Laboratory.

ANISN has been used for many shielding problems, including deep-penetration problems in which angle-dependent spectra are calculated in detail. The principal feature that makes ANISN suitable for such problems is the use of an advanced programming technique with optional data-storage configurations, which allows efficient execution of small, intermediate, and extremely large problems. ANISN also includes an efficient technique for handling general anisotropic scattering, pointwise convergence criteria, and alternate step function difference equations that effectively remove the oscillating flux distributions sometimes found in discrete ordinates solutions.

*Refers to RSIC code package number.

ANISN is written in FORTRAN IV language for use on IBM-7090 and -7094 computers and in FORTRAN IV (H) language for use on the IBM-360 computer.

BIGGI 3P (CCC-66). – The BIGGI 3P program,[79,80] developed by EURATOM, Ispra (Varese), Italy, solves the Boltzmann transport equation in plane multilayer geometry. It computes gamma-ray angular fluxes, spectra, buildup factors, and albedos. The sources must be monoenergetic and located on one outer boundary; their angular distribution can be isotropic or collimated.

BIGGI 3P integrates the Boltzmann equation numerically. The basis is the pair of coupled integral equations, discussed for the case of neutrons by Weinberg and Wigner.[1] Discrete ordinate meshes are defined in each of the three concerned dimensions (angle, space, and gamma-ray wavelength), and the integrals figuring in the transport equation are approximated by sums. The program solves the integral equations without iteration, since they are of the Volterra type (as long as only energetic downscattering is assumed). The gamma-ray cross sections (in Thompson units per electron) of each slab must be given in the input. The contribution of the low-energy tail below the cutoff energy to the four buildup factors (energy flux, particle flux, dose rate, and energy absorption rate) and to the two albedos (energy and particle current) is estimated. An exponential transformation allows rather great spatial integration steps, up to 2 or 3 mean free paths.

BIGGI 3P is written in FORTRAN language for use on the IBM-7090 computer.

3A.2. MOMENTS METHOD PROGRAMS

RENUPAK (CCC-41). – The United Nuclear Corporation's moments method code RENUPAK[81] provides a solution to the Boltzmann equation for steady-state neutron transport in one-dimensional homogeneous geometry, with elastic, inelastic, and fission processes included. Point sources or plane isotropic sources with continuous energy distributions can be used. The output consists of the dose (using response function data) and of the spatial moments, neutron flux density, and current as a function of energy and position.

After the moments are computed, they are used to reconstruct the flux and current. The flux density is assumed to consist of a linear combination of functions of given form, and constants in the expansion are adjusted so that the moments of the linear combination are the same as the computed moments of the flux density.

In the elastic slowing-down treatment the neutron energy-angle relationship is properly taken into account. The inelastic scattering of neutrons is assumed to be isotropic in the laboratory system, with several nuclear models being available to compute its energy dependence. In particular, the program permits a choice of discrete energy levels when the levels are well separated and a continuum of energy levels when the levels are very close. For heavy materials a statistical model is available.

RENUPAK is written in FAP assembly language and is operable on the IBM-7090 computer.

MOMGEM-MOMDIS (CCC-85). – The MOMGEM and MOMDIS codes[82,83] of the U.S. Naval Radiological Defense Laboratory, San Francisco, calculate the angle and energy distributions of gamma rays scattered at various depths within an infinite homogeneous medium, yielding results that closely approximate the distribution determined for a finite slab case, with the thickness of the slab the same as the depth of penetration in the infinite medium.

There are two phases of the calculation. Phase 1 is performed by MOMGEM and consists of the generation of the moments. Three sets of moments are needed to determine the required moments for third- and higher-order scattering: one set each for total, first, and second scatterings. Third- and higher-order scattering moments are obtained by adding the first and second moments together and subtracting their sum from the moments for total scattering.

In Phase 2, performed by MOMDIS, a biorthogonal polynomial expansion is used to fit the moments. The resulting distribution is for third- and higher-order scattering. Distributions for first- and second-order scattering are determined from analytical expressions. Finally, a composite spectrum is formed by adding the three distributions.

MOMGEM and MOMDIS are written in FORTRAN II and IV languages and can be used on the IBM-704 computer.

3A.3. MONTE CARLO PROGRAMS

15-2 (CCC-4). – The General Electric Monte Carlo code 15-2 (refs. 84 and 85) calculates the

energy spectrum and angular distribution of gamma rays at a point detector in an infinite homogeneous medium of air that result from single and multiple scattering of monoenergetic, monodirectional gamma rays from a point source. The single-scattering contribution is computed by numerical integration, and the contribution due to second- and higher-order scattering is determined by Monte Carlo techniques.

First-collision points for the Monte Carlo calculation are obtained by means of systematic sampling, with subsequent collision points determined randomly. A quota sampling scheme, which assigns N_k histories to the kth first-collision point, is used to allow a more intensive study of those histories that make the largest contribution to the result. Scoring is done at second- and higher-order collision points by a statistical estimation technique. At each collision point the product of the weight of the particle and the conditional probability that the particle will reach the detector without further collision, assuming that it had a scattering collision, is scored for the appropriate detector energy-angle bin. The detector-angle bins are determined by dividing the space about the detector into a number of solid angles whose apexes are at the detector. Collisions close to the detector, which would result in very large scores, are prohibited.

Two options in the program provide for further possible reduction of the variances of the estimates. One is the biased sampling of the scattering angle from an isotropic distribution. Corrections for an anisotropic distribution are made later by weighting the particle according to the Klein-Nishina relationship. In the other option, called "exponential transformation," the mean free path of a gamma ray is altered on the basis of its energy, position, and direction with respect to the detector.

The gamma-ray events treated are photoelectric effect, pair production, and Compton scattering. The total cross sections for air are computed by means of a power series fit to the ratio of the total-to-Compton cross sections. There is also an option which allows the generation and tracking of 0.5-MeV photons following pair-production events.

The 15-2 code is written in FAP language and is operable on IBM-704 and -7090 computers.

FMC-G (CCC-14). – The General Electric Monte Carlo program FMC-G,[86] together with its auxiliary routines 20-2 (ref. 87), 20-4 (ref. 88), and SG (ref. 89), solves the gamma-ray transport equation with considerable flexibility in the geometrical, material, nuclear, and source descriptions of source-shield configurations and in the variance reduction techniques. Homogeneous regions are enclosed by surfaces described by the general equation

$$AX^2 + X_0X + BY^2 + Y_0Y + CZ^2 + Z_0Z - K = 0 .$$

The output of the code includes optional absorption or energy deposition tallies, Monte Carlo entrance and leakage tallies, expectation entrance and leakage tallies, Monte Carlo or expectation flux tallies, and history tallies of particles reaching selected regions. The absorption or energy deposition, entrance, leakage, and flux tallies are made by region and energy groups. Parameters of secondary gamma rays are stored on tape for later analysis.

A nonoptional statistical estimation technique of weighting for nonabsorption is applied at each collision. Optional statistical estimation techniques may be used for scoring entrance tallies and mandatory leakage tallies. Flexibility in sampling from source spectra is achieved by using energy-group-averaged acceleration factors. Importance sampling options are (1) splitting and Russian roulette, depending on energy, region, and location within a region, (2) Russian roulette on particles whose weights fall below the weight cutoff, and (3) exponential transformation.

The auxiliary routine SG (Source Generator) applies statistical methods to generate the seven parameters required to describe source particles for FMC-G. These parameters are stored on magnetic tape for later Monte Carlo processing. The code provides three methods for generating the direction cosines of the source particle, three methods for generating the spatial coordinates, and one method for generating the source energy. Any or all of these parameters may also be entered as input.

The auxiliary code 20-2 approximates cross-section dependence on energy by discontinuous straight-line segments across specified energy groups and prepares a printed listing.

The auxiliary code 20-4 averages input differential-scattering cross sections over specified energy groups to obtain angular distribution data in the form of cumulative probability tables suit-

able for use in FMC-G. Differential-scattering cross-section input data can be in the form of either a two-dimensional tabular array of $\sigma_e^m(E,\mu)$ or a set of one-dimensional tabular arrays of Legendre polynomial coefficients. Output is available as a printed listing and as punched card input to FMC-G.

FMC-G and SG are written in FAP language, and the routines 20-2 and 20-4 are written in FORTRAN II language. The programs can be run on IBM-7090 and -7094 computers.

FMC-N (CCC-15). – A General Electric Monte Carlo program for solving the neutron transport equation is designated as FMC-N.[86] In most respects the program description is the same as that given above for FMC-G; however, FMC-N uses two additional auxiliary routines. One, identified as code 20-5 (ref. 90), applies the evaporation model of nuclear reactions to determine cumulative probability tables for energy spectra of inelastically scattered neutrons. The output from this routine includes a printed listing and punched cards suitable for input to FMC. The other routine, identified as code 20-6 (ref. 91), computes excitation and transition probabilities for excited states of the residual nucleus from a neutron inelastic-scattering reaction, given the relative gamma-ray intensities of the transitions that occur in the process and the energy level structure of the nucleus. The output is in printed form only.

FMC-N is written in FAP language, and codes 20-5 and 20-6 are in FORTRAN II language. The programs can be used on IBM-7090 and -7094 computers.

O5R (CCC-17). – The Oak Ridge National Laboratory code system O5R[28] was designed to calculate, by Monte Carlo methods, any quantity related to neutron transport in reactor or shielding problems. Arbitrary three-dimensional geometries bounded by quadric surfaces may be treated, and the sources may have arbitrary spatial, energy, and angular distributions specified by a subroutine written by the user. Anisotropic scattering can be included for both elastic and inelastic processes. Fissionable as well as nonfissionable media can be treated. Several variance reduction techniques are available.

For maximum flexibility, a calculation generally consists of two main operations. The primary routine, called the O5R Generator, is used to generate neutron case histories and produce collision tapes on which are written any, or all, of 34 distinct parameters describing each collision. These tapes are subsequently processed by analysis routines usually written by the user to produce Monte Carlo estimates of any desired quantity. Analysis routine STATEST[92] is included in the prototype of the O5R system for shielding problems (a "prototype" code is one which is a completely assembled version, including sample input and output). STATEST provides for statistical estimation of the flux in energy bins for an array of space points.

A batch system of generating case histories is employed to obtain a very detailed table of cross sections in fast memory. The cross sections in memory at one time encompass only a small energy range. All collisions of a batch for which these cross sections are needed are generated before another group of cross sections are read from tape. Cross-section data are prepared for use in O5R by XSECT, a code which performs a variety of manipulations: preparing, updating, and editing a master tape and performing cross-section arithmetic.

Source data are generated by subroutine SOURCE, usually written by the code package user for his specific problem.

A very general geometry subroutine permits the treatment of complicated geometries. As many as 16 media are permitted and boundaries may be either planes or quadric surfaces, arbitrarily oriented and intersecting in arbitrary fashion.

The O5R program is available in FORTRAN language for both the IBM-7090 and the CDC-1604 computer. It is also available in FAP language for the IBM-7090 computer and in CODAP language for the CDC-1604 computer.

TRG-SGD (CCC-25). – The Monte Carlo code TRG-SGD,[93] written by the Technical Research Group for the Air Force Weapons Laboratory (Kirtland), calculates the time and space distribution of secondary gamma-ray doses and dose rates from a nuclear weapon detonation in the atmosphere or in the ground near the surface of the earth. The neutron source is given as leakage from the exploded device. The effects of the blast and fireball on the transport of the neutrons and gamma rays are taken into account.

The neutron reactions considered are elastic scattering, inelastic scattering, radiative capture, and nonradiative capture. The $(n,2n)$ reaction is treated as inelastic scattering by cross-section modification. The prompt neutrons are degraded

14-MeV neutrons from a fusion reaction, fission neutrons, and neutrons which are assumed to have a "bomb thermal Maxwell-Boltzmann spectrum." The delayed neutrons are from a fission source with a time-dependent volume distribution. The only gamma-ray reactions considered are Compton scattering and absorption, the latter being the total of pair production and photoelectric effects.

The Monte Carlo method is used to generate the neutron distribution, the secondary gamma-ray source distribution, and the secondary gamma-ray dose distribution. The effects of the air-ground interface, an inhomogeneous atmosphere, and time-dependent hydrodynamics are taken into account. The type and yield of weapon and the detonation altitude determine the initial conditions. The geometric system is taken to be axially symmetric. In addition to statistical estimation of the gamma-ray source and dose distributions, various importance-sampling techniques are used. These include Russian roulette for low-contribution particles and generalized quota sampling. In addition, all random variables are picked from a truncated exponential distribution. This procedure is controlled by input parameters.

TRG-SGD is written in FORTRAN language and is operable on the CDC-1604 computer.

SALOMON (CCC-33). – The Monte Carlo program SALOMON[94] was developed by the Research Institute of National Defense, Stockholm, Sweden, to treat gamma-ray transport problems in multislab one-dimensional plane geometry. The program calculates the penetrating gamma-ray dose rate and energy deposition rate in a system of slabs of infinite extension and finite thickness. An isotropic monoenergetic volume source distribution is given pointwise, and one source energy at a time is calculated.

Various transformation techniques are utilized. Importance sampling is used to modify the spatial and directional distribution of the source, as well as the transport kernel. All biasing is completely contained in the program and is automatically optimized.

Two versions of the code exist, one giving better penetration accuracy and one giving better energy deposition accuracy.

SALOMON is written in FORTRAN language and can be used on IBM-7090 and -7094 computers. (Note: This program is also in the ENEA Computer Programme Library, where it carries the number ENEA 062.)

DIPSEA (CCC-35). – The Monte Carlo code DIPSEA[95] was developed by Technical Operations Research to determine the radiation dose resulting from a point isotropic gamma-ray source in an atmosphere of air whose density varies exponentially. The source may be monoenergetic or polyenergetic. A cylindrical geometry is used to describe the atmospheric region surrounding the point source. The assumed cylinder, divided into a layered series of square toroids of uniform cross section, extends from a lower altitude of 11 km to an upper altitude of 100 km and has a variable radius that normally has a maximum limit imposed by statistical fluctuations inherent in Monte Carlo calculations. The code assumes that the photon is lost after passing these boundaries.

The atmosphere is assumed to be divided into two zones, each zone having its own exponential expression for the density. The range of each zone is set equal to the altitude interval in which the gradient of the molecular-scale temperature is nearly constant.

Energies in the program are expressed in units of Compton wavelength. All interactions in the media are considered to be either Compton scattering or pair production.

The components calculated are the scattered, direct, and total doses in the center of each toroidal cross section, in units of both keV/g and ion pairs/cm^3. The scattered dose is computed by the Monte Carlo method and the unscattered dose is computed analytically.

DIPSEA is written in FORTRAN and FAP languages and can be used on IBM-704, -709, -7090 and -7094 computers.

TORN (CCC-44). – The TORN system[96–102] is a Monte Carlo neutron-transport system for slab configurations originally developed for the U.S. Army Nuclear Defense Laboratory (Edgewood Arsenal) by Technical Operations Research and later modified by Radiation Research Associates. The system has two prototypes: TORN I for homogeneous materials and TORN II for heterogeneous materials.

The TORN system determines the transmission and reflection of monoenergetic neutrons and the production of secondary gamma rays in slab configurations. The transmission is determined for shields consisting of up to five slabs and for up to five source incident angles in one run. The reflection is obtained for the maximum thickness of the slab configurations. Elastic, inelastic, and

absorption interactions are considered. The results are stored on tape in binary form. The information that may be obtained includes the number of neutrons backscattered or transmitted, the energy backscattered or transmitted, and the angular distribution of the emergent number, energy, or dose of neutrons.

The auxiliary analysis code (RRA-29) processes the output from TORN I and calculates the angular distribution of the neutron flux, current, and dose rate and the average energy of the emergent neutrons. Another analysis code (RRA-37) analyzes the characteristics of the transmitted and reflected particles recorded on magnetic tape by the TORN systems. This code calculates and prints out the angular distribution of the flux and current of the emergent particles (transmitted or backscattered) for a multilayer slab. The angular distribution of the emergent particle and dose current, dose rate, and average energy and of the unscattered particle and dose current and dose rate is also computed and is printed out and punched.

The TORN system is written in FORTRAN II and FAP languages and can be run on the IBM-7090 computer.

TORG (CCC-45). – The TORG program[103,104] is a generalized Monte Carlo program for gamma rays transported through one, two, or three slab layers. It is analogous to the TORN system for neutrons (see above) and was developed by the same group.

Information obtained from TORG includes the number and energy of gamma rays that are backscattered or transmitted and the angular distribution of the emergent number, energy, or dose. The source may be monoenergetic or polyenergetic. The source angular distribution may be isotropic, anisotropic, or described by a single incident polar angle.

The energy, angular, and spatial distribution of transmitted and reflected gamma rays is computed for arbitrary point source energy-angular distributions in slab geometry. The model is believed to be adequate up to about 200 MeV since bremsstrahlung from pair-produced and Compton-scattered electrons is accounted for. Details of emerging photons may be written on tape for further analysis.

An auxiliary analysis routine[102] (RRA-37) generates punched and printed output of the angular distribution of the emergent particle (transmitted or backscattered) dose current, dose rate, and average energy and of the unscattered particle and dose current and dose rate.

TORG is written in FORTRAN II language and can be used on the IBM-7090 computer.

OGRE (CCC-46). – The OGRE code system[105,106] was designed by Oak Ridge National Laboratory to calculate by Monte Carlo methods any quantity related to gamma-ray transport. The system is represented by two typical codes: OGRE-P1 and OGRE-G. The OGRE-P1 code is a simple prototype which calculates dose rate on one side of a slab due to a plane source on the other side. OGRE-G, a prototype of a code utilizing a general-geometry routine, calculates the dose rate at arbitrary points and provides for a very general source description by allowing the user to prepare his own source tape.

Case histories of gamma rays in the prescribed geometry are generated and then analyzed to produce averages of any desired quantity, which in the case of the prototypes is the gamma-ray dose rate. The system is designed to achieve generality by ease of modification. No importance sampling is built into the prototypes.

A very general geometry subroutine permits the treatment of complicated geometries. This is essentially the same routine used in the O5R neutron-transport system (see above). Boundaries may be either planes or quadric surfaces, arbitrarily oriented and intersecting each other in arbitrary fashion.

Cross-section data are prepared by an auxiliary master cross-section code (XSECT), which may be used to originate, update, or edit the master cross-section tape. The master cross-section tape is utilized in the OGRE codes to produce detailed tables of the macroscopic cross sections required for the Monte Carlo calculations.

OGRE is available in FORTRAN II and IV languages and in FAP language for use on the IBM-7090 computer, in FORTRAN IV for IBM-360/50 and -360/75 computers, and in FORTRAN 63 and CODAP for the CDC-1604 computer.

SPARC (CCC-58). – SPARC[107–110] is a Monte Carlo program for solving neutron- and gamma-ray transport problems in multilayer slabs. It was developed by the USAF Nuclear Aerospace Research Facility, General Dynamics, for the U.S. Army Tank Automotive Center and the U.S. Army Ballistic Research Laboratories.

SPARC analyzes the effects of radiation, either as a source incident on the shield or as distributed

sources inside the shield, to obtain spatial and energy distributions of the particle flux within the shield, angular distributions of the transmitted and reflected particle current, and angular distributions of the transmitted and reflected particles separated into ten ranges of energy.

SPARC is available in FORTRAN and FAP languages for use on the IBM-7090 and -7094 computers. [Note: The COMBINE kernel code (see below) was designed to utilize the results of SPARC to calculate flux or dose rate at detector points inside a shielded compartment.]

ADONIS (CCC-13A,B), UNC-SAM, and UNC-SAM-2 (CCC-81). – The United Nuclear Corporation stochastic approximation method, developed originally as ADONIS[111] and later as UNC-SAM,[112] calculates the solution to the Boltzmann transport equation in three-dimensional geometry by Monte Carlo methods. ADONIS tracks either neutrons or gamma rays through shields composed of rectangular parallelepipeds of different compositions. Particle splitting is used to improve the efficiency of the calculation by assigning importance weights to each of the regions. The program computes fluxes and their standard deviations in each of up to 80 regions. By use of response functions the dose and strength of secondary gamma rays from any neutron-induced reaction can be computed throughout the configuration. UNC-SAM will calculate fluxes, flux-dependent functionals such as doses, and their standard deviations in geometry comprised of rectangular parallelepipeds, which, in turn, may contain spheres, cylinders, parallelepipeds, or wedges. Importance sampling is used to increase efficiency. In evaluating neutron fluxes in small-volume detectors, a scoring by analytical estimation, referred to as "flux at a point," is used.

A modified version of UNC-SAM, identified as UNC-SAM-2,[113] treats time-dependent neutron and photon transport through matter.

ADONIS versions are available in FORTRAN-FAP language for the IBM-7090 and -7094 computers (CCC-13A) and in FORTRAN-CODAP language for the CDC-1604 computer (CCC-13B).

UNC-SAM and UNC-SAM-2 are written in FORTRAN 63 language and are operable on the CDC-1604 computer.

3A.4. PROGRAMS BASED ON KERNEL TECHNIQUE

14-0 (CCC-1). – The shielding computer program 14-0 (ref. 114), developed by the General Electric Nuclear Materials and Propulsion Operation, evaluates point-to-point kernels and integrates over source regions to perform reactor-shield penetration calculations for neutrons and gamma rays. Neutron and gamma-ray fluxes and spectra and the dose and energy absorption rates can be computed for positions in and around complex shields containing multiple sources described in a cylindrical coordinate system. In addition, the program can compute reactor shield weight. Computation of any of these quantities in a single problem is optional.

Reactor and shield geometries are described by combinations of regions formed by rotation of rectangles and trapezoids about the reactor-shield axis or parallel axes or by translation of convex quadrilaterals parallel to any axis of the rectangular coordinate system. Compositions are expressed as volume fractions for each material in the reactor-shield assembly and are associated with the appropriate geometrical regions by code numbers.

Source-region integration limits are specified for as many as six source types, and location dimensions are specified for the axis of each source region; a maximum of 200 source regions are possible. Source-region nodal points are located by intersection of axial lines in shells concentric about the source region axes and planes normal to the axes. The provisions for spacing these lines, shells, and planes permit description of cylindrical volume, cylindrical or plane surface, axial or radial line, or point sources. A different source-point spacing is permitted for each source type.

A modification of the Albert-Welton theory of neutron attenuation is used for fast-neutron flux or dose-rate calculations in hydrogenous materials. Moments-method differential number spectra and differential scattered gamma-ray energy spectra are used in the computation of differential neutron spectra and gamma-ray energy spectra. Buildup factors computed by empirical expressions are used in conjunction with exponential attenuation

to compute gamma-ray fluxes and dose and energy absorption rates.

Integration over source regions is performed according to the trapezoidal rule. The integration procedure is automatically adjusted to correctly integrate over volume, surface, or line sources. No integration is performed for point sources. Contributions from multiple source regions are summed to obtain total calculated detector responses.

An auxiliary routine (14-3)[115] performs an extensive check of input data to code 14-0 for range of values, sign, sequencing, and completeness.

This program is written in FAP language for use on IBM-704 and -7090 computers.

14-1 (CCC-2). – The shielding computer program 14-1 (ref. 114), also developed by the General Electric Nuclear Materials and Propulsion Operation, has the same description as code 14-0 (see above) except that the source density must be specified as input for each ring of source points in each different source type.

The auxiliary routine (14-3)[115] performs an extensive check of input data to 14-1 for range of values, sign, sequencing, and completeness.

Program 14-1 is written in FAP language for use on IBM-704 and -7090 computers.

14-2 (CCC-3). – The shielding computer program 14-2 (ref. 116) is a third kernel-type code developed by the General Electric Nuclear Materials and Propulsion Operation and, except for the source description, is the same as codes 14-0 and 14-1 described above. In this code the source location and dimensions are described in rectangular coordinates. Integration limits, which are specified for each space variable, may be equal for any or all variables. Planes of source region nodal points may be equally or unequally spaced between the integration limits of each space variable. Consequently, rectangular parallelepipedal volume or rectangular plane surface sources or line or point sources may be described.

Source density distributions, which must be identical for neutrons and gamma rays, are assumed to be nonseparable. They must be continuous over X, but may be discontinuous over Y and Z. A table of source densities is required as input data. Gamma-ray source energy spectra are assumed to be independent of position.

A data input check is provided by the auxiliary routine 14-3 (ref. 115).

Code 14-2 is written in FAP language for use on IBM-704 and -7090 computers.

CLOUD (CCC-32). – CLOUD[117] is a program designed by Atomics International to calculate the external gamma-ray dose rate and total integrated dose resulting from the accidental release of radioactive materials to the atmosphere.

Wind velocity, lateral and vertical diffusion coefficients, stability parameters, and the presence of physical boundaries such as a ground surface or a temperature inversion layer are considered. Depletion of the radioactive cloud due to washout and fallout is also included. The degree of hazard is estimated from the standpoint of both internal and external exposure.

A Legendre-Gauss quadrature technique is used to perform the numerical integrations of the attenuation kernel over the source regions. A two-compartment continuous-release model is assumed to simulate holdup of the source material. Decay of the source material is described either by the use of a simple parent-daughter decay scheme or by a Way-Wigner type of relationship. Either empirical or calculated fission-product-decay data may be used.

CLOUD is written in FORTRAN language for use on IBM-709, -7090, and -7094 computers.

QAD (CCC-48). – The QAD point-kernel code system[118] was developed by Los Alamos Scientific Laboratory for calculating fast-neutron and gamma-ray penetration in various shield configurations. In the gamma-ray calculation the point kernel method involves representing the gamma-ray source by a number of point isotropic sources and computing the line-of-sight distance from each source point to the detector point. From the distance through the shielding regions and the characteristics of the shielding materials, the geometric attenuation and material attenuation are calculated. The energy transferred along the line of sight is then calculated on the basis of this attenuation and the appropriate buildup factor to account for the scattered radiation. With a distributed source the point kernel including the buildup factor is integrated over the source volume for each source energy considered.

The neutron-penetration calculation is made using a kernel obtained from the moments-method solution to the Boltzmann equation which has been fit by an exponential expression. In this method the neutron spectrum penetrating a shield is de-

termined on the basis of equivalent length of a reference material between the source point and the receiver point. The equivalent length is calculated by weighting the penetration distance for each material in accordance with the material removal cross section. Provisions are also made for computing an alternate neutron dose rate based on the Albert-Welton kernel.

The input data consist of a description of the source distribution and intensity by a number of point isotropic sources, a mathematical representation of the physical geometry with quadratic surfaces, and the tabulation of attenuation coefficients, buildup factors, and conversion factors.

There are several versions of QAD:

1. QAD-IV, the general-purpose basic QAD prototype, which estimates the uncollided gamma-ray flux, dose rate, and energy deposition at specified detector points, and also the fast-neutron dose,
2. QAD-P5, which incorporates a technique for interpolating the results of neutron calculations, has additional source description routines, and has an increased number of output options,
3. QAD-HD (ref. 119), which evaluates the heat deposition and temperature rise of the propellant and the dose to a crew during nuclear rocket reactor operation,
4. QAD-P5A, another version of QAD-P5, which includes a built-in library of gamma-ray attenuation coefficients, buildup factor coefficients, neutron removal cross sections, and neutron moments-method spectra coefficients,
5. QAD-INT, which calculates gamma-ray heating rates within a source region or in a semi-infinite region surrounding the source zone, as well as unscattered and built-up fluxes and dose rates,
6. QAD-V, which permits heating calculations with a two-dimensional integration scheme,
7. QAD-B, which is an expanded version of QAD-P5 with a simplified input format and a more detailed output format and which includes a data library of many of the required input parameters.

All codes in the QAD system are available in FORTRAN IV language for use on IBM-7090 and -7094 computers. QAD-P5 is in addition available in FORTRAN II for use on IBM-7090 and -7094 computers, and in FORTRAN IV for the IBM-360 computer.

COMBINE (CCC-59). – The Combine system[120–125] was developed by the USAF Nuclear Aerospace Research Facility (GD/FW) for the U.S. Army Tank Automotive Center and the U.S. Army Ballistic Research Laboratories, Aberdeen. The system, which consists of Combine I and II, is a set of integration procedures designed to calculate the radiation flux and dose at one or more detector points inside a shielded compartment. The calculation is performed by combining the radiation incident on the shielded compartment, the transmission and reflection probabilities generated by the SPARC program (see above) or similar Monte Carlo codes, and the definition of the geometry of the shielded compartment. The transmission calculation is performed with Combine I and the reflection calculation with Combine II.

Combine I is available in FORTRAN II and FORTRAN IV languages (designated by GD/FW as E91 and E20, respectively), and Combine II is available in FORTRAN IV language. The programs can be used on the IBM-7090 and -7094 computers.

SHADRAC (CCC-84). – The shield penetration code SHADRAC[126] was developed by the USAF Nuclear Aerospace Research Facility (GD/FW) for calculating the neutron or gamma-ray spectrum, the heat generation rate, and/or dose rate at each of a group of point detectors due to each of a group of point sources. The sources may be divided into sets, with each set having a unique source spectrum. The results can also be summed over each source-point set and over the entire source group. Complex geometry may be treated.

Point-to-point kernels based on the differential energy spectrum for a point isotropic source in an infinite medium are integrated over various sources. The data used are based on the moments-method solution of the fast-neutron or gamma-ray transport equation. The stepping-point method is used to solve for the path lengths from source to detector in each region.

The gamma-ray absorption coefficients are based on interpolations of the photoelectric and pair-production cross sections so that the coefficients may be computed for all media of the system. The effective atomic number is interpolated from a table of atomic numbers versus the absorption coefficient per electron.

The source points, which are distributed either by dividing into equal intervals or by a Gaussian quadrature, locate the coordinate planes that are perpendicular to the coordinate axes. The intersections of these planes are source point locations.

SHADRAC is available in FORTRAN IV language for use on IBM-7090 and -7094 computers.

3A.5. PROGRAMS BASED ON SPINNEY REMOVAL-DIFFUSION METHOD

MAC and MAC-RAD (CCC-22). – The MAC code,[71,127] originally developed by Hanford Atomic Products Operation and placed with RSIC by Pacific Northwest Laboratory, Battelle-Northwest, calculates the neutron energy spectrum and dose rate and the gamma-ray dose rate as a function of distance through large reactor shields of concrete or hydrogenous material in slab geometry. The results are given as multigroup neutron fluxes for as many as 35 energy groups and as neutron dose rates, approximate neutron spectra, total gamma-ray dose rates (with a breakdown of the contribution from each region in the shield), and approximate gamma-ray spectra.

The code is based on the Spinney method, which uses a high-energy kernel as the source of neutrons in a multigroup diffusion procedure. This kernel is proportional to the energy-dependent removal flux, which is calculated similarly to the uncollided flux except for the use of a removal cross section equal in magnitude to the usual transport cross section. The removal flux, divided into 18 groups, is calculated for neutrons above 0.5 MeV.

The diffusion equation is reduced to a system of three first-order differential equations which are numerically integrated. In the MAC code the boundary conditions are the diffusion flux at the core-shield interface and a zero incoming flux at the outside edge of the shield. In the MAC-RAD code,[128,72] originated by Allgemeine Elektricitats-Gasellschaft, Kernenergieanlagen at Frankfurt, Germany, the removal flux is added to the diffusion flux at the core-shield interface to obtain the input boundary value. In the first group the entire flux is removal flux. Secondary gamma-ray sources are discontinuous at boundaries.

In both codes the gamma-ray dose rate is calculated for seven source energy groups by using buildup factor kernels.

MAC and MAC-RAD are available in FORTRAN II language for use on the IBM-7090 computer.

NRN (CCC-54). – NRN,[73,74,129,130] a system of codes developed by Aktiebolaget Atomenergi, Stockholm, Sweden, is built around the Spinney method of combining high-energy exponential attenuation with low-energy diffusion. The high-energy exponentially attenuating flux is broken into several energy groups, each of which requires removal cross sections.

Given a distribution of fissions (e.g., power distribution) in certain allowed geometric regions, NRN solves for neutron flux densities, absorption rates (from which secondary gamma-ray source rates may be determined), dose rates, and energy deposit rates (by energy groups) in primary knock-on atoms. Two of its auxiliary routines, REBOX and REMC, can be adapted to compute gamma-ray dose rates from gamma-ray sources in the central region (core).

The routine NECO computes all the required macroscopic quantities, including removal cross sections, from the microscopic quantities and the material compositions. The calculation of removal cross sections is a unique feature of NRN.

The exponential attenuation of the fast group fluxes (removal fluxes) is carried out by the REBOX routine if the source region is a parallelepiped or a large cylinder, and by the REMC routine if the source region is a sphere or a small cylinder. The integration over the source volume is carried out by a mesh-sum procedure in REBOX and by a Monte Carlo procedure in REMC.

NEDI, a diffusion routine, uses as sources the removal fluxes in the shield region computed by REBOX or REMC. Since the geometry of NEDI is limited to multiregion infinite slabs, infinite cylinders, and spheres, there is a geometric inconsistency, except for the sphere, with REBOX and REMC. This is to be interpreted as an approximation, not an error. NEDI further provides for transverse bucklings in the slab and cylindrical cases in order to estimate the effect of truncating the infinite systems. NEDI solves the diffusion equation by preserving the form $\nabla \cdot D \nabla \Phi$, which should allow the cross sections within a region to be continuously varied, although no such provision has actually been included.

The specification of reasonable external boundary conditions in the shield region is relatively simple, but the specification of reasonable internal boundary conditions is very difficult. If a sig-

nificant part of the final answer depends heavily upon the diffusion current or flux (rather than on the removal current or flux) at the interior shield boundary, this program should be used only with great circumspection.

NRN is available in FORTRAN IV and MAP languages for use on IBM-7090 and -7044 computers.

COMPRASH (CCC-72). – COMPRASH[70,131] is the latest code made available in a series of programs developed by the Shielding Groups of the Atomic Energy Research Establishment at Harwell for calculating fast-neutron spectra, thermal-neutron flux densities, and secondary gamma-ray dose rates for reactor shields in slab geometry. It uses the two-step Spinney removal-diffusion method of calculating neutron transport. The basic assumption is that the penetrating component from a point source can be calculated by a kernel given by

$$\Phi_0(E,R) = \frac{S\, f(E)\, e^{-\Sigma_r(E)R}}{4\pi R^2} ,$$

where

$\Phi_0(R)$ = removal flux density,

$f(E)$ = fission neutron spectrum,

S = source normalization,

$\Sigma_r(E)$ = energy-dependent removal cross section,

R = distance from source.

The removal source function

$$S(R,E) = \Sigma_r(E)\, \Phi_0(E,R)$$

is then made the source term in a conventional multigroup age-diffusion calculation to calculate the diffusing neutron spectra, including a thermal-neutron group.

The value of the removal cross section is taken to be the usual transport cross section, an assumption that is justified by the remarkable success of the model in predicting the thermal-neutron flux densities measured in bulk concrete shields.

The secondary gamma-ray transport is calculated with the use of an analytic form of the buildup factor.

COMPRASH is written in FORTRAN II and FAP languages for use on the IBM-7090 computer.

Appendix 3B. Coefficients for Gamma-Ray Buildup Factors

This appendix consists of tabulations of coefficients for the Taylor, Berger, and polynomial forms of the empirical equation for gamma-ray buildup factors. The coefficients were determined from best fits to the data of Goldstein and Wilkins (see Section 3.8.1).

Table 3B.1. Coefficients for the Taylor Form of the Dose Buildup Factor[a]

Material	E (MeV)	A	$-\alpha_1$	α_2	Maximum Deviation (%)[b]
Water	0.5	100.845	0.12687	−0.10925	−27.4, $\mu x = 10$
	1	19.601	0.09037	−0.02522	−10.8, $\mu x = 10$
	2	12.612	0.05320	0.01932	4.2, $\mu x = 1$
	3	11.110	0.03550	0.03206	1.7, $\mu x = 1$
	4	11.163	0.02543	0.03025	0.8, $\mu x = 20$
	6	8.385	0.01820	0.04164	−0.5, $\mu x = 2$
	8	4.635	0.02633	0.07097	0.6, $\mu x = 7$
	10	3.545	0.02991	0.08717	−0.7, $\mu x = 1$
Aluminum	0.5	38.911	0.10015	−0.06312	−12.2, $\mu x = 10$
	1	28.782	0.06820	−0.02973	−8.6, $\mu x = 10$
	2	16.981	0.04588	0.00271	−5.2, $\mu x = 10$
	3	10.583	0.04066	0.02514	−2.5, $\mu x = 10$
	4	7.526	0.03973	0.03860	1.8, $\mu x = 20$
	6	5.713	0.03934	0.04347	1.6, $\mu x = 20$
	8	4.716	0.03837	0.04431	−1.3, $\mu x = 15$
	10	3.999	0.03900	0.04130	1.2, $\mu x = 20$
Barytes concrete	0.5	33.026	0.06129	−0.02883	7.5, $\mu x = 2$
	1	23.014	0.06255	−0.02217	8.9, $\mu x = 20$
	2	9.350	0.05700	0.03850	9.0, $\mu x = 2$
	3	6.269	0.06064	0.04440	4.8, $\mu x = 20$
	4	4.730	0.06500	0.05883	4.8, $\mu x = 2$
	6	3.240	0.08000	0.06407	5.0, $\mu x = 2$
	8	2.167	0.09514	0.07857	1.3, $\mu x = 20$
	10	1.433	0.11201	0.13021	3.2, $\mu x = 20$
Ferrophosphorous concrete	0.5	61.341	0.07292	−0.05265	11.0, $\mu x = 2$
	1	46.087	0.05202	−0.02845	10.3, $\mu x = 2$
	2	14.790	0.04720	0.00867	3.0, $\mu x = 2$
	3	10.399	0.04290	0.02211	2.6, $\mu x = 20$
	4	6.240	0.05280	0.03765	1.7, $\mu x = 2$
	6	4.425	0.05880	0.04262	−1.0, $\mu x = 2$
	8	3.000	0.06750	0.05730	0.8, $\mu x = 4$
	10	2.279	0.07575	0.06438	0.4, $\mu x = 6$
Ordinary concrete	0.5[c]	38.225	0.14824	−0.10579	−7.5, $\mu x = 4$
	1	25.507	0.07230	−0.01843	11.1, $\mu x = 2$
	2	18.089	0.04250	0.00849	4.9, $\mu x = 2$
	3	13.640	0.03200	0.02022	4.3, $\mu x = 2$
	4	11.460	0.02600	0.02450	−5.1, $\mu x = 2$
	6	10.781	0.01520	0.02925	−2.7, $\mu x = 2$
	8	8.972	0.01300	0.02979	−3.7, $\mu x = 2$
	10	4.015	0.02880	0.06844	−2.2, $\mu x = 2$
Magnetite concrete	0.5	75.471	0.07479	−0.05534	15.9, $\mu x = 2$
	1	49.916	0.05195	−0.02796	11.5, $\mu x = 2$
	2	14.260	0.04692	0.01531	4.0, $\mu x = 2$
	3	8.160	0.04700	0.04590	5.0, $\mu x = 2$
	4	5.580	0.05200	0.05728	2.7, $\mu x = 2$
	6	3.437	0.06000	0.11520	4.3, $\mu x = 4$
	8	2.480	0.06645	0.14002	4.0, $\mu x = 20$
	10	1.743	0.08082	0.27209	5.3, $\mu x = 20$

Table 3B.1 (continued)

Material	E (MeV)	A	$-\alpha_1$	α_2	Maximum Deviation (%)[b]
Iron	0.5	31.379	0.06842	−0.03742	−6.5, $\mu x = 10$
	1	24.957	0.06086	−0.02463	−6.4, $\mu x = 10$
	2	17.622	0.04627	−0.00526	4.0, $\mu x = 2$
	3	13.218	0.04431	−0.00087	−3.0, $\mu x = 10$
	4	9.624	0.04698	0.00175	−2.7, $\mu x = 10$
	6	5.867	0.06150	−0.00186	2.1, $\mu x = 20$
	8	3.243	0.07500	0.02123	3.8, $\mu x = 4$
	10	1.747	0.09900	0.06627	3.7, $\mu x = 2$
Lead	0.5[c]	1.677	0.03084	0.30941	−0.8, $\mu x = 10$
	1	2.984	0.03503	0.13486	−1.0, $\mu x = 1$
	2	5.421	0.03482	0.04379	−0.6, $\mu x = 1$
	3	5.580	0.05422	0.00611	1.3, $\mu x = 4$
	4	3.897	0.08468	−0.02383	1.4, $\mu x = 20$
	6	0.926	0.17860	−0.04635	1.3, $\mu x = 20$
	8	0.368	0.23691	−0.05684	1.8, $\mu x = 15$
	10	0.311	0.24024	−0.02783	−0.5, $\mu x = 1$
Tin	0.5[c]	11.440	0.01800	0.03187	−1.6, $\mu x = 1$
	1	11.426	0.04266	0.01606	−2.6, $\mu x = 10$
	2	8.783	0.05349	0.01505	−2.8, $\mu x = 10$
	3	5.400	0.07440	0.02080	4.3, $\mu x = 20$
	4	3.496	0.09517	0.02598	−3.9, $\mu x = 10$
	6	2.005	0.13733	−0.01501	−2.8, $\mu x = 10$
	8	1.101	0.17288	−0.01787	−3.4, $\mu x = 15$
	10	0.708	0.19200	0.01552	2.6, $\mu x = 15$
Tungsten	0.5[c]	2.655	0.01740	0.11340	−4.9, $\mu x = 2$
	1[c]	3.234	0.04754	0.13058	−0.9, $\mu x = 10$
	2[c]	3.504	0.06053	0.08862	2.1, $\mu x = 10$
	3	4.722	0.06468	0.01404	−2.4, $\mu x = 10$
	4	5.520	0.08857	−0.04570	1.3, $\mu x = 20$
	6	1.273	0.17257	−0.12178	−2.9, $\mu x = 15$
	8	0.664	0.20710	0.04692	1.4, $\mu x = 10$
	10	0.509	0.21743	0.05025	−3.6, $\mu x = 15$
Uranium	0.5[c]	1.444	0.02459	0.35167	−0.9, $\mu x = 10$
	1[c]	2.081	0.03862	0.22639	−0.7, $\mu x = 10$
	2[c]	3.287	0.03997	0.08635	−0.5, $\mu x = 1$
	3	4.883	0.04950	0.00981	−0.9, $\mu x = 15$
	4	2.800	0.08240	0.00370	1.4, $\mu x = 4$
	6	0.975	0.15886	0.21101	−2.2, $\mu x = 15$
	8	0.602	0.19189	0.02774	−2.1, $\mu x = 15$
	10	0.399	0.21314	0.02083	−2.9, $\mu x = 15$

[a]Table taken from: S. Buscaglione and R. Manzini, *Build-Up Factors: Coefficients of the Equation of J. J. Taylor*, Oak Ridge National Laboratory Report ORNL-tr-80 [translated from Comitato Nazionale per l'Energia Nucleare Report RT/FI (65)7 (January 1965)].

[b]The values of μx given in this column are the values for which the corresponding errors are valid.

[c]For some materials the values of the buildup factor for given energies are known only in the interval of $1 \leqq \mu x \leqq 15$. In these cases, the parameters are valid up to $\mu x = 15$.

Table 3B.2. Coefficients for the Polynomial Form of the Dose Buildup Factor[a]

Material	E (MeV)	β_0	β_1	β_2	β_3	Maximum Deviation (%)[b]	Average Deviation (%)
Ordinary concrete	1	5.1902(−1)[c]	1.6152(0)	5.4702(−2)	1.8803(−3)	−3.6, $\mu x = 4$	1.8
	2	7.7342(−1)	9.1835(−1)	2.7260(−2)	−3.9911(−4)	1.2, $\mu x = 2$	0.4
	3	1.0530(0)	6.3743(−1)	1.6185(−2)	−3.8875(−4)	−3.9, $\mu x = 2$	1.2
	4	1.1506(0)	4.9800(−1)	1.0547(−2)	−2.9613(−4)	−1.9, $\mu x = 8$	0.8
	5	1.1806(0)	4.1634(−1)	7.2376(−3)	−2.2268(−4)	2.8, $\mu x = 2$	1.3
	6	1.1846(0)	3.6314(−1)	5.0942(−3)	−1.6888(−4)	2.1, $\mu x = 8$	0.9
	7	1.1784(0)	3.2590(−1)	3.6051(−1)	−1.2895(−4)	−1.3, $\mu x = 4$	0.4
Magnetite concrete	1	5.2780(−1)	1.1562(0)	9.7936(−2)	−1.4084(−3)	1.8, $\mu x = 20$	0.8
	2	9.3721(−1)	8.0638(−1)	3.1686(−2)	−4.9503(−4)	1.5, $\mu x = 8$	0.6
	3	9.5856(−1)	6.5113(−1)	1.3680(−2)	−2.0725(−4)	−1.6, $\mu x = 4$	0.6
	4	9.7216(−1)	5.3998(−1)	7.8749(−3)	−1.0316(−4)	−2.3, $\mu x = 10$	1.7
	5	9.8690(−1)	4.5747(−1)	5.8668(−3)	−6.0375(−5)	1.8, $\mu x = 10$	1.0
	6	1.0010(0)	3.9452(−1)	5.2611(−3)	−4.1859(−5)	3.0, $\mu x = 10$	2.3
	7	1.0237(0)	3.4521(−1)	5.2272(−3)	−3.4147(−5)	2.6, $\mu x = 8$	1.4
Ferrophosphorus concrete	1	5.2446(−1)	1.1570(0)	6.6197(−2)	−2.6909(−4)	1.4, $\mu x = 10$	0.7
	2	9.0796(−1)	8.0470(−1)	2.4051(−2)	−1.3747(−4)	1.4, $\mu x = 20$	0.5
	3	9.7879(−1)	6.3258(−1)	1.3122(−2)	−2.8460(−5)	−3.6, $\mu x = 20$	1.1
	4	9.9224(−1)	5.2504(−1)	8.2727(−3)	8.2210(−5)	−2.0, $\mu x = 12$	1.5
	5	9.9175(−1)	4.5156(−1)	5.5458(−3)	1.7478(−4)	2.6, $\mu x = 20$	1.0
	6	9.8751(−1)	3.9831(−1)	3.7988(−3)	2.4954(−4)	3.3, $\mu x = 20$	2.4
	7	9.8244(−1)	3.5799(−1)	2.5837(−3)	3.1005(−4)	2.4, $\mu x = 6$	1.6
Barytes concrete	1	1.4863(0)	4.2184(−1)	1.3686(−1)	−2.7616(−3)	2.1, $\mu x = 4$	1.0
	2	1.0139(0)	6.7003(−1)	3.5826(−2)	−5.2672(−4)	2.2, $\mu x = 8$	1.1
	3	9.3467(−1)	5.9469(−1)	2.0106(−2)	−2.9295(−4)	−5.4, $\mu x = 6$	2.6
	4	9.1379(−1)	5.1277(−1)	1.3442(−2)	−5.0691(−5)	−3.8, $\mu x = 14$	2.2
	5	9.0721(−1)	4.4778(−1)	9.2573(−3)	1.8044(−4)	2.4, $\mu x = 8$	1.5
	6	9.0525(−1)	3.9750(−1)	6.2307(−3)	3.8250(−4)	5.3, $\mu x = 8$	3.8
	7	9.0500(−1)	3.5806(−1)	3.8974(−3)	5.5449(−4)	4.0, $\mu x = 8$	2.9

[a]Table taken from: S. Buscaglione and R. Manzini, *On the Build-Up Factors of Concrete: Coefficients of the Polynomial Representation*, Oak Ridge National Laboratory Report ORNL-tr-349 [translated from Comitato Nazionale per l'Energia Nucleare Report CEC-94 (June 1964)].

[b]The values of μx given in this column are the values for which the corresponding errors are valid.

[c]Read: 5.1902×10^{-1}, etc.

Table 3B.3. Coefficients for Linear, Quadratic, and Berger Forms of Dose Buildup Factors Fitted over the Range 0 to 7 Mean Free Paths from Point Isotropic Source[a]

Material	E (MeV)	A_1	Maximum Error (%)[b]	A_2	b	Maximum Error (%)	C	D	Maximum Error (%)
Water	0.255	8.6524	F3.1	−0.2525	1.4984	30	1.7506	0.2609	10
	0.5	4.6800	F2.3	0.6684	0.6750	8	1.3245	0.2078	5
	1	1.9953	40	1.0053	0.1666	2	1.0622	0.1052	3
	2	1.0301	10	0.8242	0.0346	2	0.8093	0.0408	1
	3	0.7397	3	0.6962	0.0073	1	0.6876	0.0125	1
	4	0.5884	1	0.5801	0.0014	1	0.5800	0.0024	1
	6	0.4321	3	0.4616	−0.0050	1	0.4655	−0.0126	1
	8	0.3406	4	0.3782	−0.0063	1	0.3860	−0.0214	1
	10	0.2877	4	0.3251	−0.0063	1	0.3342	−0.0257	1
Aluminum	0.5	2.6461	F1.5	1.0688	0.2654	2	1.2435	0.1250	3
	1	1.6089	30	0.9316	0.1140	2	0.9589	0.0864	3
	2	0.9686	13	0.7437	0.0378	2	0.7267	0.0486	2
	3	0.7197	5	0.6355	0.0142	1	0.6294	0.0227	1
	4	0.5663	3	0.5284	0.0064	1	0.5253	0.0127	1
	6	0.4334	2	0.4142	0.0032	1	0.4177	0.0061	1
	8	0.3476	1	0.3346	0.0022	1	0.3371	0.0050	1
	10	0.2847	2	0.2715	0.0022	1	0.2752	0.0055	1
Iron	0.5	1.4283	25	0.8642	0.0949	1	0.9081	0.0752	2
	1	1.2373	20	0.8026	0.0731	1	0.8214	0.0684	2
	2	0.8556	12	0.6526	0.0342	5	0.7020	0.0319	3
	3	0.6691	9	0.5338	0.0228	1	0.5323	0.0384	1
	4	0.5403	7	0.4366	0.0175	1	0.4366	0.0358	1
	6	0.4297	8	0.3237	0.0178	1	0.3271	0.0457	1
	8	0.3391	8	0.2473	0.0154	1	0.2563	0.0464	1
	10	0.2681	8	0.1785	0.0151	1	0.1876	0.0592	1
Tin	0.5	0.5153	3	0.5479	−0.0055	2	0.5608	−0.0146	1
	1	0.7199	6	0.6153	0.0176	1	0.6219	0.0244	1
	2	0.6731	8	0.5455	0.0215	1	0.5498	0.0338	1
	3	0.5837	11	0.4284	0.0261	1	0.4379	0.0479	1
	4	0.5146	12	0.3420	0.0290	1	0.3583	0.0601	1
	6	0.4153	17	0.2082	0.0348	2	0.2369	0.0925	1
	8	0.3317	17	0.1371	0.0327	2	0.1692	0.1103	1
	10	0.2550	16	0.0945	0.0270	2	0.1232	0.1190	1
Tungsten	0.5	0.1903	8	0.2692	−0.0133	2	0.2938	−0.0751	2
	1	0.3817	5	0.4269	−0.0076	2	0.4425	−0.0255	1
	2	0.4376	2	0.4164	0.0036	1	0.4172	0.0080	1
	3	0.4171	5	0.3515	0.0110	1	0.3501	0.0295	1
	4	0.4054	12	0.2540	0.0255	1	0.2710	0.0666	1
	6	0.3363	17	0.1435	0.0324	2	0.1771	0.1049	1
	8	0.2624	16	0.0957	0.0281	2	0.1245	0.1223	1
	10	0.2073	14	0.0748	0.0223	2	0.0974	0.1238	1

Table 3B.3 (continued)

Material	E (MeV)	A_1	Maximum Error (%)[b]	A_2	b	Maximum Error (%)	C	D	Maximum Error (%)
Lead	0.5	0.1549	8	0.2273	−0.0122	3	0.2526	−0.0848	2
	1	0.2990	6	0.3613	−0.0105	2	0.3779	−0.0403	1
	2	0.3796	1	0.3787	0.0001	1	0.3862	0.0032	1
	3	0.3810	5	0.3164	0.0109	1	0.3267	0.0253	1
	4	0.3523	10	0.2389	0.0191	1	0.2530	0.0547	1
	5.1	0.3219	13	0.1747	0.0248	1	0.1936	0.0839	1
	6	0.3034	15	0.1346	0.0284	2	0.1622	0.1027	1
	8	0.2419	15	0.0894	0.0257	3	0.1220	0.1112	2
	10	0.1933	13	0.0642	0.0217	3	0.0939	0.1167	2
Uranium	0.5	0.1054	7	0.1637	−0.0098	2	0.1825	−0.0951	2
	1	0.2264	7	0.2990	−0.0122	2	0.3204	−0.0599	2
	2	0.3023	3	0.3250	−0.0038	1	0.3321	−0.0162	1
	3	0.3169	4	0.2760	0.0069	1	0.2814	0.0196	1
	4	0.3010	7	0.2199	0.0136	1	0.2283	0.0458	1
	6	0.2571	12	0.1314	0.0212	1	0.1476	0.0916	1
	8	0.2081	12	0.0885	0.0201	1	0.1081	0.1076	1
	10	0.1621	11	0.0638	0.0165	1	0.0798	0.1163	1
Ordinary concrete	0.5	3.7443	30	1.3563	0.4018	7	1.4489	0.1586	10
	1	1.9057	40	1.0980	0.1359	7	1.0448	0.1014	7
	2	1.0226	12	0.8238	0.0335	2	0.8062	0.0403	2
	3	0.7303	7	0.6189	0.0187	1	0.6267	0.0254	1
	4	0.5736	5	0.6106	−0.0062	3	0.6451	−0.0207	3
	6	0.4329	6	0.4667	−0.0057	4	0.5086	−0.0286	3
	8	0.3376	6	0.3794	−0.0070	3	0.4085	−0.0334	2
	10	0.2923	5	0.3344	−0.0071	3	0.3584	−0.0356	2
Ferrophosphorous concrete	0.5	1.9407	F1.5	0.9330	0.1696	8	0.9059	0.1283	8
	1	1.4657	30	0.8542	0.1029	3	0.8467	0.0921	5
	2	0.9264	10	0.7481	0.0300	2	0.7327	0.0397	2
	3	0.6996	4	0.6198	0.0134	1	0.6331	0.0164	1
	4	0.5611	6	0.4980	0.0106	2	0.4879	0.0237	2
	6	0.4399	2	0.4119	0.0047	2	0.4346	0.0011	2
	8	0.3493	2	0.3243	0.0042	2	0.3390	0.0043	2
	10	0.2827	3	0.2574	0.0043	1	0.2563	0.0165	1
Magnetite concrete	0.5	2.3150	F1.5	0.9510	0.2295	3	1.1049	0.1221	4
	1	1.6021	33	0.8847	0.1207	3	0.9006	0.0965	4
	2	0.9757	10	0.7636	0.0357	2	0.7770	0.0380	1
	3	0.7110	5	0.6163	0.0159	2	0.6321	0.0194	1
	4	0.5634	4	0.5177	0.0077	1	0.5241	0.0119	2
	6	0.4410	2	0.4200	0.0035	2	0.4401	−0.0004	2
	8	0.3391	2	0.3127	0.0044	1	0.3225	0.0080	1
	10	0.2840	2	0.2670	0.0029	1	0.2682	0.0096	1

Table 3B.3 (continued)

Material	E (MeV)	A_1	Maximum Error (%)[b]	A_2	b	Maximum Error (%)	C	D	Maximum Error (%)
Barytes concrete	0.5	1.4414	23	0.8769	0.0950	2	0.9313	0.0724	1
	1	1.2066	21	0.7599	0.0752	1	0.7764	0.0737	2
	2	0.8740	10	0.6886	0.0312	1	0.7006	0.0368	1
	3	0.6556	6	0.5345	0.0204	3	0.5508	0.0289	2
	4	0.5634	9	0.4682	0.0160	3	0.4413	0.0418	3
	6	0.4571	10	0.3344	0.0207	1	0.3342	0.0525	2
	8	0.3519	5	0.2836	0.0115	1	0.2901	0.0321	1
	10	0.2684	7	0.1894	0.0133	1	0.1990	0.0495	1

[a]From D. K. Trubey, *A Survey of Empirical Functions Used to Fit Gamma-Ray Buildup Factors*, Oak Ridge National Laboratory Report ORNL-RSIC-10 (February 1966).

[b]F3.1 means "factor of 3.1," etc.

Table 3B.4. Coefficients for Linear, Quadratic, and Berger Forms of Dose Buildup Factors Fitted over the Range 0 to 20 Mean Free Paths from Point Isotropic Sources[a]

Material	E (MeV)	A_1	Maximum Error (%)[b]	A_2	b	Maximum Error (%)[b]	C	D	Maximum Error (%)
Water	0.255	36.1015	F12	−12.9947	3.0515	F∞	2.5048	0.1623	30
	0.5	13.0926	F5.6	−0.9744	0.8743	F3	1.8035	0.1224	25
	1	3.4788	F2	1.1152	0.1469	6	1.2282	0.0649	11
	2	1.2549	25	0.9173	0.0210	6	0.8594	0.0240	5
	3	0.7863	6	0.7218	0.0040	2	0.7004	0.0074	2
	4	0.5951	1	0.5907	0.0003	1	0.5826	0.0014	1
	6	0.4030	5	0.4471	−0.0027	2	0.4853	−0.0082	1
	8	0.3085	7	0.3561	−0.0038	2	0.3741	−0.0124	2
	10	0.2584	7	0.3002	−0.0026	3	0.3206	−0.0139	2
Aluminum	0.5	5.7374	F3	0.6696	0.3150	20	1.4412	0.0850	12
	1	2.5385	F1.9	1.1185	0.0883	10	1.0831	0.0535	9
	2	1.1928	30	0.8751	0.0197	8	0.7869	0.0266	6
	3	0.8061	12	0.6812	0.0078	3	0.6504	0.0137	3
	4	0.6075	6	0.5503	0.0036	2	0.5343	0.0082	2
	6	0.4626	6	0.4252	0.0023	2	0.4182	0.0063	1
	8	0.3697	5	0.3395	0.0019	1	0.3366	0.0058	1
	10	0.3087	5	0.2750	0.0021	1	0.2738	0.0074	1
Iron	0.5	2.3773	F1.9	0.9019	0.0917	3	0.9814	0.0548	7
	1	1.8643	F1.6	0.9212	0.0586	7	0.8932	0.0460	7
	2	1.1194	33	0.7423	0.0234	6	0.7173	0.0277	4
	3	0.8446	25	0.5840	0.0162	4	0.5571	0.0261	4
	4	0.6942	25	0.4605	0.0145	2	0.4518	0.0268	3
	6	0.6134	34	0.3201	0.0182	1	0.3381	0.0368	3
	8	0.5245	40	0.2207	0.0189	3	0.2603	0.0428	2
	10	0.4759	50	0.1143	0.0225	6	0.1902	0.0553	1

Table 3B.4 (continued)

Material	E (MeV)	A_1	Maximum Error (%)[b]	A_2	b	Maximum Error (%)[b]	C	D	Maximum Error (%)
Tin	0.5	0.5090	4	0.5150	−0.0005	3	0.5457	−0.0063	3
	1	0.8495	18	0.6666	0.0114	3	0.6378	0.0180	3
	2	0.8521	25	0.5826	0.0168	3	0.5678	0.0254	3
	3	0.8509	40	0.4254	0.0264	1	0.4533	0.0388	3
	4	0.8643	F1.58	0.2845	0.0360	5	0.3700	0.0518	3
	6	1.0786	F2.2	−0.1374	0.0756	40	0.2401	0.0891	2
	8	1.1907	F2.8	−0.4693	0.1032	F3	0.1669	0.1145	1
	10	1.1075	F3.0	−0.6523	0.1094	F12	0.1190	0.1278	5
Tungsten	0.5	0.1550	13	0.2206	−0.0054	5	0.2692	−0.0477	5
	1	0.3382	9	0.4149	−0.0048	2	0.4279	−0.0150	2
	2	0.4671	8	0.4072	0.0037	3	0.4163	0.0070	4
	3	0.5919	30	0.3255	0.0165	2	0.3484	0.0324	2
	4	0.8102	F1.8	0.0995	0.0442	15	0.2727	0.0653	1
	6	1.2616	F3	−0.5462	0.1124	F4	0.1704	0.1160	2
	8	1.3753	F3.5	−0.9399	0.1439	F∞	0.1161	0.1405	6
	10	1.2730	F3.8	−0.9502	0.1382	F∞	0.0882	0.1510	7
Lead	0.5	0.1043	15	0.1791	−0.0047	5	0.2243	−0.0500	5
	1	0.2549	11	0.3133	−0.0036	5	0.3530	−0.0211	4
	2	0.3947	3	0.3695	0.0015	2	0.3791	0.0021	1
	3	0.5123	30	0.2990	0.0133	2	0.3244	0.0279	1
	4	0.6378	F1.6	0.1449	0.0306	10	0.2526	0.0557	1
	5.1	0.8560	F2.1	−0.1480	0.0624	40	0.1904	0.0883	2
	6	1.1247	F2.8	−0.5070	0.1014	F4	0.1554	0.1143	4
	8	1.4165	F4	−1.1408	0.1589	F∞	0.1075	0.1440	12
	10	1.2370	F4	−1.0279	0.1408	F∞	0.0824	0.1513	12
Uranium	0.5	0.0812	11	0.1262	−0.0037	5	0.1635	−0.0606	5
	1	0.1914	11	0.2556	−0.0053	5	0.2991	−0.0385	5
	2	0.2838	5	0.3185	−0.0022	2	0.3240	−0.0084	2
	3	0.4081	20	0.2614	0.0091	2	0.2781	0.0234	1
	4	0.4991	43	0.1621	0.0210	6	0.2273	0.0475	1
	6	0.8088	F2.3	−0.2492	0.0658	F2	0.1426	0.1011	2
	8	0.9323	F2.9	−0.5357	0.0912	F5	0.1004	0.1274	5
	10	0.9203	F3.3	−0.6560	0.0980	F∞	0.0721	0.1442	7
Ordinary concrete	0.5	5.0124	F2.3	0.8341	0.5016	10	1.5177	0.1413	12
	1	2.9917	F2	1.1821	0.1125	10	1.2208	0.0562	11
	2	1.2334	25	0.9344	0.0186	7	0.8579	0.0231	5
	3	0.7857	12	0.7141	0.0044	6	0.6589	0.0115	5
	4	0.5942	4	0.5662	0.0017	5	0.6056	−0.0018	4
	6	0.4145	5	0.4440	−0.0018	5	0.4769	−0.0093	4
	8	0.3200	4	0.3445	−0.0015	5	0.3789	−0.0113	4
	10	0.2737	5	0.3015	−0.0017	5	0.3318	−0.0128	4

Table 3B.4 (continued)

Material	E (MeV)	A_1	Maximum Error (%)[b]	A_2	b	Maximum Error (%)[b]	C	D	Maximum Error (%)
Ferrophosphorous concrete	0.5	3.4067	F2.2	1.1051	0.1431	15	1.1098	0.0704	15
	1	2.1096	F1.7	1.1170	0.0617	15	0.9892	0.0481	10
	2	1.1583	30	0.7992	0.0223	4	0.7703	0.0256	3
	3	0.8138	16	0.6488	0.0103	2	0.6373	0.0152	2
	4	0.6702	16	0.4923	0.0111	2	0.4966	0.0186	2
	6	0.5469	18	0.3622	0.0115	5	0.4118	0.0167	3
	8	0.4477	19	0.2692	0.0111	5	0.3207	0.0196	4
	10	0.3972	25	0.1971	0.0124	5	0.2456	0.0287	3
Magnetite concrete	0.5	4.2793	F2.5	1.4544	0.1756	23	1.3246	0.0736	18
	1	2.3058	F1.7	1.2562	0.0652	20	1.0651	0.0492	12
	2	1.1752	25	0.8756	0.0186	5	0.8208	0.0227	5
	3	0.8098	15	0.6616	0.0092	3	0.6445	0.0143	2
	4	0.6263	10	0.5280	0.0061	2	0.5265	0.0108	1
	6	0.4781	7	0.4257	0.0033	2	0.4312	0.0062	2
	8	0.3805	9	0.3195	0.0038	2	0.3204	0.0106	2
	10	0.3399	12	0.2428	0.0060	3	0.2623	0.0156	2
Barytes concrete	0.5	2.2489	F1.8	1.1064	0.0710	11	1.0183	0.0496	10
	1	1.8761	F1.7	1.0022	0.0543	14	0.8555	0.0495	12
	2	1.1122	30	0.7591	0.0219	4	0.7291	0.0265	4
	3	0.8068	24	0.6047	0.0126	6	0.5673	0.0222	4
	4	0.6873	21	0.4913	0.0122	4	0.4689	0.0242	4
	6	0.6277	30	0.3420	0.0178	2	0.3542	0.0355	4
	8	0.5574	40	0.1882	0.0229	10	0.2806	0.0409	3
	10	0.4943	50	0.0936	0.0249	10	0.1949	0.0555	2

[a]From D. K. Trubey, *A Survey of Empirical Functions Used to Fit Gamma-Ray Buildup Factors*, Oak Ridge National Laboratory Report ORNL-RSIC-10 (February 1966).

[b]F12 means "factor of 12," etc.

Appendix 3C. Graphs and Formulas of Exponential and Exponential Integral Functions

Several exponential functions that are extremely useful in shielding calculations are presented in this appendix. They include the exponential function e^{-x} and the exponential integral functions $E_n(x)$, which are expressed in integral form by

$$E_n(x) = x^{n-1} \int_x^\infty e^{-y} \frac{dy}{y^n}, \qquad \text{(C1)}$$

$$E_n(x) = \int_1^\infty e^{-xy} \frac{dy}{y^n}, \qquad \text{(C2)}$$

$$E_n(x) = \int_0^1 y^{n-2}\, e^{-x/y}\, dy\ , \qquad \text{(C3)}$$

and in series form by

$$E_n(x) = \sum_{\substack{m=0 \\ m \neq n-1}}^{\infty} \frac{(-x)^m}{(n-1-m)\, m!}$$

$$+ (-1)^n \frac{x^{n-1}}{(n-1)!} (\ln \gamma x - A_n)\ , \qquad \text{(C4)}$$

where

$$\ln \gamma = 0.577216 \ldots ,$$

$$A_1 = 0 ,$$

$$A_n = \sum_{m=1}^{n-1} \frac{1}{m} ,$$

and $n = 0, 1, 2, 3, \ldots$. The recursion relation for the exponential integrals is

$$E_n(x) = \frac{1}{n-1} [e^{-x} - x E_{n-1}(x)] \quad \text{(ref. 132)} . \qquad \text{(C5)}$$

In particular, the first-order exponential integral is given by

$$E_1(x) = \int_x^{\infty} \frac{e^{-y}}{y}\, dy \qquad \text{(C6)}$$

and the series representation by

$$E_1(x) = -\ln \gamma x - \sum_{n=0}^{\infty} \frac{(-1)^n\, x^n}{n!n} . \qquad \text{(C7)}$$

In some publications the $E_1(x)$ function is denoted by $-Ei(-x)$; that is, $E_1(x) = -Ei(-x)$. In using tables of the exponential function, caution should always be exercised so as not to confuse $-Ei(-x)$ with $-Ei(x)$, which is defined below.

For negative arguments, the $E_1(x)$ function is frequently denoted by the symbol $Ei(x)$, which is defined by

$$Ei(x) \equiv \int_{-\infty}^{x} \frac{e^y}{y}\, dy \qquad \text{(C8)}$$

and related to $E_1(-x)$ by

$$-Ei(x) = E_1(-x) = \int_{-x}^{\infty} e^y \frac{dy}{y} . \qquad \text{(C9)}$$

Graphs of e^{-x} and $E_n(x)$ for $n = 1$, 2, and 3 are presented in Figs. 3C.1 through 3C.6 (from ref. 134). The function $Ei(x)$ is plotted in Figs. 3C.7 through 3C.10 (from ref. 133).

Some approximations that are frequently useful are

$$\frac{e^{-x}}{x+n} < E_n(x) \leq \frac{e^{-x}}{x+n-1} , \qquad n \geq 1 , \qquad \text{(C10)}$$

$$E_n(x) = \frac{e^{-x}}{x} \{1 - (n/x) + [n(n+1)/x^2]$$

$$- [n(n+1)(n+2)/x^3] + \ldots\} ,$$

$$x \gg 1 , \qquad n = 0 , \qquad \text{(C11)}$$

$$E_n(x) \cong \{(1 + x + n)/[x + (x+n)^2]\}\, e^{-x} ,$$

$$x > 1 \qquad \text{(ref. 135)} , \qquad \text{(C12)}$$

$$Ei(x) \cong e^x \left[\left(\frac{1}{x}\right) + \left(\frac{1}{x^2}\right) + \left(\frac{2!}{x^3}\right) + \left(\frac{3!}{x^4}\right) + \ldots\right] ,$$

$$x > 10 . \qquad \text{(C13)}$$

Further information concerning the exponential integrals can be found in ref. 136.

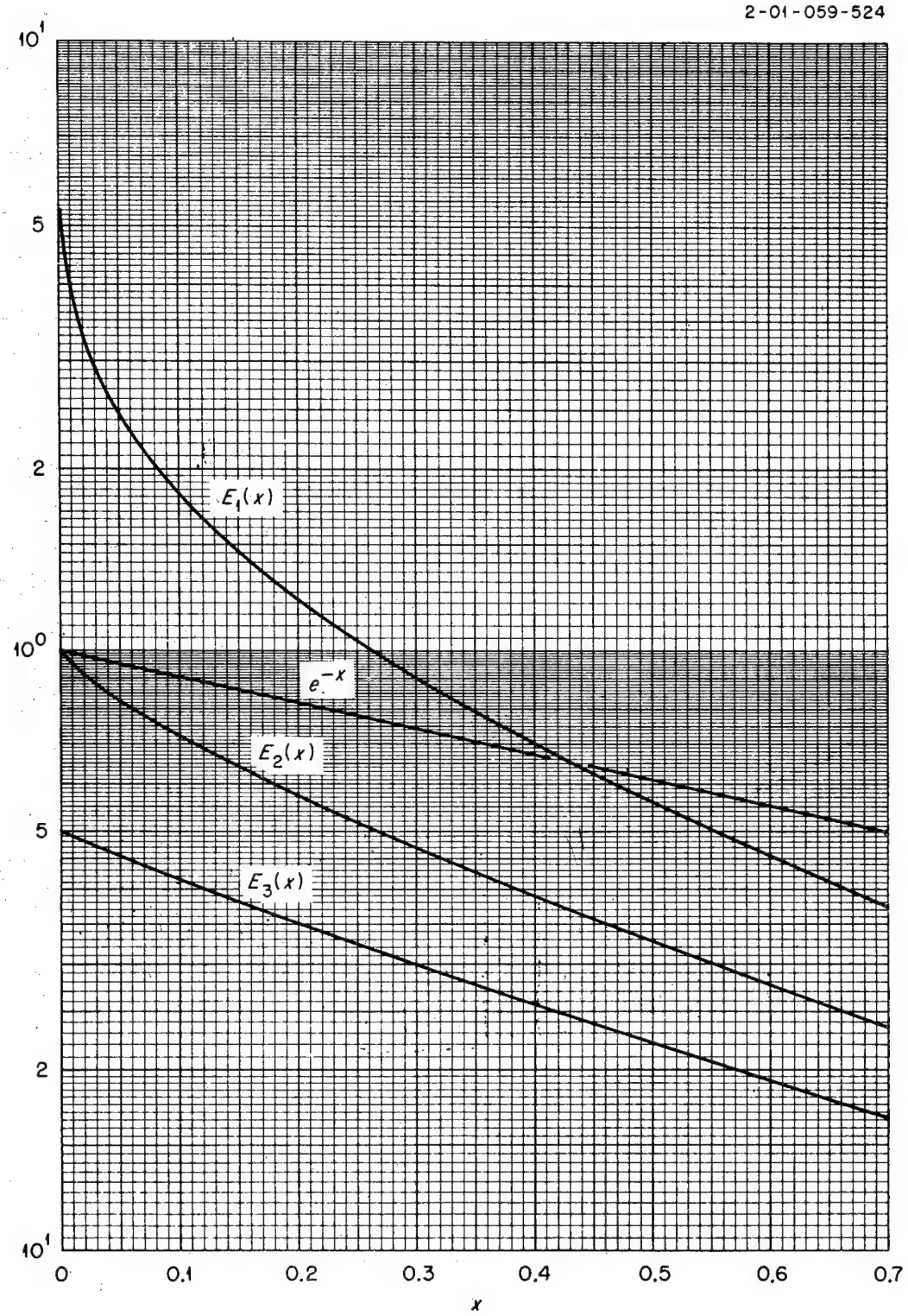

Fig. 3C.1. The Functions e^{-x}, $E_1(x)$, $E_2(x)$, and $E_3(x)$ for $x = 0$ to 0.7. (Plotted from data tabulated in ref. 133.)

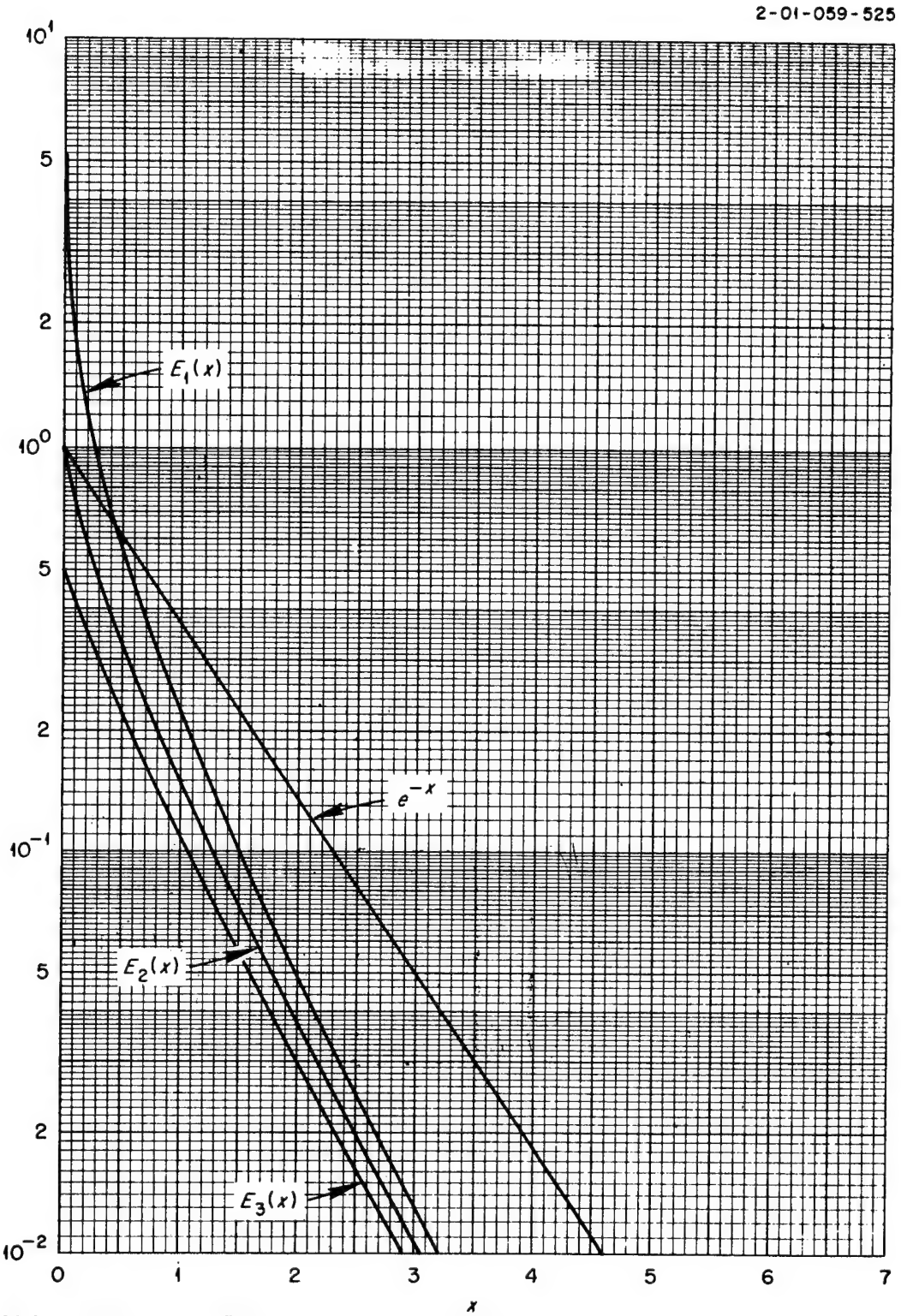

Fig. 3C.2. The Functions e^{-x}, $E_1(x)$, $E_2(x)$, and $E_3(x)$ for $x = 0$ to 3. (Plotted from data tabulated in ref. 133.)

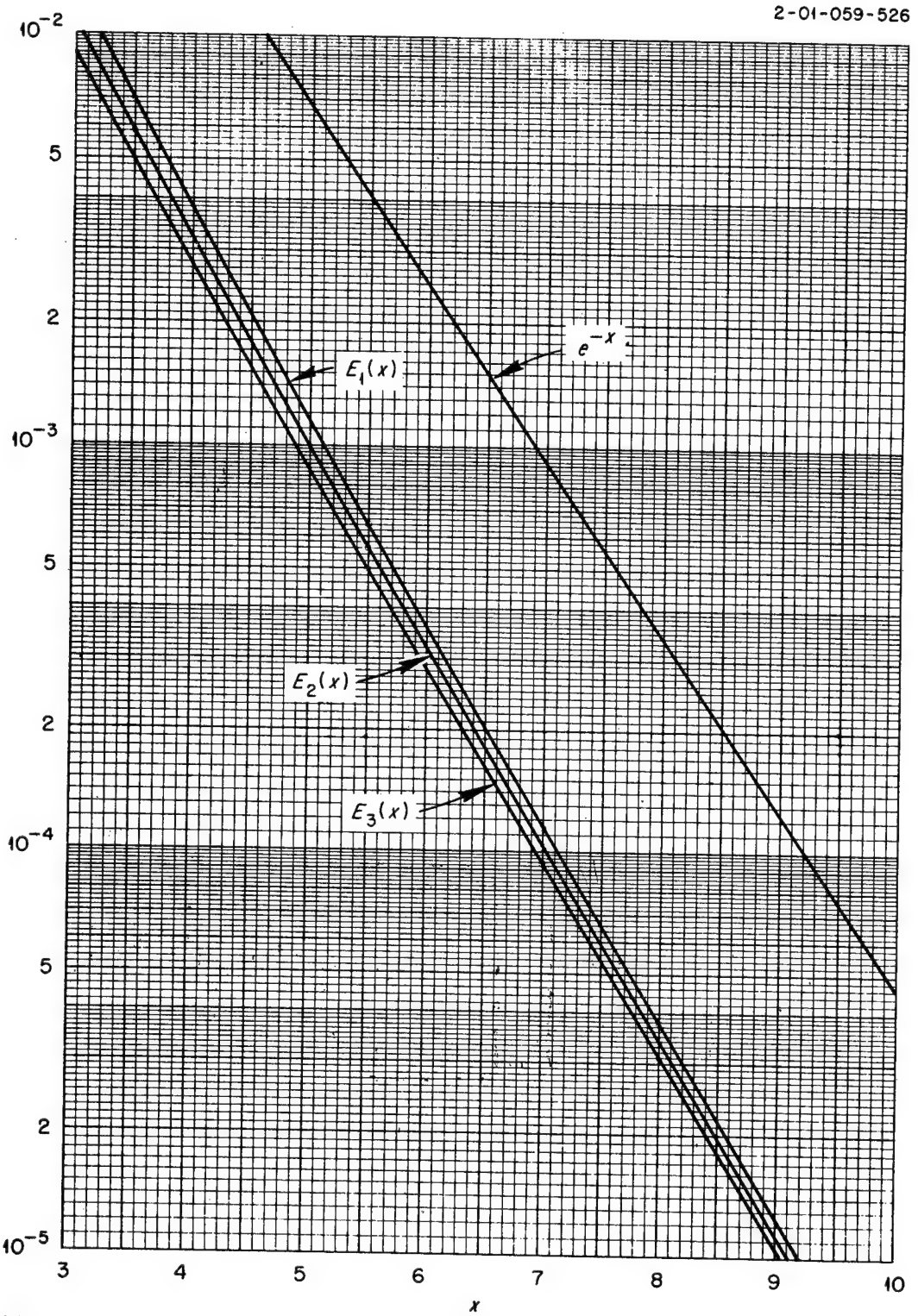

Fig. 3C.3. The Functions e^{-x}, $E_1(x)$, $E_2(x)$, and $E_3(x)$ for $x = 3$ to 9. (Plotted from data tabulated in ref. 133.)

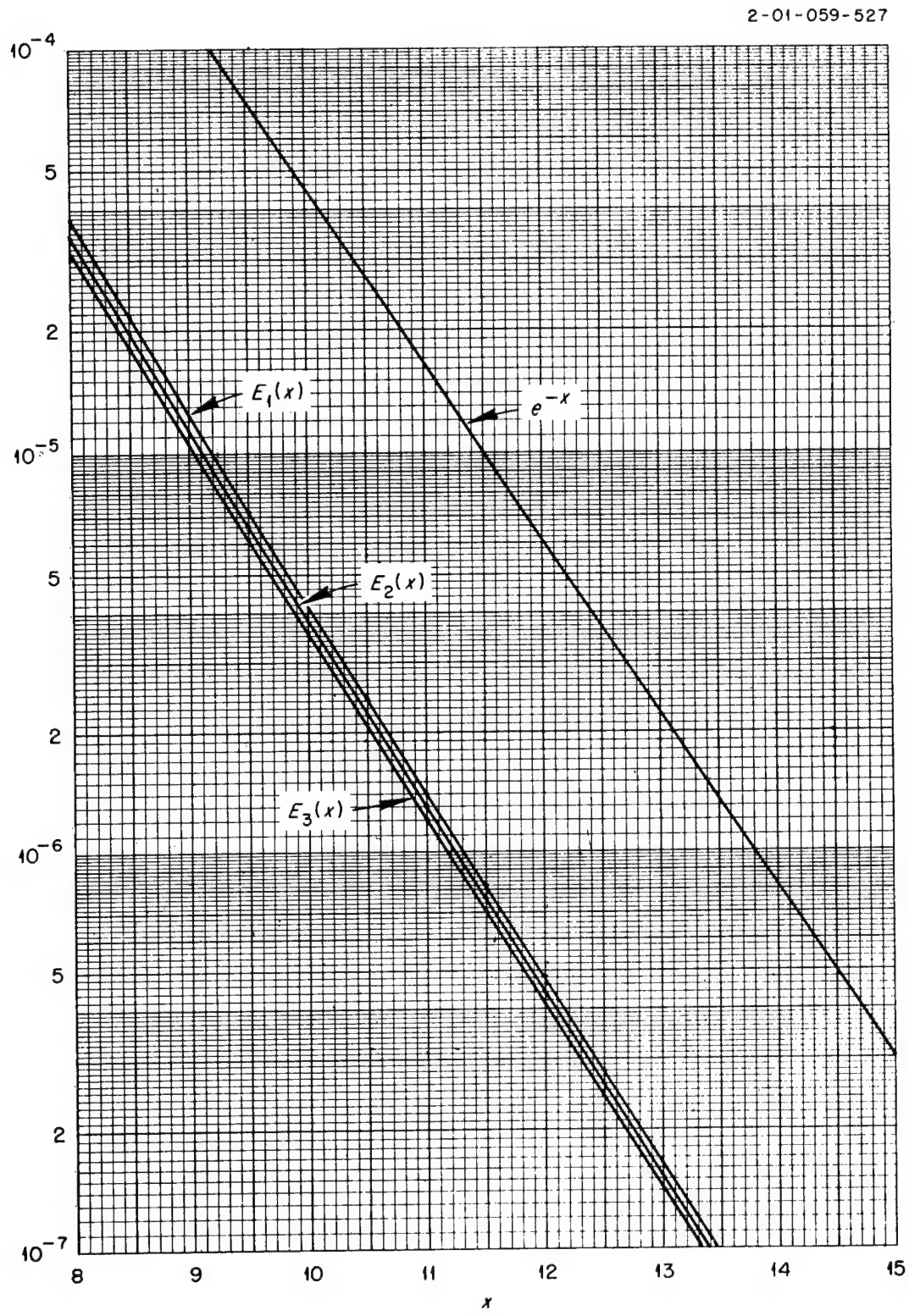

Fig. 3C.4. The Functions e^{-x}, $E_1(x)$, $E_2(x)$, and $E_3(x)$ for $x = 8$ to 15. (Plotted from data tabulated in ref. 133.)

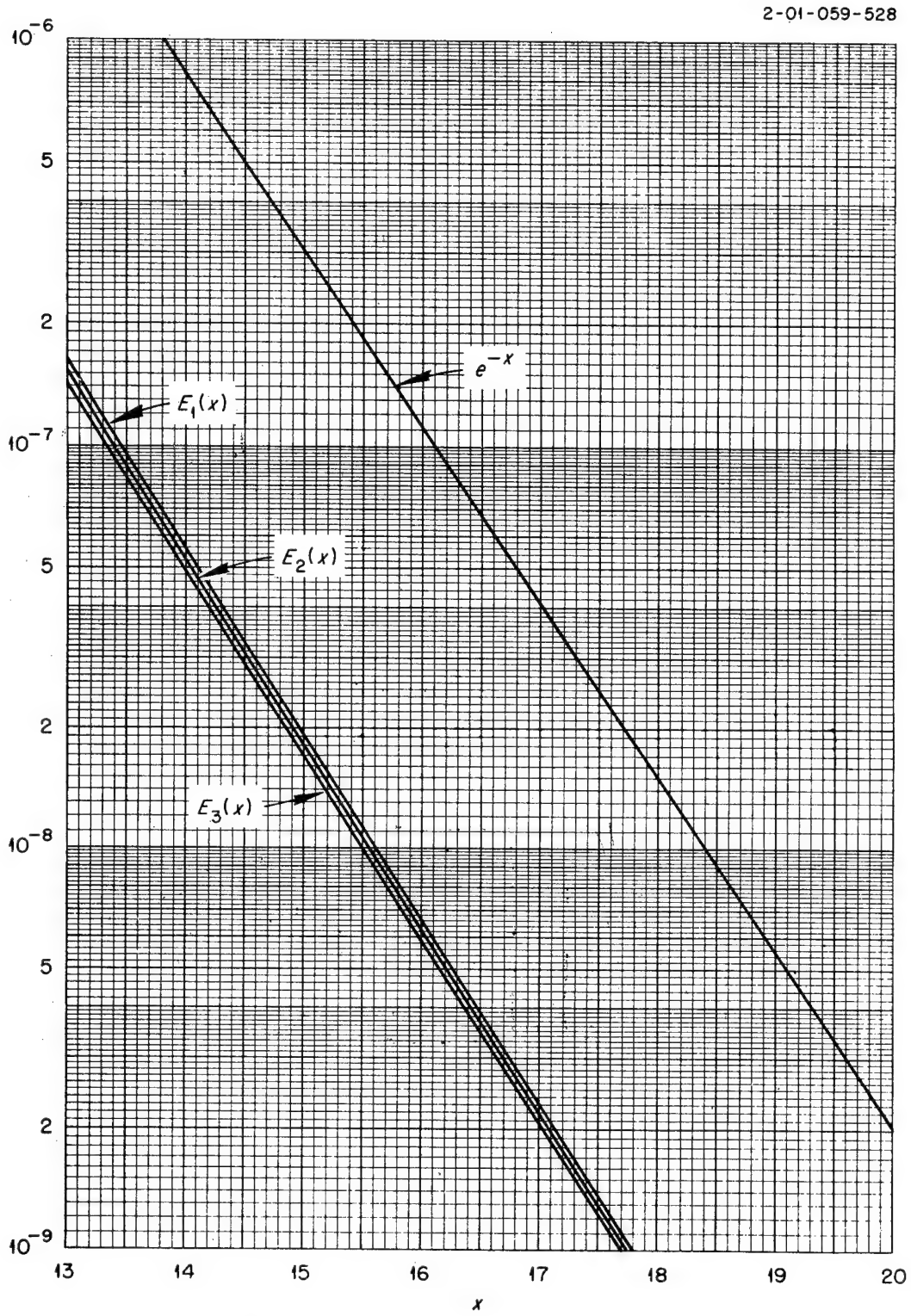

Fig. 3C.5. The Functions e^{-x}, $E_1(x)$, $E_2(x)$, and $E_3(x)$ for $x = 13$ to 20. (Plotted from data tabulated in ref. 133.)

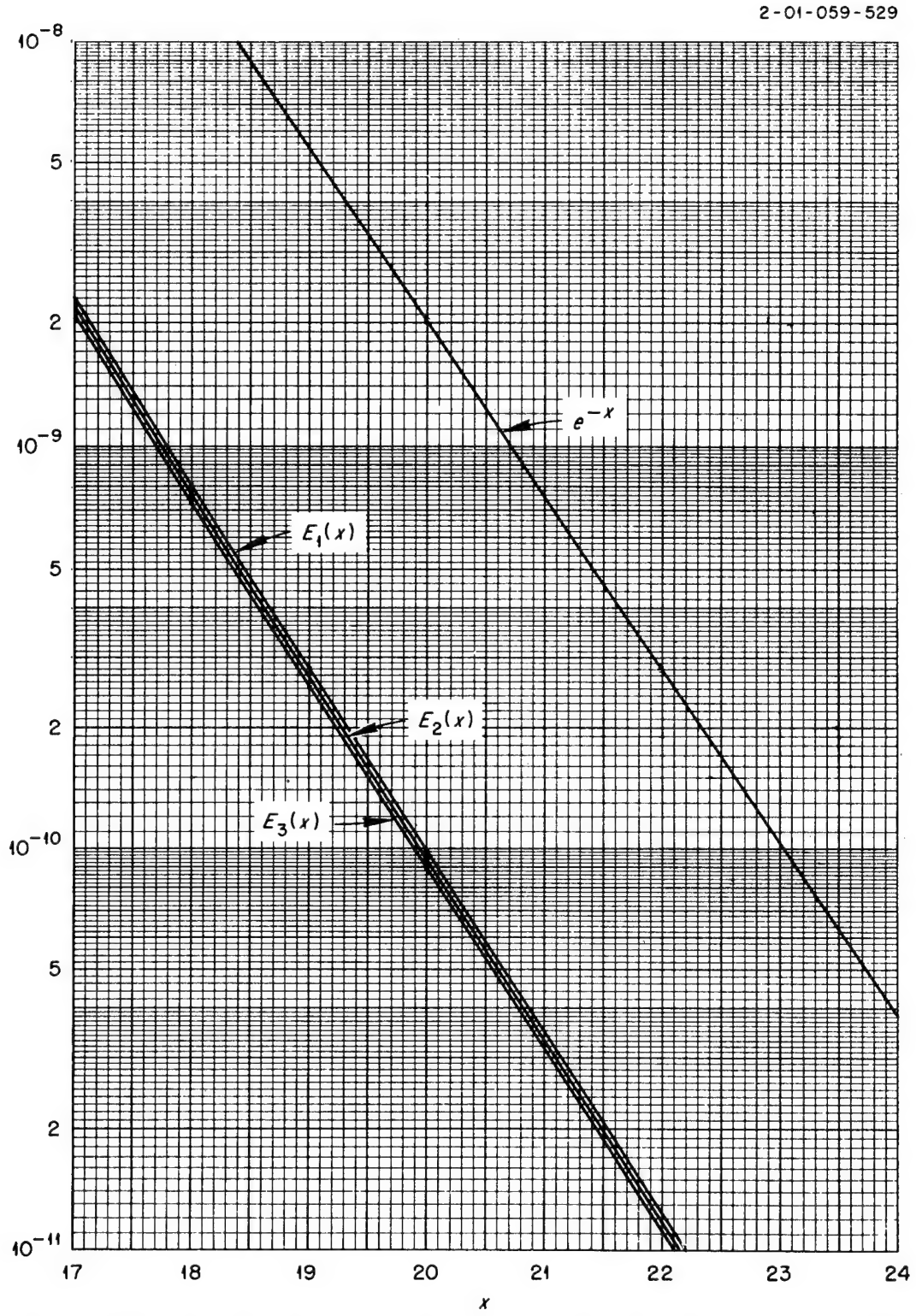

Fig. 3C.6. The Functions e^{-x}, $E_1(x)$, $E_2(x)$, and $E_3(x)$ for $x = 17$ to 24. (Plotted from data tabulated in ref. 133.)

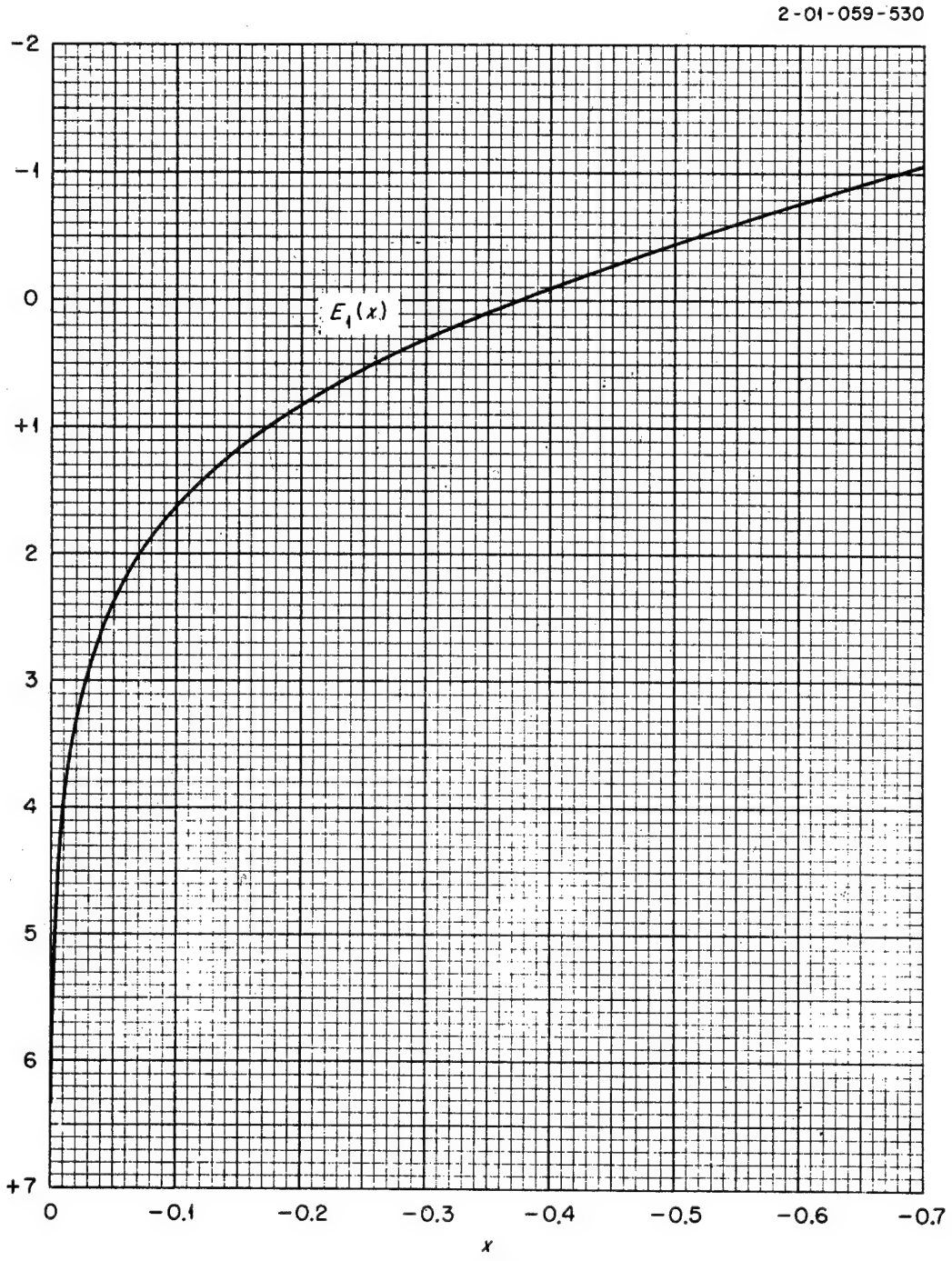

Fig. 3C.7. The Function $E_1(x)$ for Negative Arguments. (Plotted from data tabulated in ref. 134.)

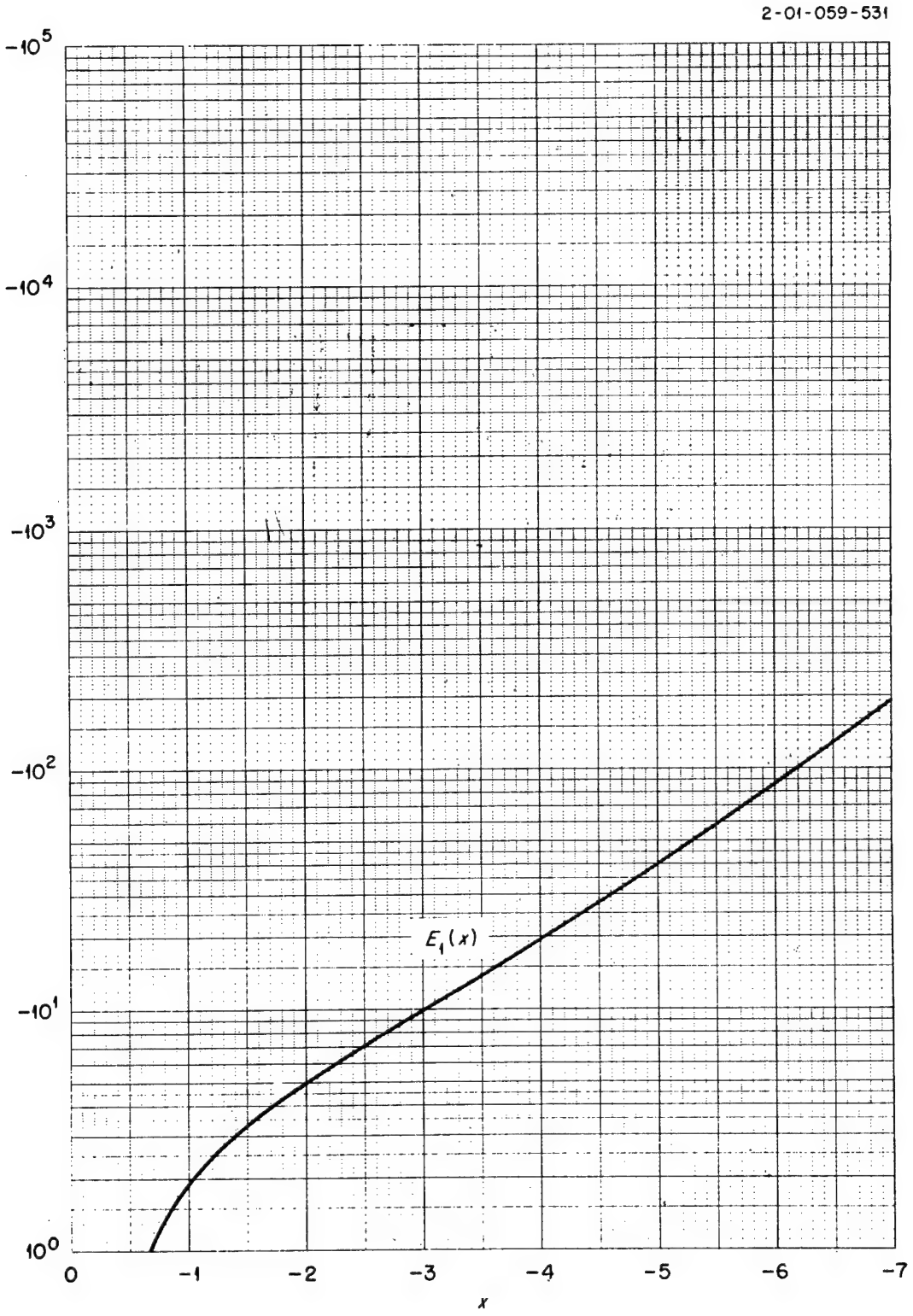

Fig. 3C.8. The Function $E_1(x)$ for Negative Arguments. (Plotted from data tabulated in ref. 134.)

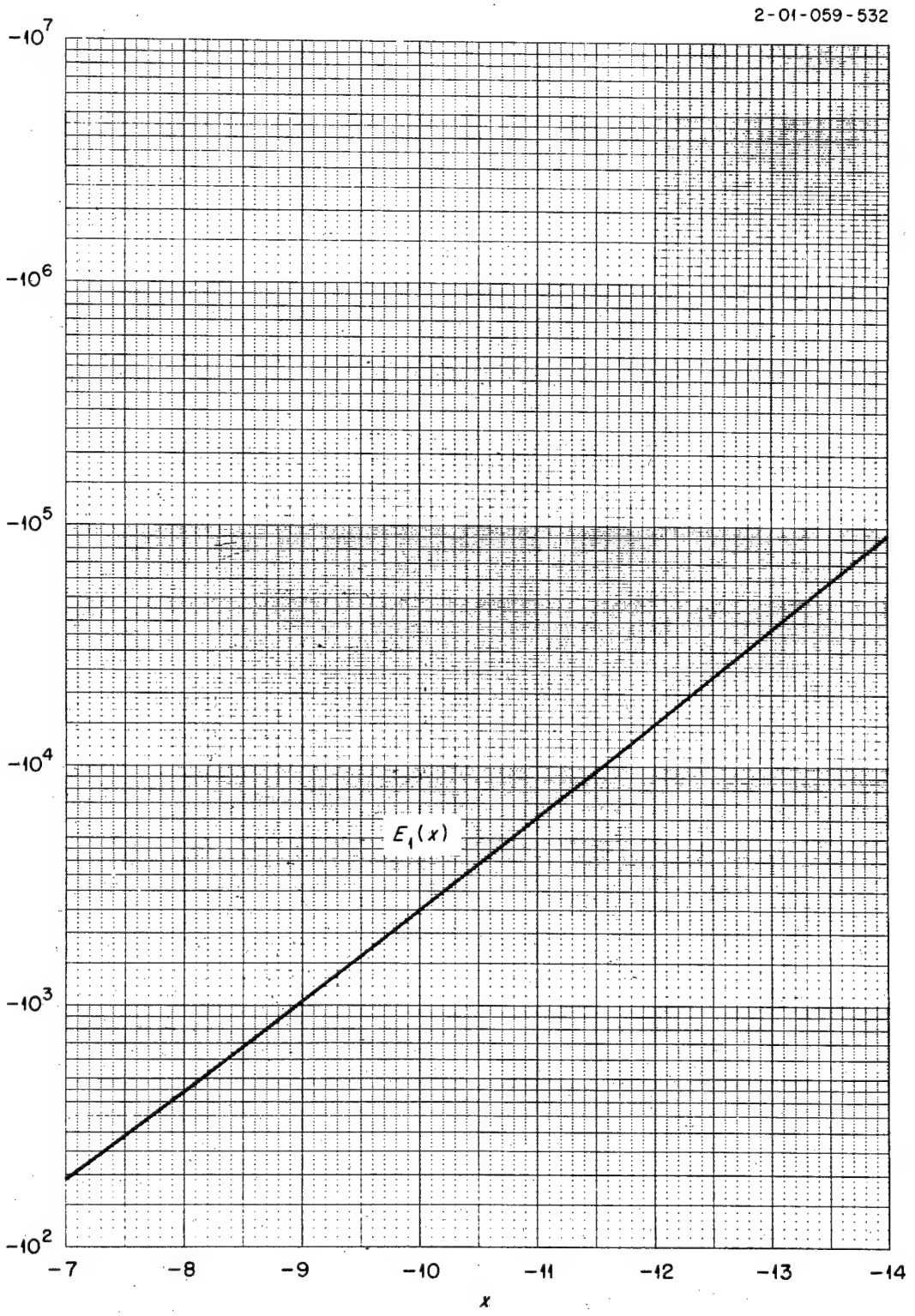

Fig. 3C.9. The Function $E_1(x)$ for Negative Arguments. (Plotted from data tabulated in ref. 134.)

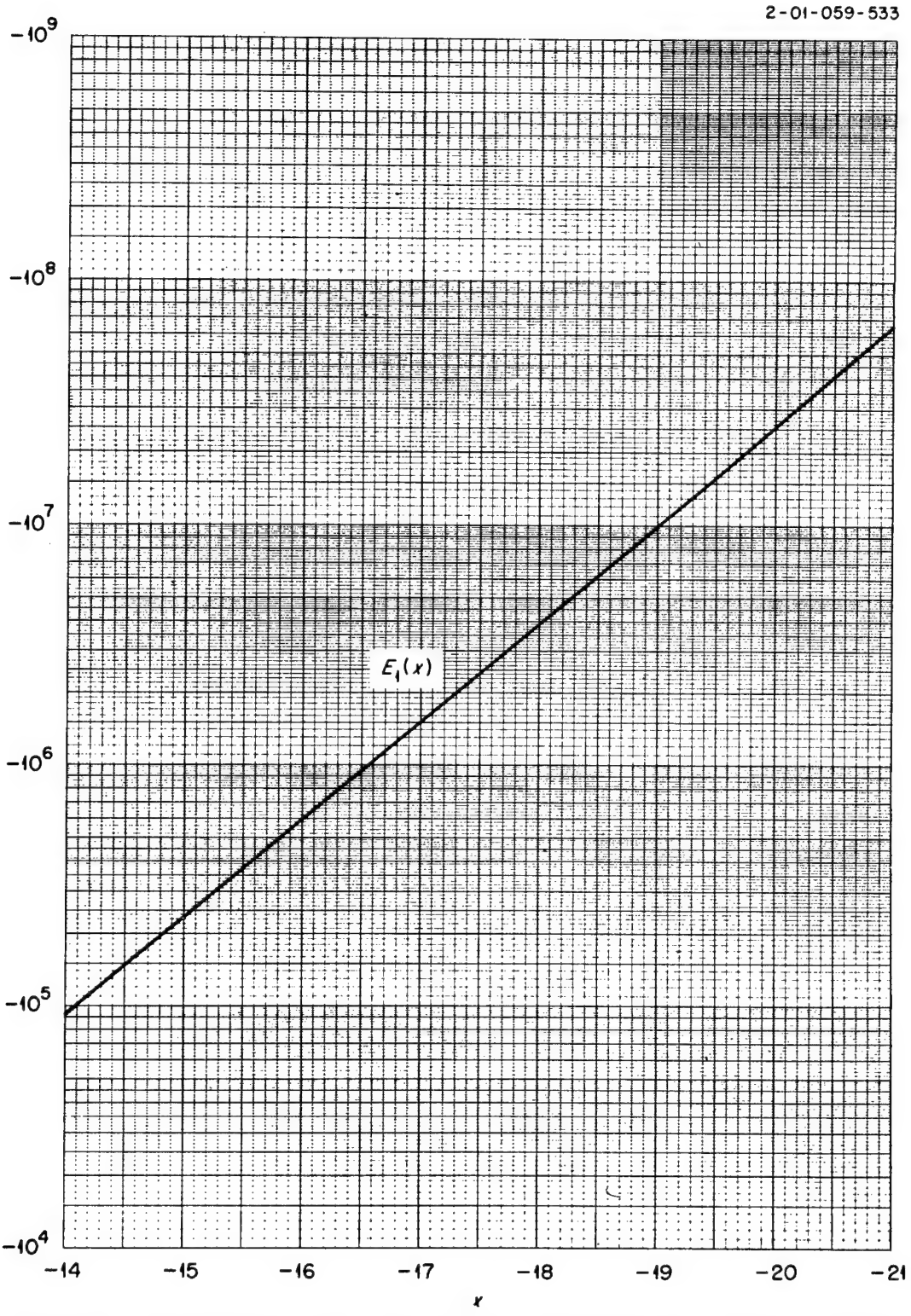

Fig. 3C.10. The Function $E_1(x)$ for Negative Arguments. (Plotted from data tabulated in ref. 134.)

Appendix 3D. Tables of Attenuation Functions for Finite Slab Geometry

This appendix consists of tabulations of attenuation functions for slab shields and disk or rectangular sources obtained by integrating over a point kernel of the form given for gamma rays in Section 3.8.1. The geometry for the disk-source configuration is shown in Figs. 3.4 and 3.5, and that for the rectangular-source configuration is shown in Fig. 3.6. Data are presented for sources with both isotropic and cosine angular distributions, the isotropic-source data being taken from the work of Hubbell *et al.*[50] and the cosine-source data from the work of Trubey.[51]

The use of these attenuation functions is explained in Section 3.8.1.

Table 3D.1. Unscattered Flux from a Disk Source with an Isotropic Angular Distribution[a]

z/r_0	μt	$4\pi\Gamma/S\ G(E)$									
		$\rho/r_0 = 0$	$\rho/r_0 = 0.2$	$\rho/r_0 = 0.5$	$\rho/r_0 = 0.8$	$\rho/r_0 = 1.0$	$\rho/r_0 = 1.2$	$\rho/r_0 = 1.5$	$\rho/r_0 = 2.0$	$\rho/r_0 = 5.0$	$\rho/r_0 = 10.0$
0.1	0	1.45(1)[b]	1.44(1)	1.36(1)	1.15(1)	7.39(0)	3.60(0)	1.83(0)	9.00(−1)	1.28(−1)	3.16(−2)
	0.01	1.39(1)	1.38(1)	1.31(1)	1.10(1)	7.03(0)	3.33(0)	1.62(0)	7.53(−1)	7.84(−2)	1.17(−2)
	0.02	1.34(1)	1.33(1)	1.26(1)	1.06(1)	6.71(0)	3.08(0)	1.44(0)	6.31(−1)	4.81(−2)	4.31(−3)
	0.05	1.20(1)	1.19(1)	1.13(1)	9.54(0)	5.86(0)	2.47(0)	1.02(0)	3.76(−1)	1.13(−2)	
	0.1	1.01(1)	1.00(1)	9.57(0)	8.11(0)	4.81(0)	1.76(0)	5.99(−1)	1.66(−1)		
	0.2	7.38(0)	7.34(0)	7.10(0)	6.12(0)	3.45(0)	9.94(−1)	2.09(−1)	4.56(−2)	1.36(−3)	1.34(−4)
	0.5	3.50(0)	3.50(0)	3.46(0)	3.17(0)	1.66(0)	2.51(−1)	2.74(−2)	3.45(−3)	2.17(−5)	1.72(−5)
	1.0	1.38(0)	1.38(0)	1.38(0)	1.32(0)	6.63(−1)	4.25(−2)	1.03(−3)	2.49(−4)		
	2.0	3.08(−1)	3.08(−1)	3.08(−1)	3.05(−1)	1.49(−1)	2.11(−3)				
	5.0	7.22(−3)	7.22(−3)	7.21(−3)	7.21(−3)	3.54(−3)					
	10.0	2.61(−5)	2.61(−5)	2.61(−5)	2.61(−5)	1.29(−5)					
0.2	0.	1.02(1)	1.01(1)	9.42(0)	7.65(0)	5.37(0)	3.25(0)	1.77(0)	8.90(−1)	1.28(−1)	3.16(−2)
	0.01	9.98(0)	9.87(0)	9.19(0)	7.44(0)	5.20(0)	3.11(0)	1.67(0)	8.13(−1)	1.00(−1)	1.92(−2)
	0.02	9.74(0)	9.62(0)	8.96(0)	7.25(0)	5.04(0)	2.98(0)	1.57(0)	7.43(−1)	7.83(−2)	1.17(−2)
	0.05	9.04(0)	8.94(0)	8.32(0)	6.71(0)	4.60(0)	2.63(0)	1.31(0)	5.70(−1)	3.76(−2)	2.63(−3)
	0.1	8.01(0)	7.92(0)	7.38(0)	5.93(0)	3.97(0)	2.15(0)	9.78(−1)	3.70(−1)	1.12(−2)	1.01(−3)
	0.2	6.35(0)	6.28(0)	5.88(0)	4.71(0)	3.17(0)	1.49(0)	5.66(−1)	1.62(−1)	3.48(−3)	3.16(−4)
	0.5	3.37(0)	3.35(0)	3.19(0)	2.60(0)	1.55(0)	5.79(−1)	1.37(−1)	2.19(−2)	1.62(−4)	4.90(−6)
	1.0	1.37(0)	1.37(0)	1.34(0)	1.14(0)	6.35(−1)	1.67(−1)	1.73(−2)	1.02(−3)		
	2.0	3.08(−1)	3.08(−1)	3.06(−1)	2.80(−1)	1.42(−1)	2.06(−2)	5.93(−4)			
	5.0	7.22(−3)	7.22(−3)	7.21(−3)	7.08(−3)	3.48(−3)	1.04(−4)	7.67(−7)			
	10.0	2.61(−5)	2.61(−5)	2.61(−5)	2.61(−5)	1.27(−5)	2.71(−8)				
0.5	0	5.06(0)	4.98(0)	4.53(0)	3.69(0)	2.96(0)	2.26(0)	1.49(0)	8.26(−1)	1.27(−1)	3.15(−2)
	0.01	4.98(0)	4.90(0)	4.46(0)	3.62(0)	2.90(0)	2.21(0)	1.45(0)	7.95(−1)	1.15(−1)	2.58(−2)
	0.02	4.90(0)	4.82(0)	4.39(0)	3.56(0)	2.84(0)	2.16(0)	1.41(0)	7.66(−1)	1.04(−1)	2.11(−2)
	0.05	4.68(0)	4.61(0)	4.19(0)	3.38(0)	2.69(0)	2.02(0)	1.30(0)	6.84(−1)	7.74(−2)	1.16(−2)
	0.1	4.34(0)	4.27(0)	3.87(0)	3.11(0)	2.45(0)	1.81(0)	1.13(0)	5.68(−1)	4.74(−2)	4.30(−3)
	0.2	3.73(0)	3.66(0)	3.32(0)	2.63(0)	2.03(0)	1.47(0)	8.69(−1)	3.94(−1)	1.79(−2)	
	0.5	2.38(0)	2.34(0)	2.11(0)	1.63(0)	1.21(0)	8.07(−1)	4.09(−1)	1.38(−1)	1.72(−3)	6.69(−5)
	1.0	1.16(0)	1.14(0)	1.03(0)	7.78(−1)	5.43(−1)	3.26(−1)	1.30(−1)	2.73(−2)	1.87(−5)	
	2.0	2.93(−1)	2.90(−1)	2.69(−1)	2.03(−1)	1.32(−1)	6.64(−2)	1.73(−2)	1.62(−3)		
	5.0	7.21(−3)	7.20(−3)	7.04(−3)	5.76(−3)	3.29(−3)	1.09(−3)	9.00(−5)	6.03(−7)		
	10.0	2.61(−5)	2.61(−5)	2.61(−5)	2.31(−5)	1.22(−5)	2.29(−6)	2.52(−8)			
1.0	0	2.18(0)	2.15(0)	1.99(0)	1.72(0)	1.51(0)	1.30(0)	1.01(0)	6.66(−1)	1.23(−1)	3.13(−2)
	0.01	2.15(0)	2.12(0)	1.96(0)	1.70(0)	1.49(0)	1.26(0)	9.95(−1)	6.52(−1)	1.17(−1)	2.83(−2)
	0.02	2.13(0)	2.10(0)	1.94(0)	1.68(0)	1.47(0)	1.20(0)	9.78(−1)	6.38(−1)	1.11(−1)	2.56(−2)
	0.05	2.05(0)	2.02(0)	1.87(0)	1.61(0)	1.41(0)	1.20(0)	9.29(−1)	5.99(−1)	9.57(−2)	1.90(−2)
	0.1	1.93(0)	1.90(0)	1.76(0)	1.51(0)	1.31(0)	1.12(0)	8.53(−1)	5.39(−1)	7.45(−2)	1.15(−2)
	0.2	1.71(0)	1.69(0)	1.55(0)	1.32(0)	1.14(0)	9.62(−1)	7.20(−1)	4.37(−1)	4.52(−2)	4.24(−3)
	0.5	1.20(0)	1.18(0)	1.07(0)	8.96(−1)	7.56(−1)	6.18(−1)	4.37(−1)	2.35(−1)	1.02(−2)	3.96(−4)
	1.0	6.64(−1)	6.51(−1)	5.85(−1)	4.73(−1)	3.87(−1)	3.02(−1)	1.95(−1)	8.65(−2)	1.06(−3)	2.27(−6)
	2.0	2.05(−1)	2.01(−1)	1.77(−1)	1.37(−1)	1.06(−1)	7.67(−2)	4.22(−2)	1.29(−2)	6.65(−6)	
	5.0	6.54(−3)	6.42(−3)	5.70(−3)	4.21(−3)	2.95(−3)	1.79(−3)	6.51(−4)	7.40(−5)		
	10.0	2.58(−5)	2.56(−5)	2.41(−5)	1.78(−5)	1.14(−5)	5.57(−6)	1.13(−6)	2.66(−8)		

Table 3D.1. (continued)

z/r_0	μt	$4\pi\Gamma/S\ G(E)$									
		$\rho/r_0 = 0$	$\rho/r_0 = 0.2$	$\rho/r_0 = 0.5$	$\rho/r_0 = 0.8$	$\rho/r_0 = 1.0$	$\rho/r_0 = 1.2$	$\rho/r_0 = 1.5$	$\rho/r_0 = 2.0$	$\rho/r_0 = 5.0$	$\rho/r_0 = 10.0$
2.0	0	7.01(−1)	6.96(−1)	6.71(−1)	6.27(−1)	5.91(−1)	5.52(−1)	4.90(−1)	3.92(−1)	1.10(−1)	3.03(−2)
	0.01	6.94(−1)	6.89(−1)	6.63(−1)	6.20(−1)	5.85(−1)	5.45(−1)	4.84(−1)	3.86(−1)	1.07(−1)	2.88(−2)
	0.02	6.86(−1)	6.81(−1)	6.56(−1)	6.14(−1)	5.78(−1)	5.39(−1)	4.78(−1)	3.81(−1)	1.04(−1)	2.74(−2)
	0.05	6.65(−1)	6.60(−1)	6.35(−1)	5.93(−1)	5.58(−1)	5.20(−1)	4.60(−1)	3.65(−1)	9.60(−2)	2.35(−2)
	0.1	6.31(−1)	6.26(−1)	6.02(−1)	5.61(−1)	5.27(−1)	4.90(−1)	4.32(−1)	3.40(−1)	8.40(−2)	1.83(−2)
	0.2	5.67(−1)	5.63(−1)	5.40(−1)	5.02(−1)	4.70(−1)	4.35(−1)	3.81(−1)	2.96(−1)	6.44(−2)	1.10(−2)
	0.5	4.13(−1)	4.09(−1)	3.91(−1)	3.60(−1)	3.34(−1)	3.05(−1)	2.62(−1)	1.95(−1)	2.91(−2)	2.41(−3)
	1.0	2.44(−1)	2.41(−1)	2.28(−1)	2.06(−1)	1.89(−1)	1.70(−1)	1.41(−1)	9.74(−2)	7.83(−3)	2.35(−4)
	2.0	8.47(−2)	8.36(−2)	7.79(−2)	6.85(−2)	6.09(−2)	5.29(−2)	4.12(−2)	2.50(−2)	6.16(−4)	
	5.0	3.59(−3)	3.52(−3)	3.17(−3)	2.60(−3)	2.16(−3)	1.72(−3)	1.14(−3)	4.77(−4)	2.28(−7)	
	10.0	1.89(−5)	1.84(−5)	1.61(−5)	1.24(−5)	9.55(−6)	6.86(−6)	3.45(−6)	9.02(−7)		
5.0	0	1.23(−1)	1.23(−1)	1.22(−1)	1.20(−1)	1.19(−1)	1.17(−1)	1.14(−1)	1.07(−1)	6.28(−2)	2.52(−2)
	0.01	1.22(−1)	1.22(−1)	1.21(−1)	1.19(−1)	1.18(−1)	1.16(−1)	1.12(−1)	1.06(−1)	6.27(−2)	2.51(−2)
	0.02	1.21(−1)	1.21(−1)	1.20(−1)	1.18(−1)	1.16(−1)	1.14(−1)	1.11(−1)	1.05(−1)	6.11(−2)	2.41(−2)
	0.05	1.17(−1)	1.17(−1)	1.16(−1)	1.14(−1)	1.13(−1)	1.11(−1)	1.08(−1)	1.01(−1)	5.85(−2)	2.25(−2)
	0.1	1.11(−1)	1.11(−1)	1.10(−1)	1.09(−1)	1.07(−1)	1.05(−1)	1.02(−1)	9.60(−2)	5.46(−2)	2.02(−2)
	0.2	1.01(−1)	1.01(−1)	9.96(−2)	9.81(−2)	9.66(−2)	9.50(−2)	9.20(−2)	8.62(−2)	4.74(−2)	1.61(−2)
	0.5	7.44(−2)	7.43(−2)	7.35(−2)	7.22(−2)	7.10(−2)	6.96(−2)	6.71(−2)	6.23(−2)	3.10(−2)	8.26(−3)
	1.0	4.49(−2)	4.48(−2)	4.43(−2)	4.33(−2)	4.25(−2)	4.14(−2)	3.97(−2)	3.62(−2)	1.53(−2)	2.71(−3)
	2.0	1.64(−2)	1.63(−2)	1.60(−2)	1.56(−2)	1.52(−2)	1.47(−2)	1.39(−2)	1.23(−2)	3.76(−3)	2.94(−4)
	5.0	7.91(−4)	7.87(−4)	7.66(−4)	7.29(−4)	6.97(−4)	6.60(−4)	5.97(−4)	4.83(−4)	5.71(−5)	3.77(−7)
	10.0	5.09(−6)	5.05(−6)	4.83(−6)	4.45(−6)	4.13(−6)	3.78(−6)	3.20(−6)	2.27(−6)	5.99(−8)	
10.0	0	3.13(−2)	3.12(−2)	3.12(−2)	3.11(−2)	3.10(−2)	3.08(−2)	3.06(−2)	3.01(−2)	2.51(−2)	1.57(−2)
	0.01	3.09(−2)	3.09(−2)	3.09(−2)	3.08(−2)	3.06(−2)	3.05(−2)	3.03(−2)	2.98(−2)	2.48(−2)	1.55(−2)
	0.02	3.06(−2)	3.06(−2)	3.06(−2)	3.04(−2)	3.03(−2)	3.02(−2)	3.00(−2)	2.95(−2)	2.45(−2)	1.53(−2)
	0.05	2.97(−2)	2.97(−2)	2.97(−2)	2.95(−2)	2.94(−2)	2.93(−2)	2.91(−2)	2.86(−2)	2.37(−2)	1.46(−2)
	0.1	2.83(−2)	2.83(−2)	2.82(−2)	2.81(−2)	2.80(−2)	2.79(−2)	2.76(−2)	2.72(−2)	2.24(−2)	1.36(−2)
	0.2	2.56(−2)	2.56(−2)	2.55(−2)	2.54(−2)	2.53(−2)	2.52(−2)	2.50(−2)	2.45(−2)	2.00(−2)	1.18(−2)
	0.5	1.89(−2)	1.89(−2)	1.89(−2)	1.88(−2)	1.87(−2)	1.86(−2)	1.84(−2)	1.80(−2)	1.43(−2)	7.75(−3)
	1.0	1.15(−2)	1.15(−2)	1.14(−2)	1.14(−2)	1.13(−2)	1.12(−2)	1.11(−2)	1.08(−2)	8.20(−3)	3.82(−3)
	2.0	4.21(−3)	4.21(−3)	4.19(−3)	4.16(−3)	4.13(−3)	4.09(−3)	4.03(−3)	3.90(−3)	2.68(−3)	9.31(−4)
	5.0	2.08(−4)	2.08(−4)	2.06(−4)	2.04(−4)	2.04(−4)	2.01(−4)	1.93(−4)	1.82(−4)	9.37(−5)	1.36(−5)
	10.0	1.39(−6)	1.38(−6)	1.37(−6)	1.34(−6)	1.31(−6)	1.28(−6)	1.22(−6)	1.10(−6)	3.53(−7)	1.26(−8)

[a] Table taken from: J. H. Hubbell, R. L. Bach, and R. J. Herbold, "Radiation Field from a Circular Disk Source," *J. Res. Natl. Bur. Std.* **65C**(4), 249 (1961).

[b] Read: 1.45×10^{1}, etc.

Table 3D.2. Unscattered Flux from a Disk Source with a Cosine Angular Distribution (Isotropic Flux)

z/r_0	μt	$2\Gamma/[\Phi(0)\,G(E)]$									
		$\rho/r_0 = 0$	$\rho/r_0 = 0.2$	$\rho/r_0 = 0.5$	$\rho/r_0 = 0.8$	$\rho/r_0 = 1.0$	$\rho/r_0 = 1.2$	$\rho/r_0 = 1.5$	$\rho/r_0 = 2.0$	$\rho/r_0 = 5.0$	$\rho/r_0 = 10.0$
0.1	0	9.01(−1)[a]	8.97(−1)	8.77(−1)	7.88(−1)	4.30(−1)	9.65(−2)	2.79(−2)	8.56(−3)	4.18(−4)	5.06(−5)
	0.01	8.78(−1)	8.75(−1)	8.55(−1)	7.70(−1)	4.19(−1)	9.10(−2)	2.51(−2)	7.25(−3)	2.57(−4)	1.87(−5)
	0.02	8.56(−1)	8.53(−1)	8.35(−1)	7.53(−1)	4.08(−1)	8.60(−2)	2.27(−2)	6.15(−3)	1.59(−4)	6.96(−6)
	0.03	8.35(−1)	8.33(−1)	8.15(−1)	7.36(−1)	3.97(−1)	8.13(−2)	2.05(−2)	5.23(−3)	9.80(−5)	2.59(−6)
	0.1	7.08(−1)	7.06(−1)	6.95(−1)	6.35(−1)	3.36(−1)	5.65(−2)	1.06(−2)	1.77(−3)	3.59(−6)	2.75(−9)
	0.2	5.70(−1)	5.70(−1)	5.64(−1)	5.23(−1)	2.71(−1)	3.57(−2)	4.55(−3)	4.24(−4)	3.73(−8)	1.84(−13)
	0.5	3.26(−1)	3.26(−1)	3.26(−1)	3.12(−1)	1.57(−1)	1.12(−2)	5.01(−4)	9.12(−6)	8.01(−14)	1.13(−25)
	1.0	1.48(−1)	1.48(−1)	1.48(−1)	1.46(−1)	7.19(−2)	2.16(−3)	1.98(−5)	2.73(−8)	6.52(−23)	[b]
	2.0	3.75(−2)	3.75(−2)	3.75(−2)	3.74(−2)	1.83(−2)	1.19(−4)	5.43(−8)	4.86(−13)	[b]	[b]
	5.0	9.96(−4)	9.96(−4)	9.96(−4)	9.96(−4)	4.91(−4)	5.05(−8)	3.72(−15)	[b]	[b]	[b]
	10.0	3.83(−6)	3.81(−6)	3.83(−6)	3.82(−6)	1.89(−6)	2.85(−13)	[b]	[b]	[b]	[b]
0.2	0	8.04(−1)	7.98(−1)	7.61(−1)	6.30(−1)	3.83(−1)	1.54(−1)	5.25(−2)	1.68(−2)	8.35(−4)	1.01(−4)
	0.01	7.88(−1)	7.82(−1)	7.46(−1)	6.18(−1)	3.74(−1)	1.49(−1)	4.98(−2)	1.54(−2)	6.55(−4)	6.15(−5)
	0.02	7.72(−1)	7.67(−1)	7.32(−1)	6.06(−1)	3.66(−1)	1.44(−1)	4.72(−2)	1.42(−2)	5.13(−4)	3.75(−5)
	0.03	7.57(−1)	7.52(−1)	7.18(−1)	5.95(−1)	3.58(−1)	1.40(−1)	4.48(−2)	1.31(−2)	4.03(−4)	2.28(−5)
	0.1	6.60(−1)	6.56(−1)	6.28(−1)	5.23(−1)	3.09(−1)	1.12(−1)	3.14(−2)	7.41(−3)	7.51(−5)	7.24(−7)
	0.2	5.46(−1)	5.43(−1)	5.23(−1)	4.39(−1)	2.54(−1)	8.37(−2)	1.94(−2)	3.42(−3)	7.13(−6)	5.49(−9)
	0.5	3.23(−1)	3.22(−1)	3.15(−1)	2.71(−1)	1.50(−1)	3.84(−2)	5.34(−3)	4.07(−4)	7.94(−9)	3.19(−15)
	1.0	1.48(−1)	1.48(−1)	1.47(−1)	1.31(−1)	6.95(−2)	1.25(−2)	8.10(−4)	1.66(−5)	1.57(−13)	2.24(−25)
	2.0	3.75(−2)	3.75(−2)	3.75(−2)	3.52(−2)	1.79(−2)	1.77(−3)	2.77(−5)	4.61(−8)	1.25(−22)	[b]
	5.0	9.96(−4)	9.96(−4)	9.96(−4)	9.84(−4)	4.82(−4)	1.01(−5)	2.90(−9)	3.20(−15)	[b]	[b]
	10.0	3.83(−6)	3.83(−6)	3.83(−6)	3.83(−6)	1.87(−6)	3.73(−9)	1.64(−15)	[b]	[b]	[b]
0.5	0	5.53(−1)	5.44(−1)	4.94(−1)	3.84(−1)	2.81(−1)	1.86(−1)	9.50(−2)	3.70(−2)	2.06(−3)	2.52(−4)
	0.01	5.45(−1)	5.36(−1)	4.87(−1)	3.78(−1)	2.77(−1)	1.82(−1)	9.27(−2)	3.57(−2)	1.87(−3)	2.06(−4)
	0.02	5.37(−1)	5.28(−1)	4.79(−1)	3.72(−1)	2.72(−1)	1.79(−1)	9.04(−2)	3.47(−2)	1.69(−3)	1.69(−4)
	0.03	5.29(−1)	5.21(−1)	4.73(−1)	3.67(−1)	2.68(−1)	1.75(−1)	8.82(−2)	3.33(−2)	1.54(−3)	1.39(−4)
	0.1	4.78(−1)	4.71(−1)	4.27(−1)	3.30(−1)	2.39(−1)	1.53(−1)	7.43(−2)	2.60(−2)	7.77(−4)	3.46(−5)
	0.2	4.14(−1)	4.08(−1)	3.70(−1)	2.84(−1)	2.03(−1)	1.27(−1)	5.85(−2)	1.85(−2)	2.96(−4)	4.80(−6)
	0.5	2.71(−1)	2.67(−1)	2.43(−1)	1.85(−1)	1.28(−1)	7.48(−2)	2.94(−2)	6.85(−3)	1.72(−5)	1.35(−8)
	1.0	1.36(−1)	1.34(−1)	1.23(−1)	9.37(−2)	5.20(−2)	3.29(−2)	1.02(−2)	1.46(−3)	1.74(−7)	8.95(−13)
	2.0	3.67(−2)	3.64(−2)	3.43(−2)	2.64(−2)	1.65(−2)	7.38(−3)	1.49(−3)	8.58(−5)	2.54(−11)	5.82(−21)
	5.0	9.96(−4)	9.95(−4)	9.79(−4)	8.07(−4)	4.57(−4)	1.37(−4)	8.77(−6)	3.79(−8)	2.39(−22)	[b]
	10.0	3.83(−6)	3.83(−6)	3.82(−6)	3.42(−6)	1.80(−6)	3.07(−7)	3.29(−9)	2.17(−13)	[b]	[b]
1.0	0	2.93(−1)	2.88(−1)	2.61(−1)	2.15(−1)	1.79(−1)	1.43(−1)	9.85(−2)	5.18(−2)	3.93(−3)	4.98(−4)
	0.01	2.89(−1)	2.84(−1)	2.57(−1)	2.12(−1)	1.76(−1)	1.41(−1)	9.69(−2)	5.08(−2)	3.74(−3)	4.51(−4)
	0.02	2.86(−1)	2.81(−1)	2.54(−1)	2.09(−1)	1.74(−1)	1.39(−1)	9.54(−2)	4.98(−2)	3.56(−3)	4.08(−4)
	0.03	2.83(−1)	2.77(−1)	2.51(−1)	2.07(−1)	1.72(−1)	1.37(−1)	9.38(−2)	4.88(−2)	3.38(−3)	3.69(−4)
	0.1	2.60(−1)	2.55(−1)	2.31(−1)	1.89(−1)	1.56(−1)	1.24(−1)	8.37(−2)	4.23(−2)	2.39(−3)	1.84(−4)
	0.2	2.31(−1)	2.27(−1)	2.04(−1)	1.66(−1)	1.37(−1)	1.08(−1)	7.12(−2)	3.46(−2)	1.46(−3)	6.79(−5)
	0.5	1.62(−1)	1.59(−1)	1.43(−1)	1.14(−1)	9.20(−2)	7.05(−2)	4.42(−2)	1.91(−2)	3.35(−4)	3.48(−6)
	1.0	9.03(−2)	8.84(−2)	7.86(−2)	6.16(−2)	4.83(−2)	3.55(−2)	2.04(−2)	7.27(−3)	3.01(−5)	2.57(−8)
	2.0	2.82(−2)	2.76(−2)	2.44(−2)	1.85(−2)	1.39(−2)	9.51(−3)	4.68(−3)	1.16(−3)	2.78(−7)	1.63(−12)
	5.0	9.29(−4)	9.13(−4)	8.17(−4)	6.02(−4)	4.14(−4)	2.41(−4)	7.93(−5)	7.24(−6)	4.16(−13)	8.52(−25)
	10.0	3.80(−6)	3.77(−6)	3.54(−6)	2.65(−6)	1.68(−6)	7.93(−7)	1.45(−7)	2.78(−9)	1.84(−22)	[b]
2.0	0	1.06(−1)	1.04(−1)	9.91(−2)	9.01(−2)	8.27(−2)	7.47(−2)	6.28(−2)	4.50(−2)	6.60(−3)	9.52(−4)
	0.01	1.04(−1)	1.03(−1)	9.81(−2)	8.91(−2)	8.17(−2)	7.39(−2)	6.20(−2)	4.44(−2)	6.43(−3)	9.05(−4)
	0.02	1.03(−1)	1.02(−1)	9.70(−2)	8.81(−2)	8.08(−2)	7.30(−2)	6.12(−2)	4.38(−2)	6.26(−3)	8.51(−4)
	0.03	1.02(−1)	1.01(−1)	9.60(−2)	8.71(−2)	7.99(−2)	7.22(−2)	6.05(−2)	4.32(−2)	6.09(−3)	8.18(−4)
	0.1	9.50(−2)	9.40(−2)	8.90(−2)	8.06(−2)	7.38(−2)	6.65(−2)	5.54(−2)	3.92(−2)	5.07(−3)	5.74(−4)
	0.2	8.55(−2)	8.45(−2)	7.99(−2)	7.22(−2)	6.59(−2)	5.91(−2)	4.90(−2)	3.41(−2)	3.89(−3)	3.46(−4)
	0.5	6.22(−2)	6.15(−2)	5.79(−2)	5.18(−2)	4.69(−2)	4.16(−2)	3.38(−2)	2.26(−2)	1.77(−3)	7.61(−5)
	1.0	3.67(−2)	3.62(−2)	3.38(−2)	2.98(−2)	2.66(−2)	2.32(−2)	1.83(−2)	1.14(−2)	4.80(−4)	6.16(−6)
	2.0	1.28(−2)	1.26(−2)	1.16(−2)	9.96(−3)	8.66(−3)	7.33(−3)	5.43(−3)	2.97(−3)	3.67(−5)	4.22(−8)
	5.0	5.43(−4)	5.32(−4)	4.75(−4)	3.84(−4)	3.14(−4)	2.45(−4)	1.55(−4)	5.95(−5)	2.07(−8)	1.78(−14)
	10.0	2.87(−6)	2.80(−6)	2.45(−6)	1.86(−6)	1.42(−6)	1.01(−6)	5.16(−7)	1.17(−7)	1.28(−13)	7.29(−25)
5.0	0	1.94(−2)	1.94(−2)	1.91(−2)	1.87(−2)	1.84(−2)	1.79(−2)	1.72(−2)	1.57(−2)	7.10(−3)	1.80(−3)
	0.01	1.92(−2)	1.92(−2)	1.90(−2)	1.85(−2)	1.82(−2)	1.78(−2)	1.70(−2)	1.56(−2)	7.00(−3)	1.76(−3)
	0.02	1.90(−2)	1.90(−2)	1.88(−2)	1.84(−2)	1.80(−2)	1.76(−2)	1.68(−2)	1.54(−2)	6.90(−3)	1.72(−3)
	0.03	1.88(−2)	1.88(−2)	1.86(−2)	1.82(−2)	1.78(−2)	1.74(−2)	1.67(−2)	1.52(−2)	6.80(−3)	1.68(−3)
	0.1	1.75(−2)	1.75(−2)	1.73(−2)	1.69(−2)	1.66(−2)	1.62(−2)	1.55(−2)	1.41(−2)	6.16(−3)	1.44(−3)

Table 3D.2. (continued)

z/r_0	μt	$2\Gamma/[\Phi(0)\,G(E)]$									
		$\rho/r_0 = 0$	$\rho/r_0 = 0.2$	$\rho/r_0 = 0.5$	$\rho/r_0 = 0.8$	$\rho/r_0 = 1.0$	$\rho/r_0 = 1.2$	$\rho/r_0 = 1.5$	$\rho/r_0 = 2.0$	$\rho/r_0 = 5.0$	$\rho/r_0 = 10.0$
	0.2	1.59(−2)	1.58(−2)	1.56(−2)	1.53(−2)	1.50(−2)	1.46(−2)	1.39(−2)	1.27(−2)	5.35(−3)	1.15(−3)
	0.5	1.17(−2)	1.17(−2)	1.15(−3)	1.12(−2)	1.10(−2)	1.07(−2)	1.02(−2)	9.16(−3)	3.51(−3)	5.91(−4)
	1.0	7.07(−3)	7.05(−3)	6.94(−3)	6.75(−3)	6.57(−3)	6.37(−3)	6.02(−3)	5.34(−3)	1.74(−3)	1.95(−4)
	2.0	2.58(−3)	2.57(−3)	2.52(−3)	2.43(−3)	2.35(−3)	2.26(−3)	2.11(−3)	1.81(−3)	4.28(−4)	2.12(−5)
	5.0	1.25(−4)	1.24(−4)	1.20(−4)	1.14(−4)	1.08(−4)	1.02(−4)	9.08(−5)	7.16(−5)	6.57(−6)	2.88(−8)
	10.0	8.00(−7)	7.93(−7)	7.57(−7)	6.94(−7)	6.41(−7)	5.82(−7)	4.88(−7)	3.36(−7)	6.77(−9)	5.46(−13)
10.0	0	4.96(−3)	4.96(−3)	4.94(−3)	4.92(−3)	4.89(−3)	4.86(−3)	4.80(−3)	4.68(−3)	3.57(−3)	1.77(−3)
	0.01	4.91(−3)	4.91(−3)	4.89(−3)	4.87(−3)	4.84(−3)	4.81(−3)	4.75(−3)	4.64(−3)	3.53(−3)	1.74(−3)
	0.02	4.86(−3)	4.86(−3)	4.85(−3)	4.82(−3)	4.79(−3)	4.76(−3)	4.71(−3)	4.59(−3)	3.49(−3)	1.72(−3)
	0.03	4.82(−3)	4.81(−3)	4.80(−3)	4.77(−3)	4.74(−3)	4.71(−3)	4.66(−3)	4.54(−3)	3.45(−3)	1.70(−3)
	0.1	4.49(−3)	4.49(−3)	4.47(−3)	4.45(−3)	4.42(−3)	4.39(−3)	4.34(−3)	4.23(−3)	3.19(−3)	1.54(−3)
	0.2	4.06(−3)	4.06(−3)	4.04(−3)	4.02(−3)	4.00(−3)	3.97(−3)	3.92(−3)	3.82(−3)	2.85(−3)	1.33(−3)
	0.5	3.01(−3)	3.00(−3)	2.99(−3)	2.97(−3)	2.95(−3)	2.93(−3)	2.89(−3)	2.81(−3)	2.04(−3)	8.73(−4)
	1.0	1.82(−3)	1.82(−3)	1.81(−3)	1.80(−3)	1.79(−3)	1.77(−3)	1.74(−3)	1.69(−3)	1.17(−3)	4.31(−4)
	2.0	6.68(−4)	6.68(−4)	6.64(−4)	6.58(−4)	6.52(−4)	6.45(−4)	6.33(−4)	6.07(−4)	3.81(−4)	1.05(−4)
	5.0	3.30(−5)	3.30(−5)	3.27(−5)	3.22(−5)	3.18(−5)	3.12(−5)	3.03(−5)	2.83(−5)	1.34(−5)	1.54(−6)
	10.0	2.20(−7)	2.19(−7)	2.16(−7)	2.11(−7)	2.06(−7)	2.01(−7)	0.91(−7)	1.72(−7)	5.06(−8)	1.37(−9)

[a] Read: 9.01×10^{-1}, etc.
[b] Effectively zero.

Table 3D.3. Unscattered Flux at a Corner Position from a Rectangular Plane Source with an Isotropic Angular Distribution[a]

μt	$4\pi\Gamma/S\,G(E)$					
	$b = 0.1$, $a = 0.1$	$b = 0.2$, $a = 0.1$	$b = 0.2$, $a = 0.2$	$b = 0.5$, $a = 0.1$	$b = 0.5$, $a = 0.2$	$b = 0.5$, $a = 0.5$
0	9.93(−3)[b]	1.97(−2)	3.90(−2)	4.62(−2)	9.16(−2)	2.16(−1)
0.01	9.83(−3)	1.95(−2)	3.86(−2)	4.57(−2)	9.07(−2)	2.14(−1)
0.02	9.74(−3)	1.93(−2)	3.82(−2)	4.53(−2)	8.97(−2)	2.11(−1)
0.05	9.44(−3)	1.87(−2)	3.70(−2)	4.39(−2)	8.69(−2)	2.05(−1)
0.1	8.99(−3)	1.78(−2)	3.52(−2)	4.17(−2)	8.25(−2)	1.94(−1)
0.2	8.13(−3)	1.61(−2)	3.18(−2)	3.75(−2)	7.43(−2)	1.74(−1)
0.5	6.02(−3)	1.19(−2)	2.35(−2)	2.75(−2)	5.44(−2)	1.26(−1)
1.0	3.64(−3)	7.18(−3)	1.42(−2)	1.64(−2)	3.23(−2)	7.38(−2)
2.0	1.34(−3)	2.62(−3)	5.14(−3)	5.79(−3)	1.14(−2)	2.53(−2)
5.0	6.60(−5)	1.28(−4)	2.47(−4)	2.60(−4)	5.04(−4)	1.04(−3)
10.0	4.37(−7)	8.26(−7)	1.54(−6)	1.50(−6)	2.83(−6)	5.15(−6)
μt	$b = 1.0$, $a = 0.1$	$b = 1.0$, $a = 0.2$	$b = 1.0$, $a = 0.5$	$b = 1.0$, $a = 1.0$	$b = 2.0$, $a = 0.1$	$b = 2.0$, $a = 0.2$
0	7.83(−2)	1.55(−1)	3.69(−1)	6.40(−1)	1.10(−1)	2.19(−1)
0.01	7.75(−2)	1.54(−1)	3.65(−1)	6.32(−1)	1.09(−1)	2.17(−1)
0.02	7.66(−2)	1.52(−1)	3.60(−1)	6.24(−1)	1.08(−1)	2.14(−1)
0.05	7.40(−2)	1.47(−1)	3.48(−1)	6.01(−1)	1.04(−1)	2.06(−1)
0.1	7.00(−2)	1.39(−1)	3.29(−1)	5.65(−1)	9.70(−2)	1.93(−1)
0.2	6.26(−2)	1.24(−1)	2.93(−1)	4.99(−1)	8.53(−2)	1.69(−1)
0.5	4.47(−2)	8.85(−2)	2.07(−1)	3.45(−1)	5.82(−2)	1.15(−1)
1.0	2.56(−2)	5.06(−2)	1.17(−1)	1.87(−1)	3.14(−2)	6.20(−2)
2.0	8.49(−3)	1.67(−2)	3.74(−2)	5.61(−2)	9.57(−3)	1.88(−2)
5.0	3.85(−4)	7.55(−4)	1.77(−3)	7.99(−3)	3.37(−4)	6.54(−4)
10.0	1.67(−6)	3.16(−6)	5.77(−6)	6.49(−6)	1.67(−6)	3.16(−6)

Table 3D.3. (continued)

μt	$4\pi\Gamma/S\ G(E)$					
	$b = 2.0$ $a = 0.5$	$b = 2.0$ $a = 1.0$	$b = 2.0$ $a = 2.0$	$b = 5.0$ $a = 0.1$	$b = 5.0$ $a = 0.2$	$b = 5.0$ $a = 0.5$
0	5.25(−1)	9.31(−1)	1.41(0)	1.37(−1)	2.73(−1)	6.57(−1)
0.01	5.18(−1)	9.18(−1)	1.38(0)	1.35(−1)	2.68(−1)	6.46(−1)
0.02	5.11(−1)	9.05(−1)	1.36(0)	1.33(−1)	2.64(−1)	6.35(−1)
0.05	4.91(−1)	8.67(−1)	1.30(0)	1.26(−1)	2.51(−1)	6.03(−1)
0.1	4.60(−1)	8.07(−1)	1.20(0)	1.16(−1)	2.31(−1)	5.55(−1)
0.2	4.03(−1)	7.01(−1)	1.02(0)	9.93(−2)	1.97(−1)	4.72(−1)
0.5	2.72(−1)	4.62(−1)	6.38(−1)	6.38(−2)	1.27(−1)	3.00(−1)
1.0	1.44(−1)	2.35(−1)	3.02(−1)	3.27(−2)	6.46(−2)	1.50(−1)
2.0	4.24(−2)	6.43(−2)	7.46(−2)	9.69(−3)	1.90(−2)	4.28(−2)
5.0	1.32(−3)	1.75(−3)	1.80(−3)	3.37(−4)	6.54(−4)	1.35(−3)
10.0	5.79(−6)	6.51(−6)	6.52(−6)	1.67(−6)	3.16(−6)	5.79(−6)
μt	$b = 5.0$ $a = 1.0$	$b = 5.0$ $a = 2.0$	$b = 5.0$ $a = 5.0$	$b = 10.0$ $a = 0.1$	$b = 10.0$ $a = 0.2$	$b = 10.0$ $a = 0.5$
0	1.19(0)	1.88(0)	2.73(0)	1.47(−1)	2.92(−1)	7.06(−1)
0.01	1.17(0)	1.84(0)	2.65(0)	1.44(−1)	2.86(−1)	6.92(−1)
0.02	1.15(0)	1.80(0)	2.58(0)	1.41(−1)	2.81(−1)	6.77(−1)
0.05	1.08(0)	1.69(0)	2.39(0)	1.33(−1)	2.65(−1)	6.38(−1)
0.1	9.92(−1)	1.53(0)	2.10(0)	1.21(−1)	2.41(−1)	5.79(−1)
0.2	8.35(−1)	1.26(0)	1.64(0)	1.02(−1)	2.02(−1)	4.84(−1)
0.5	5.14(−1)	7.27(−1)	8.53(−1)	6.42(−2)	1.27(−1)	3.01(−1)
1.0	2.47(−1)	3.20(−1)	3.44(−1)	3.27(−2)	6.47(−2)	1.50(−1)
2.0	6.51(−2)	7.57(−2)	7.69(−2)	9.69(−3)	1.90(−2)	4.28(−2)
5.0	1.75(−3)	1.80(−3)	1.80(−3)	3.37(−4)	6.54(−4)	1.35(−3)
10.0	6.51(−6)	6.53(−6)	6.54(−6)	1.67(−6)	3.16(−6)	5.79(−6)
μt	$b = 10.0$ $a = 1.0$	$b = 10.0$ $a = 2.0$	$b = 10.0$ $a = 5.0$	$b = 10.0$ $a = 10.0$	$b = 20.0$ $a = 0.1$	$b = 20.0$ $a = 0.2$
0	1.28(0)	2.07(0)	3.15(0)	3.80(0)	1.52(−1)	3.02(−1)
0.01	1.26(0)	2.02(0)	3.04(0)	3.64(0)	1.48(−1)	2.95(−1)
0.02	1.23(0)	1.97(0)	2.94(0)	3.49(0)	1.45(−1)	2.88(−1)
0.05	1.15(0)	1.83(0)	2.67(0)	3.10(0)	1.36(−1)	2.70(−1)
0.1	1.04(0)	1.63(0)	2.30(0)	2.58(0)	1.22(−1)	2.43(−1)
0.2	8.60(−1)	1.31(0)	1.74(0)	1.86(0)	1.02(−1)	2.03(−1)
0.5	5.18(−1)	7.34(−1)	8.65(−1)	8.78(−1)	6.39(−2)	1.27(−1)
1.0	2.47(−1)	3.21(−1)	3.44(−1)	3.45(−1)	3.27(−2)	6.47(−2)
2.0	6.51(−2)	7.56(−2)	7.69(−2)	7.68(−2)	9.69(−3)	1.90(−2)
5.0	1.75(−3)	1.80(−3)	1.80(−3)	1.80(−3)	3.37(−4)	6.54(−4)
10.0	6.51(−6)	6.53(−6)	6.53(−6)	6.53(−6)	1.67(−6)	3.16(−6)

Table 3D.3. (continued)

μt	$4\pi\Gamma/S\ G(E)$					
	$b = 20.0$ $a = 0.5$	$b = 20.0$ $a = 1.0$	$b = 20.0$ $a = 2.0$	$b = 20.0$ $a = 5.0$	$b = 20.0$ $a = 10.0$	$b = 20.0$ $a = 20.0$
0	7.31(−1)	1.33(0)	2.17(0)	3.38(0)	4.22(0)	4.88(0)
0.01	7.13(−1)	1.30(0)	2.10(0)	3.25(0)	4.01(0)	4.56(0)
0.02	6.96(−1)	1.27(0)	2.04(0)	3.12(0)	3.81(0)	4.28(0)
0.05	6.50(−1)	1.18(0)	1.88(0)	2.79(0)	3.30(0)	3.59(0)
0.1	5.86(−1)	1.05(0)	1.65(0)	2.36(0)	2.68(0)	2.81(0)
0.2	4.86(−1)	8.63(−1)	1.31(0)	1.75(0)	1.89(0)	1.92(0)
0.5	3.01(−1)	5.18(−1)	7.34(0)	8.63(−1)	8.79(−1)	8.82(−1)
1.0	1.50(−1)	2.47(−1)	3.21(0)	3.44(−1)	3.45(−1)	3.45(−1)
2.0	4.28(−2)	6.51(−2)	7.56(−2)	7.69(−2)	7.68(−2)	7.68(−2)
5.0	1.35(−3)	1.75(−3)	1.80(−3)	1.80(−3)	1.80(−3)	1.80(−3)
10.0	5.79(−6)	6.51(−6)	6.53(−6)	6.53(−6)	6.53(−6)	6.53(−6)

[a]Table taken from: J. H. Hubbell, R. L. Bach, and J. C. Lamkin, "Radiation Field from a Rectangular Source," *J. Res. Natl. Bur. Std.* 64C(2), 121 (1960)

[b]Read: 9.93×10^{-3}, etc.

Table 3D.4. Unscattered Flux at a Corner Position from a Rectangular Plane Source with a Cosine Angular Distribution (Isotropic Flux)

μt	$2\Gamma/[\Phi(0)\ G(E)]$					
	$b = 0.1$ $a = 0.1$	$b = 0.2$ $a = 0.1$	$b = 0.2$ $a = 0.2$	$b = 0.5$ $a = 0.1$	$b = 0.5$ $a = 0.2$	$b = 0.5$ $a = 0.5$
0	1.58(−3)[a]	3.11(−3)	6.12(−3)	7.09(−3)	1.40(−2)	3.21(−2)
0.01	1.56(−3)	3.08(−3)	6.06(−3)	7.01(−3)	1.38(−2)	3.17(−2)
0.02	1.55(−3)	3.04(−3)	6.00(−3)	6.94(−3)	1.37(−2)	3.14(−2)
0.05	1.53(−3)	3.01(−3)	5.94(−3)	6.87(−3)	1.36(−2)	3.10(−2)
0.1	1.43(−3)	2.81(−3)	5.53(−3)	6.39(−3)	1.26(−2)	2.88(−2)
0.2	1.29(−3)	2.54(−3)	5.00(−3)	5.76(−3)	1.14(−2)	2.59(−2)
0.5	9.54(−4)	1.88(−3)	3.69(−3)	4.22(−3)	8.30(−3)	1.88(−2)
1.0	5.78(−4)	1.13(−3)	2.22(−3)	2.51(−3)	4.93(−3)	1.10(−2)
2.0	2.12(−4)	4.14(−4)	8.08(−4)	8.90(−4)	1.74(−3)	3.77(−3)
5.0	1.04(−5)	2.01(−5)	3.87(−5)	4.00(−5)	7.70(−5)	1.54(−4)
10.0	6.92(−8)	1.30(−7)	2.45(−7)	2.31(−7)	4.36(−7)	7.79(−7)
μt	$b = 1.0$ $a = 0.1$	$b = 1.0$ $a = 0.2$	$b = 1.0$ $a = 0.5$	$b = 1.0$ $a = 1.0$	$b = 2.0$ $a = 0.1$	$b = 2.0$ $a = 0.2$
0	1.12(−2)	2.21(−2)	5.12(−2)	8.33(−2)	1.42(−2)	2.81(−2)
0.01	1.11(−2)	2.19(−2)	5.06(−2)	8.23(−2)	1.40(−2)	2.77(−2)
0.02	1.08(−2)	2.17(−2)	5.01(−2)	8.13(−2)	1.38(−2)	2.74(−2)
0.05	1.08(−2)	2.14(−2)	4.95(−2)	8.03(−2)	1.37(−2)	2.70(−2)
0.1	1.00(−2)	1.98(−2)	4.57(−2)	7.38(−2)	1.25(−2)	2.48(−2)
0.2	8.98(−3)	1.77(−2)	4.07(−2)	6.53(−2)	1.11(−2)	2.19(−2)
0.5	6.44(−3)	1.27(−2)	2.89(−2)	4.54(−2)	7.71(−3)	1.52(−2)
1.0	3.71(−3)	7.29(−3)	1.64(−2)	2.49(−2)	4.26(−3)	8.38(−3)
2.0	1.24(−3)	2.43(−3)	5.30(−3)	7.57(−3)	1.35(−3)	2.64(−3)
5.0	4.91(−5)	9.47(−5)	1.91(−4)	2.38(−4)	5.00(−5)	9.65(−5)
10.0	2.54(−7)	4.79(−7)	8.61(−7)	9.54(−7)	2.55(−7)	4.80(−7)

Table 3D.4. (continued)

	$2\Gamma/[\Phi(0)\, G(E)]$					
μt	$b = 2.0$ $a = 0.5$	$b = 2.0$ $a = 1.0$	$b = 2.0$ $a = 2.0$	$b = 5.0$ $a = 0.1$	$b = 5.0$ $a = 0.2$	$b = 5.0$ $a = 0.5$
0	6.55(−2)	1.09(−1)	1.48(−1)	1.56(−2)	3.08(−2)	7.23(−2)
0.01	6.47(−2)	1.08(−1)	1.45(−1)	1.53(−2)	3.04(−2)	7.12(−2)
0.02	6.39(−2)	1.06(−1)	1.43(−1)	1.51(−2)	3.00(−2)	7.02(−2)
0.05	6.30(−2)	1.05(−1)	1.41(−1)	1.49(−2)	2.95(−2)	6.92(−2)
0.1	5.77(−2)	9.52(−2)	1.27(−1)	1.35(−2)	2.68(−2)	6.26(−2)
0.2	5.08(−2)	8.32(−2)	1.09(−1)	1.18(−2)	2.34(−2)	5.45(−2)
0.5	3.49(−2)	5.58(−2)	7.05(−2)	8.02(−3)	1.58(−2)	3.64(−2)
1.0	1.89(−2)	2.92(−2)	3.49(−2)	4.33(−3)	8.53(−3)	1.93(−2)
2.0	5.78(−3)	8.34(−3)	9.26(−3)	1.35(−3)	2.65(−3)	5.81(−3)
5.0	1.95(−4)	2.44(−4)	2.49(−4)	5.00(−5)	9.65(−5)	1.95(−4)
10.0	8.63(−7)	9.56(−7)	9.58(−7)	2.55(−7)	4.80(−7)	8.63(−7)
μt	$b = 5.0$ $a = 1.0$	$b = 5.0$ $a = 2.0$	$b = 5.0$ $a = 5.0$	$b = 10.0$ $a = 0.1$	$b = 10.0$ $a = 0.2$	$b = 10.0$ $a = 0.5$
0	1.22(−1)	1.70(−1)	2.06(−1)	1.58(−2)	3.13(−2)	7.34(−2)
0.01	1.20(−1)	1.67(−1)	2.01(−1)	1.56(−2)	3.08(−2)	7.23(−2)
0.02	1.18(−1)	1.64(−1)	1.97(−1)	1.58(−2)	3.04(−2)	7.12(−2)
0.05	1.16(−1)	1.62(−1)	1.93(−1)	1.51(−2)	2.99(−2)	7.01(−2)
0.1	1.05(−1)	1.43(−1)	1.68(−1)	1.37(−2)	2.70(−2)	6.32(−2)
0.2	9.02(−2)	1.21(−1)	1.38(−1)	1.19(−2)	2.35(−2)	5.48(−2)
0.5	5.87(−2)	7.51(−2)	8.10(−2)	8.02(−3)	1.58(−2)	3.65(−2)
1.0	2.99(−2)	3.59(−2)	3.71(−2)	4.33(−3)	8.53(−3)	1.93(−2)
2.0	8.38(−3)	9.32(−3)	9.38(−3)	1.35(−3)	2.65(−3)	5.81(−3)
5.0	2.44(−4)	2.49(−4)	2.49(−4)	5.00(−5)	9.65(−5)	1.95(−4)
10.0	9.56(−7)	9.58(−7)	9.58(−7)	2.55(−7)	4.80(−7)	8.63(−7)
μt	$b = 10.0$ $a = 1.0$	$b = 10.0$ $a = 2.0$	$b = 10.0$ $a = 5.0$	$b = 10.0$ $a = 10.0$	$b = 20.0$ $a = 0.1$	$b = 20.0$ $a = 0.2$
0	1.24(−1)	1.75(−1)	2.15(−1)	2.28(−1)	1.58(−2)	3.14(−2)
0.01	1.22(−1)	1.71(−1)	2.10(−1)	2.22(−1)	1.56(−2)	3.09(−2)
0.02	1.20(−1)	1.68(−1)	2.05(−1)	2.16(−1)	1.54(−2)	3.04(−2)
0.05	1.18(−1)	1.65(−1)	2.01(−1)	2.11(−1)	1.51(−2)	3.00(−2)
0.1	1.06(−1)	1.46(−1)	1.72(−1)	1.78(−1)	1.37(−2)	2.71(−2)
0.2	9.08(−2)	1.22(−1)	1.40(−1)	1.43(−1)	1.19(−2)	2.35(−2)
0.5	5.88(−2)	7.53(−2)	8.13(−2)	8.17(−2)	8.02(−3)	1.58(−2)
1.0	2.99(−2)	3.59(−2)	3.71(−2)	3.71(−2)	4.33(−3)	8.53(−3)
2.0	8.38(−3)	9.32(−3)	9.38(−3)	9.38(−3)	1.35(−3)	2.65(−3)
5.0	2.44(−4)	2.49(−4)	2.49(−4)	2.49(−4)	5.00(−5)	9.65(−5)
10.0	9.56(−7)	9.58(−7)	9.58(−7)	9.58(−7)	2.55(−7)	4.81(−7)

Table 3D.4. (continued)

μt	$2\Gamma/[\Phi(0)\ G(E)]$					
	$b = 20.0$ $a = 0.5$	$b = 20.0$ $a = 1.0$	$b = 20.0$ $a = 2.0$	$b = 20.0$ $a = 5.0$	$b = 20.0$ $a = 10.0$	$b = 20.0$ $a = 20.0$
0	7.37(−2)	1.25(−1)	1.76(−1)	2.18(−1)	2.32(−1)	2.39(−1)
0.01	7.26(−2)	1.23(−1)	1.72(−1)	2.12(−1)	2.26(−1)	2.31(−1)
0.02	7.14(−2)	1.21(−1)	1.69(−1)	2.07(−1)	2.20(−1)	2.24(−1)
0.05	7.03(−2)	1.19(−1)	1.66(−1)	2.02(−1)	2.14(−1)	2.18(−1)
0.1	6.33(−2)	1.06(−1)	1.46(−1)	1.73(−1)	1.79(−1)	1.80(−1)
0.2	5.48(−2)	9.08(−2)	1.22(−1)	1.40(−1)	1.43(−1)	1.44(−1)
0.5	3.65(−2)	5.88(−2)	7.53(−2)	8.13(−2)	8.17(−2)	8.17(−2)
1.0	1.93(−2)	2.99(−2)	3.59(−2)	3.71(−2)	3.71(−2)	3.71(−2)
2.0	5.81(−3)	8.38(−3)	9.32(−3)	9.38(−3)	9.38(−3)	9.38(−3)
5.0	1.95(−4)	2.44(−4)	2.49(−4)	2.49(−4)	2.49(−4)	2.49(−4)
10.0	8.63(−7)	9.56(−7)	9.58(−7)	9.58(−7)	9.58(−7)	9.58(−7)

[a]Read: 1.58×10^{-3}, etc.

Appendix 3E. Graphs for Neutron Attenuation Calculations

This appendix consists of graphs of neutron penetration results obtained from Monte Carlo calculations by Clark *et al.*[61] and by Allen and Futterer.[62] Figures 3E.1 through 3E.10 show the dose (in ergs/g per incident neutron/cm^2) due to monoenergetic beams of neutrons normally incident on ordinary concrete, both on a slab and on a semi-infinite medium (half space). Figures 3E.11 through 3E.15 present plots of the neutron dose transmission factor as a function of polyethylene thickness for monoenergetic neutrons incident at various angles. When the thickness is adjusted according to the key included at the top of each figure, these latter curves apply also to water, to concrete, and to Nevada Test Site soil, both dry and water-saturated.

The use of these curves is explained in Section 3.8.2.

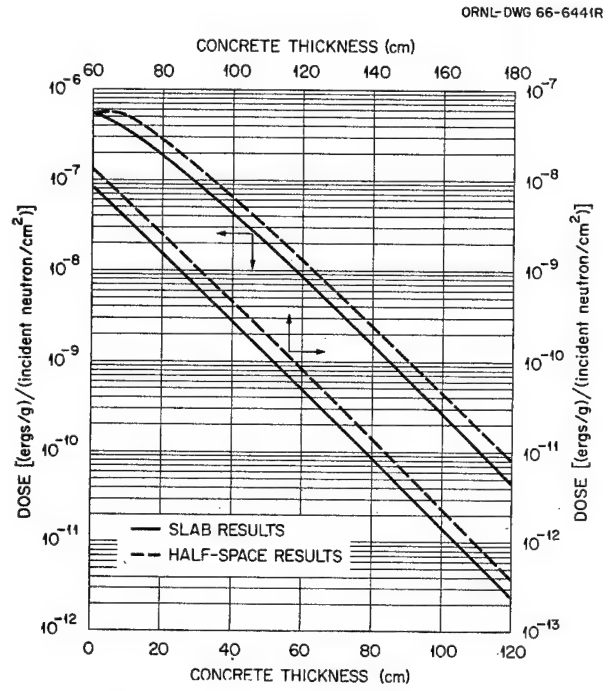

Fig. 3E.1. Penetration of 14-MeV Normally Incident Neutrons in Ordinary Concrete. (From ref. 61.)

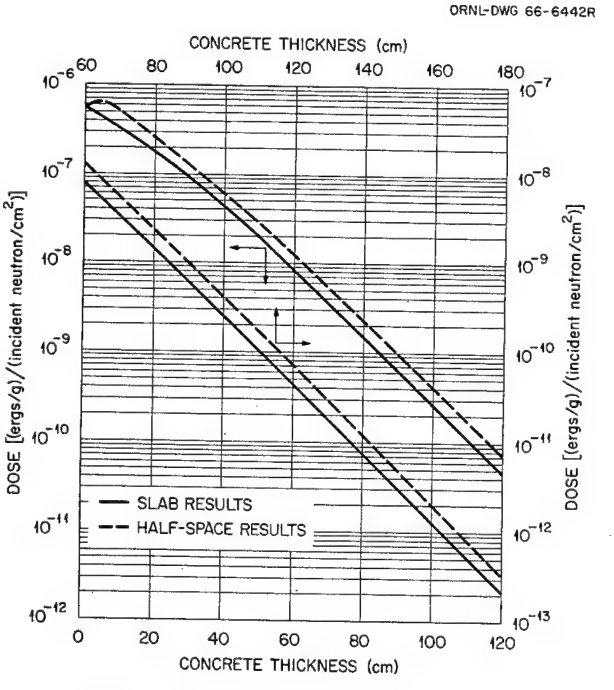

Fig. 3E.2. Penetration of 12-MeV Normally Incident Neutrons in Ordinary Concrete. (From ref. 61.)

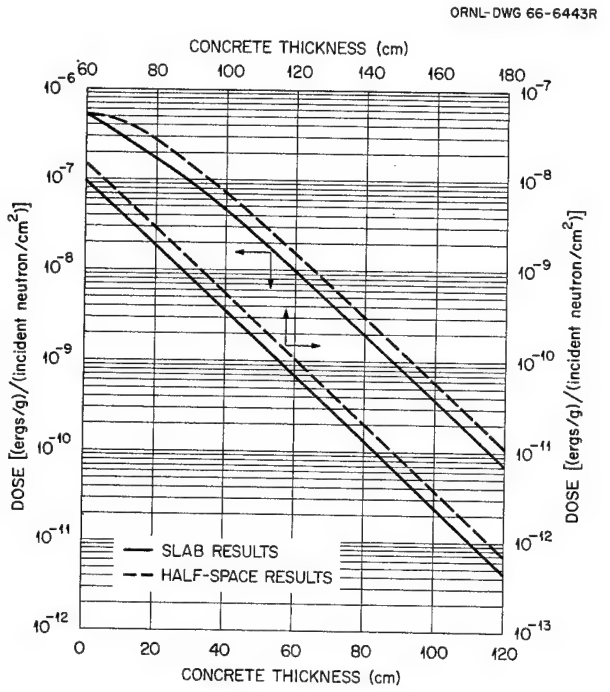

Fig. 3E.3. Penetration of 10-MeV Normally Incident Neutrons in Ordinary Concrete. (From ref. 61.)

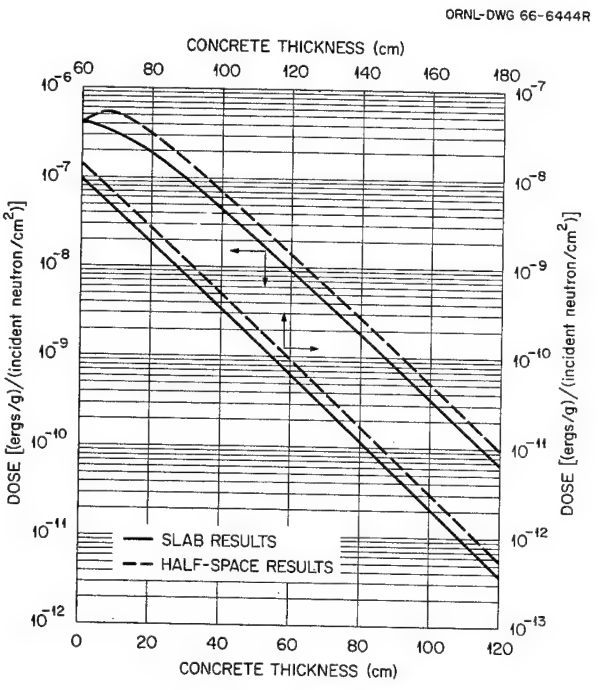

Fig. 3E.4. Penetration of 8-MeV Normally Incident Neutrons in Ordinary Concrete. (From ref. 61.)

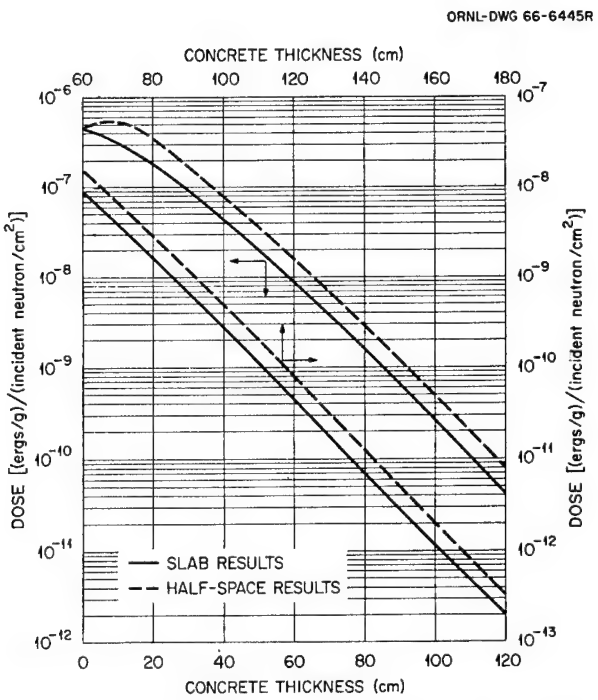

Fig. 3E.5. Penetration of 6-MeV Normally Incident Neutrons in Ordinary Concrete. (From ref. 61.)

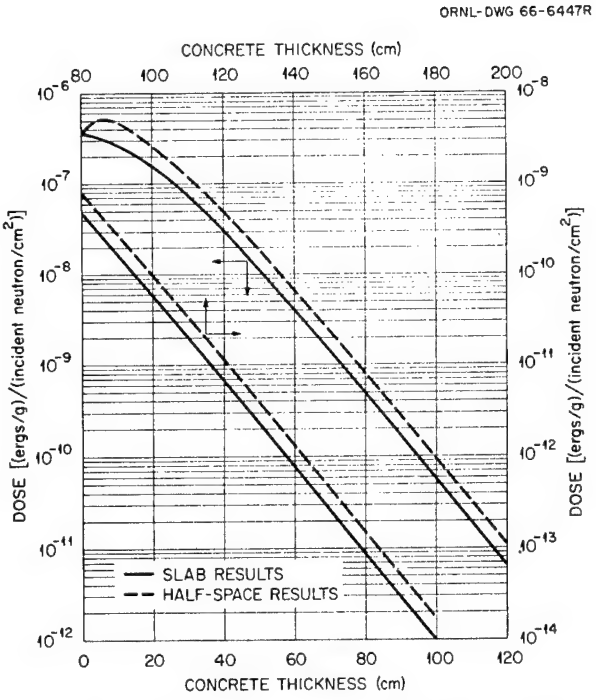

Fig. 3E.7. Penetration of 3-MeV Normally Incident Neutrons in Ordinary Concrete. (From ref. 61.)

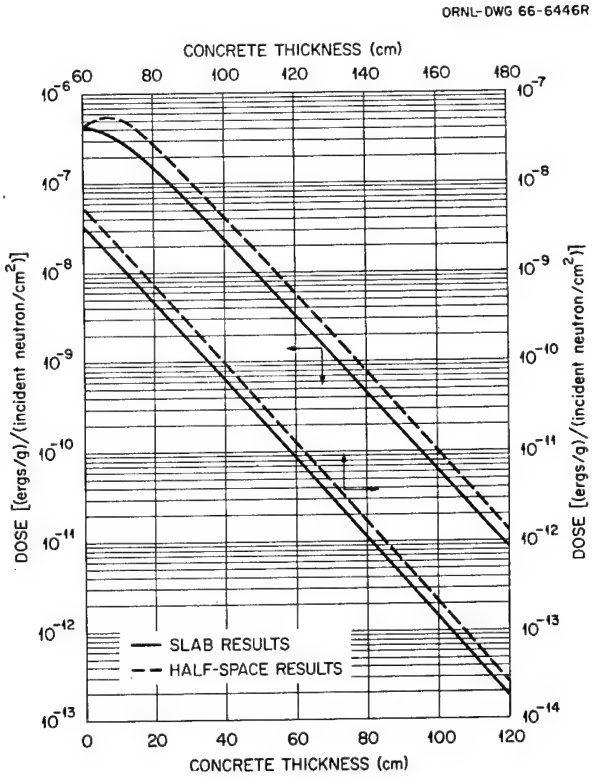

Fig. 3E.6. Penetration of 4-MeV Normally Incident Neutrons in Ordinary Concrete. (From ref. 61.)

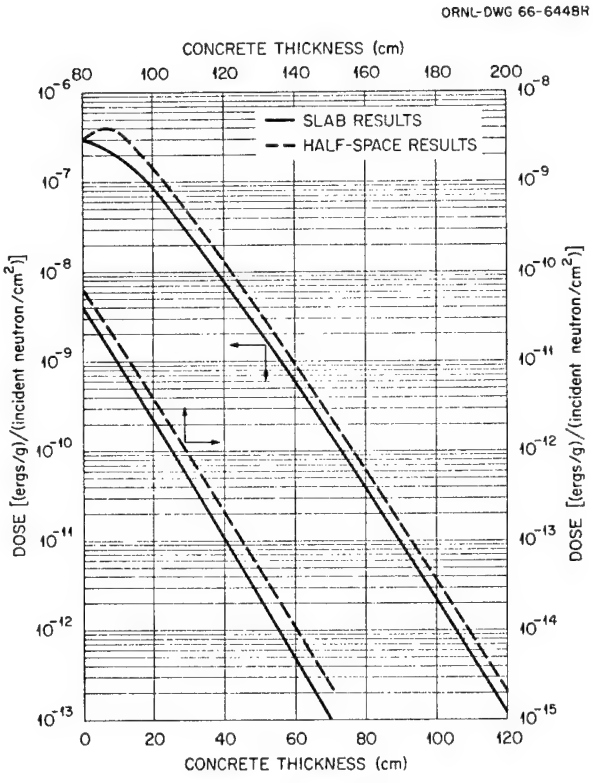

Fig. 3E.8. Penetration of 2-MeV Normally Incident Neutrons in Ordinary Concrete. (From ref. 61.)

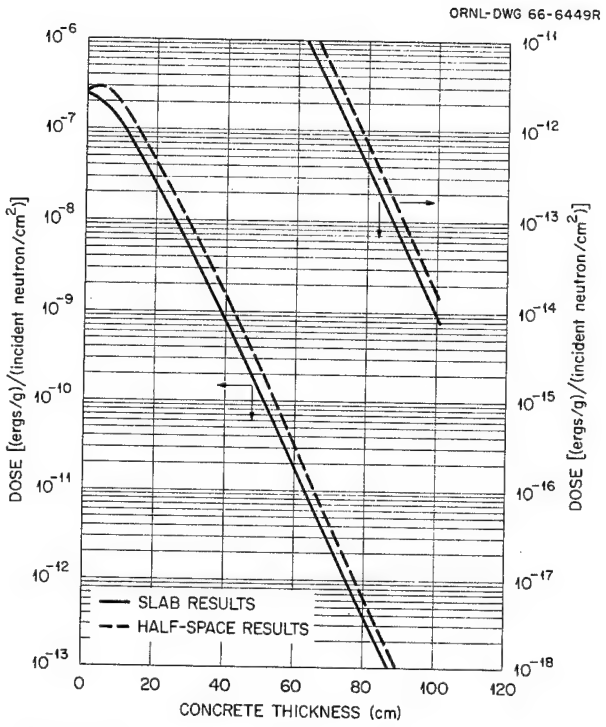

Fig. 3E.9. Penetration of 1.3-MeV Normally Incident Neutrons in Ordinary Concrete. (From ref. 61.)

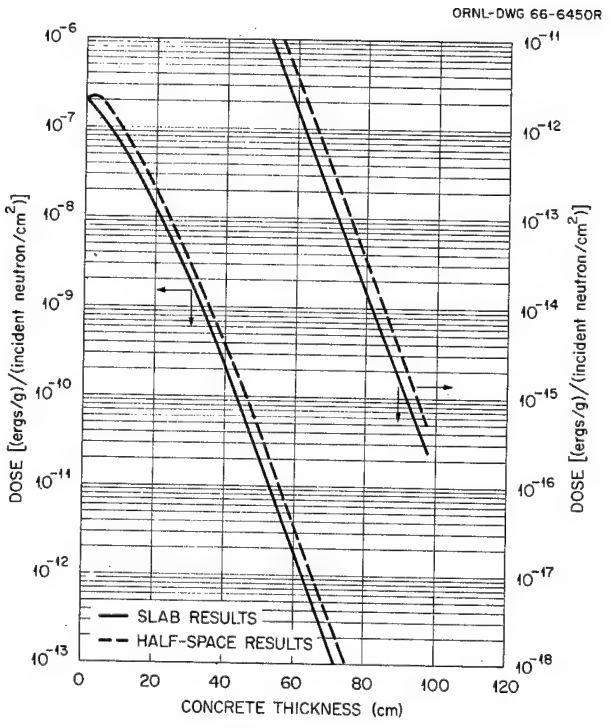

Fig. 3E.10. Penetration of 0.7-MeV Normally Incident Neutrons in Ordinary Concrete. (From ref. 61.)

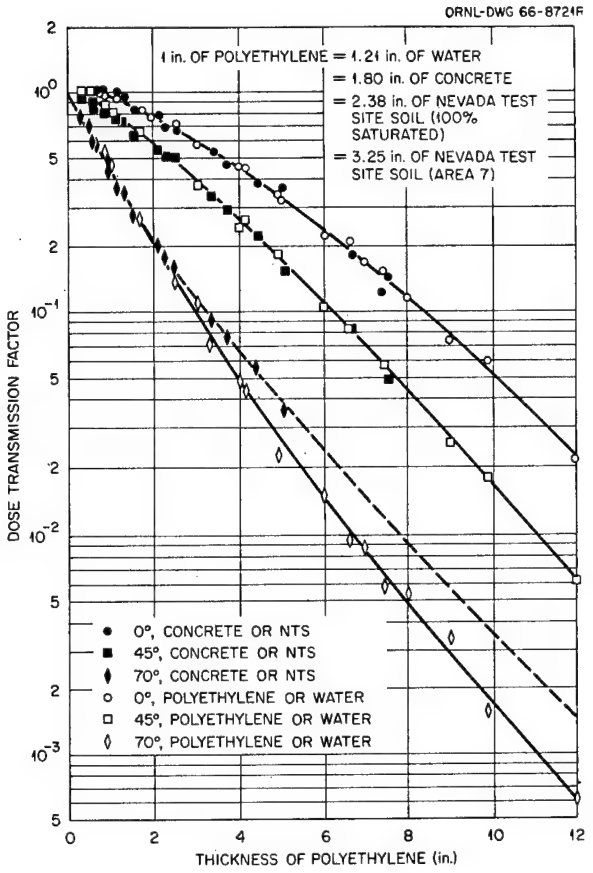

Fig. 3E.11. Penetration of 5-MeV Neutrons Incident on Various Materials at Various Angles. (From ref. 64.)

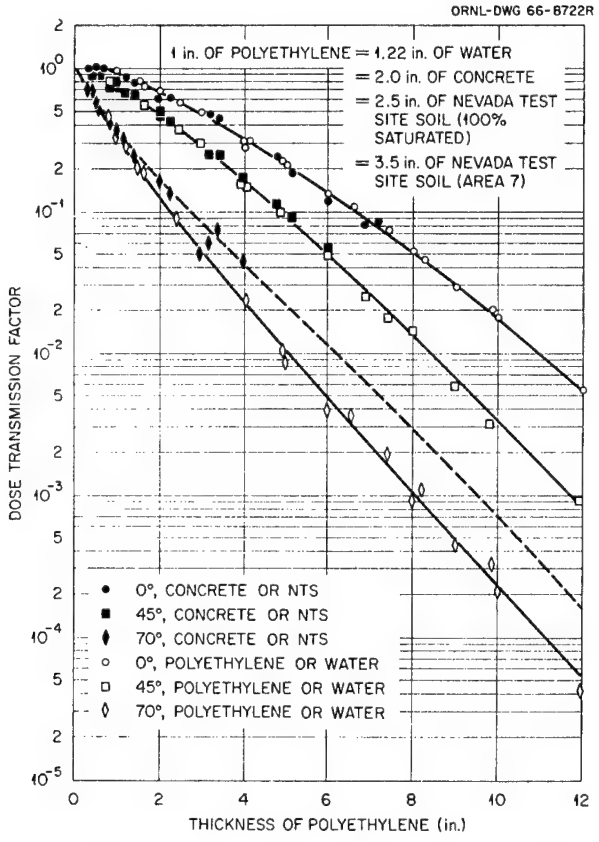

Fig. 3E.12. Penetration of 3-MeV Neutrons Incident on Various Materials at Various Angles. (From ref. 64.)

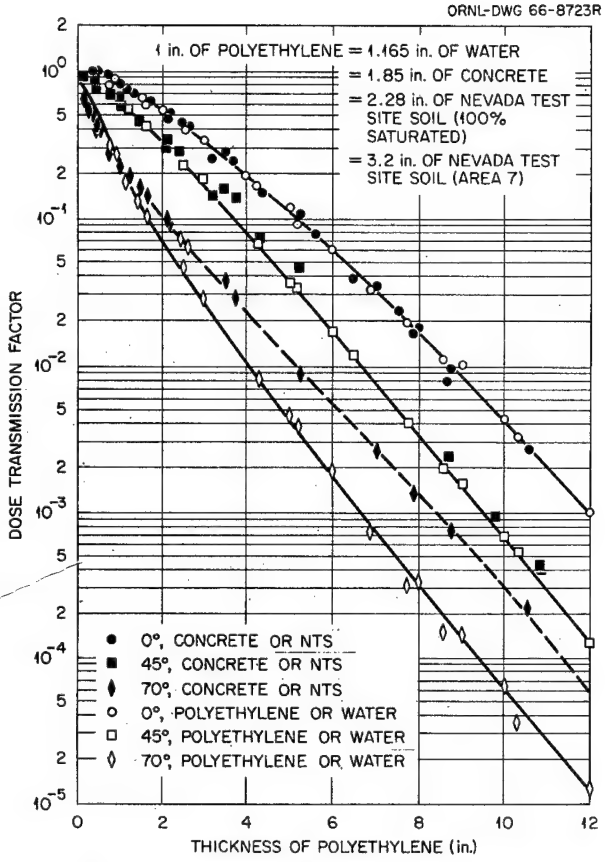

Fig. 3E.13. Penetration of 2-MeV Neutrons Incident on Various Materials at Various Angles. (From ref. 64.)

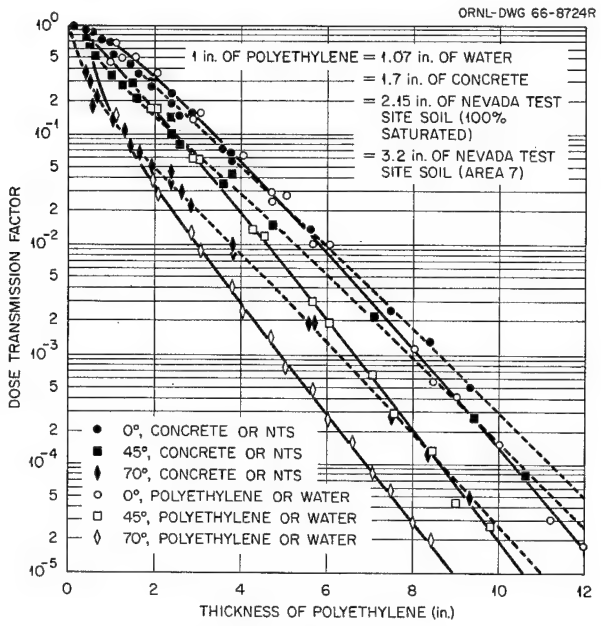

Fig. 3E.14. Penetration of 1-MeV Neutrons Incident on Various Materials at Various Angles. (From ref. 64.)

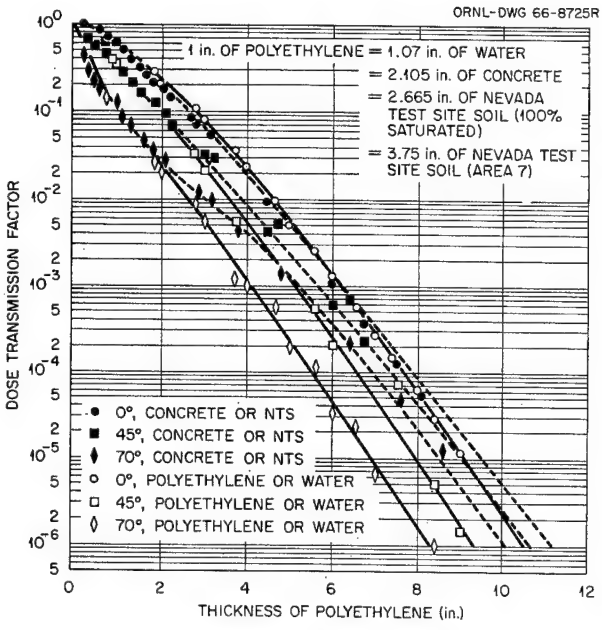

Fig. 3E.15. Penetration of 0.5-MeV Neutrons Incident on Various Materials at Various Angles. (From ref. 64.)

Appendix 3F. Graphs of the ψ Function

A useful function in calculating the shield penetration of the uncollided secondary gamma-ray flux is the ψ function, defined in Section 3.10. Values of this function have been obtained by Trubey[44] for the case of a slab shield and by Claiborne[75] for the case of a semi-infinite shield. The functions are plotted in Figs. 3D.1 through 3D.6, all of which are taken from a compilation of Trubey.[44]

ORNL-DWG 65-11934R

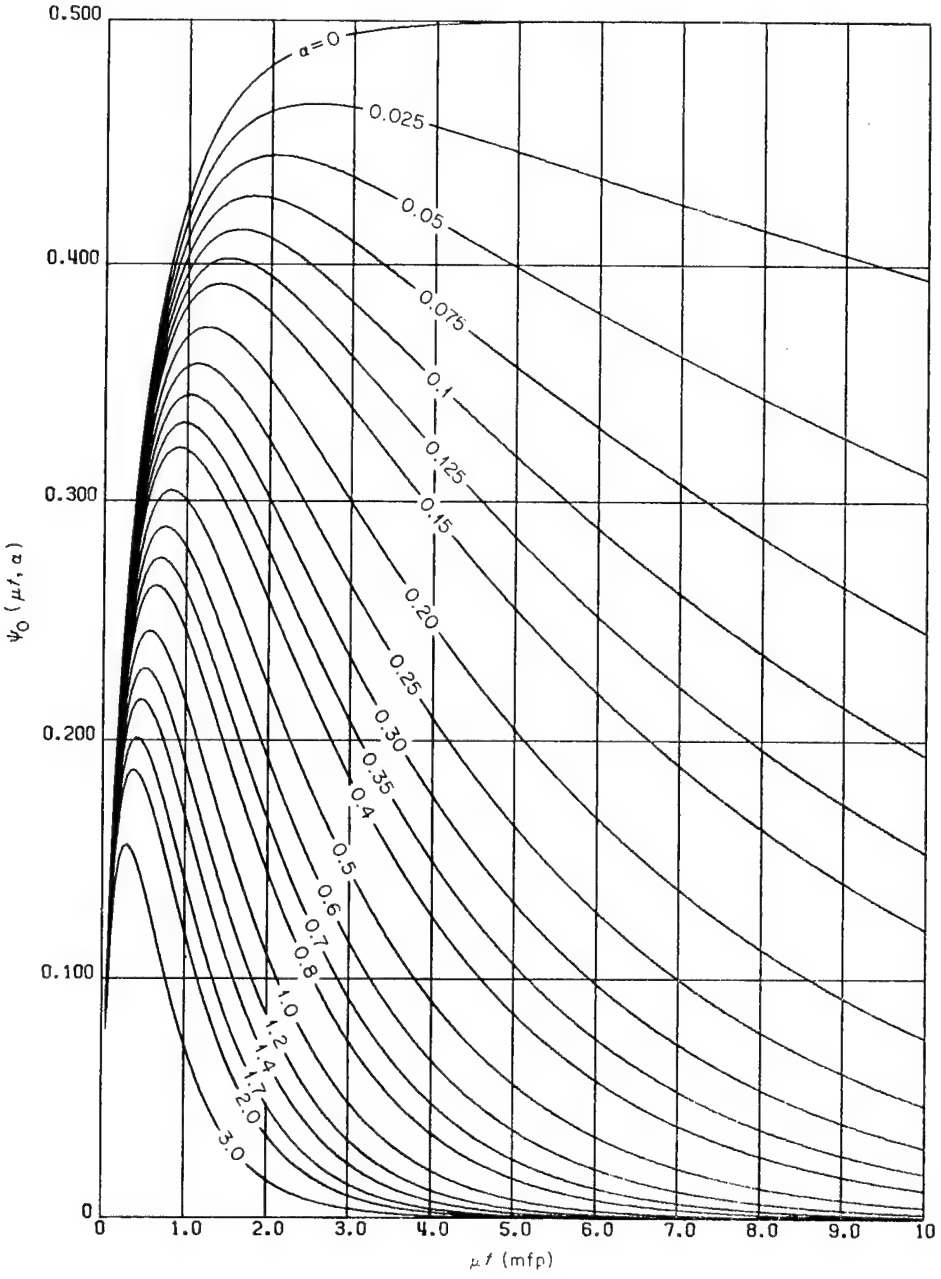

Fig. 3F.1. The Function $\Psi_0(\mu t,\alpha)$ for a Slab Shield. (From ref. 44.)

ORNL-DWG 65-11935R

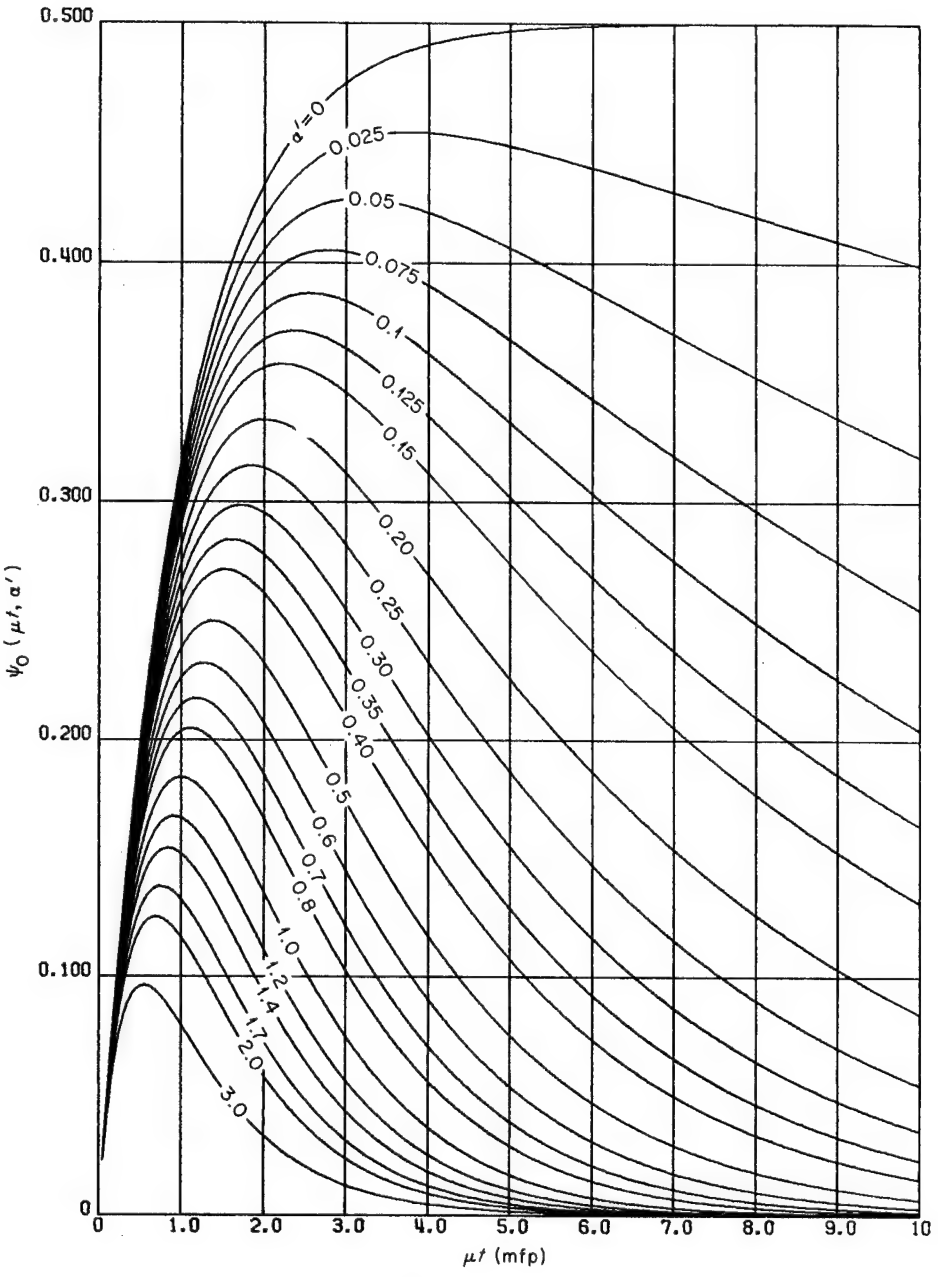

Fig. 3F.2. The Function $\Psi_1(\mu t, \alpha')$ for a Slab Shield. (From ref. 44.)

ORNL-DWG 65-11936R

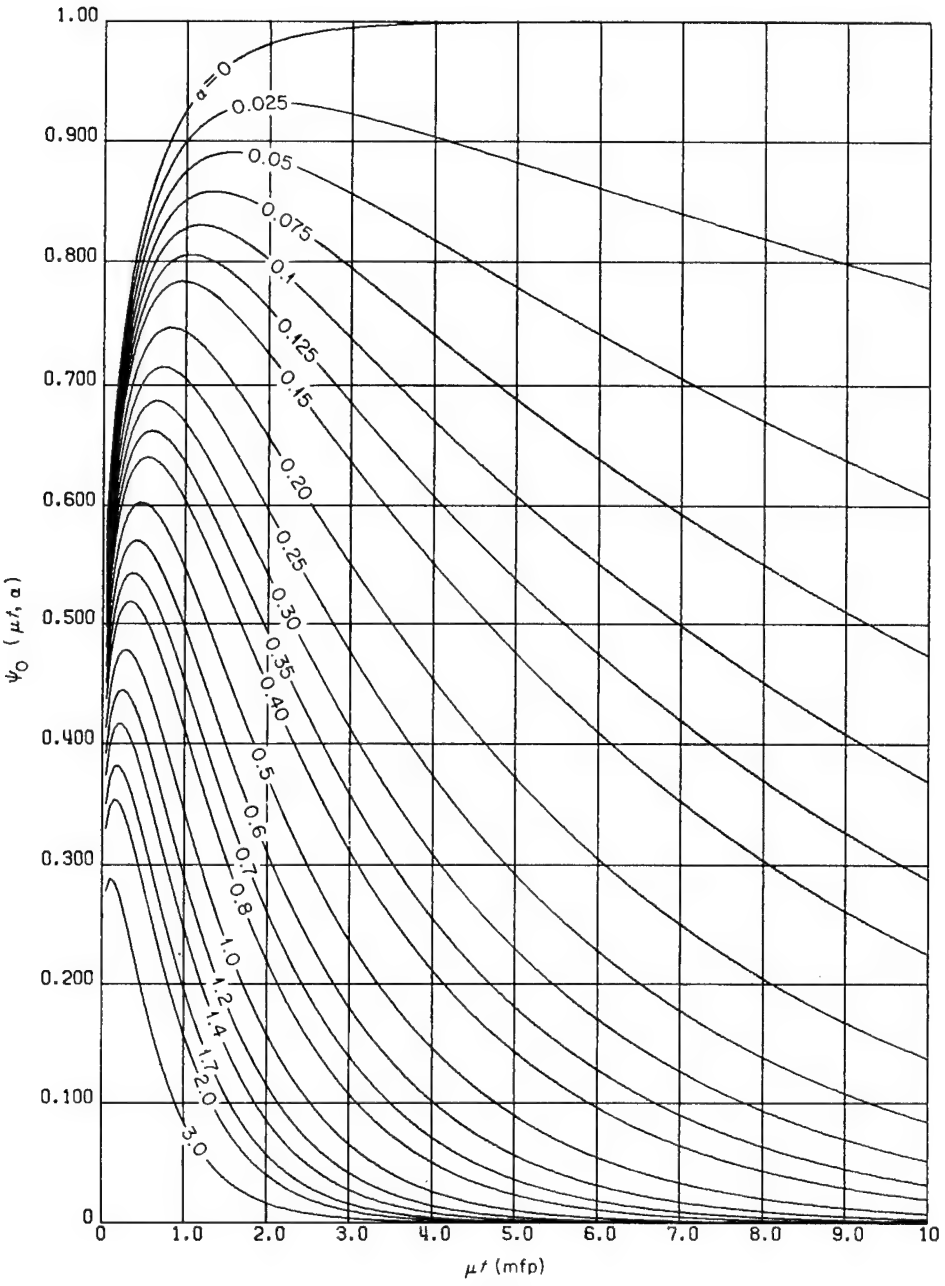

Fig. 3F.3. The Function $\Psi_0(\mu t,\alpha)$ for a Semi-infinite Shield. (From ref. 44.)

ORNL-DWG 65-11937R

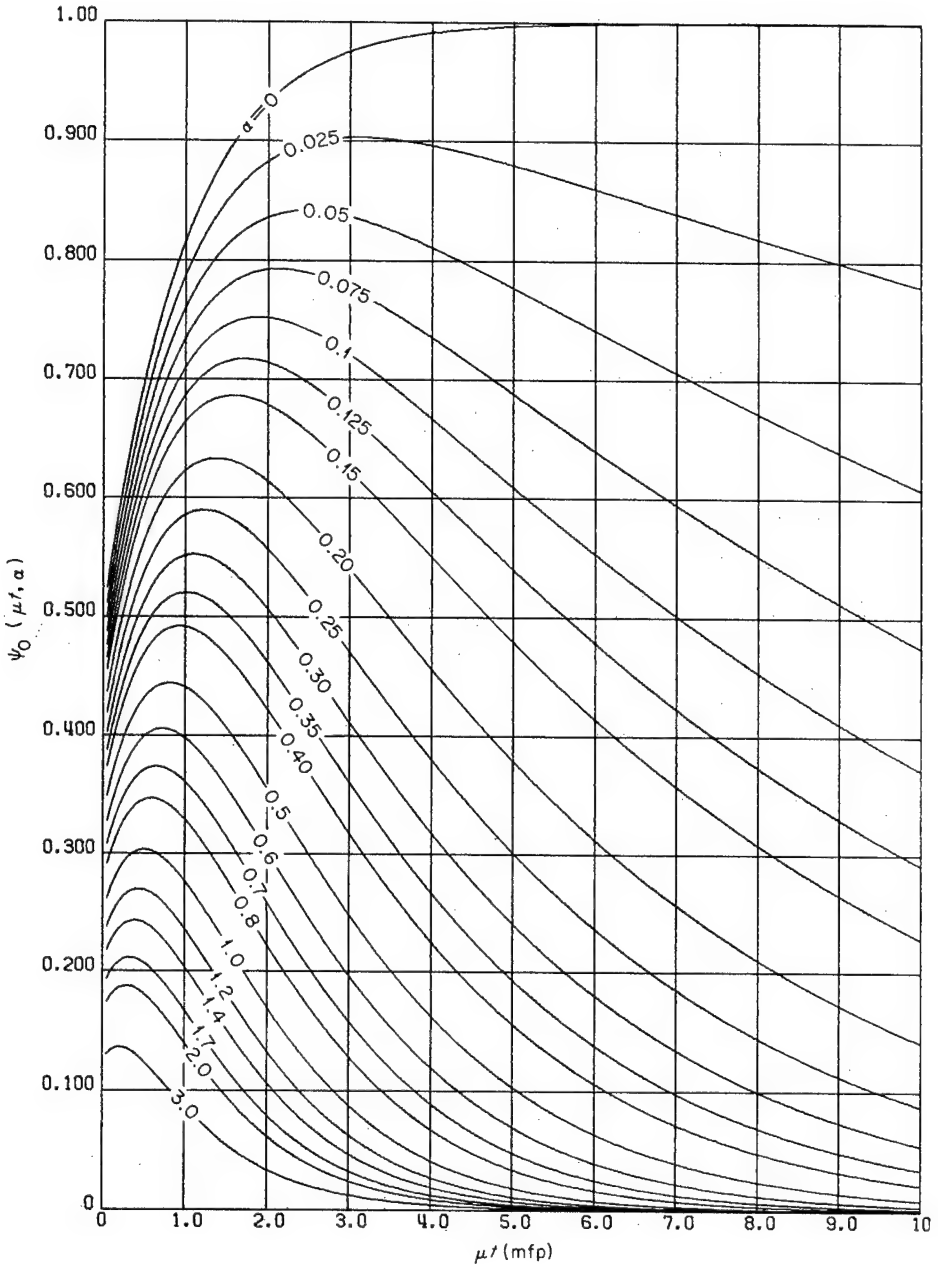

Fig. 3F.4. The Function $\Psi_1(\mu t,\alpha)$ for a Semi-infinite Shield. (From ref. 44.)

ORNL-DWG 65-11938R

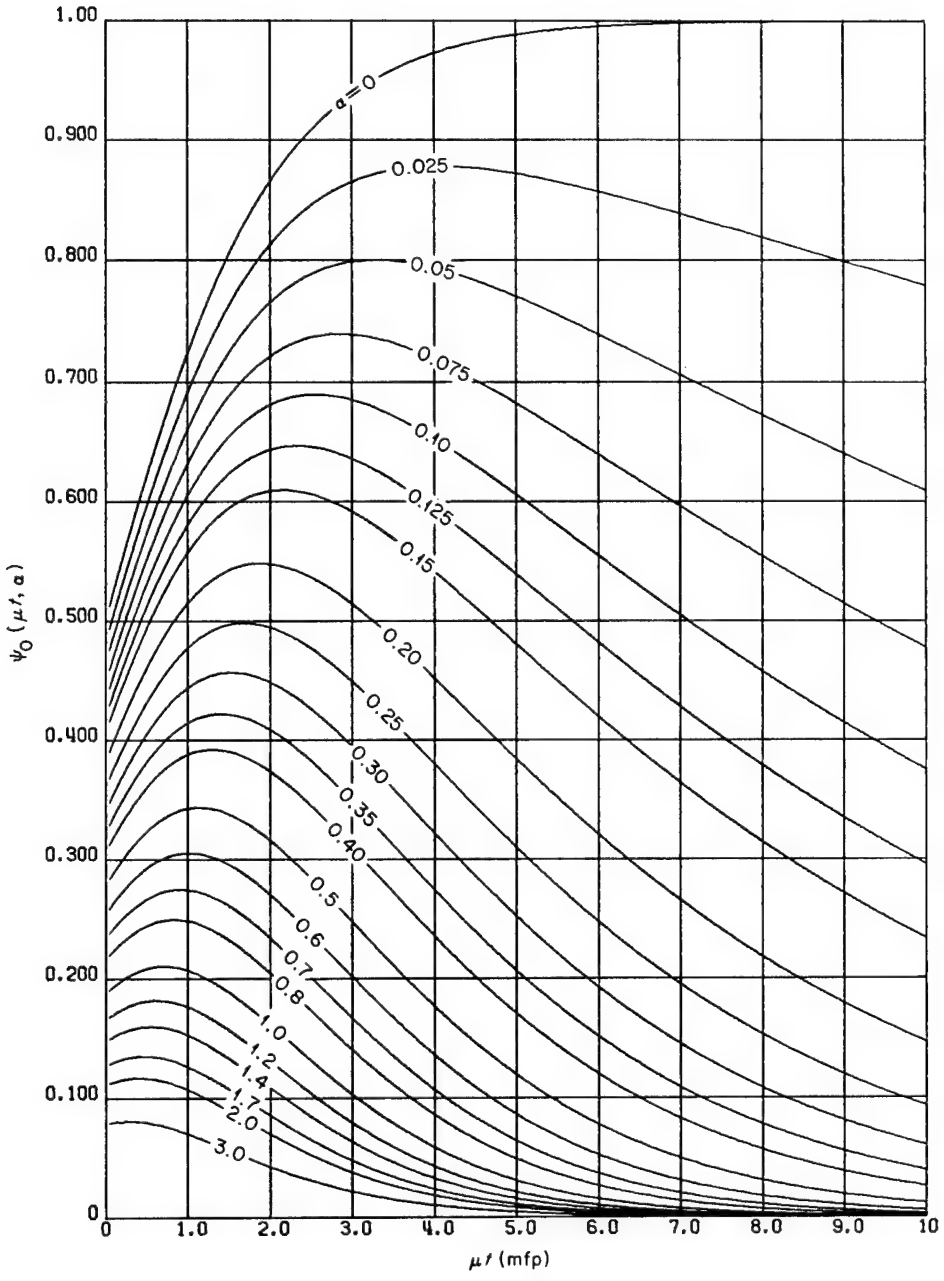

Fig. 3F.5. The Function $\Psi_2(\mu t, \alpha)$ for a Semi-infinite Shield. (From ref. 44.)

ORNL-DWG 65-11939R

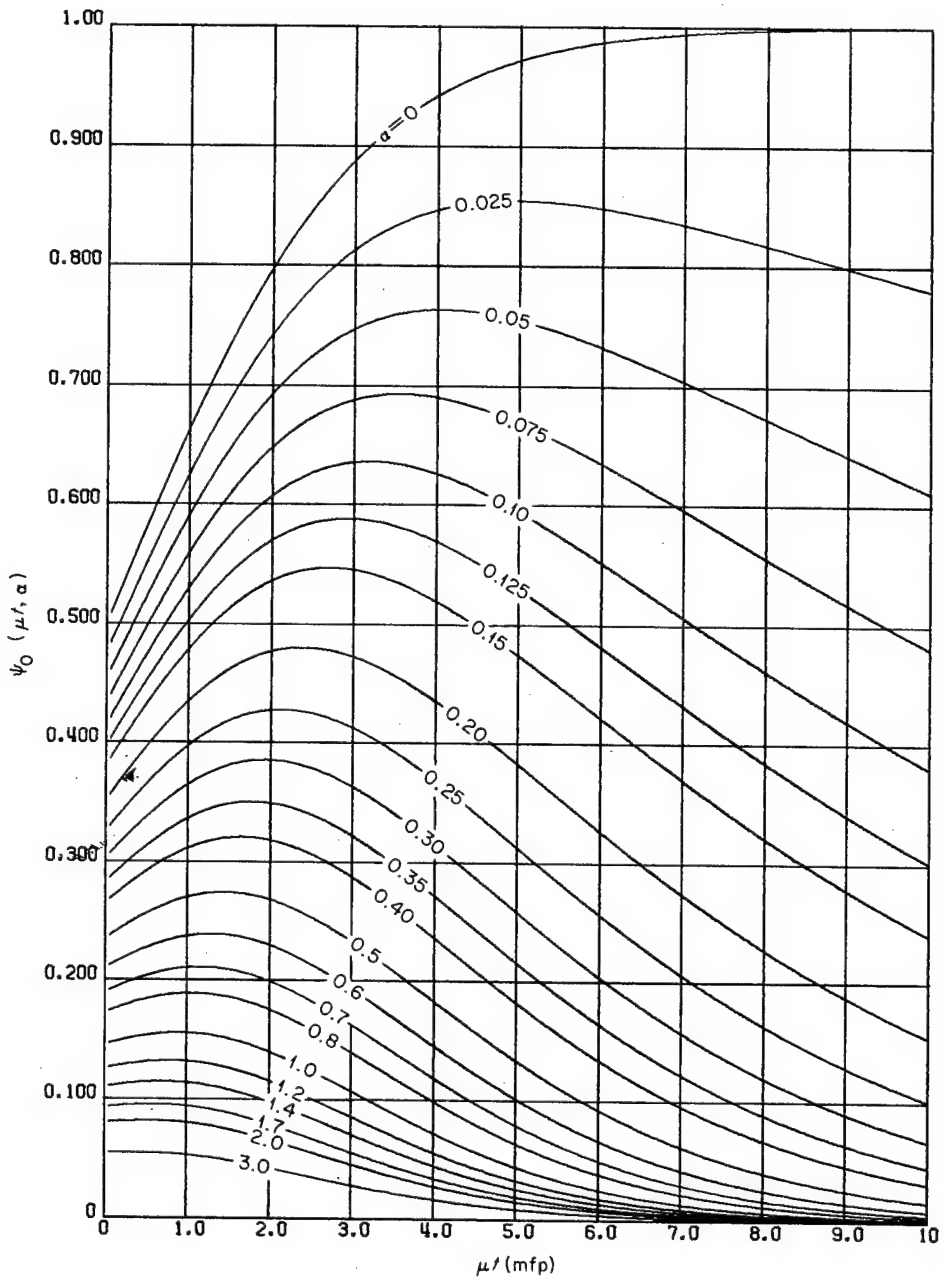

Fig. 3F.6. The Function $\Psi_3(\mu t,\alpha)$ for a Semi-infinite Shield. (From ref. 44.)

References

[1]A. M. Weinberg and E. P. Wigner, *The Physical Theory of Neutron Chain Reactors,* University of Chicago Press, Chicago, 1958.

[2]K. Shure, "P-3 Multigroup Calculations of Neutron Attenuation," *Nucl. Sci. Eng.* **19**, 310 (1964).

[3]W. D. Lanning, "Application of the Spherical Harmonics Technique to Problems in Gamma Transport," *Nucl. Sci. Eng.* **15**, 259–267 (1963).

[4]G. C. Wick, "Über ebene Diffusionprobleme," *Physick* **121**, 702 (1943).

[5]S. Chandrasekhar, *Radiative Transfer,* Clarendon Press, Oxford, 1950.

[6]B. G. Carlson, *Solution of the Transport Equation by the S_n Method,* Los Alamos Scientific Laboratory Report LA-1801 (1955).

[7]W. E. Engle, M. A. Boling, and B. W. Colston, *DTF II, A One-Dimensional Multigroup Neutron Transport Program,* North American Aviation, Los Angeles, Report NAA-SR-10951 (1966).

[8]K. D. Lathrop, *DTF-IV, A FORTRAN-IV Program for Solving the Multigroup Transport Equation with Anisotropic Scattering,* Los Alamos Scientific Laboratory Report LA-3373 (July 15, 1965).

[9]W. W. Engle, Jr., *A Users Manual for ANISN, A One Dimensional Discrete Ordinates Transport Code with Anisotropic Scattering,* Union Carbide Corp., Nuclear Division, K-25, Report K-1693 (Mar. 30, 1967).

[10]B. Carlson, C. Lee, and J. Worlton, *The DSN and TDC Neutron Transport Codes,* Los Alamos Scientific Laboratory Report LAMS-2346 (Feb. 12, 1960); C. E. Lee, *The Discrete S_n Approximation to Transport Theory,* Los Alamos Scientific Laboratory Report LA-2595 (Mar. 9, 1962).

[11]F. R. Mynatt, *A User's Manual for DOT, A Two-Dimensional Discrete Ordinates Transport Code with Anisotropic Scattering,* Union Carbide Corp., Nuclear Division, K-25, Report K-1694 (to be published).

[12]H. Goldstein and J. E. Wilkins, Jr., *Calculations of the Penetration of Gamma Rays, Final Report,* Nuclear Development Associates Report NYO-3075 (1954) (also NDA-15C-41).

[13]H. Goldstein, *Fundamental Aspects of Reactor Shielding,* Addison-Wesley, Reading, Mass., 1959.

[14]J. Certaine, *A Solution of the Neutron Transport Equation. Introduction and Part I,* New York Operations Office Report NYO-3081 (Nuclear Development Associates Report NDA-15C-43) (July 25, 1954); *Part II, NDA-UNIVAC Moments Calculation,* NYO-6268 (NDA-15C-53) (May 31, 1955); and *Part III, Reconstruction of a Function from Its Moments,* NYO-6270 (NDA-15C-61) (July 31, 1956).

[15]R. Aronson *et al., Penetration of Neutrons from a Point Isotropic Fission Source in Water,* New York Operations Office Report NYO-6267 (Nuclear Development Associates Report NDA-15C-42) (Sept. 22, 1954).

[16]R. Aronson, J. Certaine, and H. Goldstein, *Penetration of Neutrons from Point Isotropic Monoenergetic Sources in Water,* New York Operations Office Report NYO-6269 (Nuclear Development Associates Report NDA-15C-60) (Dec. 15, 1954).

[17]J. M. Hammersley and D. C. Handscomb, *Monte Carlo Methods,* Wiley, New York, 1964.

[18]N. P. Buslenko *et al., The Monte Carlo Method* (translated from the Russian), Pergamon, New York, 1966.

[19]H. Kahn, "Random Sampling (Monte Carlo) Techniques in Neutron Attenuation Problems – I and II," *Nucleonics* **6**(5), 27, and **6**(6), 60 (1950).

[20]G. Goertzel and M. H. Kalos, "Monte Carlo Methods in Transport Problems," p. 35 in *Progress in Nuclear Energy,* Series I, *Physics and Mathematics,* Vol. 2, Pergamon, New York, 1958.

[21]H. Kahn, *Applications of Monte Carlo,* Rand Corp. Report AECU-3295 (Apr. 19, 1954).

[22]E. D. Cashwell and C. J. Everett, *A Practical Manual on the Monte Carlo Method for Random Walk Problems,* Pergamon, New York, 1959.

[23]B. E. Watt, "Energy Spectrum of Neutrons from Thermal Fission of U^{235}," *Phys. Rev.* **87**, 1037 (1952).

[24]R. R. Coveyou, V. R. Cain, and K. J. Yost, "Adjoint and Importance in Monte Carlo Application," *Nucl. Sci. Eng.* **27**, 219 (1967).

[25]F. H. Clark, *The Exponential Transform as an Importance-Sampling Device – A Review,* Oak Ridge National Laboratory Report ORNL-RSIC-14 (January 1966).

[26]V. R. Cain, "Application of S_N Adjoint Flux Calculations to Monte Carlo Biasing," *Trans. Am. Nucl. Soc.* **10**, 399 (1967).

[27]F. H. Clark, "Variance of Certain Flux Estimators Used in Monte Carlo Calculations," *Nucl. Sci. Eng.* **27**, 235 (1967).

[28]D. C. Irving *et al., O5R, A General-Purpose Monte Carlo Neutron Transport Code,* Oak Ridge National Laboratory Report ORNL-3622 (February 1965).

[29]C. R. Greenhow, G. O. Mueller, and G. E. Sabian, *Use of Diffusion Theory Codes to Predict Gamma Heating,* Knolls Atomic Power Laboratory Report KAPL-M-DNA-5 (Jan. 1, 1963).

[30]V. A. Ambarzumian, "Diffusion of Light by Planetary Atmospheres," *Astron. Zh.* **19**, 30 (1942).

[31]R. Bellman, R. Kalaba, and G. M. Wing, "Invariant Imbedding and Mathematical Physics. I. Particle Processes," *J. Math. Phys.* **1**(4), 280 (1960).

[32]G. M. Wing, *An Introduction to Transport Theory,* Wiley, New York, 1962.

[33]D. R. Mathews, K. F. Hansen, and E. A. Mason, "Deep Penetration of Radiation by the Method of Invariant Imbedding," *Nucl. Sci. Eng.* **27**, 263 (1967).

[34]J. O. Mingle, "Applications of the Invariant Imbedding Method to Monoenergetic Neutron Transport Theory in Slab Geometry," *Nucl. Sci. Eng.* **28**, 177 (1967).

[35]A. Shimizu and H. Mizuta, "Application of Invariant Imbedding to the Reflection and Transmission Problems of Gamma Rays (II)," *J. Nucl. Sci. Technol. (Tokyo)* **3**, 10 (1966).

[36]J. J. Taylor, *Application of Gamma Ray Build-up Data to Shield Design,* Westinghouse Electric Corp., Atomic Power Division, Report WAPD-RM-217 (June 28, 1954).

[37]G. L. Strobel, "Additional Exponential Representations of Gamma-Ray Build-up Factors," *Nucl. Sci. Eng.* **11**, 450 (1961).

[38]S. Buscaglione and R. Manzini, *Build-Up Factors: Coefficients of the Equation of J. J. Taylor,* Oak Ridge National Laboratory Report ORNL-tr-80 (Rev.) [translated from Comitato Nazionale per l'Energia Nucleare Report RT/FI(65)7 (January 1965)].

[39]R. L. Walker and M. Grotenhuis, *A Summary of Shielding Constants for Concrete,* Argonne National Laboratory Report ANL-6443 (November 1961).

[40]T. Rockwell, editor, *Reactor Shielding Design Manual,* Van Nostrand, Princeton, 1956.

[41]A. Honig, *Dose Build-Up Factors for Concrete,* Oak Ridge National Laboratory Report ORNL-tr-502 [translated from *Kerntechnik* **6**(9), 393 (1964)].

[42]M. A. Capo, *Polynomial Approximation of Gamma Ray Buildup Factors for a Point Isotropic Source,* General Electric Co., Atomic Products Division, Report APEX-510 (August 1959).

[43]S. Buscaglione and R. Manzini, *On the Build-Up Factors of Concrete: Coefficients of the Polynomial Representation,* Oak Ridge National Laboratory Report ORNL-tr-349 [translated from Comitato Nazionale per l'Energia Nucleare Report CEC-94 (June 1964)].

[44]D. K. Trubey, *A Survey of Empirical Functions Used to Fit Gamma-Ray Build-up Factors,* Oak Ridge National Laboratory Report ORNL-RSIC-10 (February 1966).

[45]M. J. Berger, p. 47 in *Proceedings of Shielding Symposium Held at the U.S. Naval Radiological Defense Laboratory, October 17–19, 1956,* U.S. Naval Radiological Defense Laboratory Reviews and Lectures No. 29.

[46]A. B. Chilton, D. Holoviak, and L. K. Donovan, *Interim Report, Determination of Parameters in an Empirical Function for Build-Up Factors for Various Photon Energies,* Naval Civil Engineering Laboratory Report NCEL-TN-389 (AD-249195) (August 1960).

[47]A. Rudloff, "The Use of Buildup Factors in Calculating Gamma Radiation from Plane Sources Behind Absorber of Finite Extension," *Atomkernenergie* **9**, 451 (1946).

[48]A. B. Chilton, "Two-Parameter Formula for Point Source Buildup Factors," *Nucleonics* **23**(8), 119 (1965).

[49]J. H. Hubbell, "A Power-Series Buildup Factor Formulation Application to Rectangular and Off-Axis Disk Source Problems," *J. Res. Natl. Bur. Std.* **67C**, 291 (1963).

[50]J. H. Hubbell, R. L. Bach, and R. J. Herbold, "Radiation Field from a Circular Disk Source," *J. Res. Natl. Bur. Std.* **65C**, 249 (1961).

[51]D. K. Trubey, Oak Ridge National Laboratory, unpublished calculations.

[52]J. H. Hubbell, R. L. Bach, and J. C. Lamkin, "Radiation Field from a Rectangular Source," *J. Res. Natl. Bur. Std.* **64C**, 121 (1960).

[53]R. D. Albert and T. A. Welton, *A Simplified Theory of Neutron Attenuation and Its Application to Shield Design,* Westinghouse Electric Corp., Atomic Power Division, Report WAPD-15 (Nov. 30, 1950).

[54]E. Solomito and J. R. Stockton, *Modifications of the Point Kernel Code QAD-P5A: Conversion to the IBM-360 Computer and Incorporation of Ad-*

ditional Geometry Routines, Oak Ridge National Laboratory Report ORNL-4181 (in press).

[55]G. T. Chapman and C. L. Storrs, *Effective Neutron Removal Cross Sections for Shielding,* Oak Ridge National Laboratory Report ORNL-1843 (Sept. 19, 1955) (AECD-3978, Dec. 2, 1955).

[56]H. Goldstein, *Fundamental Aspects of Reactor Shielding,* pp. 310–316, Addison-Wesley, Reading, Mass., 1959.

[57]L. K. Zoller, "Fast-Neutron-Removal Cross Sections," *Nucleonics* **22**(8), 128 (1964).

[58]D. K. Trubey and G. T. Chapman, *Effective Neutron Removal Cross Sections for Carbon and Oxygen in Continuous Mediums,* Oak Ridge National Laboratory Report ORNL-2197 (Sept. 19, 1958).

[59]D. K. Trubey, Oak Ridge National Laboratory, later unpublished analysis of the homogeneous-medium data.

[60]A. W. Casper, *Modified Fast Neutron Attenuation Functions,* General Electric Co., Atomic Products Division, Report XDC-60-2-76 (Feb. 3, 1960).

[61]F. H. Clark, N. A. Betz, and J. Brown, *Monte Carlo Calculations of the Penetration of Normally Incident Neutron Beams Through Concrete,* Oak Ridge National Laboratory Report ORNL-3926 (January 1967).

[62]*Reactor Physics Constants,* Argonne National Laboratory Report ANL-5800, 2d ed. (July 1963).

[63]D. K. Trubey and M. B. Emmett, *Some Calculations of the Fast-Neutron Distribution in Ordinary Concrete from Point and Plane Isotropic Fission Sources,* Oak Ridge National Laboratory Report ORNL-RSIC-4 (June 1965).

[64]F. J. Allen and A. T. Futterer, "Neutron Transmission Data," *Nucleonics* **21**(8), 120 (1963).

[65]J. W. Haffner, "Neutron Energy Spectrum Calculations in Reactor Shields," Preprint V-84, *Nuclear Engineering and Science Conference, April 6–9, 1959, Cleveland, Ohio,* Engineers Joint Council, New York.

[66]D. C. Anderson and K. Shure, "Thermal Neutron Flux Distributions in Metal-Hydrogenous Shields," *Nucl. Sci. Eng.* **8**, 260 (1960).

[67]K. Shure, "Few-Group and Multigroup Calculations of Neutron Penetration," *Nucl. Sci. Eng.* **27**, 468 (1967).

[68]A. F. Avery *et al., Methods of Calculation for Use in the Design of Shields for Power Reactors,* United Kingdom Atomic Energy Authority Report AERE-R-3216 (February 1960).

[69]D. E. Bendall, *RASH D – A Mercury Programme for Neutron Shielding Calculations,* United Kingdom Atomic Energy Authority Report AEEW-M-261 (August 1962).

[70]J. Butler, *The Status of Theoretical Methods for Reactor Shield Design,* United Kingdom Atomic Energy Authority Report AEEW-R-361 (March 1964).

[71]E. G. Peterson, *MAC – A Bulk Shielding Code,* Hanford Atomic Products Operation Report HW-73381 (April 1962).

[72]U. Canali *et al., MAC-RAD, A Reactor Shielding Code,* European Atomic Energy Community Report EUR-2152.e (1964).

[73]L. Hjarne, editor, *A User's Manual for the NRN Shield Design Method,* Aktiebolaget Atomenergia Report AE-145 (June 1964).

[74]L. Hjarne and M. Leimdorfer, "A Method for Predicting the Penetration and Slowing Down of Neutrons in Reactor Shields," *Nucl. Sci. Eng.* **24**, 165 (1966).

[75]H. C. Claiborne, "Analytical Solutions for Heat Generation Distributions in Regular Geometries," Article 7.3 in *Engineering Compendium of Radiation Shielding,* Springer-Verlag, Berlin (to be published).

[76]B. F. Maskewitz, *Abstracts of Digital Computer Code Packages Assembled by the Radiation Shielding Information Center,* Oak Ridge National Laboratory Report ORNL-RSIC-13, Vol. I.

[77]K. D. Lathrop, *GAMLEG – A FORTRAN Code to Produce Multigroup Cross Sections for Photon Transport Calculations,* Los Alamos Scientific Laboratory Report LA-3267 (April 1967).

[78]B. G. Carlson *et al., DTF Users Manual,* United Nuclear Corp. Report UNC Phys/Math-3321, Vols. I and II (November 1963).

[79]H. Penkuhn, *A Numerical Solution of the Boltzmann Equation Applied to Numerical Slabs,* European Atomic Energy Community, Ispra, Italy, Reports EUR 2488.e and EUR 1643.e, p. 92; Argonne National Laboratory Report ANL-7050, p. 113.

[80]H. Penkuhn, *User's Manual for the Gamma Transport Codes BIGGI 4P and BIGGI 4T,* to be published as European Atomic Energy Community Report.

[81]J. Certaine, E. DeDufour, and G. Rabonowitz, *An IBM-704 Program for Neutron Moments Calculations,* United Nuclear Corp. Report NDA-2120-3 (December 1959).

[82]C. V. Smith, *A Moments Method Computer Code for Reconstructing Scattered Gamma Ray Distributions,* U.S. Naval Radiological Defense Laboratory Report USNRDL-TR-67-9 (Jan. 17, 1967).

[83]J. G. Dardis and N. E. Scofield, *Energy and Angular Distribution of Gamma Rays Scattered in Aluminum,* U.S. Naval Radiological Defense Laboratory Report USNRDL-TR-1018 (Dec. 22, 1965).

[84]N. R. Baumgardt, A. Trampus, and J. E. MacDonald, *Program 15-2, Monte Carlo Calculation of Gamma-Ray Scattering in Air,* General Electric Co., Nuclear Materials and Propulsion Operation, Report XDC 61-5-1 (May 1961).

[85]M. A. Capo, *Determination of Suitable Parameters for Compiling Gamma Ray Air Scattering Probabilities,* General Electric Co., Nuclear Materials and Propulsion Operation, Report DC-60-10-150 (Oct. 26, 1960) (declassified Oct. 2, 1964).

[86]J. J. Loechler and J. E. MacDonald, *Flexible Monte Carlo Programs FMC-N and FMC-G,* General Electric Co., Atomic Products Division, Report APEX-706 (April 1961).

[87]J. P. Yalch and J. E. MacDonald, *Program 20-2, A Program for Approximating Cross Section Dependence on Energy,* General Electric Co., Nuclear Materials and Propulsion Operation, Report GEMP-113 (June 1962).

[88]J. P. Yalch and J. E. MacDonald, *Program 20-4, A Program for Averaging Differential Scattering Cross Sections,* General Electric Co., Nuclear Materials and Propulsion Operation, Report GEMP-115 (June 1962).

[89]J. J. Loechler, *Flexible Monte Carlo Source Generation,* General Electric Co., Aircraft Nuclear Products Division, Report XDC 61-4-42 (April 1961).

[90]J. P. Yalch and J. E. MacDonald, *Program 20-5, A Program for Preparation of Spectrum Tables from Evaporation Model,* General Electric Co., Nuclear Materials and Propulsion Operation, Report GEMP-116 (June 1962).

[91]J. P. Yalch and J. E. MacDonald, *Program 20-6, A Program for Computing Nuclear Excitation and Transition Probabilities from Measured Gamma Ray Intensities,* General Electric Co., Nuclear Materials and Propulsion Operation, Report GEMP-117 (June 1962).

[92]W. E. Kinney, *Program STATEST, An Application of the Method of Statistical Estimation to the Calculation of Neutron Flux in Anisotropically Scattering Media by Monte Carlo,* Oak Ridge National Laboratory Report ORNL-3715 (November 1964).

[93]H. Steinberg and R. Aronson, *TRG-SGD, A Monte Carlo Program to Calculate Secondary Gamma Ray Dose from a Nuclear Weapon Detonation,* Kirtland Air Force Base, Weapons Laboratory, Report WL-TDR-64-46, Vols. I and II (July 1964).

[94]G. Engstrom, *A User's Manual for Salomon, An IBM-7090 Code for Gamma Transport Calculations,* Research Institute of National Defense, Stockholm, Report FOA 4A-4403-411 (November 1964).

[95]D. J. Raso and S. Woolf, *Monte Carlo Program for Calculating Doses Resulting from an Isotropic Point Source in an Exponential Atmosphere,* Technical Operations Research Report TO-B 64-12 (February 1964).

[96]J. Raso, *Final Report – Monte Carlo Codes to Investigate the Reflection and Transmission of Gamma Rays and Neutrons in Homogeneous and Heterogeneous Slabs – Vol. II. Neutron Codes,* Technical Operations Research Report TO-B 63-82 (October 1965).

[97]J. J. Long, *Utilization of the TORN-I Slab Penetration Procedure as Modified by RRA,* Radiation Research Associates Report RRA-N58 (July 1965).

[98]J. J. Long, *Utilization Instructions for Radiation Research Program RRA-29,* Radiation Research Associates Report RRA-N59 (July 1965).

[99]J. J. Long, *Utilization Instructions for Tech Ops Legendre Expansion Procedure Modified by RRA,* Radiation Research Associates Report RRA-N57 (July 1965).

[100]J. J. Long, *Utilization of the TORN-II Slab Penetration Procedure as Modified by RRA,* Radiation Research Associates Report RRA-N520 (Nov. 1965).

[101]J. J. Long, *Supplement to the TORN I (RRA-33) Procedure Customer's Utilization,* Radiation Research Associates Report RRA-N519 (October 1965).

[102]J. J. Long, *Utilization Instructions for Radiation Research Program RRA-37,* Radiation Research Associates Report RRA-N522 (November 1965).

[103]D. J. Raso and S. S. Holland, *Final Report – Monte Carlo Codes to Investigate the Reflection and Transmission of Gamma Rays and Neutrons in Homogeneous and Heterogeneous Slabs – Volume I. Gamma Ray Code,* Technical Operations Research Report TO-B 63-73 (October 1963).

[104]J. J. Long, *Utilization of the TORG Gamma-Ray Slab Penetration Procedure as Modified by RRA,* Radiation Research Associates Report RRA-N521 (Nov. 1965).

[105]S. K. Penny, D. K. Trubey, and M. B. Emmett, *OGRE, a Monte Carlo System for Gamma-Ray*

Transport Studies, Including an Example (OGRE-P1) for Transmission Through Laminated Slabs, Oak Ridge National Laboratory Report ORNL-3805 (April 1966).

[106]D. K. Trubey and M. B. Emmett, *OGRE-G, an OGRE System Monte Carlo Code for the Calculation of Gamma-Ray Dose Rate at Arbitrary Points in an Arbitrary Geometry,* Oak Ridge National Laboratory Report ORNL-TM-1212 (January 1966).

[107]J. W. Stokes and J. L. Hunter, *Radiological Armor Program Methods and Data Compilation, Volume 5A. Computer Procedures: Slab Penetration and Reflection Calculation (SPARC, P09),* General Dynamics, Fort Worth, Report FZK-200-5A (June 1965).

[108]J. L. Hunter *et al., Radiological Armor Program Methods and Data Compilation, Volume 5A. Computer Procedures: Slab Penetration and Reflection Calculation (SPARC, P09) – Programmer's Manual Supplement,* General Dynamics, Fort Worth, Report FZK-200-5A SUPP. (June 1965).

[109]J. R. Stokes and J. L. Hunter, *Computer Procedure: Slab Penetration and Reflection Calculation (SPARC, E59),* General Dynamics, Fort Worth, Report FZK-234 (June 1965).

[110]J. L. Hunter, *Computer Procedure: Slab Penetration and Reflection Calculation (SPARC, E59) – Programmer's Manual Supplement,* General Dynamics, Fort Worth, Report FZK-234, SUPP. (June 1965).

[111]B. Eisenman and E. Hennessy, *Adonis: An IBM-7090 Monte Carlo Shielding Code Which Solves for the Transport of Neutrons or Gamma Rays in Three-Dimensional Rectangular Geometry,* United Nuclear Corp. Report UNUCOR-635 (March 1963).

[112]B. Eisenman and F. R. Nakache, *UNC-SAM: A FORTRAN Monte Carlo System for the Evaluation of Neutron or Gamma-Ray Transport in Three-Dimensional Geometry,* United Nuclear Corp. Report UNC-5093 (Aug. 31, 1964).

[113]E. S. Troubetzkoy, *UNC-SAM-2: A FORTRAN Monte Carlo Program Treating Time-Dependent Neutron and Photon Transport Through Matter,* United Nuclear Corp. Report UNC-5157 (September 1966).

[114]J. T. Martin, J. P. Yalch, and W. E. Edwards, *Shielding Computer Programs 14-0 and 14-1, Reactor Shield Analysis,* General Electric Co., Nuclear Materials and Propulsion Operation, Report XDC 59-2-16 (Jan. 23, 1959).

[115]M. D. McDonald, *Shielding Computer Program 14-3, Data Check for Shielding Computer Programs 14-0, 14-1, and 14-2,* General Electric Co., Nuclear Materials and Propulsion Operation, Report XDC-59-3-52 (Dec. 10, 1958).

[116]J. T. Martin, J. P. Yalch, and W. E. Edwards, *Shielding Computer Program 14-2, Reactor Shield Analysis,* General Electric Co., Nuclear Materials and Propulsion Operation, Report XDC-59-6-173 (June 15, 1959).

[117]D. S. Duncan *et al., CLOUD – An IBM-709 Program for Computing Gamma-Ray Dose Rate from a Radioactive Cloud,* Atomics International Report NAA-SR-Memo-4822 (April 1959).

[118]R. E. Malenfant, *QAD: A Series of Point Kernel General-Purpose Shielding Programs,* Los Alamos Scientific Laboratory Report LA-3537 (April 1967).

[119]G. P. Lahti, *QAD-HD Point Kernel Radiation Shielding Computer Code to Evaluate Propellant Heating and Dose to Crew,* National Aeronautics and Space Administration Report NASA-TM-X-1397 (April 1967).

[120]R. F. Falkenbury, J. L. Hunter, and J. R. Stokes, *Radiological Armor Program, Methods and Data Compilation. Volume 5B. Computer Procedures: Combine Transmission Calculation (E20),* General Dynamics, Fort Worth, Report FZK-200-5B (June 24, 1965).

[121]J. L. Hunter *et al., Radiological Armor Program, Methods and Data Compilation. Volume 5B. Computer Procedures: Combine Transmission Calculation (E20), Programmers Manual Supplement,* General Dynamics, Fort Worth, Report FZK-200-5B SUPP. (June 24, 1965).

[122]R. F. Falkenbury, J. L. Hunter, and J. R. Stokes, *Computer Procedure: Combine Transmission Calculation (E91),* General Dynamics, Fort Worth, Report FZK-235 (June 8, 1965).

[123]J. L. Hunter, C. W. Austin, and J. B. Wyatt, *Computer Procedure: Combine Transmission Calculation (E91) Programmers Manual Supplement,* General Dynamics, Fort Worth, Report FZK-235 SUPP. (June 1965).

[124]R. F. Falkenbury and J. L. Hunter, *Radiological Armor Program Methods and Data Compilation. Volume 5C. Computer Procedures: Combine Reflection Calculation (F29),* General Dynamics, Fort Worth, Report FZK-200-5C (June 30, 1965).

[125]J. L. Hunter *et al., Radiological Armor Program Methods and Data Compilation. Volume 5C. Computer Procedures: Combine Reflection Calculation (F29), Programmers Manual Supplement,* General Dynamics, Fort Worth, Report FZK-200-5C SUPP. (June 1965).

[126]J. A. Moore *et al., Shield Heating and Dose Rate Attenuation Calculation (SHADRAC)*, General Dynamics, Fort Worth, Report NARF-DC-Memo 1.097 (Mar. 25, 1966).

[127]J. Greenborg, *Two Cross Section Libraries for Use with MAC Shielding Code*, Hanford Atomic Products Operation Report HW-73381 SUPP. 1 (January 1964).

[128]H. Preusch and H. Ilsemann, *MAC-RAD, A Multigroup Attenuation Code for Plane Geometry*, Oak Ridge National Laboratory Report ORNL-tr-610 (October 1963) (translated from Allgemeine Elektricitats-Gesellschaft, Kernenergieanlagen, Hochhaus, Germany, Report AEG-KEA-116).

[129]Kj. Nyman *et al., A Preliminary User's Manual for the NRN Shield Design Method in FORTRAN IV Language*, Aktiebolaget Atomenergia, Stockholm, Report AE-FFA-673-RFN-213 (October 1965).

[130]E. Aalto, R. Fraki, and K. Malen, "The Fine Adjustment of the Neutron Penetration in the NRN Method," *Nucl. Sci. Eng.* **22**, 443 (1965).

[131]A. F. Avery, J. Clarke, and A. Hartley, *COMPRASH (A Preliminary User's Guide Prepared for the ENEA Seminar-Workshop on Shielding Programmes Held at Ispra, April 1966)*, United Kingdom Atomic Energy Authority Report AEEW-M648 (March 1966).

[132]G. Placzek, *The Functions* $E_n(x) = \int_1^\infty \times e^{-xu}u^{-n}dx$, National Research Council of Canada, Division of Atomic Energy, Report NRC-1547 (Dec. 2, 1946).

[133]D. K. Trubey, *A Table of Three Exponential Integrals*, Oak Ridge National Laboratory Report ORNL-2750 (June 18, 1959).

[134]Federal Works Agency, Works Project Administration, *Tables of Sine, Cosine, and Exponential Integrals*, Vols. I and II, under sponsorship of National Bureau of Standards, 1940.

[135]F. Clark, *Approximation to All Orders of the Exponential Integral*, Wright Air Development Center Report WADC-TR-57-771 (Feb. 1958).

[136]M. Abramowitz and I. A. Stegun, editors, *Handbook of Mathematical Functions with Formulas, Graphs, and Mathematical Tables*, National Bureau of Standards, Applied Mathematics Series 55, GPO, Washington, 1964.

Unclassified

Security Classification

DOCUMENT CONTROL DATA - R & D

(Security classification of title, body of abstract and indexing annotation must be entered when the overall report is classified)

1. ORIGINATING ACTIVITY *(Corporate author)*

Oak Ridge National Laboratory
Oak Ridge, Tennessee

2a. REPORT SECURITY CLASSIFICATION
Unclassified

2b. GROUP

3. REPORT TITLE

"Methods for Calculating Neutron and Gamma-Ray Attenuation," Chapter 3 of Weapons Radiation Shielding Handbook

4. DESCRIPTIVE NOTES *(Type of report and inclusive dates)*
Handbook

5. AUTHOR(S) *(First name, middle initial, last name)*

Authors: Paul N. Stevens and David K. Trubey
Editors: Lorraine S. Abbott, H. Clyde Claiborne, Charles E. Clifford

6. REPORT DATE	7a. TOTAL NO. OF PAGES	7b. NO. OF REFS
December 1967	48	51

8a. CONTRACT OR GRANT NO.
Interagency Agreement: 40-36-64

b. PROJECT NO.
DASA Task: A2-11.033

c. IACRO EO 804-64

d.

9a. ORIGINATOR'S REPORT NUMBER(S)
DASA-1892-3

9b. OTHER REPORT NO(S) *(Any other numbers that may be assigned this report)*

10. DISTRIBUTION STATEMENT

This document has been approved for public release and sale; its distribution is unlimited.

11. SUPPLEMENTARY NOTES

12. SPONSORING MILITARY ACTIVITY
Defense Atomic Support Agency
Washington, D.C. 20301

13. ABSTRACT

Calculations of the attenuation of neutrons and gamma rays in shields can be performed by several techniques, the best technique for a particular problem depending on the type of problem to be solved and the degree of accuracy required. This chapter of the Handbook surveys the calculational methods used most frequently and provides summaries of digital computer codes based on the various methods. The methods covered are those of spherical harmonics, discrete ordinates, moments, Monte Carlo, diffusion theory, invariant imbedding, and kernels, plus a method which combines a removal kernel with diffusion theory. Except for the invariant imbedding method, all these techniques are either approximate solutions to the well-known Boltzmann equation or are based on kernels obtained from solutions to the equation. A discussion of the Boltzmann equation is also included in the chapter. (U)

DD FORM 1 NOV 65 1473

Unclassified

Security Classification

Unclassified
Security Classification

14. KEY WORDS	LINK A		LINK B		LINK C	
	ROLE	WT	ROLE	WT	ROLE	WT
Neutron attenuation						
Gamma-ray attenuation						
Secondary gamma-ray attenuation						
Boltzmann transport equation						
Spherical harmonics method						
Discrete ordinates S_n method						
Moments method						
Monte Carlo method						
Diffusion theory						
Invariant imbedding						
Point kernels						
Buildup factors						
Removal cross sections						
Albert-Welton kernel						
Removal-diffusion method						
Spinney method						

Unclassified
Security Classification

INTERNAL DISTRIBUTION

1–9. L. S. Abbott
10. R. G. Alsmiller, Jr.
11. J. R. Buchanan
12–21. H. C. Claiborne
22–24. C. E. Clifford
25. S. J. Cromer
26. V. M. Hamrick
27. W. H. Jordan
28. P. R. Kasten
29. Joanne S. Levy
30–31. F. C. Maienschein
32. F. R. Mynatt
33. B. F. Maskewitz
34. R. B. Parker
35. S. K. Penny
36. A. M. Perry
37. P. H. Pitkanen
38. F. A. R. Schmidt
39–78. P. N. Stevens
79. D. A. Sundberg
80. D. K. Trubey
81. A. M. Weinberg
82. H. Yamakoshi
83. G. Dessauer (consultant)
84. B. C. Diven (consultant)
85. W. N. Hess (consultant)
86. M. H. Kalos (consultant)
87. L. V. Spencer (consultant)
88–1088. RSIC Distribution
1089–1091. Central Research Library
1092. Document Reference Section
1093–1112. Laboratory Records Department
1113. Laboratory Records ORNL R. C.
1114. ORNL Patent Office

EXTERNAL DISTRIBUTION

1115–1119. Capt. R. W. Enz, Radiation Physics Branch, DASA, Washington, D. C. 20301
1120. P. B. Hemmig, Division of Reactor Development and Technology, U. S. Atomic Energy Commission, Washington, D. C.
1121–1122. J. W. Keller, NASA Headquarters, Washington, D. C.
1123. Lt. Col. G. C. Reinhardt, Radiation Physics Branch, DASA, Washington, D. C.
1124. R. Reetz, NASA Headquarters, Washington, D. C. 20546
1125. Robert Roussin, 1213 West Clark, Urbana, Illinois
1126–1135. W. Selph, Radiation Research Associates, Fort Worth, Texas
1136. I. F. Zartman, Division of Reactor Development, U. S. Atomic Energy Commission, Washington, D. C.
1137–1150. Division of Technical Information Extension (DTIE)
1151. Laboratory and University Division, AEC, ORO
1152. Director, Advanced Research Projects Agency, Washington, D. C. 20301
1153–1154. Commanding Officer, Armed Forces Radiobiology Research Institute National Naval Medical Center, ATTN: Technical Library; Bethesda, Maryland 20014
1155–1156. Director, Defense Atomic Support Agency, ATTN: APTL; STMD (For Canadian Def. Research Bd), Washington, D. C. 20305
1157. Director, Defense Communications Agency; ATTN: NMCSSC, B-210, Washington, D. C. 20305
1158–1177. Defense Documentation Center, Cameron Station, Alexandria, Virginia 22314
1178. Director, Defense Intelligence Agency, ATTN: DIAAP-8B, Washington, D. C. 20301
1179. Office of Defense Research and Engineering, Assistant Director (Nuclear Programs), Room 3E1071, The Pentagon, ATTN: Technical Library, Washington, D. C. 20301
1180. Joint Chiefs of Staff, Department of Defense, ATTN: Technical Library, Washington, D. C. 20301

1181. Commander, Joint Task Force Eight, ATTN: Technical Library, Sandia Base, New Mexico 87115
1182. Chief, National Military Command System Support Center, Room BE-685, The Pentagon, ATTN: Technical Library, Washington, D.C. 20301
1183. Director, Weapons Systems Evaluation Group, ATTN: Library/Col Holden/C. Beckel, Washington, D.C. 20305
1184. Joint Strategic Target Planning Staff, Offutt AFB, Nebraska 68113
1185. Commanding Officer, U.S. Army Combat Developments Command, Institute of Nuclear Studies, Fort Bliss, Texas 79916
1186. Chief of Research and Development, Department of the Army, ATTN: Nuclear, Chemical-Biological Div., Washington, D.C. 20310
1187. Commanding General, U.S. Army Electronics Command, ATTN: AMSEL-RD-DO/S
1188. Commanding General, U.S. Army Electronics Proving Ground, ATTN: Technical Library, Fort Huachuca, Arizona 85613
1189. Chief of Engineers, Department of the Army, ATTN: ENGMC-EM, Washington, D.C. 20315
1190. Commanding Officer, U.S. Army Mobility Equipment Research & Development Center; ATTN: Technical Info & Library Branch, Fort Belvoir, Virginia 22060
1191. Director, U.S. Army Engineer Waterways Experiment Station, ATTN: Library, Vicksburg, Mississippi 39180
1192. Commanding Officer, Harry Diamond Laboratories, ATTN: Technical Reference Branch, Washington, D.C. 20438
1193. Commanding General, U.S. Army Materiel Command, ATTN: AMCRD-BN/Nuclear Branch, Washington, D.C. 20315
1194. Nike-X Project Office, U.S. Army Materiel Command, Redstone Arsenal, ATTN: Technical Library, Huntsville, Alabama 35809
1195. Commanding Officer, U.S. Army Nuclear Defense Laboratory, ATTN: Library, Edgewood Arsenal, Maryland 21010
1196. Surgeon-General, Department of the Army, Room 1616, Main Navy Bldg., Washington, D.C. 20315
1197. Commanding General, White Sands Missile Range, ATTN: Technical Library/ORDBS-OM-TL, Las Cruces, New Mexico 88002
1198. Commanding Officer, Picatinny Arsenal, Dover, New Jersey 07801
1199. Commanding Officer, U.S. Army Research Office (Durham), Box CM, Duke Station, ATTN: Technical Library, Durham, North Carolina 27706
1200. Commanding General, U.S. Army Tank-Automotive Center, Warren, Michigan 48090
1201. Commanding General, U.S. Army Test & Evaluation Command, ATTN: NBC Office, Aberdeen Proving Ground, Maryland 21005
1202. Office of the Secretary of the Army, Director of Civil Defense, ATTN: Research, Washington, D.C. 20310
1203. Commanding General, Frankford Arsenal, Bridge & Tacony Street, Philadelphia, Pennsylvania 19137
1204. Commanding Officer, U.S. Army Materials Research Agency, ATTN: Technical Library Section, Watertown Arsenal, Watertown, Massachusetts 02172
1205. Commanding Officer, Naval Civil Engineering Laboratory, Port Hueneme, California 93041
1206. Chief of Naval Operations, Department of the Navy, ATTN: OP 75, Washington, D.C. 20350
1207. Superintendent, Naval Postgraduate School, ATTN: Technical Library, Monterey, California 93940
1208–1209. Commanding Officer, Naval Radiological Defense Laboratory, ATTN: Tech Info Div., San Francisco, California 94135 ATTN: J. Ferguson
1210. Director, Naval Research Laboratory, ATTN: Technical Library, Washington, D.C. 20390
1211. Commander, Naval Ship Systems Command, Department of the Navy, ATTN: L. E. Seiffert, CODE 03541, Washington, D.C. 20360

1212. Commanding Officer, Nuclear Weapons Training Center Atlantic, ATTN: Technical Library, Norfolk, Virginia 23511
1213–1215. Commander, Air Defense Command, ATTN: ADLMD-W, Missile & Space Weapon Div.; ADLDC, DCS/Plans; ADCSG, Box 35 (Col Kossuth), Ent Air Force Base, Colorado 80912
1216. Director, Air University Library, Maxwell AFB, Alabama 36112
1217. Arnold Engineering Development Center, ATTN: AELR, Arnold AFB, Tennessee 37389
1218. ATC, ATTN: Office of the Surgeon, Randolph AFB, Texas 78148
1219. Air Force Avionics Laboratory, ATTN: AVPT, Wright-Patterson AFB, Ohio 45433
1220–1223. Space & Missile Systems Organization (SAMSO), AF Unit Post Office, ATTN: SMQN; SMTSM-1; SMSDM/STINFO/Technical Library; SMTSS, Los Angeles, California 90045
1224. Directorate of Nuclear Safety, ATTN: AFINS, Kirtland AFB, New Mexico 87117
1225. Air Force Materials Laboratory, ATTN: MAS (Maj H. S. Reinert) Wright-Patterson AFB, Ohio 45433
1226. Medical Service School/114, ATTN: MSSMDM, Sheppard AFB, Texas 76311
1227. AF Office of Aerospace Research, Office of Research Analysis, ATTN: RRRD, Holloman AFB, New Mexico 88330
1228. Commander, AF Office of Aerospace Research, 1400 Wilson Blvd., ATTN: RROSP, Arlington, Virginia 22209
1229. Commander, USAF RADL Health Laboratory, ATTN: SGHW, Wright-Patterson AFB, Ohio 45433
1230. Commander Rome Air Development Center, ATTN: EMTLD (Documents Library), Griffiss AFB, New York 13440
1231. School of Aviation Medicine, USAFSC Aerospace Med Ctr, ATTN: Chief Radiobiology Branch, Brooks AFB, Texas 78235
1232. AF Strategic Air Command, ATTN: OAI; DPLBIC (LTC Tye), Offutt AFB, Nebraska 68113
1233–1234. Air Force Systems Command, ATTN: SCS-7; SCTSW, Andrews AFB, Washington, D.C. 20331
1235. AFSC STLO, Air Force Unit Post Office, ATTN: TRSAL, Los Angeles, California 90045
1236. Systems Engineering Group (ASD), ATTN: SENS, Wright-Patterson AFB, Ohio 45433
1237–1242. Headquarters, USAF, ATTN: AFCSAMI-2; AFOCC-A; AFRDQSN; AFRDDF; AFRDD; AFOCE-KA, Washington, D.C. 20330
1243–1244. Hq, USAF, TEMPO-8, ATTN: AFMSR; AFTAC/SDP-R, Washington, D.C. 20333
1245–1250. AF Weapons Laboratory, ATTN: WLRP; WLRB; WLDC; WLDN; WLIL; WLPM, Kirtland AFB, New Mexico 87117
1251. Argonne National Laboratory, 9700 South Cassave, ATTN: Library Services Dept/Report Section, Argonne, Illinois 60440
1252. Atomic Energy Commission, ATTN: Headquarters Library, Reports Section, Mail Station G-17, Washington, D.C. 20545
1253. Brookhaven National Laboratory, ATTN: Research Library, Upton, New York 11973
1254. University of California, Lawrence Radiation Laboratory, P.O. Box 808, ATTN: Technical Library, Livermore, California 94551
1255–1258. University of California, Los Alamos Scientific Laboratory, P.O. Box 1663, ATTN: R. F. Taschek/J. A. Phillips/G. A. Sawyer/E. J. Stovall, Los Alamos, New Mexico 87544
1259. President, Sandia Corporation, P.O. Box 5800, ATTN: Document Library, Albuquerque, New Mexico 87115
1260. National Bureau of Standards, Radiation Theory Section, ATTN: C. M. Eisenhauer, Washington, D.C. 20239
1261. National Center for Atmospheric Research, ATTN: Tech Library, Boulder, Colorado 80302
1262. Public Health Service, 4th and Jefferson Drive, S.W., ATTN: C. L. Weaver, Washington, D.C. 20201
1263. USPHS, Research Branch, Division of Radiological Health, 1901 Chapman Ave., Rockville, Maryland 20853

1264. Gilbert J. Ferber and L. Machta, Air Resources Laboratory, ESSA, Georgia Ave., Silver Spring, Maryland
1265. Aerojet-General Corp., San Ramon Plant, P. O. Box 86, San Ramon, California 94583 ATTN: Technical Library
1266–1267. Aerospace Corporation, San Bernardino Operation, 1111 E. Mill St., San Bernardino, California 92402 ATTN: E. W. Ray and Benveniste
1268. Battelle Memorial Institute, 505 King Avenue, Columbus, Ohio 43201 ATTN: John E. Davis
1269. Battelle Northwest Laboratory, P. O. Box 999, Richland, Washington 99352
1270. Philco-Ford Corporation, Aeronutronic Division, Ford & Jamboree Roads, Newport Beach, California ATTN: Technical Library
1271. The Bendix Corporation, Missile Systems Division, 400 South Beiger Street, Mishawaka, Indiana 46544 ATTN: Technical Library
1272. Boeing Aircraft Company, P. O. Box 3707, Seattle, Washington 98108, ATTN: Technical Library
1273. Columbia University, Low Memorial Library, New York, New York 10027, ATTN: H. Goldstein, Nuclear Eng. Dept.
1274. Gulf General Atomic, P. O. Box 1111, San Diego, California 92112, ATTN: R. J. Beyster
1275. General Dynamic/Convair (Astronautics), 5001 Kearny Villa Road, P. O. Box 1128, San Diego, California 92112 ATTN: Technical Library, D. Hamlin
1276. General Dynamics Corporation, Fort Worth Division. P. O. Box 748, Fort Worth, Texas 76101 ATTN: Technical Library
1277. General Electric Company, TEMPO, Center for Advanced Studies, 816 State Street, Santa Barbara, California 93102 ATTN: DASA Information and Analysis Center, W. W. Chan
1278. Holmes and Narver, Inc., 828 S. Figueroa Street, Los Angeles, California 90017 ATTN: Nuclear Division Library
1279. IIT Research Institute, 10 West 35th Street, Chicago, Illinois 60616 ATTN: Technical Library
1280. University of Illinois, Urbana Campus, Urbana, Illinois 61801 ATTN: A. B. Chilton
1281. Institute for Defense Analyses, 400 Army-Navy Drive, Arlington, Virginia 22202 ATTN: Technical Information Office
1282. Kaman Aircraft Corporation, Nuclear Division, Garden of the Gods Road, Colorado Springs, Colorado 80907
1283. Knolls Atomic Power Laboratory, P. O. Box 1072. Schenectady, New York 12301 ATTN: Document Library
1284. Massachusetts Institute of Technology, Instrumentation Laboratory, 68 Albany Street, Cambridge, Massachusetts ATTN: Technical Library
1285. Lockheed Missiles and Space Company, 3251 Hanover Street, Palo Alto California 94304
1286. Martin-Marietta Corporation, P. O. Box 179, Denver, Colorado 80201 ATTN: Technical Library
1287. Massachusetts Institute of Technology, 68 Albany Street, Cambridge, Massachusetts 02139 ATTN: MIT Libraries-Technical Reports
1288. University of Michigan, P. O. Box 618, Ann Arbor, Michigan 48107, ATTN: Technical Library
1289. North American Aviation, Space & Information Systems Division, 12214 Lakewood Blvd., Downey, California 90241 ATTN: Engineering Library
1290. Northrop Corporate Laboratories, 3401 West Broadway, Hawthorne, California 90250 ATTN: D. A. Hicks
1291. Radiation Research Associates, 1506 West Terrell Avenue, Fort Worth, Texas 76104
1292. The RAND Corporation, 1700 Main Street, Santa Monica, California 90406 ATTN: J. I. Marcum
1293. Stanford Research Institute, Menlo Park, California 94025 ATTN: Technical Library
1294. Sylvania Electronic Products, 190 Whisman Avenue, Mountain View, California 94042

1295. Technical Operations, Inc., South Avenue, Burlington, Massachusetts 01803
1296. LFE, Inc., Tracerlab Division, 2030 Wright Avenue, Richmond, California 94804
1297. TRW Systems, One Space Park, Redondo Beach, California 90278 ATTN: Nancy Hammond, Librarian
1298. Union Carbide Corporation, Union Carbide Research Institute, P. O. Box 278, Tarrytown, New York 10592
1299. United Nuclear Corporation, Grasslands Rd., Elmsford, New York 10523
1300. University of Virginia, Charlottsville, Virginia 22901 ATTN: Nuclear Engineering Department, Reed Johnson
1301. National Academy of Sciences, 2101 Constitution Avenue, Washington, D.C. 20418
1302. Space Technology Laboratories, 5771 West 96th Street, Building 12, Los Angeles, California
1303. TRW, RAMO-Woolridge Division, 8433 Fallbrook Avenue, Canoga Park, California ATTN: Technical Library
1304. Research Triangle Institute, P. O. Box 12194, Research Triangle Park, North Carolina 27709
1305. Hughes Aircraft Company, 3011 Malibu Canyon Road, Malibu, California 90265 ATTN: Doris Foehner
1306. University of Maryland, Department of Chemical Engineering, College Park, Maryland 20740
1307. Kansas State University, Department of Nuclear Engineering, Manhattan, Kansas 66502 ATTN: W. Kimel
1308. Associated Nucleonics, Inc., 975 Stewart Avenue, Garden City, New York 11552
1309. Carnegie Institute of Technology, Department of Physics, Pittsburgh, Pennsylvania 15213
1310. Marquardt Corporation, 16555 Saticoy Street, Van Nuys, California 91406
1311. Nuclear-Chicago Corporation, 333 E. Howard Avenue, Des Plaines, Illinois 60018
1312. Texas Nuclear Corporation, Box 9267, Allendale Station, Austin, Texas 78756
1313. University of California, Civilian Defense Research Project, 741 University Hall, 2200 University Avenue, Berkeley, California 94720
1314–1570. Given distribution as shown in TID-4500 under Reactor Technology category (25 copies – CFSTI)